Todd, Christopher Noel (2020) ***The sedimentary evolution of Permian to Cretaceous basins in Queensland, Australia: insights from lithostratigraphy, U–Pb zircon geochronology, sedimentary facies, and provenance analysis.*** **PhD Thesis, James Cook University.**

https://doi.org/10.25903/x1pq%2Dxc37

The sedimentary evolution of Permian to Cretaceous basins in Queensland, Australia: insights from lithostratigraphy, U–Pb zircon geochronology, sedimentary facies, and provenance analysis

Thesis submitted by

Christopher Noel Todd

Bachelor of Geology (Honours)

April 2020

For the degree of Doctor of Philosophy (Natural and Physical Sciences)

College of Science and Engineering

James Cook University

Statement of Access

I, the undersigned author of this thesis, understand that James Cook University will make this thesis available for use within the library and allow access in other approved libraries after its submission. All users consulting this thesis will have to sign the following statement:

> *In consulting with this thesis, I agree not to copy or closely paraphrase it in whole or in part without the written consent of the author; and to make proper public written acknowledgement for any assistance which I have obtained from it.*

Beyond this, I do not wish to place any restrictions on access to this thesis.

Christopher Noel Todd
April 2020

Declaration

I declare that this thesis is my own work and has not been submitted in any form for another degree or diploma at any university or other institute or tertiary education. Information derived from the published or unpublished work of others has been acknowledged in the text and a list of references is given.

Christopher Noel Todd
April 2020

Acknowledgements

I would like to acknowledge and thank the countless people in my professional and personal life whose support has helped me achieve this thesis. A broad thank you to all my family and friends and, at the risk of becoming sentimental, I would like to make mention some particular individuals who made significant contributions to the ultimate submission of this dissertation.

First and foremost, I must thank my parents; without their love and support of my passions over the long years, I would never have even considered that this achievement was within my reach. Allowing me to chase my dreams and learn from my own mistakes is the best thing you could have ever done for me. If not for your willingness to support my endeavours, even whilst not understanding the why or how of it all, I would not be here. I would also like to thank the rest of my family and friends who have always been there to ride high with my successes and comfort me in my failures.

I also owe a significant debt of gratitude, and likely few cartons of beer, to Eric Roberts. It was your classes in undergraduate that encouraged me to begin research, and then to believe in my abilities to continue from an Honours to a PhD. Furthermore, you provided me with the opportunities to improve my employability. I apologise for tormenting you with seemingly endless drafts, pestering questions, practical jokes, and my deadpan smart-arse comments delivered with perfect comedic timing; but nonetheless you still continuously took time out of your every increasingly busy schedule to help me out – and that is appreciated beyond words. I would also like to thank Carl Spandler and Bob Henderson for helping to shape and formulate ideas and hypotheses that could are explored in this work, and then to read and review these ideas brought to fruition; it provided a great deal of polish to my thesis.

I also wish to share my appreciation to the multitude of people with who I shared my PhD journey. A PhD is a tough assignment in a vast many a way, and people who have never attempted one are often ill-equipped to offer the necessary advice and comforting words to make life better again. Without all of you, it is highly likely that I would never have reached this point in my life.

Statement of Contribution of Others

Nature of Assistance	Contribution	Names, Titles and Affiliations of Co-contributors
Intellectual Support	Supervision	Assoc. Prof. Eric Roberts (JCU) Assoc. Prof. Carl Spandler (JCU)
	Proposal Writing/Literature Review	Assoc. Prof. Eric Roberts (JCU); Prof. Bob Henderson (JCU)
	Data Analysis	Assoc. Prof. Eric Roberts (JCU)
	Thesis Writing/Structure	Assoc. Prof. Eric Roberts (JCU) Dr. Maree Corkeron (JCU)
Financial Support	Research Funding	JCU Higher Degree by Research Enhancement Scheme; International Association of Sedimentologists Post-Graduate Scheme; Jurassic Foundation Research Grant; Australian Research Council Discovery Project
	Stipend	Australian Postgraduate Award
Data Collection	Palynology Analysis	Dr. Adam J. Charles (MGPalaeo)
	Mineral Separation	Dr. Cassian Pirard (JCU) Dr. Hui-Qing Huang (JCU)
	Advanced Analytical Centre	Dr. Yi Hu (JCU) Dr. Shane Askew (JCU)

Statement of Contribution

Chapter	Publication on which chapter is based	Nature and extent of intellectual input
1	Todd, C.N., Roberts, E.M. and Charles, A.J.	
2	Todd, C.N. and Roberts, E.M.	
3	Todd, C.N. and Roberts, E.M.	
4	Todd, C.N., Roberts, E.M., Knutsen, E.M., Rozefelds, A.C., Spandler, C., Huang, H.	
I confirm the candidate's contribution to this paper and consent to the inclusion of the paper in this thesis: Name: Eric Roberts Signature: Date:		

Chapter	Publication on which chapter is based	Nature and extent of intellectual input
1	Todd, C.N., Roberts, E.M. and Charles, A.J.	
I confirm the candidate's contribution to this paper and consent to the inclusion of the paper in this thesis: Name: Adam Charles Signature: Date:		

<table>
<tr><th>Chapter</th><th>Publication on which chapter is based</th><th>Nature and extent of intellectual input</th></tr>
<tr><td>4</td><td>Todd, C.N., Roberts, E.M., Knutsen, E.M., Rozefelds, A.C., Spandler, C., Huang, H.</td><td></td></tr>
<tr><td colspan="3">I confirm the candidate’s contribution to this paper and consent to the inclusion of the paper in this thesis:

Name: Espen Knutsen

Signature:

Date:</td></tr>
</table>

<table>
<tr><th>Chapter</th><th>Publication on which chapter is based</th><th>Nature and extent of intellectual input</th></tr>
<tr><td>4</td><td>Todd, C.N., Roberts, E.M., Knutsen, E.M., Rozefelds, A.C., Spandler, C., Huang, H.</td><td></td></tr>
<tr><td colspan="3">I confirm the candidate’s contribution to this paper and consent to the inclusion of the paper in this thesis:

Name: Andrew Rozefelds

Signature:

Date:</td></tr>
</table>

Chapter	Publication on which chapter is based	Nature and extent of intellectual input
4	Todd, C.N., Roberts, E.M., Knutsen, E.M., Rozefelds, A.C., Spandler, C., Huang, H.	
I confirm the candidate's contribution to this paper and consent to the inclusion of the paper in this thesis: Name: Carl Spandler Signature: Date:		

Chapter	Publication on which chapter is based	Nature and extent of intellectual input
4	Todd, C.N., Roberts, E.M., Knutsen, E.M., Rozefelds, A.C., Spandler, C., Huang, H.	
I confirm the candidate's contribution to this paper and consent to the inclusion of the paper in this thesis: Name: Hui-Qing Huang (Jeffrey) Signature: Date:		

Abstract

The Jurassic represents one of the least understood times in eastern Australia's geological history. It is difficult to study rocks of this age primarily because outcrop exposure is sparse, typically covered by a thick Cretaceous succession and Cainozoic to Quaternary cover sequences, and contemporaneous igneous bodies are rare or are absent. These bodies were likely removed during rifting, uplift, and erosion of the eastern Australian margin due to plate reorganisation in the Late Cretaceous. In lieu of primary magmatic rocks along the continental margin, provenance studies on proximal sedimentary basin infill can be a useful proxy for reconstructing the geological history of this continental succession. This study utilises a mostly continuous Mesozoic sedimentary succession exposed in Porcupine Gorge National Park on the north-eastern margins of the overlying Galilee and Eromanga basins in the Hughenden area of central northern Queensland, along with three nearby stratigraphic drill cores from the Geological Survey of Queensland (GSQ) Hughenden collection (cores 5, 6 and 7), to address a number of questions regarding the tectonic and environmental history of north-eastern Australia during the Triassic–Cretaceous. In order to characterise these strata, a multi-faceted approach, incorporating lithostratigraphy, palynology, U–Pb zircon geochronology, sedimentary facies analysis, and sedimentary provenance methodologies was applied to the sedimentary succession in the Hughenden area, with particular interest in the Jurassic.

The first objective of this study was to test and refine the existing stratigraphic and temporal framework for Permian–Cretaceous strata in the north-eastern Galilee and Eromanga basins through the application of lithostratigraphy, U–Pb zircon geochronology and palynology in outcrop and core. An updated stratigraphy was developed, including the identification and formal definition of two new sedimentary units: the upper Permian Galah Tuff Bed (251.5 ± 2.5 Ma) at the top of the Betts Creek beds, and the Upper Triassic Porcupine Gorge

Formation (229.4 ± 3.6 Ma), which replaces the lowermost ~18 m of the Warang Sandstone in the gorge. Based on the inclusion of the Galah Tuff Bed it is recommended that the Betts Creek beds be upgraded to the Betts Creek Group. Maximum depositional ages were confirmed for other key units in the Jurassic (Injune Creek Group, 161.9 ± 3.1 Ma) and Cretaceous (Hooray Sandstone, 129.7 ± 2.3 Ma; Gilbert River Formation, 122.5 ± 4 Ma). Zircon ages and palynology results suggest the need for further revision of many Mesozoic units and correlations regionally.

Secondly, this study characterised the lithofacies and alluvial architecture of long-lived fluvial systems in the Triassic to Jurassic of the Galilee and Eromanga basins for use in palaeoenvironmental reconstruction as well as for documenting reservoir and aquifer properties of prospective units in these basins. The similarity in lithofacies and architecture between each formation reveals the presence of a low accommodation setting, bed-load-dominated, braided fluvial system that characterises the Mesozoic in the study area. A short-lived shift to increased channel sinuosity and suspended load channels, likely associated with increased accommodation space caused by tectonic movement along the eastern Australian margin, is recognised in the lower Blantyre Sandstone. A brief marine incursion onto the craton during the Late Jurassic, to the north and south of the study area, may have affected the region by resulting in strong coastal winds, which would explain the presence of remobilisation of braid bar tops into aeolian dunes in the upper Blantyre Sandstone.

The third objective was to apply U–Pb zircon geochronology, sandstone petrology and palaeocurrent analysis to reconstruct the Permian to Cretaceous palaeodrainage evolution and patterns into the north-eastern Galilee and Eromanga basins. Provenance studies suggest that upper Permian to Middle Jurassic stratigraphic section was predominantly sourced from the North Australian Craton and Thomson Orogen, and from intrusive and extrusive rocks of the Kennedy Igneous Association to the north and north-east. Uplift in the Middle Jurassic changed provenance patterns, leading to the input of recycled sediments from basement metamorphics of the Anakie Province to the south. Subsequently, palaeodrainage shifted again in the Early Cretaceous with a return to a north-eastern source area associated with erosion of the Kennedy Igneous Association. Syn-depositional Mesozoic provenance sources are recognised in Triassic, Jurassic, and Cretaceous formations, which are interpreted to be derived from a distal volcanic arc on the eastern Australian margin.

The final objective of this thesis was to refine the age and stratigraphic context of important Jurassic vertebrate taxa from the eastern Australia. Only a handful of Jurassic vertebrates are known from Australia, including *Rhoetosaurus brownei* and *Siderops kehli* from the Surat Basin in Queensland, which were collected in the 1920s and 1960s, respectively, and lack precise stratigraphic context. Detrital zircons were sampled directly from matrix still attached to the fossilised bones housed in the Queensland Museum Collections, and these zircon grains were utilised to refine the maximum depositional age interpretation of both localities. The results of this analysis provide significantly refined age estimates for both specimens: 176.6 ± 2.0 Ma (upper Toarcian) for *S. kehli* and 162.6 ± 1.1 Ma (lower Oxfordian) for *R. brownei*. Lithological analysis of the *Siderops* and *Rhoetosaurus* matrix material, in addition to the ages, confirms the Toarcian Westgrove Ironstone Member of the Evergreen Formation and the Callovian–Oxfordian Walloon Coal Measures, respectively, as the sources of the two fossils.

Table of Contents

List of Tables

List of Figures

Chapter 1

Chapter 2

Chapter 3

Chapter 4

Chapter 5

List of Digital Appendices

Chapter 1:

Introduction

Geological background of the late Palaeozoic to Mesozoic basins of north-eastern Australia

Introduction

The geology of eastern Australia consists of six geological provinces: the Neoarchean to Palaeoproterozoic North Australian Craton, and the five orogenic belts that form the Cambrian to Triassic Tasman Orogenic Zone, or Tasmanides (Glen, 2005, 2013; Rosenbaum, 2018). The Tasmanides, from oldest to youngest, are the Delamerian, Lachlan, Thomson, Mossman, and New England orogens. Their formation was driven by subduction along a long-lived convergent margin on the eastern side the Australian continent. This subduction zone was active from the early Cambrian (~510 Ma) until at least the early Late Triassic (~230 Ma), and possibly until the Late Cretaceous (Veevers, 2006; Tucker et al., 2016; Wainman et al., 2015, 2018a, b; Hoy and Rosenbaum, 2017; Hoy et al., 2018) and, whilst it is considered to have controlled subsidence and formation of basins above these basement provinces, its influence during the Jurassic and Early Cretaceous is still poorly understood. Some of these overlying basins are of particular importance due to their hydrocarbon and groundwater resources, specifically the Carboniferous to Triassic basins (i.e. the Bowen, Galilee, Cooper, Sydney and Gunnedah basins), and the overlying Jurassic to Cretaceous basins (i.e. the Carpentaria, Eromanga, Surat, Laura, and Clarence-Moreton basins) (Fig. 1). These Jurassic to Cretaceous basins are often considered together as parts of a single superbasin system called the Great Artesian Basin, or alternatively the Great Australian Superbasin (Cook et al., 2013). For this thesis, Great Artesian Basin (GAB) will be used to refer to this collection of basins.

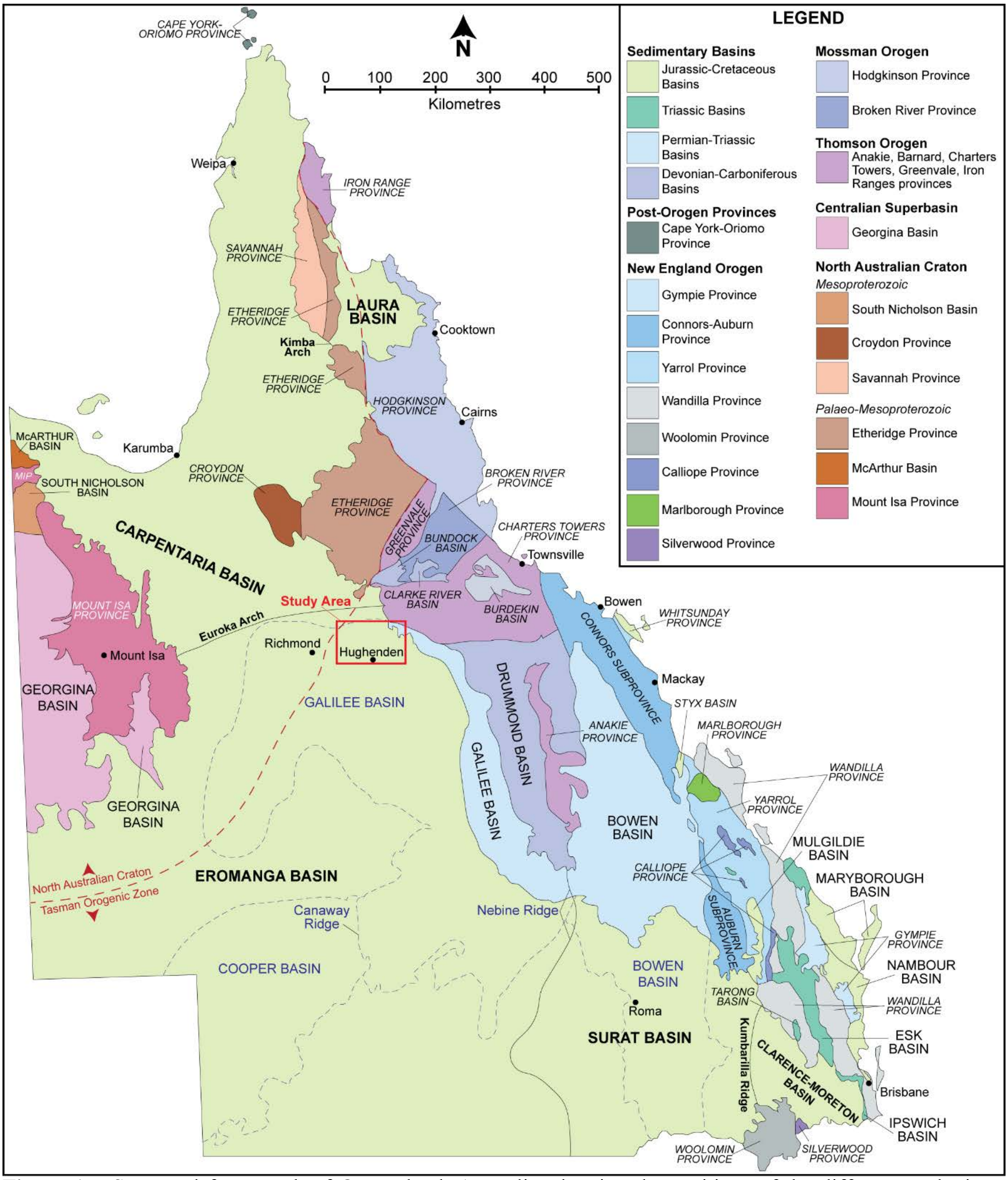

Figure 1 – Structural framework of Queensland, Australia, showing the positions of the different geologic – provinces, including the important Palaeozoic to Mesozoic sedimentary basins and orogenic belts. Modified from Withnall et al. (2013). Dotted lines indicate portions of Carboniferous to Triassic basins that are buried beneath the Jurassic to Cretaceous basins.

Geological Evolution of the Galilee Basin

The Galilee, Cooper and Bowen basins (Fig. 2) are separated by the basement structures the Canaway Ridge (Galilee and Cooper basins) and Nebine Ridge (Galilee and Bowen basins), however the basins are considered to have developed coevally between the late Carboniferous and Middle Triassic (de Caritat and Braun, 1992). Sedimentation between the Galilee and Bowen basins is considered continuous from the late Permian–Middle Triassic and so the two are often interpreted to be tectonically linked (e.g. de Caritat and Braun, 1992; Phillips et al., 2018b). However, sediment exchange between the Galilee Basin and the more southerly Cooper Basin is not thought have occurred (Hoffman, 1988). In contrast to the Bowen Basin, the tectonic evolution of the Galilee Basin is poorly documented, with competing hypotheses existing for its formation, including foreland-style subsidence due to lithospheric flexure of the uplifting Anakie Province (de Caritat and Braun, 1992), a result of a dextral shear couple (Evans and Roberts, 1980), or dynamic platform tilting (Waschbursch et al., 2009). Counter to these ideas, Van Heeswijck (2018) instead interpreted that the northern Galilee Basin was initiated by a continuation of thermal subsidence, which is a mechanism that is more characteristic of the evolution of the underlying Drummond Basin. During the late Carboniferous to early Permian, glaciogenic fluvial and lacustrine sediments were deposited in the Galilee Basin (Jones, 2003; Gray, 1977).

The middle Permian, ~270–260 Ma, was a period of non-deposition or non-preservation within the Galilee and Bowen basins (Evans, 1980; Van Heeswijck, 2004, 2010; Allen and Fielding, 2007a; Phillips et al., 2017a). At this time, the first of three compressive events related to the Hunter–Bowen Orogeny is interpreted to have uplifted the eastern Australian margin (Holcombe et al., 1997; Van Heeswijck, 2018). Widespread deposition resumed in the late Permian, which has been attributed to passive thermal subsidence in the Galilee Basin – and to foreland tectonics in the Bowen Basin relating to the second Hunter–Bowen deformation event

(Holcombe et al., 1997) – and these regimes continued into the Middle Triassic. Late Permian infill of the Galilee Basin is dominated by volcanolithic fluviatile sandstones, carbonaceous shales, and coals of the Betts Creek beds or Betts Creek Group (Allen and Fielding, 2007a, b; Phillips et al., 2017a). In the Early to Middle Triassic coal formation ceased in the basin and a shift to slightly drier fluvial-dominated sandstone and pedogenic floodplain shales is recorded in the basin (e.g. Vine et al., 1964; Gray, 1977; Balfe, 1979).

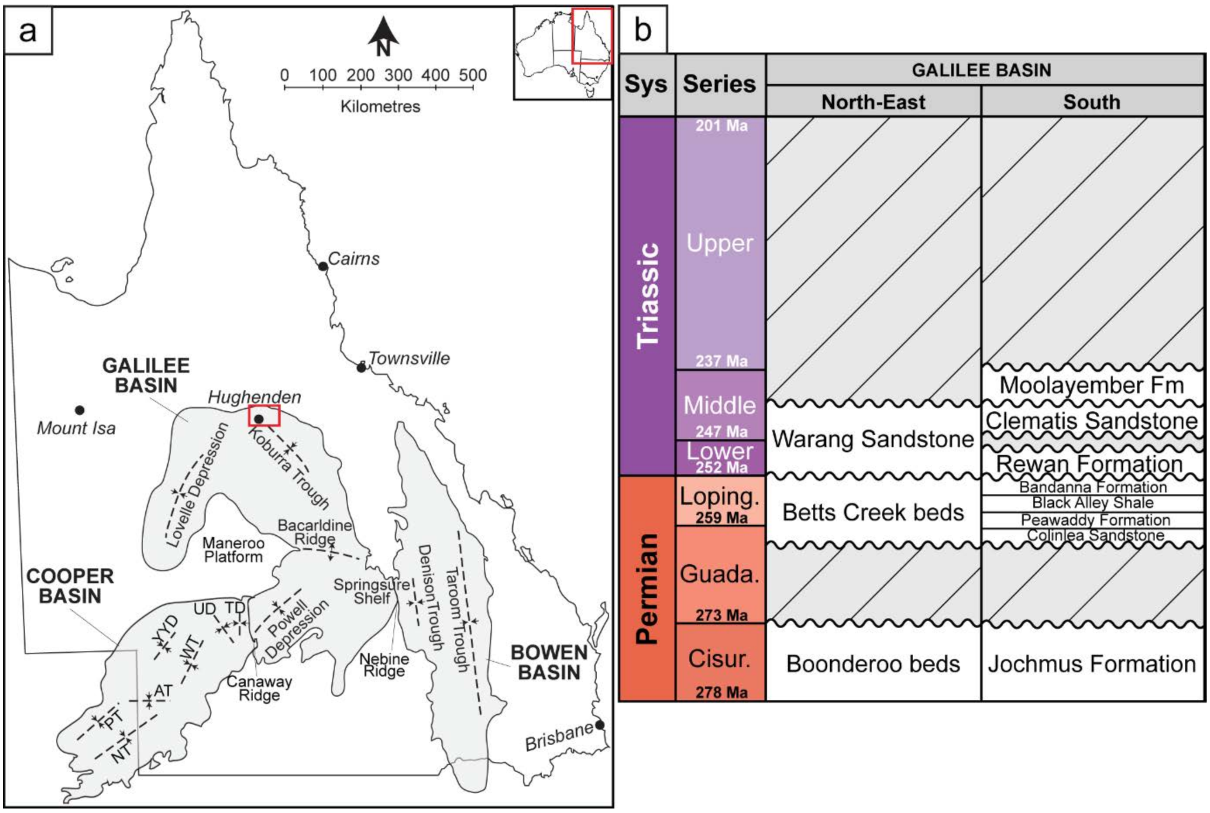

Figure 2 – (a) Extent of the Galilee, Cooper, and Bowen basins in Queensland and the structural elements. (b) Stratigraphy of the Galilee Basin.

In the early Late Triassic (~235–230 Ma), the final compressive phase of the Hunter–Bowen Orogeny uplifted and inverted the eastern Australian margin, causing substantial deformation in the form of large-scale thrusting and folding of the Permian to Triassic strata in the Bowen Basin and New England Orogen (Korsch et al., 2009; Hoy and Rosenbaum, 2017;

Hoy et al., 2018). Sedimentary deposition into the Bowen, Galilee, Cooper, Sydney and Gunnedah basins also ceased as a result of this large-scale deformation and uplift.

An extended period of tectonic stability during the Late Triassic and into the Early Jurassic is interpreted from seismic surveys, where erosion of the Bowen Basin and New England Orogen sequences formed a peneplain surface over which Jurassic and Cretaceous strata of the Surat Basin were then deposited (Korsch et al., 2009). Similar seismic surveys in the northern Galilee Basin sequence showed no deformation in the sedimentary sequences, indicating it remained mostly unaffected by the final Hunter–Bowen compression event (Van Heeswijck, 2010, 2018). The stratigraphic boundary marking the contact between the Galilee and Eromanga basins can, therefore, be characterised as a paraconformable surface.

Geological Evolution of the Eromanga Basin

In the GAB, the Eromanga, Carpentaria and Surat basins also evolved coevally. Sediment exchange between the Eromanga and Surat basins across the Nebine Ridge is interpreted to have occurred sporadically between the Middle Jurassic and Early Cretaceous (Korsch et al., 2009; Wainman et al., 2015), whereas exchange between the Eromanga and Carpentaria basins wasn't initiated until the Early Cretaceous (Smart and Senior, 1980). Localised sedimentary deposition was initiated in places within the south-west Eromanga Basin in the latest Triassic; however, widespread deposition did not occur until the Early Jurassic (Draper, 2002). The process and timing of formation of the Eromanga Basin is also debated, and attempts to resolve it debate are hampered by a sparsity of outcrop exposure of Early Jurassic strata in Queensland (Bianchi et al., 2018). In addition, primary magmatic rocks of this same age that could help determine the nature of the eastern continental margin (e.g. subduction and presence of an active magmatic arc; back arc magmatism and rifting; intraplate rifting and volcanism; or a large igneous province) are rare (Turner et al., 2009; Waschbursch et al., 2009; Bryan et al., 2012).

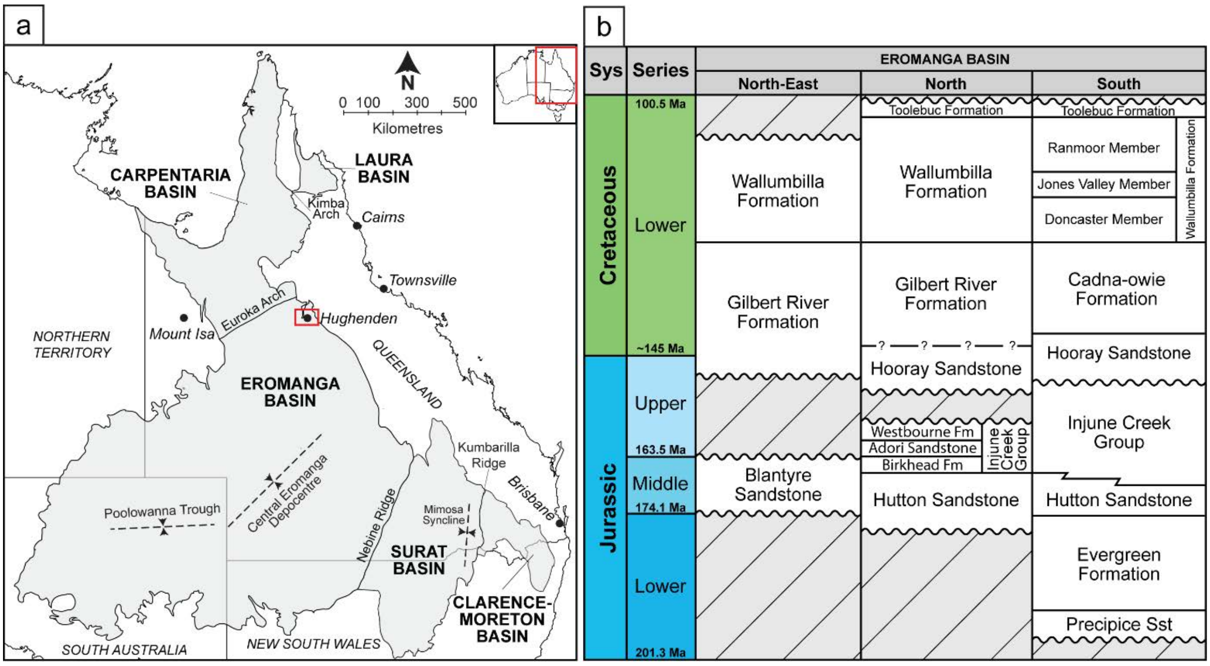

Figure 3 – (a) Extend of the Great Artesian Basin and associated structural elements. (b) The stratigraphy of the Eromanga Basins.

The saucer-shaped Eromanga Basin is commonly described as an intracratonic sag basin (Cook et al., 2013) but different tectonic models have also been suggested, including (1) foreland basin development to better account for periods of accelerated subsidence (Gallagher, 1990); (2) thermal contraction of the lithosphere causing subsidence far inboard of the continental margin (Gallagher and Lambeck, 1989); (3) deep crustal metamorphism resulting in crustal densification and subsidence (Middleton, 1980); and (4) subduction-related dynamic platform tilting (Gallagher, 1990; de Caritat & Braun 1992; Gallagher et al. 1994; Russell & Gurnis 1994; Gurnis et al. 1998; Waschbursch et al., 2009). Each of these hypotheses implies that an active convergent margin was located along the eastern Australian continental margin during the Jurassic. A separate hypothesis, however, invokes failed incipient rifting in an intraplate setting as the formation mechanism for the Eromanga Basin (e.g. Fielding, 1996;

Yago and Fielding, 1996). This interpretation indicates the position of the margin as being further to the east, or that subduction ended in the Late Triassic with the final compression of the Hunter-Bowen Orogeny. Evidence for volcanism in the Middle to Late Jurassic has been documented in the form of tuff horizons in the sedimentary basin record (Wainman et al., 2015, 2018a), and are interpreted to be sourced from an arc-related volcanic chain, rather than intraplate volcanism. A mechanism for initiation of subsidence in the latest Triassic or Early Jurassic is not explained by these models, and indeed a more complex combination of these models may be more likely (Waschbursch et al., 2009).

With the exception of a short-lived marine influence in the Early Jurassic (Bianchi et al., 2018; Wang et al., 2019; La Croix et al., 2019) and Late Jurassic (Wainman and McCabe, 2019), the sedimentary infill of the Eromanga Basin during the Early Jurassic to Early Cretaceous was dominated by continental depositional systems consisting of highly permeable fluvial sandstones and carbonaceous floodplain deposits (e.g. Balfe, 1979; Draper, 2002; Ransley et al., 2015; Wainman et al., 2015). In the Aptian (Early Cretaceous), a marine transgression blanketed the Eromanga Basin in shallow marine mudstones (Cook et al., 2013). Deposition continued into the Late Cretaceous as the sea retreated, which is tracked by a progressive shift to continental depositional systems (e.g. Tucker et al., 2017).

Arc-related volcanism along the eastern Australian margin continued into the Late Cretaceous (~92 Ma) until a switch to an extensional regime induced continental rifting beginning ~83 Ma and opened the Tasman Sea (Tucker et al., 2016). These rifted pieces, consisting of the Lord Howe Rise and parts of Zealandia, now lie submerged beneath the Tasman Sea (Willcox et al., 2001; Exon et al., 2004; Mortimer et al., 2008, 2017). Mesozoic detrital zircon signatures observed in Vanuatu and New Caledonia suggest that these areas were also once attached to the ancient Australian continent (Buys et al., 2014). Cessation of subduction further led to isostatic rebound of the remaining eastern margin and created significant relief in the form of the present-day Great Dividing Range, thereby terminating deposition into the GAB and draining the sediments west and south-westward into the contemporaneously forming Ceduna Delta in the Great Australian Bight (Jones and Veevers, 1983; Gallagher et al., 1994; Gurnis et al., 1998; Veevers, 2006; Bryan et al., 2012; MacDonald et al., 2013; Lloyd et al., 2016).

Despite our understanding of these geological events, the tectono-sedimentary history of Eastern Australia between the Late Triassic and Early Cretaceous is still poorly resolved. In particular, it is unclear if subduction-related volcanism continued along the eastern margin between the final Hunter–Bowen Orogenic compressional event at ~230 Ma and the onset of rifting at ~83 Ma. Further, if subduction was continuous, it is unknown if it was located proximal enough to the continental margin (i.e., onshore or offshore) to have influenced the development of, and infill into, the GAB. In addition, if subduction did continue, was basin formation largely a result of compression (foreland-style basin) or lithospheric attenuation caused by backarc extension (resulting in a backarc or intracratonic basin)?

Exacerbating this uncertainty issue is the sparsity of magmatic or other igneous rocks from the Middle Triassic, Jurassic and earliest Cretaceous that could shed light on the tectonic processes operating at this time (Turner et al., 2009). Fortunately, however, the widespread intracratonic sedimentary basins of eastern Australia can provide insight into these issues. Although outcrop of Middle Triassic, Jurassic and Lower Cretaceous sequences across the GAB is limited, a number of good exposures and a significant number of stratigraphic drill cores are available that can provide critical clues to deciphering the tectonic and sedimentary record during this time (e.g. Gray, 1977; Balfe, 1979). This period is of particular importance because it contains economic hydrocarbon reservoirs (e.g. Wainman et al., 2015) and groundwater resources (Ransley et al., 2015), and preserves some of Australia's most important Mesozoic fauna (dinosaurs and other rare vertebrates; e.g. Longman, 1926; Warren and

Hutchinson, 1983; Thulborn, 1994; Kear, 2012; Nair and Salisbury, 2012) and flora (Turner et al., 2009).

This multi-faceted thesis forms part of the larger Australian Research Council funded Jurassic Arc Project that aims to better understand the geology and sedimentology of this understudied period in the eastern Australian geological record. The primary focus of this investigation is the Middle Triassic to Lower Cretaceous succession in the Galilee and Eromanga basins in North Queensland, with additional field localities elsewhere in Queensland. Special emphasis was placed on studying the exposures in Porcupine Gorge National Park in North Queensland because of the unrivalled exposure and access to study this sequence in a single locality. Drill cores from stratigraphic bored located proximal to Porcupine Gorge National Park were also utilised to provide a broader regional context. The main issues this thesis aims to resolve include (1) utilising modern provenance analysis to track the sources and sediment dispersal patterns in order to test the location and timing of key tectonic events in north-eastern Queensland, (2) improving age constraint of rock units in the Galilee and Eromanga basins, and of critical Jurassic faunas in the Surat Basin, thereby also resolving stratigraphic issues in the Mesozoic record of Queensland, and (3) characterising the sedimentary architecture of potential hydrocarbon and groundwater reservoirs in the northern Galilee and Eromanga basins.

Thesis structure

Thesis body

This thesis is written and organised as a series of individual manuscripts to be submitted as papers to international journals. As such, the thesis has been organised as a series of four stand-alone chapters, with a common thread of late Palaeozoic to Mesozoic geology and geochronology in Queensland. This structure causes some repetition in the introductory sections of each paper, such as the geological setting and methods, but as each paper has a different focus, this repetition is necessary. At time of thesis submission, Chapter 5 has been published in *Gondwana Research*, and the remaining chapters (2, 3 and 4) are either in review, in revision or will be submitted following completion of the thesis. A single reference list encompassing all references used across all the chapters/sections follows Chapter 6: Thesis Summary.

Chapter 2 utilises lithostratigraphy and geochronology (palynology and U–Pb zircon geochronology) to provide a robust and detailed revised stratigraphic framework for the north-eastern Galilee and Eromanga basins utilising the sedimentary successions exposed in Porcupine Gorge National Park and in nearby Geological Survey of Queensland (GSQ) stratigraphic drill core. This chapter is the first study to present U–Pb detrital zircon data for this interval in northern Queensland and is crucial for correlating the sedimentary strata both within each basin and across basin boundaries.

Chapter 3 presents a detailed sedimentological investigation into the Triassic–Jurassic fluvial depositional system in the Galilee and Eromanga basins. The objectives of this chapter are to describe and interpret the facies and architecture of each unit in order to better understand the depositional setting and environments during this time, and to characterise the aquifer characteristics of these extensive sandstone-dominated fluvial deposits, which are key producing units in other parts of the GAB. This study has implications for better understanding of groundwater capacity and flow within this portion of the GAB, and Jurassic hydrocarbon reservoirs in Queensland.

Chapter 4 represents a comprehensive, modern sedimentary provenance analysis, utilising U–Pb detrital zircon geochronology, sandstone petrography, palaeocurrent analysis, and pebble counts to model the palaeodrainage evolution and tectonic history of north-eastern Australia during the Permian to Cretaceous. This work synthesises the concepts established in Chapter 2 and 3 with the results from additional analyses to determine the source terranes for each of the major detrital zircon populations, and interprets the major provenance changes that are observed and how they may relate to the tectonic evolution of the eastern Australian margin. In addition, this chapter aims to test whether a subduction-related volcanic arc was active along the North Queensland margin during the Late Triassic to Early Cretaceous and if it was influencing basin evolution and/or contributing to the sedimentary infill.

The aim of Chapter 5 is to provide robust ages and geological context to two of Australia's most important Jurassic megafaunas by analysing the sedimentary matrix collected directly from the fossilised bones. U–Pb detrital zircon analysis of material from the giant amphibian *Siderops kehli* and Australia's only recorded pre-Cretaceous sauropod dinosaur *Rhoetosaurus brownei*, both discovered in the Surat Basin, was ultimately able to provide both taxa with strict numerical ages and stratigraphic control.

Appendices

In addition to each individual data chapter presented herein (Chapters 2–5), there are four appendices attached to the back of this thesis, including three that detail research conducted as part of my PhD, but in which I was not the primary investigator. Appendix 1, published in the *Australian Journal of Earth Sciences*, combines detrital zircon results from my thesis work with additional (U–Th)/He data collected by my colleagues at James Cook University to present evidence for a Jurassic uplift event of the eastern Australian margin. Although I am not the lead author, I contributed at least 30% of the data, writing and interpretation for this co-authored manuscript that directly relates to my thesis work. Appendices 2 and 3, published in *Plos One* in 2016 and in Australasian Science in 2017, present the oldest known fossil evidence for agriculture in insects with a description of a number of fungus-farming termite nests from the East African Rift in Tanzania. Appendix 4 presents the fully tabulated pebble count data that is used to determine sedimentary provenance in Chapter 5; however, it was excluded from the text for being too cumbersome for a journal manuscript.

Chapter 2:
A stratigraphic framework for the Galilee and Eromanga basins, Queensland, Australia: evidence from lithostratigraphy, palynology, and U–Pb zircon geochronology

Abstract

Despite many lithological and geochronological studies within the north-eastern Galilee and Eromanga basins, the Mesozoic stratigraphy within these basins remains problematic. This study integrates lithostratigraphy, palynology, and U–Pb zircon geochronology of well-exposed Permian–Cretaceous sedimentary units and proximal stratigraphic cores from northern Queensland to test existing correlations and to establish new correlations. The newly defined Galah Tuff Bed, at the top of the Betts Creek beds in Porcupine Gorge, dated at 251.5 ± 2.5 Ma, provides an important age constraint and tie point for correlation with coeval units in the adjacent Bowen Basin. Overlying the Betts Creek beds, a newly recognised Upper Triassic stratigraphic unit, defined herein as the Porcupine Gorge Formation, is identified. Based on detrital zircon maximum depositional age control, the overlying Warang Sandstone and Moolayember Formation are determined to be considerably younger (locally) than previously reported (Middle to Late Triassic rather than Early to Middle Triassic). Despite no new age constraining data for the overlying Jurassic Blantyre Sandstone, existing lithostratigraphic and palynologic data suggest a correlation between the lower Blantyre Sandstone and the Hutton Sandstone. Further, the upper Blantyre Sandstone is correlated with the Injune Creek Group based on petrographic and detrital zircon provenance attributes. The maximum depositional age calculated in this study for the Injune Creek Group (161.9 ± 3.1 Ma) suggests widespread correlation of this unit across the Eromanga and Surat basins. Detrital zircon maximum depositional age constraints for the overlying Hooray Sandstone and the Gilbert River Formation suggest depositional ages no older than Barremian and Aptian, respectively.

Introduction

The Carboniferous–Triassic Galilee Basin and overlying Jurassic–Cretaceous Eromanga Basin dominate the Phanerozoic geology in northern Queensland. Both basins represent sub-basins of larger sedimentary systems: the Galilee-Cooper-Bowen-(±Sydney-Gunnedah basins) system and the Laura-Carpentaria-Eromanga-Surat-(±Clarence-Moreton basin) system, also known as the Great Artesian Basin or Great Australian Superbasin. Importantly, both basin systems yield critical economic hydrocarbon and/or groundwater resources. Thus, a refined stratigraphic framework that establishes more precise correlations within and across these vast basin systems is crucial to our understanding of their genesis and evolution, as well as the spatiotemporal distribution of important resources.

Prior to the advent of cheap and efficient U–Pb dating techniques, constraining the ages of the nonmarine late Palaeozoic to Mesozoic strata of the Galilee and Eromanga basins, and correlating units between regions, relied exclusively on lithostratigraphic and biostratigraphic interpretations (e.g. Evans, 1964; Burger and Kemp, 1972; Burger, 1973; McKellar, 1977, 1979; Burger and Senior, 1979; de Jersey and McKellar, 1980). More recently, the discovery and dating of rare intercalated volcanic units, coupled with widespread application of U–Pb detrital zircon geochronology, has dramatically improved the resolution with which we can correlate strata in continental basins of eastern Australia (Tucker et al., 2013; Wainman et al., 2015, 2018a, 2018b; Phillips et al., 2018a, 2018b; Bell et al., 2019). Moreover, many of these studies have demonstrated the value of combining U–Pb maximum depositional ages from detrital zircons with palynology in refining the temporal resolution of the eastern Australian spore-pollen zonations.

Outcrop exposure of the Mesozoic succession across Queensland is generally limited to basin margins and deeply incised gorge systems, which tends to hinder our understanding of this succession. Porcupine Gorge National Park in northern Queensland provides an opportunity to study ~200 M.y. of Permian–Cretaceous sedimentary strata, with tens of kilometres of cliff-face exposures that contains strata recorded from both the Galilee and Eromanga basins (e.g. Vine et al., 1964). However, aside from a brief lithological overview by Vine et al. (1964) and three sedimentological investigations into the Palaeozoic formations (Jones, 2003; Allen and Fielding, 2007a,b), the stratigraphy of Porcupine Gorge remains an untapped archive on the history of northern Queensland.

This study, therefore, aims to refine the stratigraphic framework for the north-eastern Galilee and Eromanga basins by (1) describing the lithology and stratigraphy in core and in outcrop from the Hughenden region, including the spectacular Porcupine Gorge National Park and Geological Survey of Queensland (GSQ) Hughenden cores, (2) combining palynology and U–Pb detrital zircon and tuff zircon geochronology from both outcrop and core to provide better age controls on the Permian–Cretaceous succession, and (3) using these data to test current stratigraphic correlations and to establish newer and more accurate correlations.

Background Geology

Galilee Basin

The Carboniferous to Triassic intracratonic Galilee Basin is subdivided into three depocentres: the Koburra Trough in the north-east, the Lovelle Depression in the north-west, and the Powell Depression in the south, which cover a combined area of 247,000 km^2 across Queensland (Fig. 1a). Mechanical extension or thermal subsidence are generally interpreted as the mechanism for basin opening during the late Carboniferous (Van Heeswijck, 2010; Phillips et al., 2017a, 2017b). Sedimentation is thought to have been continuous between the Galilee and Bowen basins during the late Permian to Middle Triassic, with sediments generally draining westward across the Nebine Ridge (Vine, 1973; Hawkins, 1977; Casey, 1970; Fielding et al., 1990). The Galilee Basin is separated from the Cooper Basin in the south-west by the Canaway Ridge, which blocked sediment transfer between the two basins (Hoffman, 1988). A final compressive phase of the Hunter-Bowen Orogeny inverted and closed the basin in the Late Triassic (Van Heeswijck, 2018).

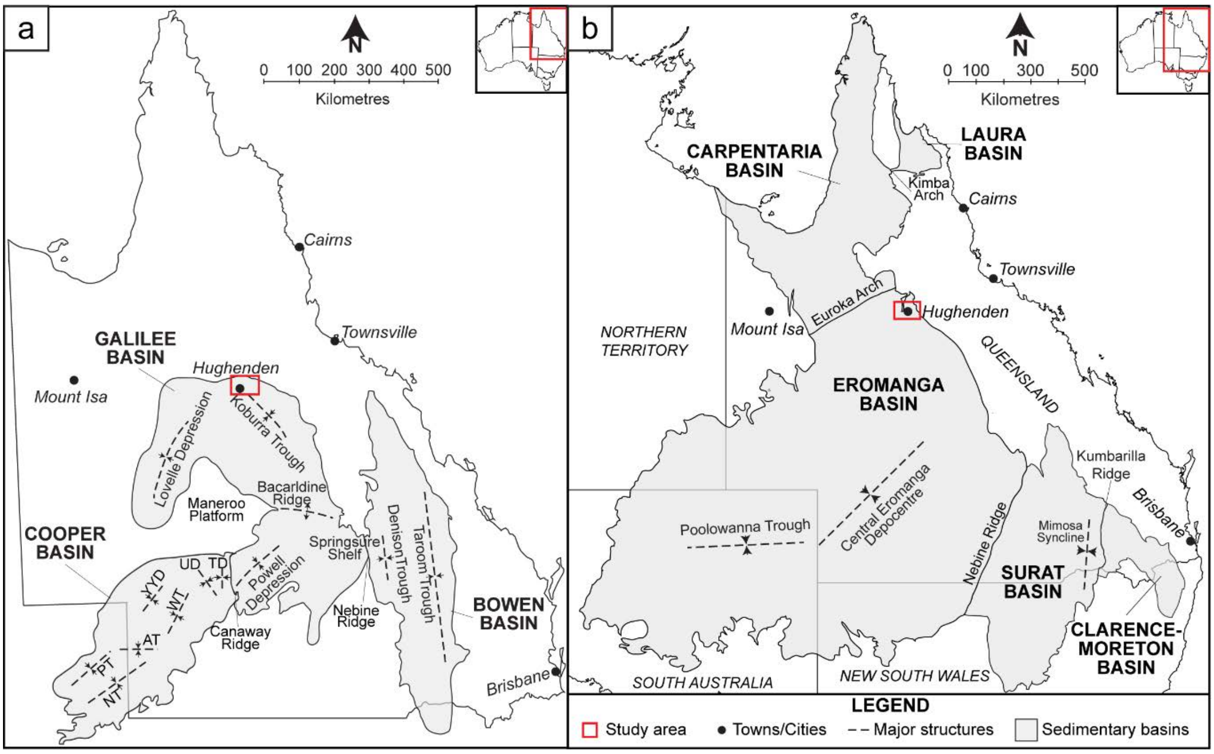

Figure 1 – (a) Extent of the Galilee, Bowen, and Cooper basins in Queensland and their associated structural features. (b) Extent of the Great Artesian Basin system and its associated structural features.

Eromanga Basin

The Jurassic to Cretaceous intracratonic Eromanga Basin overlies the Galilee and Cooper basins and covers 1.2 million km^2 across much of Queensland and South Australia, and parts of the Northern Territory and New South Wales (Fig. 1b). Localised subsidence in southern Queensland and South Australia during the Late Triassic initiated basin development, before widespread subsidence commenced in the Early Jurassic (Gray et al., 2002). Seismic surveys and lithostratigraphic studies suggest that the stratigraphy is continuous across the Nebine

Ridge between the south-eastern Eromanga Basin and western Surat Basin throughout the Jurassic and Early Cretaceous (Wake-Dyster et al., 1987). The Euroka Arch separates the Eromanga and Carpentaria basins; however, sedimentation only became continuous during the Early Cretaceous (Smart and Senior, 1980). Rifting of the eastern Australian margin during the Late Cretaceous uplifted the remaining continental crust, which filled and closed the Eromanga Basin (Cook et al., 2013).

Local Geology and Stratigraphy

The north-eastern portions of the Galilee and Eromanga basins are exposed within Porcupine Gorge, ~65 km north of Hughenden in central northern Queensland (Fig. 1a, b). The Porcupine Creek, a tributary of the Flinders River, has incised ~100–150 m through the shallowly southward-dipping succession over the last one million years to reveal dramatic, cliff-forming exposures of the Permian to Lower Cretaceous stratigraphy through the gorge (Coventry et al., 1985). A combined thickness of ~350 m of sedimentary strata is exposed along a NNE-SSW transect through Porcupine Gorge. The lithostratigraphy as observed in Porcupine Gorge represented by Hughenden North (Fig. 3) was initially described in its entirety by Vine et al. (1964) and includes the first lithological definitions of the Triassic Warang Sandstone and Jurassic Blantyre Sandstone. The description of each formation, as identified by Vine et al. (1964) in Porcupine Gorge, is incorporated herein and modified where necessary.

Between 1974 and 1977, five stratigraphic cores were drilled in the Hughenden area by the GSQ: GSQ Hughenden 1-2R, GSQ Hughenden 3-4R, GSQ Hughenden 5, GSQ Hughenden 6 (Gray, 1977), and GSQ Hughenden 7 (Balfe, 1979). The lithostratigraphy observed in cores 1-6 by Gray (1977) is very similar to that of Vine et al. (1964) for Porcupine Gorge, and is also represented on Figure 2 as Hughenden North. A different lithostratigraphic succession was observed in GSQ Hughenden 7 by Balfe (1979), represented as Hughenden South (Fig. 3), which shows a transition between the basin margin stratigraphy in Porcupine Gorge and that which is observed closer to the depocentres of each basin (*sensu* Almond, 1983; Gray et al., 2002; Van Heeswijck, 2010; I'Anson et al., 2018). The various lithostratigraphic frameworks established for Hughenden region are compiled in Figure 2.

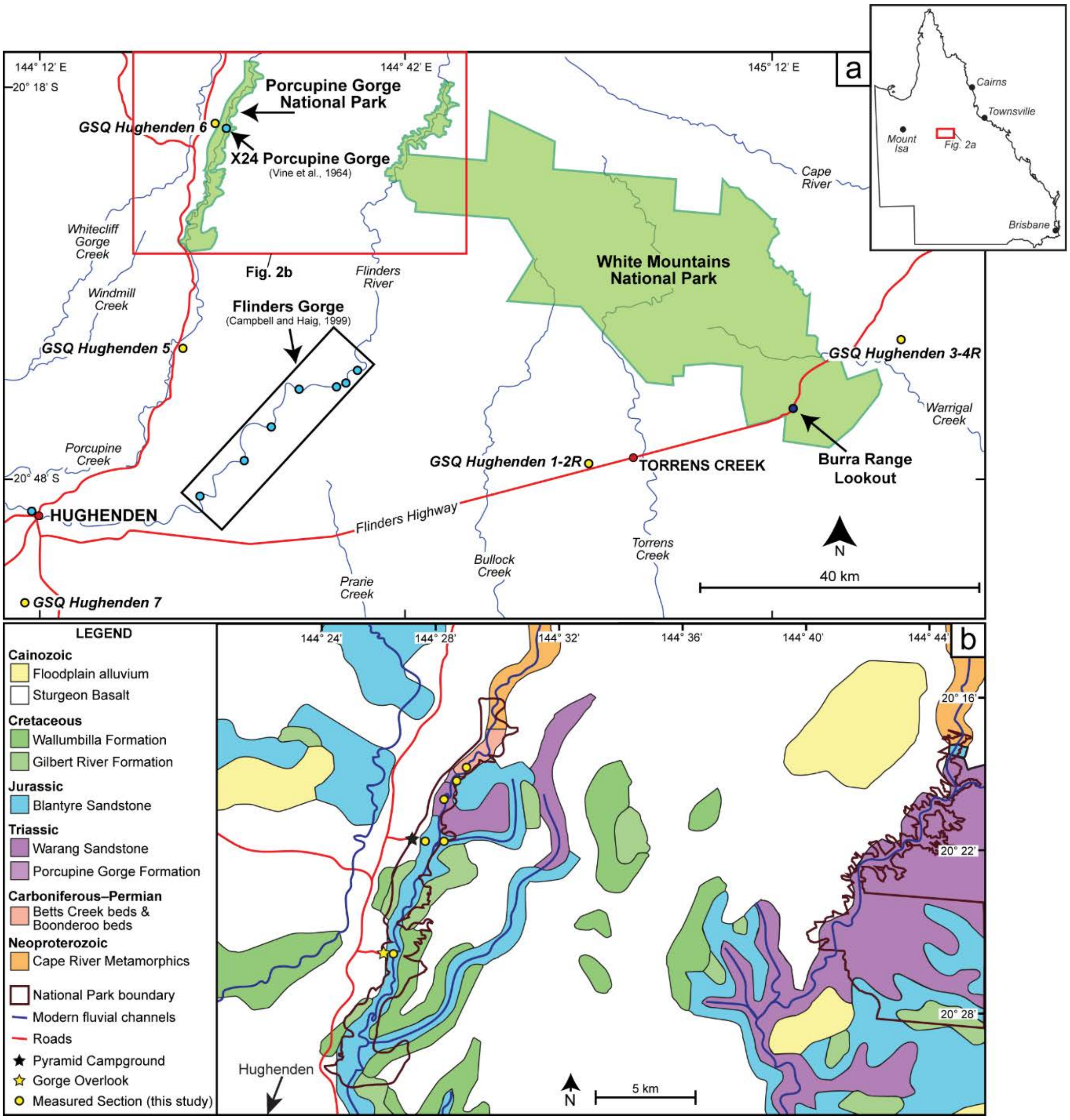

Figure 2 – (a) Geographic map of the Upper Flinders River area, including national park boundaries, stratigraphic core locations, and locations of stratigraphic sections measured by other authors (blue dots). (b) Geological map of the Porcupine Gorge, north of Hughenden, including location of measured stratigraphic sections.

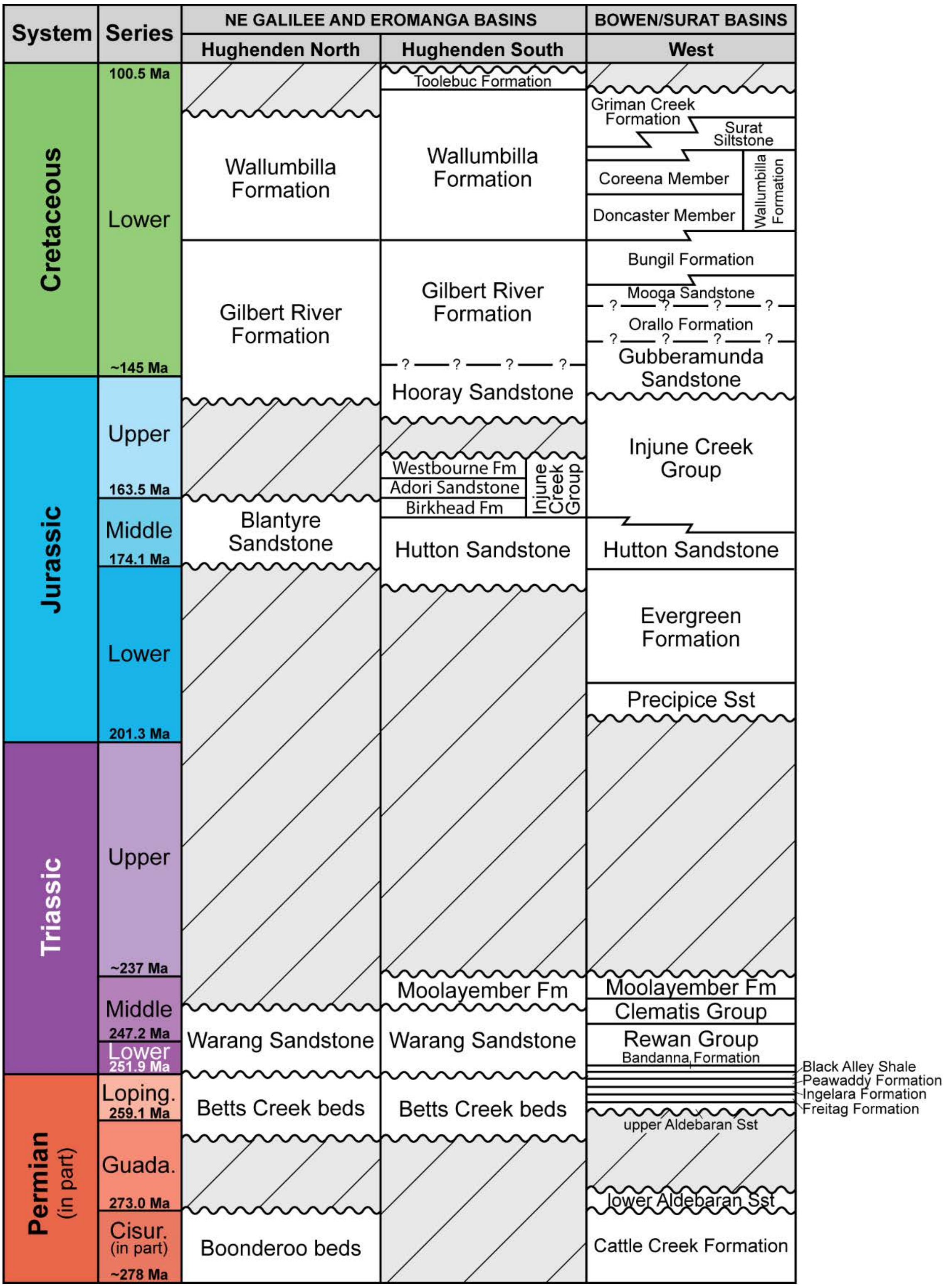

Figure 2 – Comparisons of the stratigraphies of the north-eastern Galilee and Eromanga basins in the Hughenden area and their equivalents in the Bowen and Surat basins prior to this study. Data collected from Vine et al. (1964), Gray (1977), Balfe (1979), Phillips et al. (2018a), and Wainman et al. (2018a). Grey lined boxes indicate periods of lack of preservation or depositional hiatuses. Boundary dates taken from the International Commission on Stratigraphy (Cohen et al., 2013).

Methods

Lithostratigraphy

Fieldwork was undertaken in Porcupine Gorge National Park between 2014 and 2017. Nine decimetre scale lithostratigraphic sections were measured using a Jacob's staff, Abney level, GPS, and compass (Appendix 4). From these, a composite lithostratigraphic section through the gorge was established. In addition, description, and sampling of the GSQ Hughenden 5, 6, and 7 stratigraphic drill cores was conducted at the GSQ Core Facility in Brisbane, Queensland (locations given in Fig. 2b). Lithological descriptions by Vine et al. (1964) in Porcupine Gorge and the White Mountains, and by Campbell and Haig (1999) in the Flinders River Gorge, are also incorporated into this study for comparison (Fig. 2b).

Palynology

Six siltstone/mudstone samples were collected in Porcupine Gorge for palynological investigation: four from the siltstone of the Porcupine Gorge Formation (newly described in lithostratigraphy section below) (55 m and 57 m), and one from each of the lower and upper Blantyre Sandstone exposures (108 m and 262 m). Sample selection in the field was dictated by the availability of unweathered and non-oxidised siltstone or mudstone layers to avoid oxidation of palynomorphs. An additional three samples were collected from the Blantyre Sandstone in GSQ Hughenden 5 core at 41 m, 84 m, and 155 m depths. All samples were analysed by Dr Adam Charles at MGPalaeo in Perth, Australia. Approximately 5 g of sample was processed using standard techniques outlined by Wood et al. (1996) and references therein. Following washing and crushing of the sample, 25 ml of 34% hydrochloric acid was added to remove any carbonates, with subsequent decanting and further washing, with the addition of 25 ml of 48% hydrofluoric acid to digest silicate minerals. The sample was sieved using a 100 µm mesh to remove the coarse, organic component, with the remaining residue passed through a 10 µm sieve. Finally, the residual organics were subjected to heavy liquid separation using lithium heterometatungstate, mixed with a PVA solution and mounted on glass coverslips using Norland Optical Adhesive 61. Quantitative palynological data were collected by counting the first 100 microfossils observed, to estimate the relative abundance of palynomorphs, with the remainder of the sample scanned for diagnostic marker species.

In addition, previous relevant palynological datasets from the Hughenden area were reviewed. Revised zonal designations were applied to samples described by Evans (1964) and McKellar (1977, 1979), in order to provide robust comparisons with the samples analysed in this study. Triassic and Jurassic assignments follow the zonation of Helby et al. (1987) and Partridge (2006), respectively.

Detrital zircon & tuff zircon geochronology

Sampling

Nine 2-3 kg sandstone samples were collected in Porcupine Gorge for U–Pb detrital zircon geochronology (Table 1). In ascending stratigraphic order, these include one sample from the Betts Creek beds (2 m), one from the Porcupine Gorge Formation (51 m), three from the Warang Sandstone (63 m, 66 m, and 107 m), three from the Blantyre Sandstone (116 m, 182 m, and 286 m), and one from the Gilbert River Formation (293 m).

In addition, a single volcanic tuff layer was discovered from near the top of the Betts Creek beds (42 m) in Porcupine Gorge. This important bed was sampled (~3 kg) and mapped as a local marker horizon directly below the unconformable Permian–Triassic contact. GPS locations for the tuff and all nine detrital zircon samples are given in Table 1.

Ten additional detrital zircon samples were collected from the GSQ stratigraphic drill cores for comparison to outcrop samples. Locations and depths are summarised in Table 2.

These include two samples from GSQ Hughenden 5 (Blantyre Sandstone, 53.5 m and 105 m), four samples from GSQ Hughenden 6 (Porcupine Gorge Formation, 199 m; Warang Sandstone, 169 m and 120 m; Blantyre Sandstone, 41 m), and four samples from GSQ Hughenden 7 (Hutton Sandstone, 341 m; Injune Creek Group, 230 m; Hooray Sandstone, 198 m; Gilbert River Formation, 184 m).

Table 1 – Outcrop samples collected for zircon geochronology from Porcupine Gorge National Park, their associated formations, heights in composite section of Figure 4, and their coordinates.

Sample	Formation	Height (m)	Coordinates
Wall1	Gilbert River Formation	293	20°24'31.33"S 144°26'11.81"E
GRF01	Blantyre Sandstone	286	20°24'31.36"S 144°26'12.32"E
BGR01		182	20°24'14.29"S 144°26'14.77"E
BSS-2004		116	20°22'28.19"S 144°27'15.96"E
WSS-Top	Warang Sandstone	107	20°21'5.16"S 144°27'59.98"E
WSS-0409		66	20°20'7.67"S 144°28'8.84"E
WSS-2908		63	20°20'7.26"S 144°28'8.73"E
PGF01	Porcupine Gorge Formation	51	20°20'6.91"S 144°28'8.48"E
BCTuff01	Betts Creek beds	42	20°19'58.22"S 144°28'15.45"E
BCB01		2	20°19'38.58"S 144°28'4.53"E

Zircon Separation

The samples were crushed and milled to achieve a <500 µm particle size before being passed through a Wilfley Table to remove the clays and lighter density particles. Once dried, the magnetic fraction was removed from the dense fraction using a Frantz magnetic separator, with successive runs on 0.8, 1.0 and 1.2 amperes. The non-magnetic portion was then separated using a lithium polytungstate (LST) heavy liquid (~2.85 g/cm^3). From the remaining heavy material, 100-120 zircons were randomly picked for each sample using a binocular microscope and mounted in an epoxy resin that was then polished to expose the zircons.

Table 2 – Drill core samples for zircon geochronology from the Hughenden region, their relative positions, and associated formations.

<table>
<tr><th>Sample Location</th><th>Coordinates</th><th>Depth (m)</th><th>Sample</th><th>Stratigraphic Unit</th></tr>
<tr><td rowspan="2">GSQ Hughenden 5</td><td rowspan="2">20°37'60.00"S
144°24'0.00"E</td><td>53.5</td><td>H5B5</td><td rowspan="2">Blantyre Sandstone</td></tr>
<tr><td>105</td><td>H5B21</td></tr>
<tr><td rowspan="4">GSQ Hughenden 6</td><td rowspan="4">20°20'48.77"S
144°27'11.60"E</td><td>41</td><td>H6B8</td><td>Blantyre Sandstone</td></tr>
<tr><td>120</td><td>H6B26</td><td rowspan="2">Warang Sandstone</td></tr>
<tr><td>169</td><td>H6B38</td></tr>
<tr><td>199</td><td>H6B47</td><td>Porcupine Gorge Formation</td></tr>
<tr><td rowspan="4">GSQ Hughenden 7</td><td rowspan="4">20°56'60.00"S
144°10'60.00"E</td><td>184</td><td>H7B55</td><td>Gilbert River Formation</td></tr>
<tr><td>198</td><td>H7B59</td><td>Hooray Sandstone</td></tr>
<tr><td>230</td><td>H7B66</td><td>Injune Creek Group</td></tr>
<tr><td>341</td><td>H7B101</td><td>Hutton Sandstone</td></tr>
</table>

Zircon Analysis

The epoxy puck with mounted zircons was imaged using a scanning election microscope with cathodoluminescence detector (SEM-CL) to determine the grains most suitable for analysis. The samples were subsequently analysed by laser ablation-inductively coupled plasma-mass spectrometry (LA-ICP-MS) at the Advanced Analytical Centre at James Cook University. For further instrument set up and methodology, see Tucker et al. (2013). A 32 µm beam diameter with 10 Hz analysis frequency was used for all samples. Total time for analysis was 70 s, which includes 30 s for background intensity measurement followed by 40 s of sample ablation. Up to 101 grains were analysed for each sample with standard bracketing after each 10-15 unknown analyses using two analyses of primary standard GJ1 (Jackson et al., 2004) and two analyses of in-house secondary standard Temora 2 (Black et al., 2004). Data reduction was completed using licensed software GLITTER^{TM} and plotted using the Microsoft Excel add-in programme Isoplot, version 4.15 (Ludwig, 2008).

Maximum Depositional Age Calculation

To achieve a more robust and accurate representation of the maximum depositional age of each sample, numerous statistical methodologies were applied to the resulting detrital zircon data (e.g. Dickinson and Gehrels, 2009; Coutts et al, 2019). In this study, we employ similar methodologies after Dickinson and Gehrels (2009), Tucker et al. (2013) and Bell et al. (2019), with some modifications. The common methods are (1) youngest single grain age (YSG), (2) youngest graphical peak (YPP), (3) youngest grain cluster at 1σ (YGC 1σ), (4) youngest grain cluster at 2σ (YGC 2σ), (5) youngest detrital zircon (YDZ), and (6) Zircon age extractor (TuffZirc). The youngest detrital zircon (YDZ) and the Isoplot function or zircon age extractor method (TuffZirc) methodologies were discounted by both Dickinson and Gehrels (2009) and Tucker et al. (2013) for providing either spuriously young ages due to Pb-loss issues in certain grains, or much older ages because of the reliance on large populations (n>6) to calculate a maximum depositional age, which is often quite difficult to achieve with detrital datasets. We have, therefore, also chosen to exclude these parameters from this study. Maximum depositional age estimates were calculated using only the youngest single grain (YSG), youngest population peak (YPP), youngest grain cluster at 1σ error with two or more grains (YGC 1σ [2+]), and youngest grain cluster at 2σ using three or more grains (YGC 2σ [3+]). A 15% discordance cut off was used for the U–Pb detrital zircon results for ages <1000 Ma where the $^{238}U/^{206}Pb$ ratio was used, whereas a 30% cut off was used for ages >1000 Ma where the $^{207}Pb/^{206}Pb$ ratio was used.

Lithostratigraphy

Permian Units

Two Permian units are exposed in the north-eastern Galilee Basin succession and have been studied in detail: the lower Permian Boonderoo beds (Vine et al., 1964; Jones, 2003; Jones and Fielding, 2004), and the upper Permian Betts Creek beds (Vine et al., 1964; Gray, 1977; Allen and Fielding, 2007a,b). The work from these authors are summarised in the sections below. A section of the upper ~47 m of Betts Creek beds is included in Figure 4 from work herein.

Boonderoo beds

The Boonderoo beds were studied in Porcupine Gorge, and GSQ Hughenden 3-4R and 6 cores (Gray, 1977; Allen and Fielding, 2007a). In outcrop, they overlie the basement metamorphics with an angular unconformity. The Boonderoo beds attain a maximum thickness of 257 m in GSQ Hughenden 3-4R and 220 m in GSQ Hughenden 6. Up to 172 m of the Boonderoo beds was measured in outcrop in Porcupine Gorge, although the presence of numerous faults makes it difficult to assess the true thickness. The lithology is composed of interbedded sandstone, shales, mudstones, diamictites, and lesser conglomerates that have been interpreted to be the result of deposition during a glacial period (Vine et al., 1964; Norvick, 1974; Jones, 2003; Jones and Fielding, 2004).

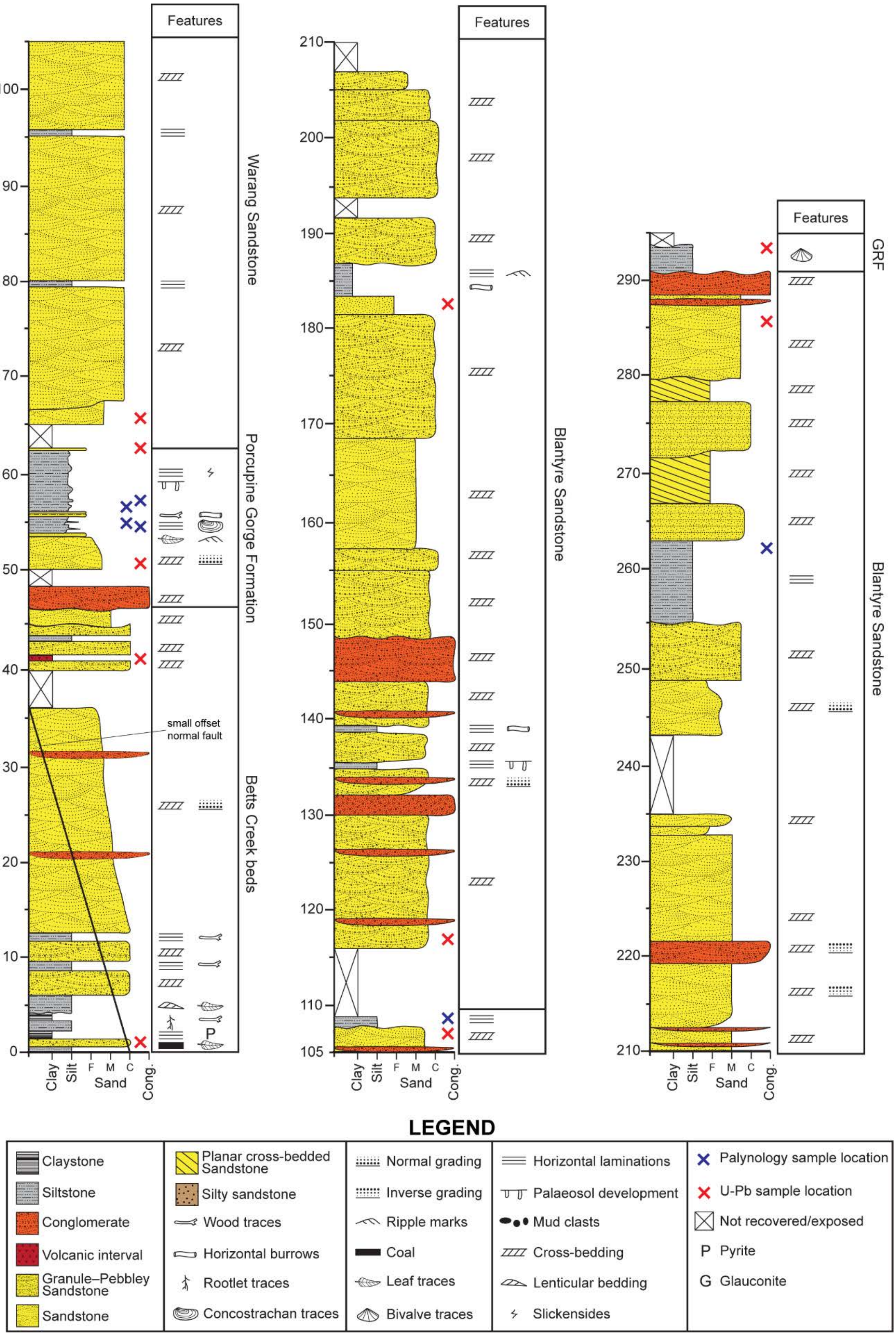

Figure 4 – Composite lithostratigraphic section through Porcupine Gorge National Park, including sedimentary structures and sample locations. Height measured in metres. GRF = Gilbert River Formation.

Betts Creek beds

The Betts Creek beds rest unconformably above the Boonderoo beds in Porcupine Gorge, and is also identified in GSQ Hughenden 6 and 7 cores (Gray, 1977; Balfe, 1979). T–he thickness of the Betts Creek beds varies from >19 m in GSQ Hughenden 7 to 110 m in GSQ Hughenden 6, and between 45–60 m in Porcupine Gorge (Balfe, 1979; Gray, 1977; Allen and Fielding, 2007a). The Betts Creek beds outcropping in Porcupine Gorge comprises pebble to cobble conglomerate, thick white, quartzose, cross-bedded sandstones interbedded with siltstones, carbonaceous shales, coal, and diamictite (Fig. 4).

Triassic Units

The Triassic succession in the north-eastern Galilee Basin consists of the Warang Sandstone and the Moolayember Formation (Vine et al., 1964; Gray, 1977; Balfe, 1979). The Moolayember Formation is only observed in the GSQ Hughenden 7 core and overlies the Warang Sandstone (Balfe, 1979). Allen and Fielding (2007a) suggested that the Lower Triassic Rewan and Clematis groups crop out in Porcupine Gorge but did not discuss in any further detail. We, like earlier authors were unable to identify evidence to support the existence of either of these units in the gorge or in nearby cores. However, in seeking to confirm Allen and Fielding's (2007a) observations, we were able to confirm that a separate lithostratigraphic unit does crop out between the Betts Creek beds and Warang Sandstone. Interestingly, it is clearly different from either the Rewan or Clematis groups based on both its sedimentology and age (see discussion). Instead, the lithological and geochronological evidence collected during this study support the establishment of a new lithostratigraphic unit that we term the Porcupine Gorge Formation.

Porcupine Gorge Formation

The 18 m thick Porcupine Gorge Formation is defined herein. It lies unconformably on the Betts Creek beds, and consists of a pebble conglomerate unit at the base, fining-upward into a fine- to medium-grained trough cross-bedded sandstone, followed by a 1 m thick carbonaceous mudstone interbedded with sandstone, and is capped by 8 m of red-orange coloured sandy siltstone with slickensides and minor mottling (Fig. 4). This formation is interpreted to represent a fluvial floodplain succession capped by a well-developed palaeosol. This differs significantly from the surrounding units which show little to no evidence of palaeosol development and are typified by coarser-grained sandstones. The Porcupine Gorge Formation was also recognised in the GSQ Hughenden 6 core (Fig. 5), but the GSQ Hughenden 5 core does not penetrate deep enough to reach the Porcupine Gorge Formation, and the base of the Triassic succession in GSQ Hughenden 7 was not studied here. A formal definition of the new Porcupine Gorge Formation is provided in Supplementary Materials 1.

Warang Sandstone

The Warang Sandstone crops out in Porcupine Gorge and the nearby White Mountains National Park, and was intercepted in the GSQ Hughenden 5, 6, and 7 cores; however, it was not re-logged in GSQ Hughenden 5 due to poor preservation, nor in GSQ Hughenden 7 due to time restraints. It reaches a maximum thickness of ~700 m in the Hughenden region (Withnall et al., 1997), but more commonly varies from ~61 m in Porcupine Gorge (Fig. 4), to 67 m in GSQ Hughenden 6 (Fig. 5), to 340 m in GSQ Hughenden 7 (Balfe, 1979). Based on our recognition of the Porcupine Gorge Formation and better understanding of the regional stratigraphy and facies distribution, the original thickness of 128 m for the Warang Sandstone in Porcupine Gorge estimated by Vine et al. (1964) was revaluated and is better estimated at about 61 m. Vine et al. (1964) had

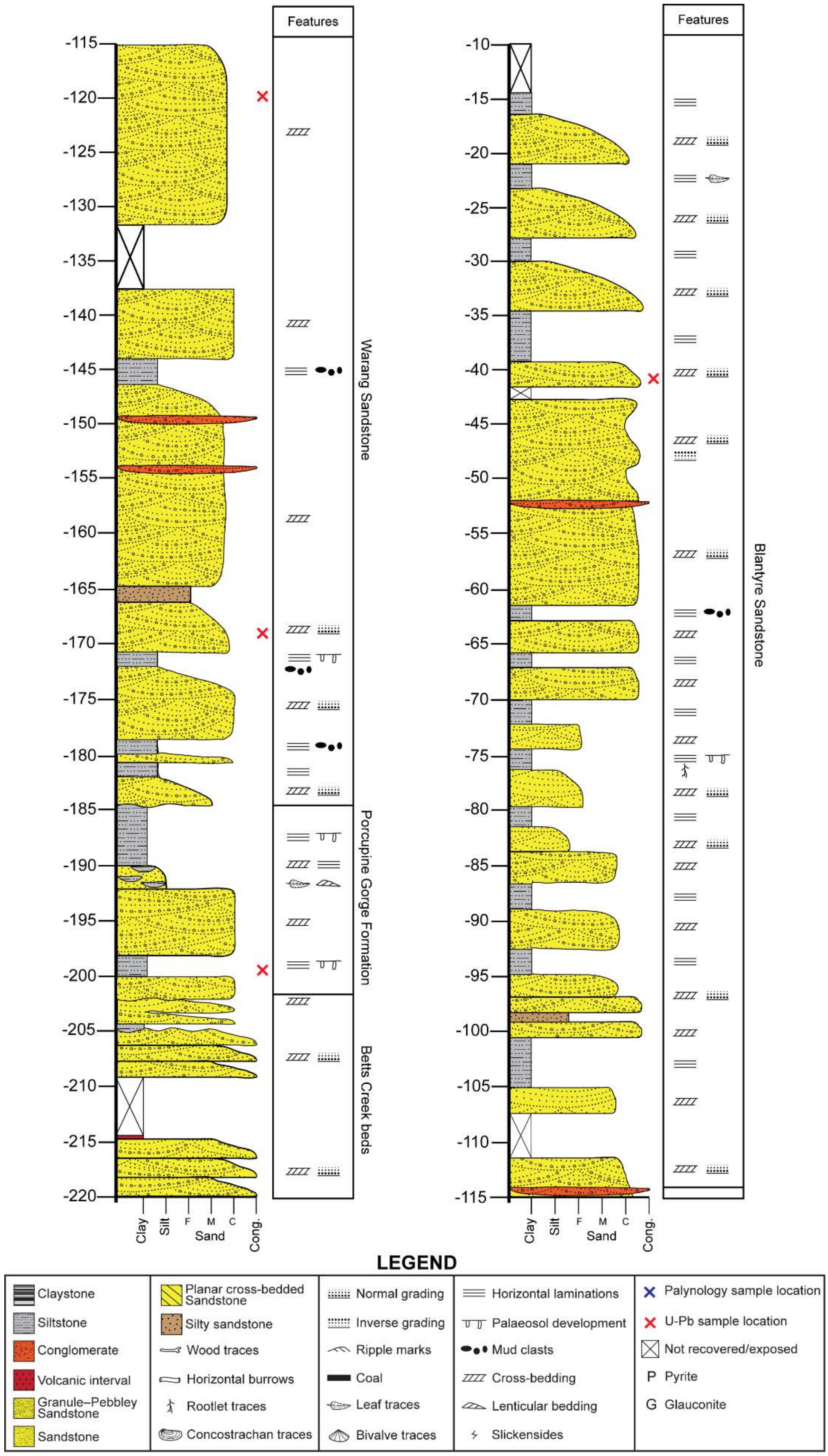

Figure 5 – Lithostratigraphic section of the GSQ Hughenden 6 drill core, including sedimentary structures and locations of detrital zircon sampling. Depths measured in metres.

included about 43 m above the top of what we consider to be the base of the Blantyre Sandstone in their original thickness estimates. This interval is characterised by heterogeneous yellowish, coarse-grained sandstones and pebble conglomerates that do not match the lithology of the underlying homogeneous, white, cross-bedded sandstone that is most typical of the Warang Sandstone (e.g. the White Mountains; Vine et al., 1964). More specifically, the lithology of the Warang Sandstone is best described as a dominantly homogeneous, white, kaolinitic, medium- to coarse-grained, trough cross-bedded sandstone with minor interbedded mudstones or siltstones (between 0.3–0.5 m thick) and rare conglomeratic lenses (<0.5 m thick). This formation is interpreted to have been deposited in a large fluvial braidplain environment.

Moolayember Formation

The Moolayember Formation was only identified in the interval between 434.5–386 m (48.5 m) in the GSQ Hughenden 7 core (Fig. 6), although it reaches a maximum thickness of ~150 m. This 48 m interval consists predominantly of siltstone and claystone, ranging between 4 m and 13 m thick, and less abundant medium- to coarse-grained cross-bedded sandstones in fining-upwards intervals between 4–9 m thick. The claystone is generally reddish-brown in appearance and the siltstone is a lighter greyish colour with occasional reddish-brown intervals. The sandstone is also a light greyish colour and has three fining-upwards sequences of medium- to fine-grained sandstone. The siltstones and cross-bedded sandstones are suggestive of a fluvial and floodplain environment. The claystone layers indicate a very low-energy depositional environment which, with the proximity to the silts and sands, is likely an oxbow lake. The overall fluvio-lacustrine setting is consistent with the interpretation of Vine and Paine (1974).

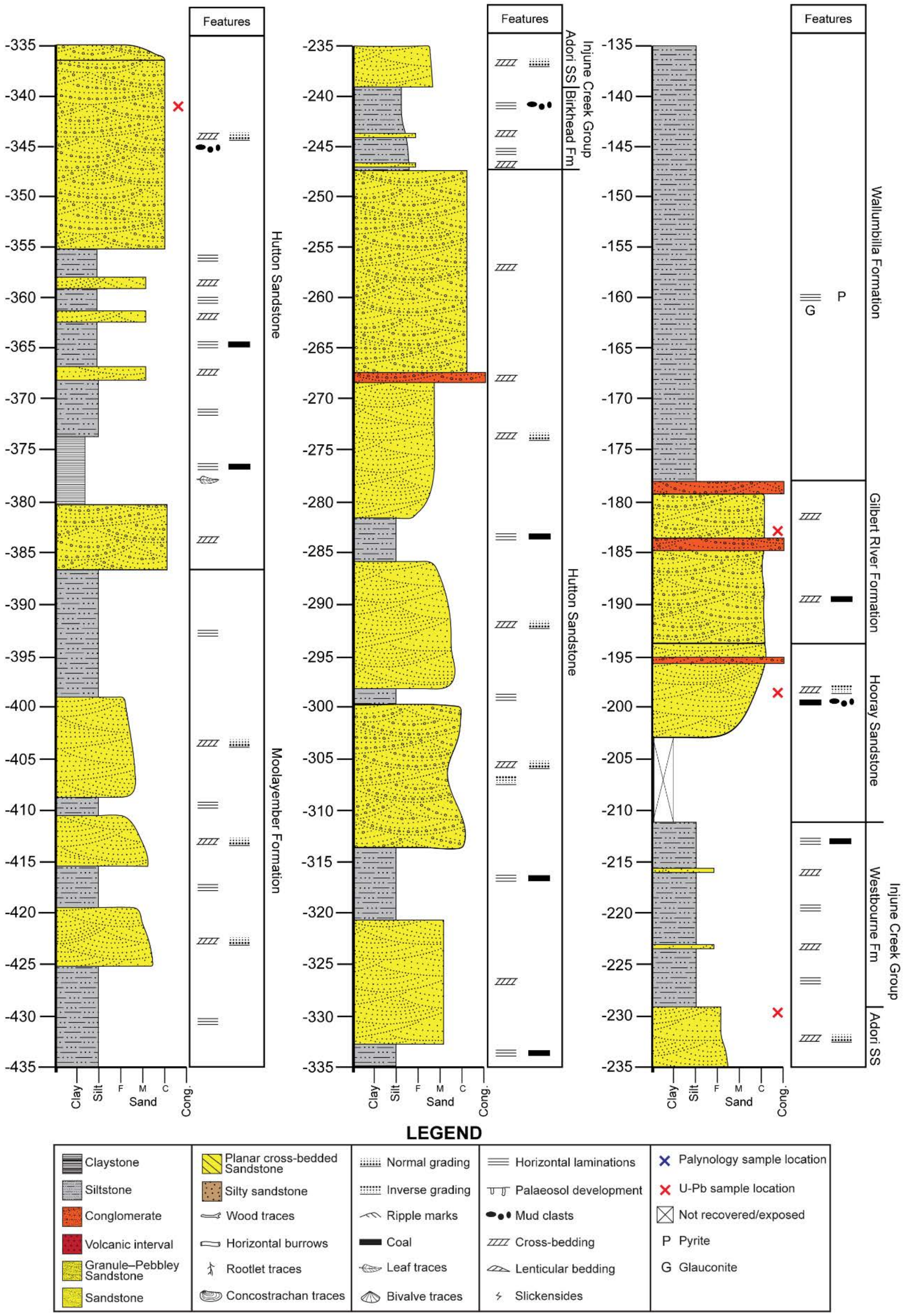

Figure 6 – Lithostratigraphic section through the GSQ Hughenden 7 drill core, including sedimentary structures and detrital zircon sampling. Depths in metres. Formation boundaries taken from Balfe (1979).

Jurassic Units

The Blantyre Sandstone is the only Jurassic unit observed to crop out on the north-eastern margin of the Eromanga Basin. Further south in the GSQ Hughenden 7 core, an expanded Jurassic succession has been recognised that includes the Hutton Sandstone and Injune Creek Group. The Blantyre Sandstone is not recognised in the GSQ Hughenden 7 core.

Blantyre Sandstone

An erosional disconformity is recognised between the Warang and Blantyre sandstones in Porcupine Gorge and marks a significant time gap between the cessation of Galilee Basin deposition and the initiation of the Eromanga Basin depositional cycle. This surface is also distinct in core from GSQ Hughenden 6. However, in GSQ Hughenden 5, this surface cannot be precisely identified due to a ~38 m interval of unrecovered open hole. Outcrop investigations in Porcupine Gorge presented in this study provide strong evidence to suggest that the thickness of the Blantyre Sandstone has been underestimated in outcrop studies. The formation varies from ~100 m in GSQ Hughenden 6 (Fig. 5), to >76 m in GSQ Hughenden 5 (Fig. 7) and ~184 m in Porcupine Gorge (Fig. 4). This outcrop thickness is expanded from the ~38 m thick estimate of Vine et al. (1964) based on our observations in the Porcupine Gorge that demonstrate a lower position for the Warang Sandstone/Blantyre Sandstone boundary, and hence a considerably thicker sequence. The previous maximum thickness of ~123 m for the Blantyre Sandstone was recorded in the north-west of the Hughenden 1:250,000 sheet area (Vine et al., 1964).

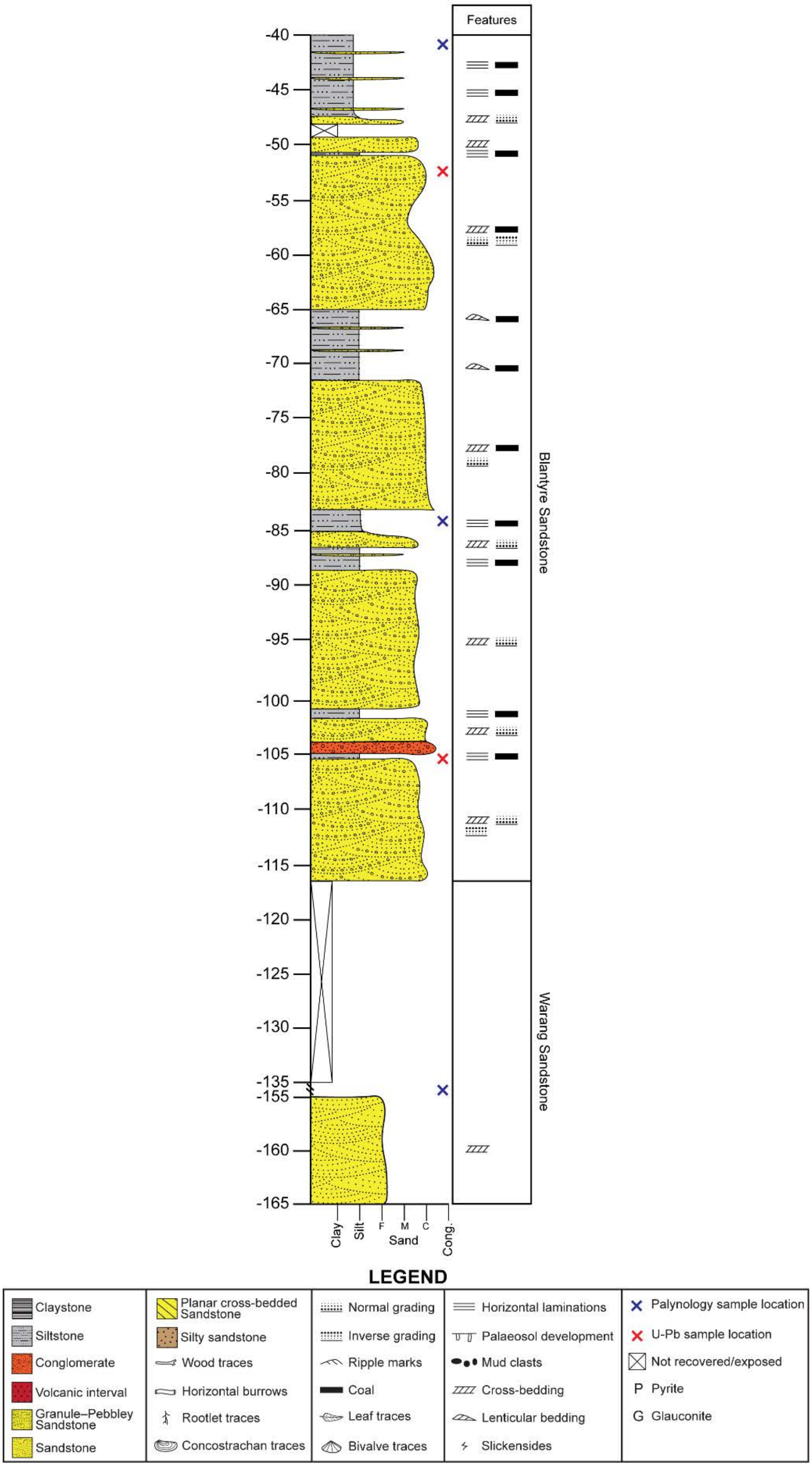

Figure 7 – Lithostratigraphic section of GSQ Hughenden 5 drill core, including sedimentary structures and the locations of detrital zircon sampling. Depths in metres. Formation boundary between Warang Sandstone and Blantyre Sandstone taken from Gray (1977).

The outcrop exposure of the Blantyre Sandstone is subdivided into distinct lower and upper units. The lower unit is ~71 m thick, and is characterised by medium- to very coarse-grained, cross-bedded sandstones alternating with abundant polymictic pebble conglomeratic intervals and less common sandy siltstones. The sandstone is weathered, revealing a typically reddish yellow to yellow or white appearance, and is more heterogeneous than the Warang Sandstone in regards to grain size, sorting and rounding. The conglomerate units range in thickness from 0.3–0.5 m, and contain abundant quartz and rhyolite clasts, with lesser chert, intraformational mudstones and recycled sandstones. These pebbles range from 1–4 cm in diameter. The siltstones are generally grey to yellow, however, rare red claystones with mottling are observed near the base, which most likely represent post-depositional weathering processes. The siltstones range in thickness from 0.2–8.0 m. The upper unit's lithology is very similar, except the conglomerates and sandstone are much more quartz-rich. An exception to this is a unique ~1.5 m thick and massive polymictic, cobble paraconglomerate near the top of the formation, which is composed of a diverse assemblage of poorly sorted and randomly orientated clasts that appear to represent a proximal debris flow deposit. Thin coal beds (<10 cm) were identified in the GSQ Hughenden 5 core, but not in GSQ Hughenden 6 or in outcrop. Overall, the presence of cross-bedded sandstones associated with developing soils and coal beds suggests a fluvial floodplain depositional setting.

Hutton Sandstone

A continuous section of the Hutton Sandstone was identified in the GSQ Hughenden 7 core at 244–386 m depth (Fig. 6). Lithologically, the Hutton Sandstone is dominated by medium- to very coarse-grained, cross-bedded fluvial channel sandstone, with up to 5 m of floodplain siltstones that are locally carbonaceous or coaliferous, and very minor pebble conglomerates.

The sandstone is typically weathered, with cut surfaces revealing a yellow to white colour, and is heterogeneous in nature, with sandstone packages ranging in thickness between 0.3–20 m. The conglomerate is polymictic, consisting of abundant quartz with lesser chert and minor intraformational mudstones, and is 0.8 m thick.

Injune Creek Group

The overlying Injune Creek Group, which in the Hughenden area consists of the Birkhead Formation, Adori Sandstone, and Westbourne Formation, has a thickness of 35.9 m in the GSQ Hughenden 7 core (Fig. 6). Previous authors working on this drill core did not differentiate the group into individual formations (Balfe, 1979), but they are identified herein based on lithological evidence. Individual thicknesses are 7.8 m, 9.5 m, and 18.6 m, respectively. By contrast, the Injune Creek Group in the Surat Basin attains a maximum thickness of 905 m (Swarbrick, 1975). The Birkhead Formation consists of siltstone interbedded with minor sandstone lenses. The Adori Sandstone consists of white, quartzose, fine-grained, cross-bedded sandstone interbedded with very thin (<5 cm) carbonaceous mudstones. The Westbourne Formation contains predominantly 3–4 m thick interbedded siltstones and mudstones with minor (0.3 m thick) sandstones. The siltstones are micaceous and carbonaceous, containing thin coal bands that are <10 cm thick. Overall, the Injune Creek Group is interpreted to have been deposited under the influence of fluvial and lacustrine settings.

Cretaceous Units

In outcrop, the Gilbert River Formation and Wallumbilla Formation are the only two units observed on the north-eastern margin of the Eromanga Basin, and in Porcupine Gorge only the Gilbert River Formation crops out. These units are not observed in the GSQ Hughenden 5 or 6 cores, but are recorded in GSQ Hughenden 7, along with the Hooray Sandstone, which lies beneath the Gilbert River Formation, which in turn is overlain by the Wallumbilla Formation (Balfe, 1979).

Hooray Sandstone

The Hooray Sandstone is limited in extent in the Hughenden region, having been identified only in the GSQ Hughenden 7 core, achieving a thickness of ~18 m (Balfe, 1979; Fig. 6). It occurs as a dominantly yellow to white coarsening-upward fine- to coarse-grained, cross-bedded quartzose sandstone. Minor conglomerate lenses (<0.4 m thick) and a very thin (<5 cm) coal layer are also present. The formation was deposited in a fluvial floodplain environment.

Gilbert River Formation

The Gilbert River Formation disconformably overlies the Blantyre Sandstone in Porcupine Gorge and in the GSQ Hughenden 7 core it overlies the Hooray Sandstone, though the nature of this boundary is unclear (Fig. 6). The Gilbert River Formation's thickness is ~3 m in the Flinders River Gorge (Campbell and Haig, 1999), ~4 m in Porcupine Gorge (Fig. 4), and ~16 m in GSQ Hughenden 7 (Fig. 6). In GSQ Hughenden 7, the Gilbert River Formation is dominated by 3–8 m thick medium to very coarse-grained cross-bedded sandstones, 0.2–0.3 m-thick pebble conglomerates and <0.1 m-thick siltstones. The sandstones and conglomerates are highly quartzose and generally whiter and cleaner than the underlying Hooray Sandstone. From this, the Gilbert River Formation is interpreted as being terrestrial in origin, probably fluvial (Balfe, 1979). However, in Porcupine Gorge, the unit is a ~4 m-thick, massive, orange to pink to white siltstone with rare bivalve and wood moulds. The depositional environment of the outcrop is considered marginal to shallow marine, which is more consistent with Campbell and Haig's (1999) description of a ~3 m thick succession of muddy transgressive sandstones mapped as the Gilbert River Formation in the Flinders River Gorge.

Wallumbilla Formation

The Wallumbilla Formation was identified only in the GSQ Hughenden 7 core where it attains a thickness of 156 m (Fig. 6). The unit reaches a maximum thickness of 350 m in the south-west Eromanga Basin (Gray et al., 2002). Lithologically, the Wallumbilla Formation is composed of marine planar and cross-laminated siltstones, typically dark grey to black, and are locally glauconitic and pyritic.

Age

Palynology

Of the six Mesozoic outcrop samples in Porcupine Gorge analysed at MGPalaeo, only two yielded sufficient palynomorphs to constrain a relative age and depositional environment (Table 3). The samples at 53 m and 54 m (Fig. 3), were taken from the base of the siltstone unit in the Porcupine Gorge Formation. Spores and pollen make up >90% of the microfossil assemblages, with <10% freshwater algal content (*Botryococcus* spp.). No saline algae were observed, suggesting a non-marine depositional environment. Both samples contained abundant *Falcisporites australis* (>70%) and frequent *Protohaploxypinus* spp. (<10%). Rare palynomorphs include *Aratrisporites* spp., *Chordasporites* spp., *Plaesiodictyon mosellanum* and *Striatopodocarpidites* spp. (Fig. 8). The overall assemblages are characteristic of the Triassic, although individual zonal designations were not possible owing to the absence of marker taxa. However, the presence of rare *Staurosaccites quadrifidus* (at 53 m only) and *Enzonalasporites vigens* (at 54 m only), suggests a ranged *C. rotundus* to *A. parvispinosus* zonal assignment, consistent with a Middle–Late Triassic (Anisian–Carnian) age (Helby et al., 1987).

Two of the three samples collected from GSQ Hughenden 5 returned sufficient material to constrain ages, each coming from the Blantyre Sandstone (at 41 m and 84 m). Both contained spinose acritarchs without dinoflagellate cysts suggesting a brackish depositional environment. Each sample contained a greater proportion of *Callialasporites dampieri* relative to *Callialasporites turbatus*, with rare *Klukisporites scaberis*, *Striatella* spp., and *Coronatispora perforata* (the latter observed at 84 m only). This indicates the *D. complex* Zone of Bajocian (Middle Jurassic) age is the oldest possible age designation (Partridge, 2006). However, McKellar (1977) noted the presence of younger marker species *Contignisporites cooksoniae* at 84.25m in GSQ Hughenden 5. The latter species can be rare and inconsistent towards the base of its range, which may explain its absence from the samples analysed herein. Data from McKellar (1977) suggests the Blantyre Sandstone samples assessed within this study should reside within the stratigraphically higher *C. cooksoniae* Zone. Ranged *C. cooksoniae – D. complex* zonal assignments (Bajocian–Callovian) are applied to the samples at 41 m and 84 m to take this uncertainty into account. Further updated zonal interpretations based on Evans (1964) and McKellar (1977, 1979) data are given in Table 4.

Table 3 – Palynological data for all core and outcrop samples analysed at MGPalaeo. Diversity column definitions: very low = 1-4 species, low = 5-9 species, moderate = 10-19 species, high = 20-29 species, very high ≥ 30 species. Key datum column definitions: common = 5-19% of the microfossil assemblage, superabundant ≥ 50% of the microfossil assemblage. Outcrop locations are in Porcupine Gorge, and all core locations are GSQ Hughenden 5.

Sample	Top Depth / Height (m)	Base Depth (m)	Sample Type	Micro-fossil Yield	Preservation	Percentage				Diversity		Age	Spore-pollen Zone (Subzone)	Environment	Key Datums
						Microplankton			Spore-pollen	Micro-plankton	Spore-pollen				
						Dinoflag	Spiny acritarchs	Other							
H5-PB1 (Blantyre Sandstone)	41.04	41.18	Core	Very high	Good	0	<1	4	96	Very low	Very high	Callovian – Bajocian	*C. cooksoniae - D. complex*, Upper	Brackish	*Striatella* spp., *R. circolumenus*, *K. scaberis*, *C. dampieri* > *C. turbatus*
H5-PB14 (Blantyre Sandstone)	84.33	84.46	Core	Very high	Good	0	<1	7	93	Very low	Very high	Callovian – Bajocian	*C. cooksoniae - D. complex*	Brackish	*Striatella* spp., *C. perforata*, *K. scaberis*, *C. dampieri* > *C. turbatus* [out of count], *A. australis* (common)
H5-PB24 (Warang Sandstone)	154.73	154.85	Core	Extremely low	Good	N/A	N/A	N/A	N/A	N/A	N/A	Indet.	Indet.	Indet.	Near Barren of microfossils
GRF1 (Blantyre Sandstone)	262	-	Outcrop	Extremely low	Moderate	N/A	N/A	N/A	N/A	N/A	N/A	Indet.	Indet.	Indet.	Near Barren of microfossils. Abundant fungal hyphae
BSS1 (Blantyre Sandstone)	108	-	Outcrop	Extremely low	Moderate	N/A	N/A	N/A	N/A	N/A	N/A	Indet.	Indet.	Indet.	Near Barren of microfossils.
LTR3 (Porcupine Gorge Formation)	58	-	Outcrop	Barren	N/A	N/A	N/A	N/A	N/A	N/A	N/A	Indet.	Indet.	Indet.	Barren of microfossils.
LTRI2 (Porcupine Gorge Formation)	57	-	Outcrop	Extremely low	Moderate	N/A	N/A	N/A	N/A	N/A	N/A	Indet.	Indet.	Indet.	Near Barren of microfossils. Abundant opaque & brown phytoclasts
LTRI1 (Porcupine Gorge Formation)	54	-	Outcrop	Moderately low	Moderate - poor	0	0	2	98	Very low	Low	Carnian – Anisian	*C. rotundus-A. parvispinosus*	Non-marine	*F. australis* (superabundant), *Protohaploxypinus* spp., *Aratrisporites* spp., *Chordasporites* spp., *Plaesiodictyon mosellanum*, *Striatopodocarpidites* spp. & *Enzonalasporites vigens*
LTR4 (Porcupine Gorge Formation)	53	-	Outcrop	High	Moderate	0	0	6	94	Very low	Moderate	Carnian – Anisian	*C. rotundus-A. parvispinosus* (*S. speciosus-S. quadrifidus* equivalent)	Non-marine	*F. australis* (superabundant), *Protohaploxypinus* spp. (common), *Staurosaccites quadrifidus*, ?*Plaesiodictyon mosellanum*, *Striatopodocarpidites* spp.

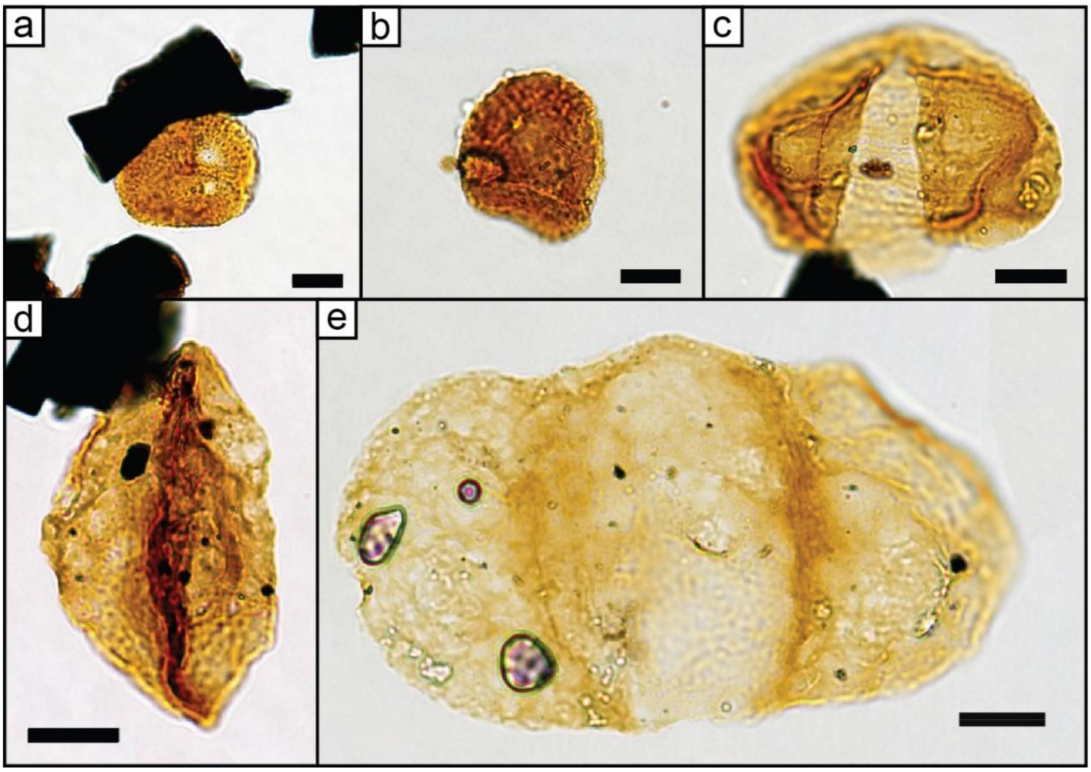

Figure 8 – Selected palynomorphs from sample LTRI1 (Porcupine Gorge Formation): (a) and (b) *Enzonalasporites vigens*, (c) *Protohaploxypinus* spp., (d) *Aratrisporites* spp., (e) *Falcisporites australis*. (Scale bar = 10 μm).

Table 4 – Revised palynology results for the Hughenden region based on the work by Evans (1964) and McKellar (1977, 1979).

Well	Formation	Depth (m)	Key Species	Ref.	Previous Age / interpretation	Revised Interpretation	Revised Age	Comments
GSQ Hughenden 2	Warang Sandstone	381.99	Abundant *S. quadrifidus* with striate and non-striate bisaccate pollen, *A. carnarvonensis* and rare *Aratrisporites* spp. Absence of *D. problematicus*.	McKellar (1977)	Middle Triassic	*S. quadrifidus* Zone (equivalent to the uppermost parts of the *A. parvispinosus* Zone in true Ipswich floras where *S. quadrifidus* markers do not occur)	Carnian – Anisian	
GSQ Hughenden 5	Blantyre Sandstone	84.25	Rare *C. cooksoniae*, *C. perforata*, dominance of Araucariaceae-type pollen, (e.g. *C. dampieri*, *C. turbatus*). Absence of *M. florida*	McKellar (1977)	Middle – Late Jurassic	*C. cooksoniae* Zone	Callovian – Bajocian	
GSQ Hughenden 5	Blantyre Sandstone	105.11	*Contignisporites* sp. indet. (one specimen), dominance of Araucariaceae-type pollen, (e.g. *C. dampieri*, *C. turbatus*). Absence of *M. florida*	McKellar (1977)		?*C. cooksoniae* Zone	?Callovian – Bajocian	
GSQ Hughenden 5	Warang Sandstone	378.45	*S. quadrifidus*, *A. carnarvonensis*, *D. problematicus*, *R. trisinus*. Dominance of *Alisporites* spp., absence of *Aratrisporites*.	McKellar (1977)	Middle Triassic	*S. quadrifidus* Zone (equivalent to the uppermost parts of the *A. parvispinosus* Zone in true Ipswich floras where *S. quadrifidus* markers do not occur)	Carnian – Anisian	
GSQ Hughenden 5	Warang Sandstone	428.16	Common to moderately common *Alisporites* spp. with *Aratrisporites* sp., *P. samoilovichii*, *I. reticulata*, *L. limatulus*, *P. reticulatus*	McKellar (1977)	Early? – Middle Triassic	*A. parvispinosus* Zone or older	Anisian or older	Low yield assemblage
GSQ Hughenden 6	Porcupine Gorge Formation	191.48	*T. playfordii*, *F. mimosae*, *A. carnarvonensis*, minor *Aratrisporites* spp., dominance of *Alisporites* spp.	McKellar (1977)	Middle Triassic	*A. parvispinosus* - *A. tenuispinosus* zones (equivalent to the *T. playfordii* Zone)	Ladinian – Olenekian	Interval reassigned PGF (lithostrat). DZ sample at 199 m = rough 239 Ma MDA
GSQ Hughenden 7	Injune Creek Group	220.7	Rare *C. cooksoniae*, *K. scaberis*, *R. circolumenus*, moderately common *C. turbatus*, *C. dampieri*. Minor *Classopollis* and absence of *M. florida*	McKellar (1979)	Middle Jurassic	*C. cooksoniae* Zone	Callovian – Bajocian	DZ sample at 230 m = rough 162 Ma MDA (Oxfordian) Conservative DZ @ ~170 Ma
GSQ Hughenden 7	Injune Creek Group	246.38	Abundant *Classopollis* with rare *C. dampieri* and *S. pseudoalveolatus*	McKellar (1979)		*D. complex* - *C. turbatus*, Upper	Bajocian – Aalenian	Reworking horizon?
GSQ Hughenden 7	Hutton Sandstone	283.82	Rare *C. turbatus* with *C. perforata* and *S. manifestus*, minor *Classopollis*	McKellar (1979)		*C. cooksoniae* - *D. complex* zones*	Callovian – Bajocian	*ranged assignment owing to the rare and inconsistent occurrence of *C. cooksoniae* towards the base of its range

GSQ Hughenden 7	Hutton Sandstone	371.54	*R. circolumenus*, cf. *D. complex*, *S. pseudoalveolatus*, *S. manifestus*, *C. turbatus*, rare *Classopollis*. Absence of *C. cooksoniae*	McKellar (1979)		*C. cooksoniae - D. complex*, Upper zones*	Callovian – Bajocian	*ranged assignment owing to the rare and inconsistent occurrence of *C. cooksoniae* towards the base of its range
GSQ Hughenden 7	Hutton Sandstone	375.88	Rare *S. pseudoalveolatus*, *S. manifestus*. Minor proportions of *C. dampieri* and *C. turbatus*. *Classopollis* predominates	McKellar (1979)		*C. turbatus*, Upper	Bajocian – Aalenian	
GSQ Hughenden 7	Hutton Sandstone	377.77	Predominant *Classopollis* and moderately common *A. fissus*, rare *C. dampieri*, *C. turbatus*	McKellar (1979)	Middle – Early Jurassic	*C. turbatus - C. torosa*, Upper	Bajocian – Pliensbachian	
GSQ Hughenden 7	Hutton Sandstone	380.38	Abundant *Classopollis* and moderately common *A. fissus*, rare *C. dampieri*, *C. turbatus* & *S. caminus*	McKellar (1979)		*C. turbatus - C. torosa*, Upper	Bajocian – Pliensbachian	
GSQ Hughenden 7	Hutton Sandstone	385.40	Predominance of *Classopollis* spp., *P. elatoides*, *A. fissus* and *C.* sp. cf. *segmentatus*	McKellar (1979)		*C. turbatus - C. torosa*	Bajocian – Hettangian	
GSQ Hughenden 7	Moolayember Formation	525.80	*C. senectus*, *R. trisinus*, *I. clara*, rare *Aratrisporites* spp. Abundant *Alisporites* spp. and rare striate bisaccates	McKellar (1979)	Middle Triassic	*A. parvispinosus* Zone	Ladinian – Anisian	
GSQ Hughenden 7	Warang Sandstone	557.84	*L. limatulus*, *R. trisinus*, abundant *Alisporites* spp., *F. mimosae*. Rare striate bisaccates	McKellar (1979)	?Middle Triassic	?*A. parvispinosus* or older	Anisian or older	
GSQ Hughenden 7	Warang Sandstone	843.09	Striate and non-striate bisaccate pollen predominate. Rare *L. pellucidus*, *P. samoilovichii*, *D. playfordii*, *T. playfordii*, and frequent *L. brevicula*. *M. tentula*	McKellar (1979)	Early Triassic	*P. samoilovichii - L. pellucidus* zones	Olenekian – Induan	
Whitecliff No. 2	Warang Sandstone	210.31 (690 ft)	Common *Alisporites* spp. with *Thymospora* sp. cf. *ipsviciensis*	Evans (1964)	Triassic	Indeterminate	Triassic (undifferentiated)	
Flinders Gorge	Blantyre Sandstone	outcrop	*C. cooksoniae*, *C. perforata*, *C. dampieri*	Evans (1964)	Jurassic, no older than Callovian	*C. cooksoniae* Zone	Callovian – Bajocian	

Detrital zircon maximum depositional age assessment

Eighteen U–Pb detrital zircon samples were collected from the Hughenden area for both sedimentary provenance and maximum depositional age analysis. Only the youngest grain-ages from five of these samples (BCB01, PGF01, H7B66, H7B59, and H7B55) are directly relevant to resolving stratigraphic issues, and these are presented here. In addition, a single volcanic ash bed (BCTuff01) was collected from the Betts Creek beds and a robust U–Pb zircon age for this sample is also presented here. The maximum depositional age results were calculated and compared using different approaches, which are presented below and summarised in Table 5.

Betts Creek beds

The detrital zircon sample collected from the base of the Betts Creek beds in Porcupine Gorge (BCB01) produced 60 concordant grains from 72 analyses. Of these 60 grains, 17 produced Permian ages, with the four youngest Guadalupian (middle Permian). The maximum depositional age methodologies produced the following results: YSG at 266.2 ± 3.1 Ma; YPP at 270 Ma; YGC 1σ (2+) at 267.7 ± 3.5 Ma from three grains; and YGC 2σ (3+) at 267.7 ± 3.5 Ma from three grains. Each of these ages are consistent with the others, indicating that they all represent viable maximum ages. Based on a comparison of each of the results, the maximum depositional age of 267.7 ± 3.5 Ma – produced by both YGC 1σ (2+) and YGC 2σ (3+) – are considered to be the most plausible interpretation for the oldest possible age for the base of the Betts Creek beds (Fig. 9c). The volcanic tuff sample (BCTuff01), herein defined as the Galah Tuff Bed (Supplementary Materials 2), was discovered ~20 m above the DZ sample and 4 m below the top of the formation and yielded a stratigraphically conformable age of 251.5 ± 2.5 Ma (Fig. 9b). Considered together, these new results suggest that the Betts Creek beds in Porcupine Gorge range from at least 267.7 Ma to 251.5 Ma, suggesting a depositional period of no more than ~15 million years. However, it is entirely possible that deposition of the Betts Creek beds began significantly later than 267.7 Ma. Interestingly, the age of the Galah Tuff suggests that the upper age bracket for the Betts Creek Beds roughly coincides with the Permo-Triassic boundary. We observed an unremarkable fluvial disconformity surface with evidence of erosional incision at the boundary, which suggests that the boundary itself is probably not present, likely because of erosional incision prior to deposition of the overlying Porcupine Gorge Formation.

Porcupine Gorge Formation

One hundred zircon grains were analysed from the sample collected above the base of the Porcupine Gorge Formation in outcrop (PGF01), of which 89 were concordant. Seventeen grains were of Triassic age, including three from the Early Triassic, 10 from the Middle Triassic, and four from the Late Triassic. The different maximum depositional age analysis metrics all yielded a consistent Late Triassic age as follows: 228.0 ± 3.0 Ma (YSG); 229 Ma (YPP); 229.4 ± 3.6 Ma (YGC 1σ (2+)), and 229.4 ± 3.6 Ma (YGC 2σ (3+)). We interpret both the YGC 1σ (2+) and YGC 2σ (3+) ages of 229.4 ± 3.6 Ma age to be the most robust interpretations for the maximum depositional age (Fig. 9a); which is consistent with the younger estimate (Carnian) from our palynology results above. Indeed, the zircon results help us to refine the Middle to Upper Triassic stratigraphic assignment suggested by the palynology to perhaps solely Upper Triassic.

A further 100 detrital zircon grains were analysed from the GSQ Hughenden 6 core sample of the Porcupine Gorge Formation (H6B47), producing 92 concordant ages. A single Late Triassic grain was also recovered from this sample (223.4 ± 10.7 Ma), which doesn't permit us to assess the maximum depositional age for this sample in the core but does lend additional support to the interpretation of a Late Triassic age for the Porcupine Gorge Formation in the north-eastern Galilee Basin. A robust 238.7 ± 6 Ma maximum depositional age from three grains was also recovered from this sample, which still permits a Middle to Late Triassic age interpretation for the Porcupine Gorge Formation, similar to the palynological results.

Injune Creek Group

The Injune Creek Group sample (H7B66) was collected from the Adori Sandstone at 230 m depth from FSQ Hughenden 7. A total of 98 zircon grains were analysed that provided 80 concordant ages, including 12 Jurassic grains: five Early Jurassic, four Middle Jurassic, and three Late Jurassic. The maximum depositional age results are: YSG at 155.0 ± 2.0 Ma; YPP at 155 Ma; YGC 1σ (2+) at 161.9 ± 3.1 Ma from two grains; and YGC 2σ (3+) at 170.3 ± 2.6 Ma from three grains. The YSG method was discounted for this sample as the 1σ age error did not overlap with the next youngest grain and may therefore be a product of contamination or Pb-loss. Youngest graphical peak (YPP) was also discounted as the peak was the same age as the YSG. The most reliable of these methods is considered to be YGC 2σ (3+), which produced a mean square weighted deviation (MSWD) of 1.01. Therefore, the more robust maximum depositional age is considered to be 170.6 ± 2.6 Ma (Fig. 10c), which is older than what we expect the true depositional age to be, based on the 162.39 Ma and 161.11 Ma tuff ages for the Birkhead Formation, which sits below the Adori Sandstone, in the southern Eromanga Basin (Wainman et al., 2015).

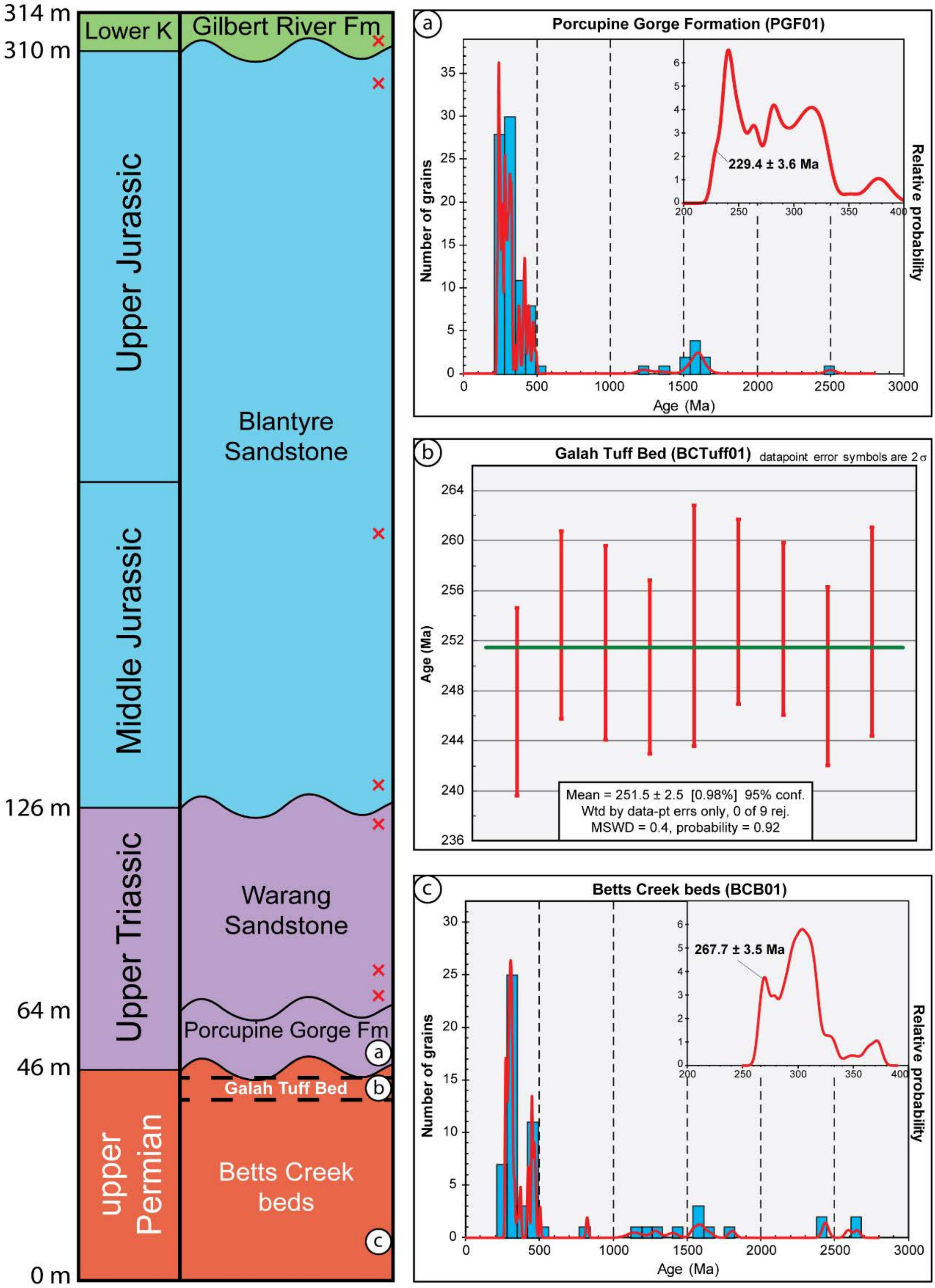

Figure 9 – Maximum depositional ages, and tuff ages, from the zircon results in Porcupine Gorge. Letters on the column correspond to the charts. (a) Porcupine Gorge Formation. (b) Weighted average of the youngest zircons from the Galah Tuff Bed. (c) Betts Creek beds. Insets show maximum depositional ages. Conf. = confidence; wtd = weighted; pt = point; errs = errors; ref. = rejected.

Hooray Sandstone

The Hooray Sandstone sample (H7B59) was collected at 198 m depth in the GSQ Hughenden 7 core, ~5 m below the upper contact. From 100 analyses, a total of 69 grains were concordant, with six Early Cretaceous grains. The maximum depositional ages range from the YSG age at 127.6 ± 2.2 Ma, to the YPP age of 130 Ma, to the YGC 1σ (2+) age of 128.8 ± 2.8 Ma and YGC 2σ (3+) age of 129.7 ± 2.3 Ma. All four methods produce dates that overlap within 1σ error, suggesting that each of these results coincides with the true depositional age. The most robust interpretation is the YGC 2σ (3+) age of 129.7 ± 2.3 Ma, which we interpret to closely approximate the depositional age of the Hooray Sandstone based on the presence of syn-depositional volcanics that can be traced to the Whitsunday Volcanic Province to the east (~135–95 Ma; Bryan et al., 2012) (Fig. 10b).

Gilbert River Formation

The Gilbert River Formation sample (H7B55) was taken from GSQ Hughenden 7 at 184 m depth, ~7 m below the upper contact. Ninety-four out of 101 grains analysed were concordant grains, producing consistent maximum depositional age estimates of 119.4 ± 1.7 Ma (YSG), 120 Ma (YPP), 120.4 ± 2.4 Ma (YGC 1σ (2+)) and 122.5 ± 4.1 Ma (YGC 2σ (3+)). The MSWD of the YGC 2σ (3+) method was calculated at 2.3, whereas the MSWD for the YGC 1σ (2+) method was determined to be 0.72 and is, therefore, considered the more reliable age (Fig. 10a). The YGC 2σ (3+) is taken to be the maximum depositional age and, given that the ages can be correlated to the Whitsunday Volcanic Province, is interpreted to be close to the true depositional age.

Table 5 – Maximum depositional ages calculated by different statistical techniques for the five samples with robust age constraints. BCB = Betts Creek beds, PGF = Porcupine Gorge Formation, ICG = Injune Creek Group, Hooray = Hooray Sandstone, GRF = Gilbert River Formation.

Unit	**Sample**	**YSG**		**YPP**	**YGC 1σ (2+)**				**YGC 2σ (3+)**				**YDZ**			**TuffZirc**			
		Age	**Err**	**Age**	**Age**	**Err**	**MSWD**	**n**	**Age**	**Err**	**MSWD**	**n**	**Age**	**Range**	**Conf**	**Age**	**Range**	**Conf.**	**n**
GRF	H7B55	119.4	1.7	120	120.4	2.4	0.72	2	122.5	4.1	2.3	4	119.5	+2.7/ -3.9	95%	125.2	+2.8/ -3.8	93.8%	6
Hooray	H7B59	127.6	2.2	130	128.8	2.8	0.25	3	129.7	2.3	0.71	4	127.0	+3.3/ -5.8	95%	130.9	+5.1/ -3.3	96.9%	6
ICG	H7B66	155.0	2.0	155	161.9	3.1	0.11	2	170.3	2.6	1.01	3	160.8	+3.8/- 4.7	95%	171.8	+3.2/ -3.9	87.8%	6
PGF	PGF01	228.0	3.0	229	229.4	3.6	0.46	3	229.4	3.6	0.45	3	226.3	+5.0/ -6.1	95%	234.3	+3.7/ -6.3	96.9%	6
BCB	BCB01	266.2	3.1	270	267.7	3.5	0.48	3	267.5	3.5	0.48	3	265.0	+4.3/ -6.9	95%	270.5	+7.6/ -4.3	96.9%	6

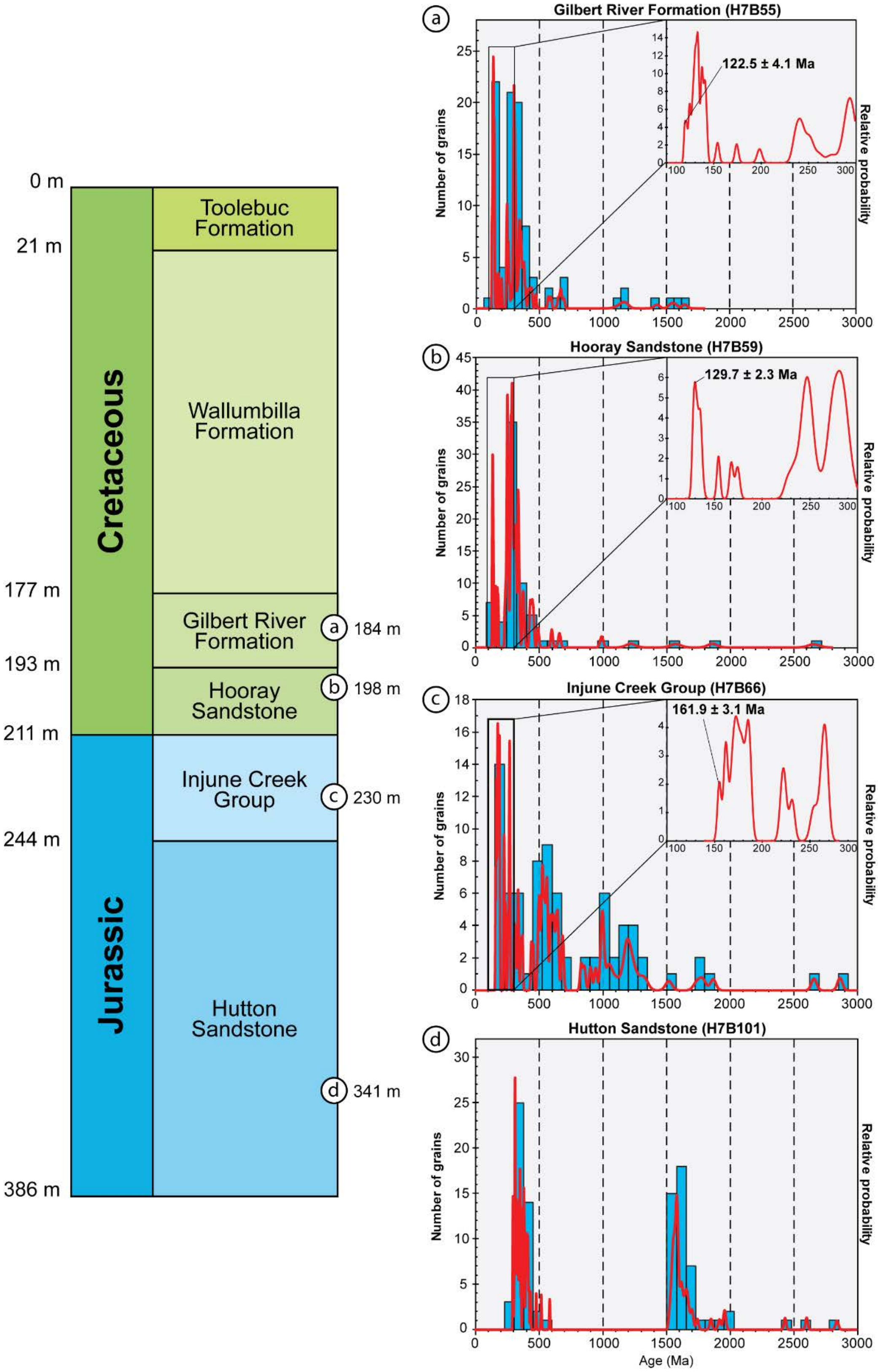

Figure 10 – Probability density plots from the detrital zircon results in GSQ Hughenden 7 drill core. Letters on the column correspond to the charts. (a) Gilbert River Formation. (b) Hooray Sandstone. (c) Injune Creek Group. (d) Hutton Sandstone. Insets show the maximum depositional age determinations.

Revisions to Existing Stratigraphic Concepts

Based on the measured sections through outcrop and re-logged core, in combination with the palynology and geochronology, several adjustments were made to the stratigraphy in the Hughenden region, which are discussed below.

Permian-Triassic transition

Widespread igneous activity persisted along the eastern Australian margin during the late Permian and resulted in numerous volcanic tuff deposits and voluminous volcanic detritus being shed into contemporaneous sedimentary basins. In the Bowen Basin at least three distinct tuff units were observed in the Blackwater Group, including the Platypus Tuff (256.01 – 258.9 Ma; Michaelsen, et al., 2001; Collins, 2009; Smith and Mantle, 2013; Metcalfe et al., 2015), the Black Alley Shale Tuff (254.34 ± 0.08 Ma – 254.10 ± 0.05 Ma; Metcalfe et al., 2015), and the Yarrabee Tuff (253.07 – 252.58 Ma; Metcalfe et al., 2015; Ayaz et al., 2016). Two further tuffs were observed in the Sydney Basin, Nobbys Tuff (255.02 – 255.26 Ma; Metcalfe et al., 2015), and the Awaba Tuff (253.14 – 253.21 Ma; Metcalfe et al., 2015). In the central Galilee Basin, Phillips et al. (2018a) identified five late Permian tuffs in the Betts Creek Group succession, including Black Alley Shale Tuff equivalents at 254.41 ± 0.07 Ma, 254.32 ± 0.10 Ma, and 254.09 ± 0.06 Ma, as well as a Yarrabee Tuff equivalent at 252.81 ± 0.07 Ma, and a Nobbys Tuff equivalent at 255.13 ± 0.09 Ma. The LA-ICP-MS date presented here for the Galah Tuff Bed at 251.5 ± 2.5 Ma, plus the abundance of syn-depositional detrital zircons in the lower part of the Betts Creek beds, provides further evidence for this widespread late Permian igneous activity. Furthermore, the Galah Tuff Bed presented here is correlative with the age of the Gibraltar Rhyolite from the Texas Orocline of southern Queensland and northern New South Wales (251.6 ± 3.5 Ma; Campbell et al., 2015). This unit was highlighted by

Phillips et al. (2018a) as a possible source for the Yarrabee Tuff in the Galilee and Bowen basins and, therefore, we also consider this a possible source for the Galah Tuff Bed in Porcupine Gorge. In addition, we consider the Yarrabee Tuff to be correlative with the Galah Tuff Bed. The formalisation of the Galah Tuff Bed in the Hughenden area necessitates the upgrade of the Betts Creek beds to the Betts Creek Group. This upgrade makes it consistent with the nomenclature of Phillips et al., (2017a) for the northern and eastern Galilee Basin.

The Late Triassic maximum depositional age calculated for the Porcupine Gorge Formation in outcrop (~229.4 ± 3.6 Ma; YGC 2σ), presents a significantly refined age assessment for understanding the temporal relationships of the Permian–Triassic transition in the north-eastern Galilee Basin. Elsewhere in the Galilee and Bowen basins, widespread sedimentary deposition occurred during the Early and Middle Triassic with the Rewan and Clematis groups (e.g. Vine, 1973; Allen and Fielding, 2007a, 2007b); however, the surprisingly young zircon population recovered from the base of the Porcupine Gorge Formation, ~4 m above the contact with the top of the Betts Creek beds (Group) in Porcupine Gorge, demonstrates the possibility of an extended depositional hiatus of ~16–29 million years between Permian and Triassic deposition in the north-eastern Galilee Basin. This may represent a period of localised basin inversion during the Early and Middle Triassic and is evidenced by the erosional surface that marks the boundary between the two formations.

Age and correlation of Triassic strata

Both the Middle–Late Triassic age assessment from the palynology and the Late Triassic detrital zircons present in the Porcupine Gorge Formation from outcrop provide support for the lithostratigraphic interpretations that the this unit represents a valid, new stratigraphic unit in the region that is too young to be correlated with either the Rewan Group (latest Lopingian–Early Triassic; Laurie et al., 2016) or the Clematis Group (Early–Middle Triassic;

Green et al., 1997). Moreover, the core and outcrop investigations highlight that neither the Rewan nor the Clematis Group was deposited in the north-eastern Galilee Basin, which is consistent with most previous interpretations (e.g. Gray, 1977; Balfe, 1979; Hawkins and Green, 1993). The detrital zircon results for this sample do, however, reveal a significant Middle Triassic zircon population that is consistent with continuous igneous activity through the Triassic along the eastern Australian margin.

The Great Artesian Basin system formed following the final compressive phase of the Hunter-Bowen Orogeny, which deformed and inverted many of the Permian–Triassic terranes in eastern Australia between ~230–235 Ma (Li et al., 2015; Hoy and Rosenbaum, 2017). Erosion of these terranes, which include the New England Orogen and the Bowen Basins, provided a peneplain surface over which the Great Artesian Basin was deposited. This deformation is absent in the in the north-eastern Galilee Basin (Van Heeswijck, 2010), and the Galilee and Eromanga basin boundary is marked by a disconformity. The detrital zircon maximum depositional age of the Porcupine Gorge Formation at ~229.4 Ma is coincident with, or younger than, the final Hunter-Bowen compression and, based on the above criterion, suggests both this unit and the overlying Warang Sandstone could be included in the Eromanga Basin stratigraphy.

Despite no useful maximum depositional age constraints confirmed from detrital zircons or palynology collected herein, the Late Triassic age of the Porcupine Gorge Formation unambiguously indicates that the overlying Warang Sandstone and Moolayember Formation must also be Late Triassic. However, the majority of previous palynological results for the Warang Sandstone returned Early to Middle Triassic palynological ages (Evans, 1964; McKellar, 1977, 1979; de Jersey and McKellar, 1980), with only two samples taken closer to the basin margin (GSQ Hughenden 1-2R and GSQ Hughenden 5) indicating any Late Triassic component (Carnian–Anisian; Table 5). A plausible explanation for these conflicting ages is that the Triassic spore-pollen zonations, similar to the Permian zones after Laurie et al. (2016), are poorly constrained and are in need of readjustment, utilising new radioisotopic techniques. However, it is also plausible that these results suggest the Triassic succession in the north-eastern Galilee Basin may be diachronous with deposits closer to the basin margins recording younger ages than those closer to the depocentre in the south. Indeed, with no firm chronostratigraphic control, the possible diachroneity also calls into question all correlations of Triassic strata across the Galilee Basin, and whether to include the Porcupine Gorge Formation and Warang Sandstone from Porcupine Gorge into the Eromanga Basin stratigraphic succession. This work highlights the need for further basinwide isotopic age control and resampling of the palynology to provide greater constraint for the succession.

Apatite fission-track (AFT) dating was applied to the Moolayember Formation in the Bowen Basin (Raza et al., 2009), providing an age range between 240–231 Ma (Middle–Late Triassic). The lower end of this range is roughly coincident with the maximum depositional age of the Porcupine Gorge Formation at 229.4 ± 3.6 Ma (YGC 2σ) but, given the supposed stratigraphic continuity between the Galilee and Bowen basins and the respective stratigraphic positions of each formation, this temporal correlation is problematic. This result further highlights the need for additional basinwide chronostratigraphic age control and resampling of the palynology to provide greater temporal constraints on correlations between the Bowen and Galilee basins.

Age and correlation of Jurassic strata

Detrital zircon maximum depositional ages were of limited utility in refining the ages of the Hutton or Blantyre sandstones in the north-eastern Eromanga Basin due to a lack of contemporaneous Jurassic grains. However, the new palynological samples and revised results of McKellar (1977) for the Blantyre Sandstone in GSQ Hughenden 5 provide further constraints for the age of this unit, with Middle Jurassic assemblages present throughout, consistent with a Callovian–Bajocian age (Tables 3 & 4). These results appear to be broadly consistent with those from the upper part of the Hutton Sandstone in GSQ Hughenden 7 (371.54 m, 283.82 m; McKellar, 1979), as well as previously documented ages and zones for this unit from the Surat Basin (e.g. Price 1997; Gallagher et al., 2008; Todd et al., 2019). Indeed lithologically, the Hutton Sandstone and the lower Blantyre Sandstone are comparable (Fig. 11), sharing a similar sandstone lithofacies and alluvial architecture indicative of fluvial depositional environments (Chapter 3). In palynology, spore-pollen zones are defined by the first occurrence of certain species. Unfortunately for the Middle and Late Jurassic zones, these species are typically rare and are inconsistent in their occurrence near the base of their ranges. This means that analysis of additional samples is required to more accurately constrain these units and refine how they correlate to each other.

In the north-eastern Eromanga Basin, the Injune Creek Group can be subdivided, oldest to youngest, into the Birkhead Formation, Adori Sandstone and Westbourne Formation (Balfe, 1979). The conservative YGC (2σ) age at 170.3 ± 2.6 Ma (Bajocian–Aalenian) determined for the Adori Sandstone for the GSQ Hughenden 7 core herein (H7B66) is consistent with both of the updated palynology samples for this interval (Table 4). However, the age of the Adori Sandstone has been given elsewhere in the Eromanga Basin as upper Oxfordian to Tithonian (Cook et al., 2013) or strictly Tithonian (Gallagher et al., 2008). The less conservative YGC (1σ) age of 161.9 ± 3.1 Ma (early Oxfordian) for the Adori Sandstone, though roughly coincident with the Oxfordian interpretation and the results for the Birkhead Formation in the southern Eromanga Basin (162.39 Ma and 161.11 Ma; Wainman et al., 2018a), is inconsistent with the updated palynology (Callovian–Bajocian) based on McKellar (1979) from the

GSQ Hughenden 7 drill-hole. This discrepancy suggests local age differences in the separate localities, as well as the need for more work on both the palynology and the U–Pb geochronology of the Injune Creek Group to improve stratigraphic correlation within the group across the Eromanga Basin.

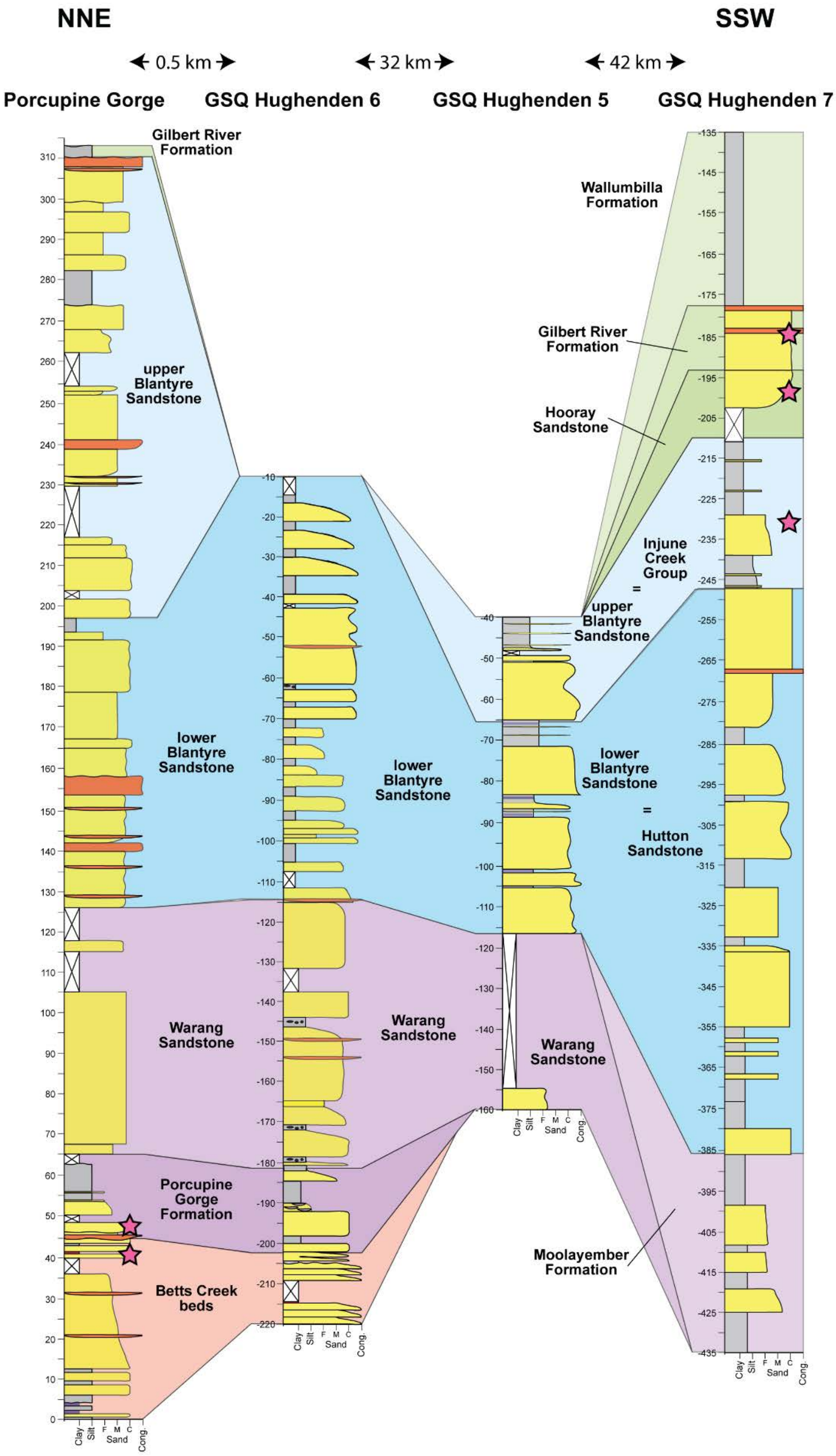

Figure 11 – Lithostratigraphic correlation between outcrop in Porcupine Gorge and the GSQ Hughenden 5, 6, and 7 stratigraphic drill cores based on lithology, palynology and U–Pb detrital zircon geochronology.

The youngest single grain (YSG) age for sample GRF01 (upper Blantyre Sandstone) in Porcupine Gorge is 162.7 ± 2.3 Ma, roughly coincident with the less conservative 161.9 ± 3.1 Ma maximum age from the Injune Creek Group (H7B66), which suggests that these two units are temporally correlative (Fig. 11). Indeed, the whole detrital zircon spectra for both samples shows remarkable similarities in source materials, further suggesting their correlation. However, a single grain is not typically considered a reliable indication for a maximum depositional age constraint. Furthermore, the key index taxon typically found in the Injune Creek Group was not found in any of the Blantyre Sandstone samples, highlighting the need for further study on the Jurassic interval in northern Queensland.

Until recently, evidence for continued volcanic arc activity along the eastern Australian margin in the Jurassic was largely non-existent. The subduction zone on the eastern margin was present since at least the middle Cambrian (e.g. Glen, 2005), but much of the Mesozoic volcanolithic sediments deposited in the interior basins has not been preserved or have been deeply buried. However, Tucker et al. (2016) identified a relatively continuous assemblage of Jurassic detrital zircons from the Upper Cretaceous Winton Formation, and more recently, a series of Middle to Late Jurassic tuffs was reported in the Injune Creek Group by Wainman et al. (2018a, b) across the Eromanga, Surat and Clarence-Moreton basins in south-eastern Queensland. The detrital zircon data for the Injune Creek Group reported here support the hypothesis that volcanics were draining westward off the arc and into the Great Artesian Basin. The paucity of primary tuff horizons in Jurassic strata in the northern Eromanga Basin and Carpentaria Basin, and lack of Jurassic zircons in these same rocks, may be a result of fluvial reworking of ash beds or the more distal geographical location of northern Queensland in comparison to the active portion of the arc. Further work is required to establish the true nature of this magmatism, and indeed where the volcanic centres were located during this interval.

Age and correlation of Cretaceous strata

The youngest population of detrital zircons from the Hooray Sandstone in GSQ Hughenden 7 yielded a maximum depositional age of 129.7 ± 2.3 Ma (YGC 2σ), which significantly refines the previous latest Jurassic to Early Cretaceous depositional age estimates based on palynology (e.g. Burger & Senior, 1979; Cook et al., 2013). This also indicates that the contact between the Injune Creek Group and the Hooray Sandstone is likely unconformable, representing a temporal gap of >20 million years.

Detrital zircon analysis of the overlying Gilbert River Formation in GSQ Hughenden 7 yielded a maximum depositional age of 122.5 ± 4 Ma, suggesting an Aptian or younger age for the formation in the north-eastern Eromanga Basin. Preliminary detrital zircon studies of the Gilbert River Formation in the southern Carpentaria Basin (Drochmann, 2015) revealed a single 120.1 ± 1.8 Ma grain age from the GSQ Dobbyn 1 drill core, which is roughly consistent with the maximum depositional age determined herein for the Eromanga Basin, indicating that the two units are likely correlative. Palynological assessments placed the GSQ Dobbyn 1 core sample in the Barremian (Early Cretaceous; ~129.4–125 Ma; Drochmann, 2015), which is further evidence for the likely temporal equivalence of these two samples.

While the Gilbert River Formation nomenclature is common to the northern Eromanga Basin, the Carpentaria Basin and the Laura Basin, the unit varies significantly between each observed outcrop and each core interval. The stratotype description of Smart et al. (1971) in the Carpentaria Basin divided the formation into a lower terrestrial and an upper lagoonal to marine unit, each with separate lithologies, but neither unit is always identified. The lower terrestrial unit is not observed in the Laura Basin (de Keyser and Lucas, 1968; Hawkins and Williams, 1990) or in Porcupine Gorge and Flinders River Gorge (Campbell and Haig, 1999), while the upper lagoonal to marine unit is not identified in GSQ Hughenden 7 in the Eromanga

Basin. In addition, age estimate of the Gilbert River Formation can also be highly varied (E. Foley, pers. comm). These variations in lithology and depositional environments outline the difficulties in correlating the Gilbert River Formation both within and across basin boundaries. Further work is required to clarify the lithology, age, and depositional environment of the Gilbert River Formation to better correlate it across the Great Artesian Basin.

Conclusions

This study provides critical stratigraphic and temporal refinement of a number of key formations in the Hughenden area that have wide-reaching implications for our understanding of Mesozoic geology in Queensland. A new volcanic tuff (Galah Tuff Bed) discovered at the top of the Betts Creek Group yields an age of 251.5 ± 2.5 Ma (Fig. 12), which is close in age to the Yarrabee Tuff marker horizon in the Bowen Basin, providing strong evidence for extensive volcanism in the upper Permian throughout eastern Australia, including into northern Queensland. Further, this age, together with the maximum age of the overlying – and newly defined – Porcupine Gorge Formation (229.4 ± 3.6 Ma; Fig. 12) from detrital zircon studies, reveals a significant hiatus or unconformity between the upper Permian and Upper Triassic strata in the north-eastern margin of the Galilee Basin. This study also confirms the generally held interpretation that the Rewan and Clematis groups do not outcrop in the north-eastern Galilee Basin, and also suggests that the Triassic succession may be diachronous within the Galilee Basin, calling into question current correlations of Triassic units across Queensland.

The Jurassic Blantyre Sandstone is subdivided into two units, with the lower unit correlating to the Hutton Sandstone, and the upper unit correlating to the Injune Creek Group of GSQ Hughenden 7. The discovery of Jurassic zircon populations in this study also provides further support to a growing body of evidence for widespread igneous activity at this time, possibly related to a volcanic arc off Australia's eastern continental margin. The young, maximum depositional age zircon populations in the Hooray Sandstone and Gilbert River Formation are Early Cretaceous (Fig. 12), demonstrating neither unit can be Upper Jurassic, as previously assumed. The maximum depositional ages identified for a number of the stratigraphic units investigated during this study suggest generally younger ages than are suggested by ages ascribed utilising the Mesozoic spore-pollen zone framework in eastern Australia. This indicates that more systematic and higher-precision analytical approaches to U–Pb detrital zircon analysis, such as chemical abrasion-isotope-dilution-thermal ionisation mass spectrometry (CA-ID-TIMS), could be successfully employed in the basin for improved temporal calibration of the spore-pollen zones.

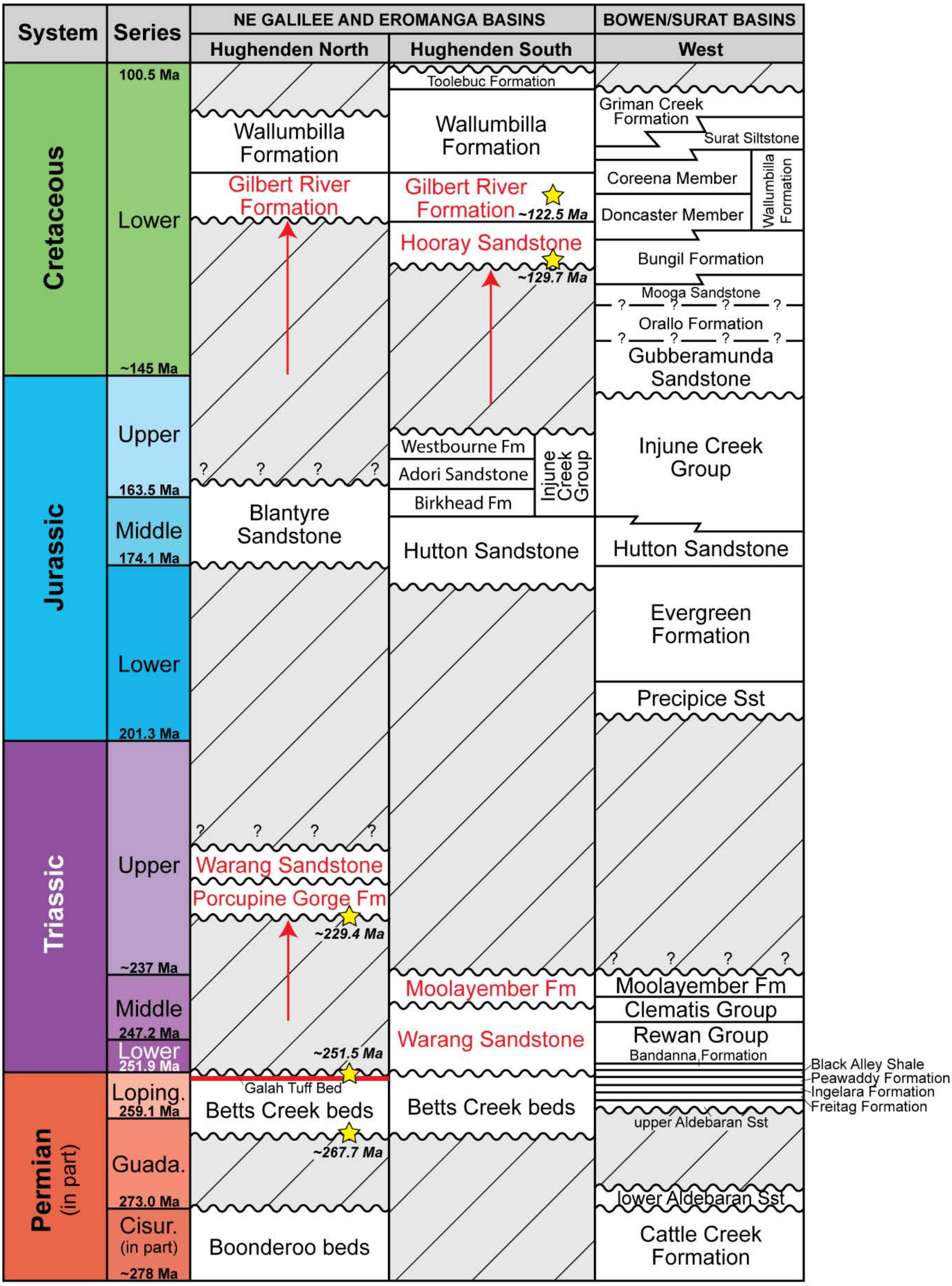

Figure 12 – New comparison of stratigraphies from the north-eastern Galilee and Eromanga basins and the Bowen and Surat basins with new ages and new units included. Formation names in red indicate updated ages. Yellow stars indicate samples where robust maximum depositional ages were calculated.

Supplementary Materials 1: Definition of the Porcupine Gorge Formation

Derivation of Name

A previously unrecognised stratigraphic unit discovered in this study is here defined as the Porcupine Gorge Formation. The name for the unit is derived from the Porcupine Gorge in which the unit was discovered, and in which the type section is described.

Type and Reference Sections

The type locality is defined as an 18.4 m thick interval of sedimentary rock, accessible on the eastern cliff-face ~1.8 km north of the base of the Pyramid Trail in Porcupine Gorge National Park, ~63 km north-east of the town of Hughenden in northern Queensland, Australia (WGS84 20°20'6.91"S 144°28'8.48"E). An additional 18.2 m thick interval of the Porcupine Gorge Formation was observed in the GSQ Hughenden 6 stratigraphic drill core (184.6–202.8 m), which is housed in the Department of Minerals and Energy Exploration Data Centre in Zillmere, Brisbane, Queensland.

Lithology

The 18.4 m thick formation consists of four main lithologies. The basal 2.9 m (15.8% of the formation) contains a yellow to red, poorly to moderately sorted, polymictic pebble conglomerate, with sub-rounded to rounded clasts. Clast types are dominated by quartz and rhyolite with lesser intraformational mudstones and cherts. Above the conglomerate is a 2.2 m covered interval where lithology is indeterminable. This is followed by a 3.8 m thick very pale yellow quartzose, cross-bedded sandstone (20.7% of the formation). The sandstone fines upwards from medium- to fine-grained, is typically subangular to subrounded and moderately to well sorted. Overlying this unit is 2.2 m of localised bluish grey carbonaceous siltstone interbedded with minor claystones and fine-grained sandstone (12.0%). The siltstone is typically thinly laminated but may also contain small ripple cross-stratification. Carbonaceous leaf and wood fragments are common within the laminations, with less abundant conchostracan and *Planolites* trace fossils occurring. Capping the formation is a distinctive, 6.7 m thick, mottled palaeosol succession, with minor interbedded fine-grained sandstones and numerous slickensides (40%). A very thin sandstone (<10 cm) is interbedded with the palaeosol at the very top.

Distribution

The Porcupine Gorge Formation replaces 18 m of strata that had been previously assigned to the overlying Warang Sandstone. However, the distinct lithology of this unit, coupled with the erosional unconformity above and the distinct difference in mean palaeocurrent vectors (south-west for Porcupine Gorge Formation, south for Warang Sandstone), is sufficient to determine it as a separate lithostratigraphic unit. The Porcupine Gorge Formation is confined in its extent to Porcupine Gorge and to the GSQ Hughenden 6 stratigraphic drill core, located ~1.2 km west of the gorge. The Warang Sandstone is poorly preserved in GSQ Hughenden 5 and so it is not possible to ascertain whether the Porcupine Gorge Formation extends to this bore location.

Stratigraphic Relationships

In the type section in Porcupine Gorge, the Porcupine Gorge Formation overlies the medium- to very coarse-grained sandstones of the Betts Creek beds at a disconformable surface. The white, medium-grained, cross-bedded sandstone Warang Sandstone then overlies the palaeosol of the Porcupine Gorge Formation at a paraconformity. These same relationships are observed in the GSQ Hughenden 6 drill core.

Age

Using U–Pb detrital zircon geochronology through LA-ICP-MS, a maximum depositional age of the Porcupine Gorge Formation was determined to be 229.4 ± 3.6 Ma. Palynology conducted on the mudstone unit returned an Anisian to Carnian age for the unit; however, the detrital zircon age is considered more robust and is preferred over the palynological age. Further, based on this age, this unit cannot be considered to belong to either the Rewan or Clematis group, which overlie the Betts Creek beds in more southerly exposures of the Galilee Basin.

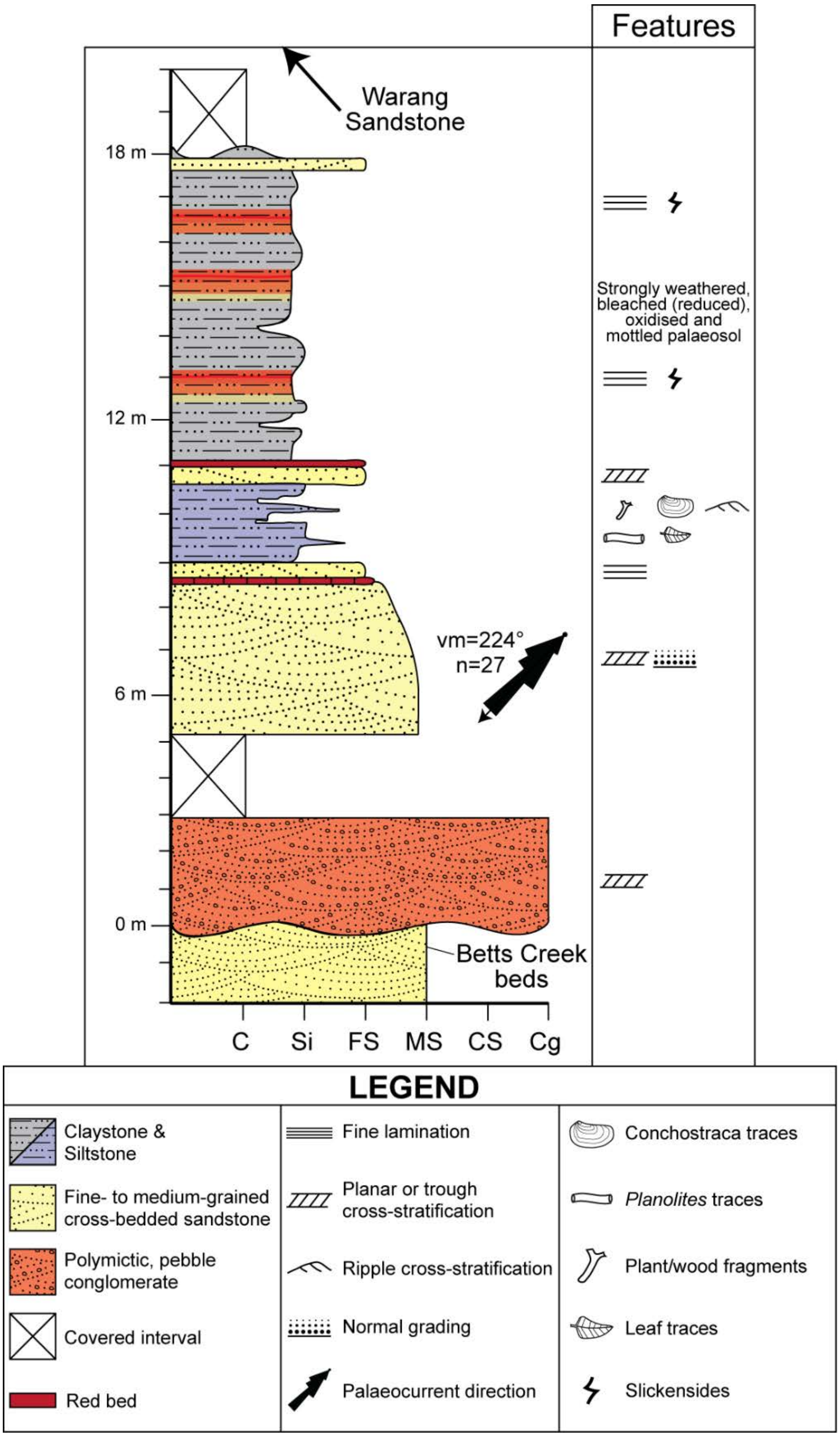

Supplementary Figure 1 – Type section of the Porcupine Gorge Formation in Porcupine Gorge, including sedimentary structures and palaeocurrent markers.

Supplementary Materials 2: Definition of the Galah Tuff Bed

Derivation of Name

This distinctive tuff horizon in the Betts Creek beds is named for the Galah Creek (also known as the Porcupine Creek) which flows through the Porcupine Gorge where the type section is located.

Type and Reference Sections

The type section is recognised within a 10 m thick succession of medium- to very coarse-grained quartzose sandstone in the uppermost exposures of the Betts Creek beds, ~2 km NNE of the base of the Pyramid Trail in Porcupine Gorge National Park, ~63 km north-east of the town of Hughenden, North Queensland, Australia (WGS84 20°19'58.22"S 144°28'15.45"E).

Lithology

The Galah Tuff Bed is white, porphyritic, and typically internally massive. It contains rounded phenocrysts of coarse-grained quartz clasts and clay clasts that range in size from 0.2 mm to 3.0 mm but are generally <1 mm. These phenocrysts constitute ~5–10% of the tuff and are evenly distributed within a very fine-grained matrix. The clay clasts are likely the result of feldspar weathering and give a soapy feel to the rocks. Based on this grain size and distribution, the Galah Tuff Bed is classified as a volcanic ash-fall tuff.

Distribution

The Galah Tuff Bed is confined to outcrop exposures in Porcupine Gorge National Park in North Queensland, observable in lateral extent for ~80 m in the cliff face. While a similar stratigraphic interval was intercepted in drill core GSQ Hughenden 6, no tuff horizon was recorded. However, it is notable that ~3 m of core was not recovered from this bore traversing the boundary between the Betts Creek beds and Porcupine Gorge Formation, and this may have contained the Galah Tuff Bed.

Thickness

In the type section, the Galah Tuff Bed attains a maximum thickness of 1.5 m but averages 0.5 m.

Age

LA-ICP-MS zircon geochronology provided an age of 251.5 ± 2.5 Ma (latest Permian-earliest Triassic) for the Galah Tuff Bed. This confirms the late Permian assignation of the Betts Creek beds and provides a robust stratigraphic marker for the overlying Triassic strata.

Stratigraphic Relationships

The Galah Tuff Bed is limited in extent in Porcupine Gorge, where it is situated ~5 m below the top of the Betts Creek beds. Based on the age assignment of 251.5 ± 2.5 Ma, the Galah Tuff is roughly equivalent in age to the Gibraltar Ignimbrite (251.6 ± 3.2 Ma; Campbell et al., 2015), as well as the Yarrabee Tuff (252.54 ± 0.04 Ma – 253.07 ± 0.22 Ma; Phillips et al., 2018).

Chapter 3:
Facies architecture of a long-lived Triassic to Jurassic fluvial system, north-eastern Galilee and Eromanga basins, northern Queensland

Abstract

The Triassic and Jurassic sandstones of the Great Artesian Basin in eastern Australia are highly important reservoirs for groundwater, yet little is known about their facies architecture or reservoir characteristics. Here we present a detailed lithofacies and alluvial architectural analysis of the Upper Triassic Porcupine Gorge Formation and Warang Sandstone, and the Middle to Upper Jurassic Blantyre Sandstone. A suite of 12 lithofacies and six distinct architectural elements, including channel elements, sandy bedforms, gravel bedforms, downstream accretion, lateral accretion, and floodplain fines, were documented in this study. Each of these architectural elements is interpreted to represent a particular depositional environment within a long-lived fluvial-dominated depocentre. Indeed, the similarity in facies associations between the successive Triassic and Jurassic depositional units reveals the existence of a low-accommodation, dominantly braided channel-dominated fluvial system that occupied the basin(s) throughout much of the Mesozoic. A notable change in fluvial architecture in the succession is a ~30 m interval where individual sandstone channel bodies are bounded by fine-grained facies in the lower Blantyre Sandstone. This suggests a significant increase of accommodation space that is possibly linked to a marine incursion that has been recently documented in the Surat and Carpentaria basins. Following this depositional interval, a return to a low-accommodation, braided channel-dominated fluvial system is recorded by the upper Blantyre Sandstone. The presence of aeolian-reworked braid bar tops suggests the influence of strong winds, possibly a result of the proximity to the regressive marine shorelines. A distinctive change in facies and provenance is recorded in the uppermost part of the Blantyre Sandstone where a matrix-supported, polymictic cobble conglomerate suggests significant basin reorganisation, with associated uplift and changes to palaeodrainage networks. Each of

these formations was deposited in a bed-load-dominated system that is laterally extensive and vertically and laterally homogeneous, which gives them potential as aquifers.

Introduction

The Great Artesian Basin (GAB) is the world's largest artesian aquifer system (Ransley et al., 2015), covering an area of over 1.7 million km^2 across central and eastern Australia. The estimated 64.9 million gigalitres of contained groundwater is largely held within the highly permeable Jurassic and Cretaceous sandsheets of the Carpentaria, Eromanga and Surat basins (± Clarence-Moreton Basin) (Habermehl, 1980, 1983; Ransley et al., 2015) but is also stored within Triassic sandstones of the underlying Bowen and Galilee basins (Moya et al., 2014, 2015). The depositional environments of these sandsheets have traditionally been interpreted as laterally extensive fluvial systems in internally draining basins at relatively high latitudes (>60°S; Veevers, 2006; Scotese, 2016). Recent studies in the Surat and Carpentaria basins (Bianchi et al., 2018; Wainman and McCabe, 2019; E. Foley, pers. comm.) indicates sporadic epicontinental marine flooding of the GAB during the Jurassic as shown by marginal marine to shallow marine microfaunal and microfloral assemblages elsewhere in the GAB. However, due to a paucity of detailed sedimentological analyses of correlative Triassic and Jurassic units in the central portion of the GAB (i.e., Galilee and Eromanga basins), additional work is necessary to fully understand the depositional system, and the nature and extent of marine transgressions into the interior of the continent.

In addition to the necessity of improved facies and alluvial architectural analysis for reconstructing Mesozoic palaeoenvironments and palaeogeography, such studies are also necessary to characterise the reservoir properties and connectivity of sandstone aquifer units of the GAB. To date, most of our understanding of this vast aquifer system is based on petroleum drill hole data, stratigraphic wells and water bores (e.g. Wray, 2009; Bianchi et al., 2018). Only a limited number of outcrop studies, particularly in the Eromanga Basin, have investigated the alluvial architecture of these vast fluvial sandsheets. Thus, the spatial and stratigraphic variability and connectivity of these units on both local and regional scales is unclear and warrants further investigation.

A number of authors, including Anderson (1989), Anderson et al. (1999), Huggenberger and Aigner (1999), Klingbeil et al. (1999) and Zappa et al. (2006), have outlined the importance of a detailed qualitative sedimentary approach to characterise aquifer heterogeneity. On an outcrop scale, factors such as lateral and vertical facies relationships, alluvial architecture and sedimentary structures, petrology, and porosity and permeability are all important to understanding and modelling the hydraulic properties of aquifers, specifically with respect to groundwater flow-through rates (Huggenberger and Aigner, 1999). Ancient bed load dominated river deposits associated with braided channel systems are considered to be among the best aquifers due to their high sand/mud ratios, and presence of laterally extensive and interconnected sandsheets. In contrast, the deposits of ancient mixed-load systems like meandering, and particularly anastomosing, channel belts are typically associated with low sand/mud ratios and the sandbodies tend to be less extensive and less interconnected (e.g. Anderson et al., 1999; Hornung and Aigner, 1999; Lunt et al., 2004; Medici et al., 2018). As groundwater usage in central Queensland and throughout the GAB continues to expand with increased climate variability, a greater understanding of the lateral and vertical interconnectivity and facies relationships associated with the Mesozoic sandstones that comprise the GAB aquifer system is required (i.e. bed-load-dominated versus mixed-load-dominated channel systems), and the starting point for this is at the outcrop scale.

Porcupine Gorge National Park, on the north-eastern margins of the overlapping Galilee and Eromanga basins in North Queensland, exposes a ~350 m thick succession of largely fluvial lower Permian–lower Cretaceous strata (Vine et al., 1964; Vine and Paine, 1974; Gray, 1977; Chapter 2, herein) , with superb outcrop exposures of the Upper Triassic Porcupine

Gorge Formation and Warang Sandstone, and the Middle–Upper Jurassic Blantyre Sandstone. Each of these formations is considered temporally and/or lithologically correlative to important aquifer units elsewhere in the GAB (Chapter 2).

Despite a long history of exploration in the area, detailed sedimentary investigations into these formations have been sparse, and mostly limited to geological survey reports, drilling logs, and geological map notes. Most of the previous studies of this nature have provided basic lithological information and primarily focused on stratigraphic correlation and palynology. This study presents a detailed lithofacies and architectural element investigation of the Porcupine Gorge Formation, Warang Sandstone, and Blantyre Sandstone in Porcupine Gorge, and of nearby wells (GSQ Hughenden 5 and 6), on the north-eastern margins of the Galilee and Eromanga basins, eastern-central Great Artesian Basin in North Queensland (Fig. 1). The goal of this study is twofold: first, to develop a better understanding of the depositional environments that characterise this portion of the GAB during the Mesozoic and the evolution of these environments through time; and second, to combine facies and alluvial architecture analysis of outcrop exposures with their correlative sub-surface units to better understand the lateral and vertical interconnectivity and heterogeneities within and between these locally and regionally important aquifer units in the GAB.

Background Geology

Galilee Basin

The upper Carboniferous to Upper Triassic Galilee Basin is an intracratonic system that extends ~247 000 km^2 across central Queensland (Fig. 1a). It is separated into three major depocentres: the Koburra Trough in the north-east, the Lovelle Depression in the north-west, and the Powell Depression in the south. The sediment package reaches a maximum thickness of ~3 km in the east and thins to <900 m in the west (de Caritat and Braun, 1992; Phillips et al., 2018b). The

Galilee Basin is coeval with the Bowen Basin to the east, with the two basins considered tectonically and stratigraphically linked (de Caritat and Braun, 1992). The Galilee Basin also formed contemporaneously with the Cooper Basin to the west, though the Cooper Basin developed in tectonic and stratigraphic isolation from the other two basins (Hoffman, 1988).

Eromanga Basin

The Early Jurassic to Late Cretaceous Eromanga Basin stretches ~1.2 million km^2 across much of Queensland and South Australia, and parts of the Northern Territory and New South Wales (Fig. 1a) with a maximum thickness of 3 km. The Galilee and Eromanga basins are separated by a peneplanation surface (Korsch et al., 2009; van Heeswijck, 2010, 2018), as a consequence of uplift and erosion of the eastern Australian margin spanning ~50 Mya. The Eromanga Basin is contemporaneous with the Surat and Carpentaria basins, with a shared stratigraphy between the Middle Jurassic to Early Cretaceous with the Surat Basin, and from the Early to Late Cretaceous with the Carpentaria Basin (e.g. Smart and Senior, 1980; Korsch et al., 2009).

Local Geology

Porcupine Gorge National Park is located ~65 km north of the town of Hughenden in North Queensland (Fig. 1a), on the north-eastern margins of the Galilee and Eromanga basins. The gorge trends NNE to SSW for ~25 km with the Permian to Cretaceous sedimentary package dipping variably between 1° and 7° to the south-west (Fig. 1b). The gorge reaches a maximum depth of ~90–150 m and, due to the variable dip, a stratigraphic interval of ~350 m of upper Palaeozoic and Mesozoic strata is exposed. In the headwaters of the gorge, the sedimentary succession rests on an angular unconformity with Neoproterozoic basement rocks of the Cape River Metamorphics. A series of five Miocene to Pleistocene (~6–0.9 Ma) basalt flows of the

Sturgeon Sub-province (Coventry et al., 1985) blanket the local landscape (Fig. 1b) and cap the sedimentary succession along the length of Porcupine Gorge.

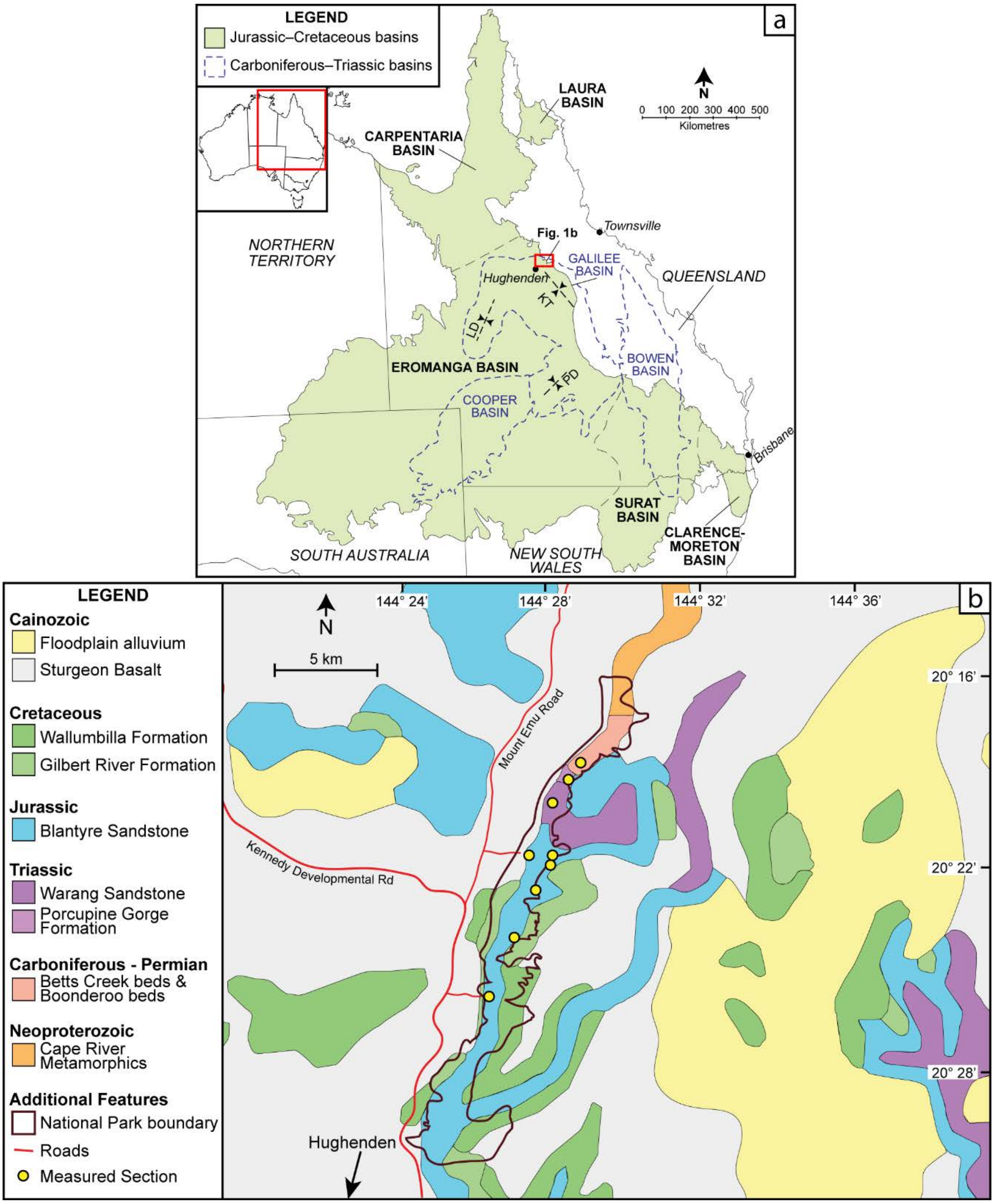

Figure 1 – (a) Basin extent in north-eastern Australia from the late Carboniferous to Late Cretaceous. (b) Local geology of the Porcupine Gorge National Park (modified from Chapter 2, Fig. 1). KT = Koburra Trough; LD = Lovelle Depression; PD = Powell Depression.

Local Stratigraphy

The stratigraphy in the north-eastern Galilee and Eromanga basins (Fig. 2), near the town of Hughenden, was first established by Vine et al. (1964) with later contributions by Vine and Paine (1974), Gray (1977), Balfe (1979), Allen and Fielding (2007a, b), van Heeswijck (2010) and herein (Ch. 2). The sedimentary infill in the north-east of the Galilee Basin consists of upper Carboniferous to lower Permian glaciogenic fluvio-lacustrine deposits of the Boonderoo beds (Vine et al., 1964; Jones, 2003, Jones and Fielding, 2004), upper Permian coaliferous alluvial and coastal-plain units of the Betts Creek beds (Allen and Fielding, 2007a, b), and Upper Triassic quartzose fluvial deposits of the Porcupine Gorge Formation and Warang Sandstone (Van Heeswijck, 2010, 2018; Ch. 2) (Fig. 2). The Warang Sandstone is diachronous, having been deposited during the Early to Middle Triassic in the Koburra Trough (e.g. Balfe, 1977; McKellar, 1977; de Jersey and McKellar, 1980) based on palynology, and in the Late Triassic on the margins of the basin based on detrital zircon geochronology and palynology from outcrop and core (Ch. 2).

On its north-eastern margin, the Eromanga Basin is characterised by Jurassic fluvial sandstones of the Blantyre Sandstone overlain by Lower Cretaceous shallow marine mudstones of the Gilbert River Formation and Wallumbilla Formation (Vine and Paine, 1974; Balfe, 1979) (Fig. 2). The Middle to Upper Jurassic Blantyre Sandstone is restricted to the basin margins but is lithologically and temporally correlative with the more widespread Hutton Sandstone and lower Injune Creek Group (Balfe, 1979; Ch. 2). The Gilbert River Formation is considered a stratigraphic correlative of the Cadna-owie Formation, with both representing the onset of a major transgression in the Early Cretaceous (e.g. Campbell and Haig, 1999; Gray et al., 2002).

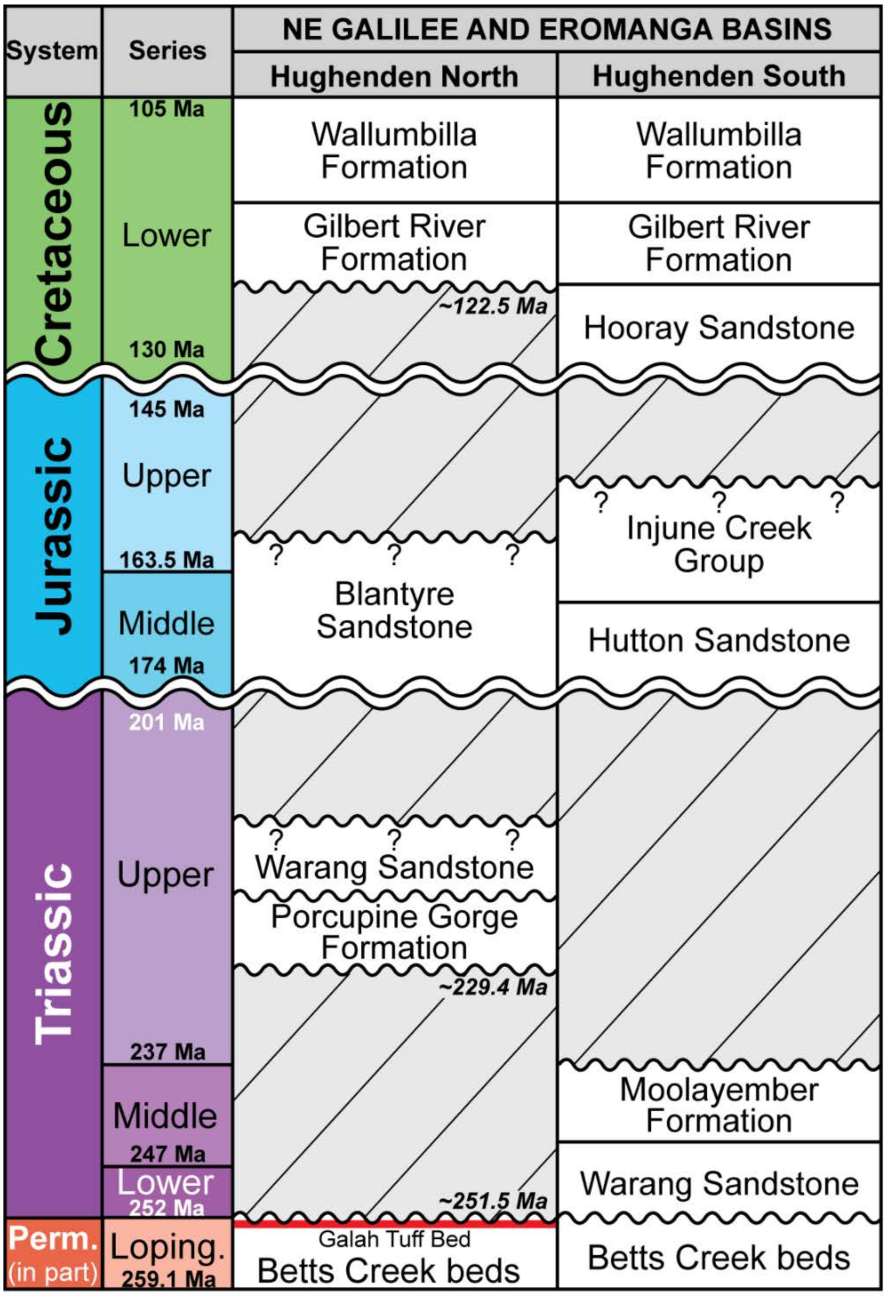

Figure 2 – Mesozoic stratigraphy of the north-eastern Galilee and Eromanga basins described from outcrop and stratigraphic drill core investigations. Hughenden North represents Porcupine Gorge, and the GSQ Hughenden 5 and 6 cores, whereas Hughenden South represents the GSQ Hughenden 7 core. Ages and stratigraphic correlations from Chapter 2.

Methods

Fieldwork was conducted within Porcupine Gorge National Park between 2014 and 2017. A total of nine localities along a 9 km NNE-SSW transect within the gorge (Appendix 4), many of which traversed formation boundaries, were selected to describe the sedimentology of the Porcupine Gorge Formation, Warang Sandstone, and Blantyre Sandstone. Decimetre-scale stratigraphic sections were measured at each locality using a Jacob's staff, compass, clinometer, and GPS. Each of the units was walked out, utilising distinct marker horizons, in order to characterise its lateral extent, and to correlate it and observe and describe the variation between stratigraphic sections. A composite ~248 m thick section of the entire Mesozoic stratigraphy was constructed by compiling data from the nine sections. Inaccessible cliff exposures were hand-drawn and photographed, then redrawn using Adobe® Illustrator®, to create photomosaics to distinguish and map the lithofacies and alluvial architecture of each formation. Palaeocurrent analysis was performed by measuring the axes of three-dimensionally exposed cross-beds, bar forms and ripple marks, and vector means were then calculated for each formation using these data.

Lithofacies and Architectural Elements

This study utilises the well-established and extensively described lithofacies classification scheme of Miall (1977, 1996), and considers specific modifications from Roberts (2007), Jinnah and Roberts (2011) and Tucker et al. (2017). Twelve individual lithofacies were identified and detailed from the three formations studied in outcrop in Porcupine Gorge (Table 1). Key characteristics and significant variations from the Miall (1977, 1996, 2010) scheme are briefly discussed below, and a new lithofacies code is described and interpreted. Lithofacies were observed in particular combinations and, together with their geometry, bounding surfaces, and lateral and vertical extent, were used to infer six two-dimensional and three-dimensional architectural elements (Table 2). Bounding surfaces after Miall (1977, 1996, 2003) were interpreted in the field and laboratory from field sketches and photographs.

Channels are higher-order elements based on bounding surface hierarchy [5^{th} order of Miall and Jones (2003)] and so may contain any lower (4^{th}) order "within channel" elements.

Table 1 – Sedimentary lithofacies types observed in the Upper Triassic to Upper Jurassic succession in Porcupine Gorge. Adapted from Miall (1977, 1996, 2010), Roberts (2007), Jinnah and Roberts (2011) and Tucker et al., (2017). Listed in order of grain-size (gravels, sands, fines), followed by most to least common.

Facies Code	Lithofacies	Photographic Example	Description	Features
Gt	Matrix-supported trough cross-bedded granule, pebble or cobble conglomerate		***Clasts***: quartz, some rhyolite, rare volcanic chert, sandstone, weathered granite, intraformational mudstone. Sub-rounded to rounded, moderate to well-sorted. Imbrication, normal grading. ***Matrix***: medium- to very coarse-grained sandstone.	Commonly laterally and vertically associated with St and Sp at erosional basal and upper contacts. Is locally oligomictic with quartz clasts. Individual sets are 0.4–1.6 m thick.
Gm	Massive matrix-supported pebble or cobble extraformational conglomerate		***Clasts***: abundant quartz and rhyolite, rare volcanic chert, sandstone, weathered granite, intraformational mudstone. Well-rounded, moderately sorted. ***Matrix***: Fine- to coarse-grained sandstone.	Commonly overlain by, or grades into, sets of Sp or St. Typically grades into Sp or St. Thicknesses typically <0.5 m.
Gms	Massive matrix-supported pebble to boulder extraformational conglomerate		***Clasts***: abundant quartz and rhyolite, rare volcanic chert, recycled sandstone, weathered granite. Sub-angular to well-rounded, poorly sorted. ***Matrix***: Medium- to very coarse-grained sandstone.	Localised facies. Is overlain by St or Gt. Overlies St at a 4th order erosional surface. Unit is 0.1–0.3 m thick.
St	Medium- to coarse-grained trough cross-bedded sandstone		Medium- to coarse-grained, yellow to white, quartzose sandstone, typically sub-angular to sub-rounded and moderate to well-sorted. Granules or pebbles of quartz or rhyolite may occur as lags on basal surfaces.	Commonly overlies Gt, Gm and Gms. Often displays erosional basal and upper surfaces. Individual sets may be 0.1–2.0 m thick and usually extend laterally for >100 m.
Sp	Medium- to coarse-grained planar (tabular) cross-bedded sandstone		Medium- to coarse-grained, yellow to white, quartzose sandstone, generally sub-angular to sub-rounded with moderate to well-sorting. Fining upwards sets.	Commonly overlies Gt, Gm and Gms. Typically occur in individually overlaying sets. Sets may be 0.1–3.0 m thick and typically extend for >100 m.
Sh	Fine- to coarse-grained horizontally laminated sandstone		Fine- to coarse-grained, white, quartzose sandstone, typically sub-rounded and well-sorted. Surficial oxidation to reddish-brown colour.	Commonly interbedded with St and Sp. Granules of quartz or rhyolite may be locally abundant but are typically rare. Beds are 10–30 mm thick and extend laterally <100 m.
Spe	High-angled planar (tabular) cross-stratified sandstone		Medium- to coarse-grained, sub-rounded, well-sorted quartzose sandstone. Alternating fining and coarsening upwards. Fine and coarse layers are different colours, giving a pinstripe texture. Granules and pebbles accumulate at toe of sets.	Commonly associated with Sr and Sh, typically at 3rd order erosional bounding surfaces. May be cross-cut by CH (Table 2) elements at 5th order surfaces.
Sr	Fine- to medium-grained ripple cross-laminated sandstone		Fine- to medium-grained, yellow to white, quartzose sandstone. Sub-rounded to rounded and moderately to well-sorted Ripple index (RI) and ripple symmetry index (RSI) indicative of current ripples.	Localised facies, typically bounded between sets of St, Sp, or Spe. Usually occur in sets <0.3 m. Individual beds <25 mm.
Fr	Massive mottled siltstone or claystone		Oxidised red, purple or orange siltstone or claystone. Highly weathered, blocky texture.	Overlies Sp, St, Sh. Rootlet traces 8–20 mm thick. Localised slickensides also present.
Fl	Thinly laminated or ripple cross-laminated sandstone and siltstone		Siltstone to fine or very fine, yellow sandstone. Commonly oxidised to red or purple.	Commonly overlies and is overlain by St and Sp elements at 3rd or 4th order erosional surfaces. Beds are 5–25 mm thick.
Fm	Massive to weakly laminated siltstone or claystone		Oxidised reddish purple siltstone or claystone.	Overlies St, Sp, Sr facies. Thinly bedded (<30 mm). Desiccation cracks common, horizontal (*Planolites*) or vertical burrows (*Skolithos*) are locally abundant but overall rare.
Fsc	Carbonaceous siltstone or claystone		Slightly oxidised, carbonaceous, purple to gray siltstone or claystone. May be locally micaceous.	Overlies St or Sp. Is overlain by Fl or Fr. Can be massive or weakly laminated in beds <15 mm. Contains carbonaceous wood fragments 2–10 mm diameter. Concostrachan traces (~2 mm) are rare.

Table 2 – Architectural element classification from outcrop in Porcupine Gorge. Adapted from Allen (1983), Miall (1985, 2006), Jones et al. (2001), Miall and Jones (2003), Allen and Fielding (2007a), and Ghazi and Mountney (2009). Elements are listed in order of bounding surface hierarchy.

Architectural Element	Generalised Cross-section	Description & Geometry	Bounding Surfaces	Interpretation
Channel element				
CH Channel deposits		Channelised bodies, lenticular to tabular with irregular often pebbly basal surfaces, containing any combination of lithofacies Gt, Gm, St, Sp, Sh, and Sr. May include components of GB, SB, DA or LA. May be bounded by SB or FF. Highly variable scale ~1.5–8 m thick and 5 m to >100 m wide.	Erosional 5^{th} order basal surfaces. Sharp to erosional upper surfaces.	Channel deposits accumulated via the amalgamation of individual braided channel forms.
Within-channel elements				
SB Sandy bedforms		Tabular to sheet-like bodies dominated by multiple stacked and amalgamated lithofacies St and Sp, and may grade up into Sr or Sh. May locally incorporate granules or pebbles. Often bounded by GB or FF. Range between 1 m and >10 m thick, extending laterally for >300 m.	Sharp to erosional basal 4^{th} order surfaces. Upper surfaces may be gradational.	Deposition and accumulation via unidirectional dune migration in mid-channel bars.
GB Gravel bedforms	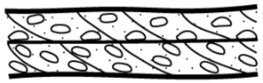	Tabular or sheet-like bodies dominated by stacked and amalgamated sets of lithofacies Gt, St and rare Gm. Typically pebble or cobble conglomerates in sandstone matrix. Often grades upwards into SB. Range between 0.5–3 m, extending laterally for <300 m.	Sharp to erosional 4^{th} order basal surfaces. Sharp to gradational upper surfaces.	Bedload deposits moved during flood events and accumulating as channel lags or mid-channel bars.
DA Downstream accretion		Characterised by multiple stacked sets of Sp or St lithofacies in a tabular to wedge geometry. Sets are typically normally graded and oriented parallel to palaeoflow direction. Individual cosets range from 0.3–1.5 m with stacked sets reaching >20 m thick and extending laterally >100 m.	Erosional basal 4^{th} order surfaces and sharp to gradational upper surfaces.	Deposited by downstream accreting, low-sinuosity, bedload dominated fluvial system.
LA Lateral accretion		Stacked sets of low-angle lithofacies Sp, minor St and rare Sr. Sets fine upwards and are orientated perpendicular to palaeoflow direction. May be laterally associated with CH elements and vertically with FF. Stacked cosets are typically 1.5–5 m thick, and laterally extend up to 20 m.	Erosional 4^{th} order basal and upper surfaces.	Deposited by laterally accreting, bedload dominated fluvial system.
Overbank element				
FF Floodplain fines		Sheet-like bodies dominated by fine-grained lithofacies Fr, Fl, and Fm with rare Fsc. May show evidence of pedogenesis. Often bounded by SB below at a gradational contact and GB above at an erosional contact. Range from 0.5–6 m thick, average <1 m, and may extend laterally ~2 m to >200 m.	Sharp to erosional 4^{th} order basal and upper surfaces.	Low-energy deposits accumulated in flood events/depositing up to distally, soil development.

Key Characteristics of Established Lithofacies

Gravelly Lithofacies

Lithofacies Gt is the most common of the three gravelly facies observed in outcrop. It consists of matrix-supported, trough cross-bedded conglomerates that occurs in clast sizes from granule to pebble to cobble with a medium- to very coarse-grained sandstone matrix. Typically, the conglomerates are polymictic and contain abundant quartz, common rhyolite, and rare volcanic chert, sandstone, granite, and intraformational mudstone; however, on rare occasion they are oligomictic and contain only quartz. Imbrication of the clasts is common but normal grading of the deposits are rare. Individual trough cross-bedded sets range from 0.4–1.6 m thick, which is a variation from the description of a maximum thickness of 3 m by Miall (1977). These sets typically occur with broad, channel geometries with erosive basal surfaces, contacting St or Sp lithofacies below. Lithofacies Gt is interpreted to represent channel fills during high-velocity flows (Miall, 1977, 2010).

The second most common gravelly lithofacies, Gm, occurring as massive, matrix-supported conglomerates, with a clast size of pebble to cobble in a fine- to coarse-grained matrix. In the original description by Miall (1977), these types of deposits are typically clast-supported. In addition, lenticles of clay and silt do not occur in lithofacies Gm in Porcupine Gorge. Most other features of these deposits are consistent with the original description, however, so this warrants definition as Gm. The clasts in this lithofacies are common quartz and rhyolite, with rare volcanic chert, sandstone, granite, and intraformational mudstones. Individual units are <0.5 m thick with erosive bases and are overlain by St or Sp sets. Lithofacies Gm is interpreted to represent longitudinal bars or in-channel debris flows (Miall, 1977, 2010).

Lithofacies Gms is the least abundant of the gravelly lithofacies occurring only once in the Mesozoic succession. It consists of a massive, matrix-supported pebble to boulder conglomerate with a medium- to very coarse-grained sandstone matrix. It is similar to the Gmm lithofacies of Roberts (2007), Miall (2010), and Tucker et al. (2017), but the size of the clasts is typically much greater, and no grading was observed. Clasts are typically quartz and rhyolite, with less abundant volcanic chert, sandstone, and granite that are sub-angular to well-rounded and poorly sorted. Unit thickness varies from 0.1–0.3 m, overlaying St lithofacies with an erosional surface, and is typically overlain by St or Gt lithofacies at a sharp contact. Lithofacies Gms is interpreted to represent a debris flow (Tucker et al., 2017).

Sandy Lithofacies

Lithofacies St is the most common sandy lithofacies, and the most common of all lithofacies observed. This facies consists of sets of medium- to coarse-grained, trough cross-bedded sandstone that are typically 0.1–2.0 m thick. In the Warang and Blantyre sandstones, set thickness is frequently >1.0 m, which is greater than the 5–60 cm thickness typically expected by Miall (1977), and <1.4 m by Roberts (2007). Cosets of stacked St deposits occur in thicknesses from 2–6 m, where they typically overlie Gt, Gm, or Gms lithofacies at erosional contacts, and are overlain by St or any of the fine-grained lithofacies. The sandstone is typically sub-angular to sub-rounded and moderately- to well-sorted, often grading normally, with granules or pebbles of quartz and rhyolite occurring rarely at the base of sets. Based on the scale and features of lithofacies St, it is interpreted to be deposited as 3D dunes (Miall, 1977, 2010; Tucker et al., 2017).

The second most common sandy lithofacies is Sp, consisting of medium- to coarse-grained planar (tabular) cross-bedded sandstones in sets 0.1–3.0 m thick. Cosets can be stacked to reach a total thickness of over 5 m, which is consistent with the original description of Miall (1977). Lithofacies Sp most commonly overlies gravelly lithofacies Gt and Gm, and in turn are overlain by sandy lithofacies St or fine-grained lithofacies Fr, Fl, Fm, and Fsc. The sandstone is sub-angular to sub-rounded and moderately- to well-sorted and may be normally graded. Similar deposits were interpreted by Miall (2010) and Tucker et al., (2017) as 2D dunes.

Lithofacies Sh consists of fine- to coarse-grained horizontally bedded sandstones, with beds ranging between 10–30 mm thick. Deposits of Sh may be up to 2 m thick and are interbedded with sandy lithofacies St or Sp. Lithofacies Sh typically overlies St at graded or sharp boundaries. The sandstone is typically sub-rounded are is well-sorted. Rare granules of quartz and rhyolite occur locally. Due to the nature of the exposure, any additional sedimentary structures such as parting lineations (Miall, 1977; Roberts, 2007; Tucker et al., 2017) were not observed. Due to the sharp contacts, lithofacies Sh is interpreted to represent planar bed flow in upper flow regime (Miall, 1977, 2010).

The least abundant of the sandy lithofacies is Sr, consisting of localised fine- to medium-grained ripple cross-stratified sandstones, occurring in sets <0.3 m thick. Individual laminae or beds may be up to 25 mm thick, but average closer to 10 mm, and typically overlie sets of St, Sp or Spe. The sandstone is highly quartzose, sub-rounded to rounded and moderately- to well-sorted. Wavelengths vary from 3–7 cm, averaging 5 cm; stoss sides are usually 1–2 cm, and lee sides 4–5 cm. Ripple index calculations of >12, and ripple symmetry index calculations of >3, are consistent with a unidirectional current flow. Lithofacies Sr is interpreted to have formed in a lower flow regime to form asymmetrical 2D ripples (Miall, 1977, 2010).

Fine-grained Lithofacies

The most common of the fine-grained lithofacies is Fr, consisting of massive siltstones or claystones occurring in deposits that vary greatly between 0.1–3.0 m. Fr lithofacies typically overlie Sp, Sh, or St deposits at sharp contacts. These silts and clays usually display a blocky texture, which is highly weathered and heavily oxidised to red, purple, and orange. Common features of this lithofacies include mottling, as well as rootlet traces that range from 8–20 mm wide, and locally abundant slickensides. These types of features, particularly rootlet traces, are characteristic of the Fr lithofacies of Miall (2010), for which an incipient soil was interpreted.

Lithofacies Fl contains thinly laminated or ripple cross-stratified very fine-grained sandstone and siltstone, occurring in deposits between 0.1–2.0 m. Individual laminae or beds range from 5–25 mm thick, and overlie St and Sp lithofacies at sharp contacts. Where present, very fine-grained sandstone appears rounded and well-sorted. This lithofacies is characteristic for its undulatory bedding or ripple cross-stratification, but is typically barren of bioturbation, rootlet traces and coal, which is more reminiscent of the Miall (2010) facies table than the Miall (1977) table. Ripples are highly variable, but typically indicate unidirectional current. Lithofacies Fl is interpreted to have formed as either overbank or waning flood deposits (Miall, 1977, 2010).

The third most abundant fine-grained lithofacies is Fm, which consists of massive to weakly laminated siltstones or claystones, occurring in deposits up to 0.5 m thick. Individual laminar or beds occur up to 30 mm thick, and typically overlie the St, Sp, or Sr lithofacies. The characteristics described here borrows more from the Miall (2010) than the Miall (1977), with the presence of desiccation cracks and bioturbation (specifically *Planolites* and other horizontal burrows, and *Skolithos* traces). Desiccation cracks are typically <20 mm in width and are infilled with coarser material, likely from the overlying sandy facies. *Planolites* and *Skolithos* traces are typically rare and are typically <10 mm in width or diameter, respectively. These deposits are interpreted to have formed in overbank processes on the floodplains, which is consistent with Miall (2010).

The least abundant of the fine-grained lithofacies is the localised Fsc, consisting of massive to weakly laminated carbonaceous siltstones or claystones in deposits up to 2 m thick. Individual laminae or beds occur at <15 mm in thickness, and overlie St, Sp, or Sr lithofacies.

The characteristic features of Fsc are the carbonaceous nature of the sediments, together with locally abundant wood fragments from 2–10 mm in diameter, and very rare concostrachan traces up to 2 mm in diameter. Thin laminae are very weakly preserved and strong oxidation events have likely destroyed much of the other sedimentary structures in this interval. The depositional interpretation by Tucker et al. (2017) for their description of lithofacies Fsc is a backswamp setting, which is the same conclusion we can draw for this lithofacies in Porcupine Gorge based on the evidence presented here.

Description of New Lithofacies

Description: Lithofacies Spe – high-angled tabular cross-stratified sandstone

Lithofacies Spe consists of medium to coarse-grained, sub-rounded, very well-sorted, quartzarenitic sandstone sets, up to 8 m thick, characterised by internal tabular cross-bedding. Individual beds display both fining and coarsening upwards textures, with the latter more prevalent. The finer laminae are white, and the coarse laminae are yellow to orange, giving the unit a distinctive pinstripe character (Fig. 3a). Granules to small pebbles of sub-rounded quartz clasts are observed on the toes of numerous foresets (Fig. 3b). Foreset dip angles were measured between 27° and 32°, with an average of 29°. The lower boundary of Spe are typically sharp and flat, commonly bounded by lithofacies Sh, Sr or St, whereas the upper contact is usually erosional and commonly cross-cut by the channel element (CH) (Fig. 3c).

Interpretation: Lithofacies Spe – high-angled tabular cross-stratified sandstone

Lithofacies Spe is interpreted to be the result of transport and deposition by aeolian processes. Inverse grading of the strata is commonly associated with this style of depositional process (Hunter, 1977, 1981), and the presence of pinstripe textures (Freyberger and Schenk, 1988) and grain accumulations – interpreted as grainfall (Kocurek, 1991; Day and Kocurek, 2017) –

are also evidence for wind-driven transportation. The high angle of the foresets (>20°) is indicative of the sand reaching the angle of repose, which is more commonly associated with aeolian deposition than with fluvial processes and is well documented in deposits such as the Jurassic-aged Navajo Sandstone of the south-western United States of America (e.g. Marzolf, 1988).

Figure 3 – Lithofacies Spe (a) Evidence for pinstripe bedding between finer-grained (white) and coarser-grained (orange) sand. Pencil scale is 15 cm. (b) Shallowing of the foreset angle and grain accumulations at the toes of the tabular cross-bed sets (red box). Hand lens scale is 5 cm. (c) Truncation of lithofacies Spe (lower unit) by overlying architectural element CH (channel deposits), specifically lithofacies St, evidenced by pebble lag in the erosional contact (white arrows).

Facies Architecture

The sedimentary lithofacies and 2D and 3D architectural elements observed, described, and interpreted from the nine stratigraphic sections taken in Porcupine Gorge are used below to discuss the depositional environments and fluvial evolution of the Porcupine Gorge Formation, Warang Sandstone, and Blantyre Sandstone during the Late Triassic to Late Jurassic in North Queensland. The Blantyre Sandstone is divided into lower and upper lithostratigraphic units (Chapter 2) which are described separately below.

Porcupine Gorge Formation

Description

Structural dip in the Porcupine Gorge Formation averages ~2° to the SSW and, coupled with the relatively thin nature of the formation (~18 m) and the modern geomorphology of the gorge, means that lateral exposure is limited to ~450 m along a SSW-NNE transect. Some parts of the formation are inaccessible for detailed sedimentological analysis due to vertical cliff faces or are covered by scree; however, a single section was measured (Fig. 4). The Porcupine Gorge Formation consists of a well-defined, generally fining-upwards trend of architectural elements from gravelly bedforms (GB) to sandy facies (SB) and associated channels forms (CH), then to into the floodplain fines (FF) with occasional interbedded SB elements.

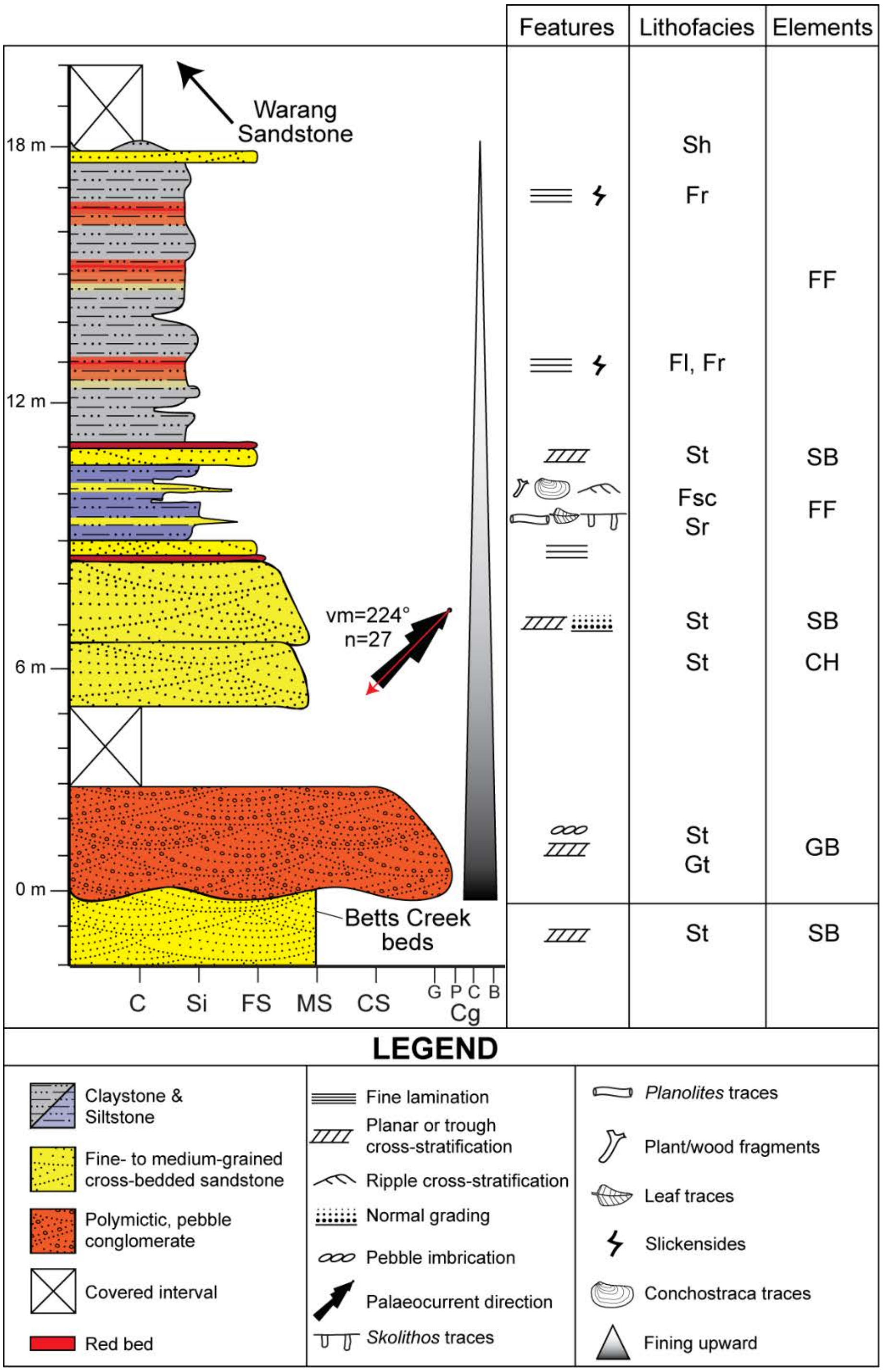

Figure 4 – Lithostratigraphy of the Porcupine Gorge Formation, showing the facies associations and architectural elements as exposed in Porcupine Gorge National Park, northern Queensland. vm = vector mean.

The succession begins with a GB element, composed of lithofacies Gt that grades into St, directly overlying an SB unit of the Betts Creek beds at an undulating erosional unconformity

(Fig. 5a). The GB is 2.9 m thick and generally tabular in form, with rare imbrication. The lateral extent of the element is unknown due to poor exposure. Clasts in the Gt sets are typically granule to pebble-sized (up to 6 cm), are sub-angular to sub-rounded, and are predominantly quartz with less common rhyolite and rare intraformational mud clasts.

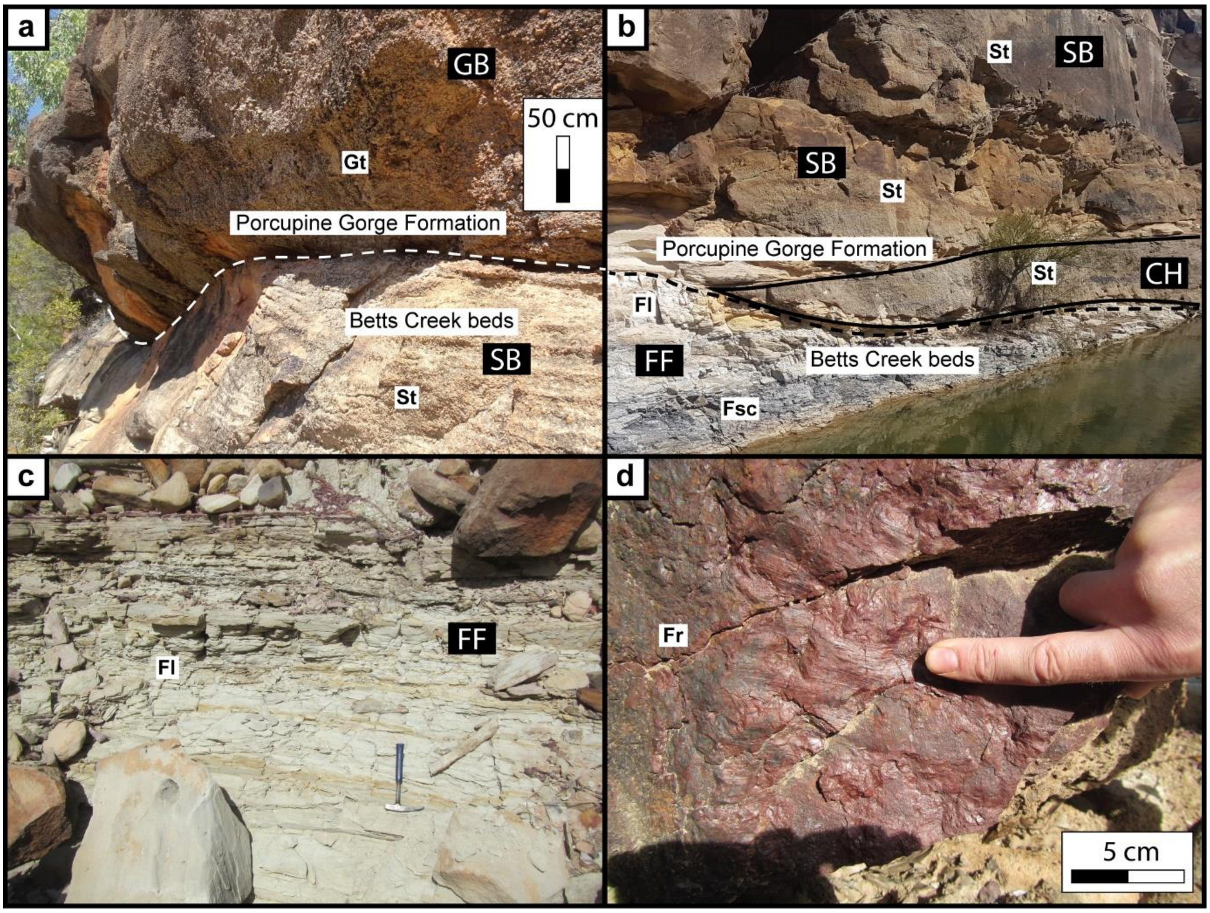

Figure 5 – Field photographs of the Porcupine Gorge Formation showing the lithofacies and architectural elements and their relationships with each other. (a) Amalgamated Gt lithofacies within a GB element at the base of the Porcupine Gorge Formation (overlying the Betts Creek beds). (b) CH and SB elements in the base of the formation directly above the contact with the Betts Creek beds. (c) example of an FF element, which is dominated by lithofacies Fl in this photo. Rock hammer is 32 cm. (d) Slickensides in lithofacies Fm associated in an FF element.

Up section is a 3.8 m thick, tabular SB element; however, downstream this unit can be seen directly overlying the Betts Creek beds (Fig. 5b). It is composed of stacked sets of amalgamated lithofacies St in sets between 0.3–1.6 m thick, which thin towards the top of the formation (Fig. 5b), and are bounded by other elements at 4th order surfaces. The SB deposits extends laterally for at least 150 m and is traceable downstream for at least 400 m, which is the limit of exposure in the base of the gorge. The geometry of the SB elements suggests the presence of the higher-order CH element. Internally, St sets are white with the sandstones being sub-angular to sub-rounded, well-sorted and quartzose with clay matrix common, fining upwards from a medium-grained to fine-grained sandstone bounded by 3rd order surfaces. Palaeocurrents were measured on 3D cross-bedding that is well exposed on benches, which indicate flow direction of 208°–242° (vector mean of 227°).

The uppermost 8.9 m of the formation is dominated by a suite of lenticular to tabular shaped FF elements. Internally, thinly laminated (<10 mm) Fsc lithofacies dominate this interval, and is characterised by purple siltstones that contain abundant carbonaceous wood and leaf traces and fragments between 2–10 mm, horizontal burrows (*Planolites*) and conchostracan impressions. Muscovite is locally abundant on the tops of some of the laminae. Two thin beds of lithofacies Sr (<10 cm) are interbedded within the Fsc sequence, and are highly weathered and massive or weakly ripple cross-stratified, and consist of fine- to medium-grained sandstone. The upper part of this FF succession is laterally extensive and caps the Porcupine Gorge Formation (Fig. 5c). Near the top of the formation lithofacies Fl and Fr are very highly weathered and oxidised, expressed as purple, red, and orange blocky siltstones and claystones. Horizontal bedding is very weakly preserved, and mottling and vertical burrows (*Skolithos*) were observed but are of rare abundance. Similarly, slickensides are present but also rare (Fig. 5d).

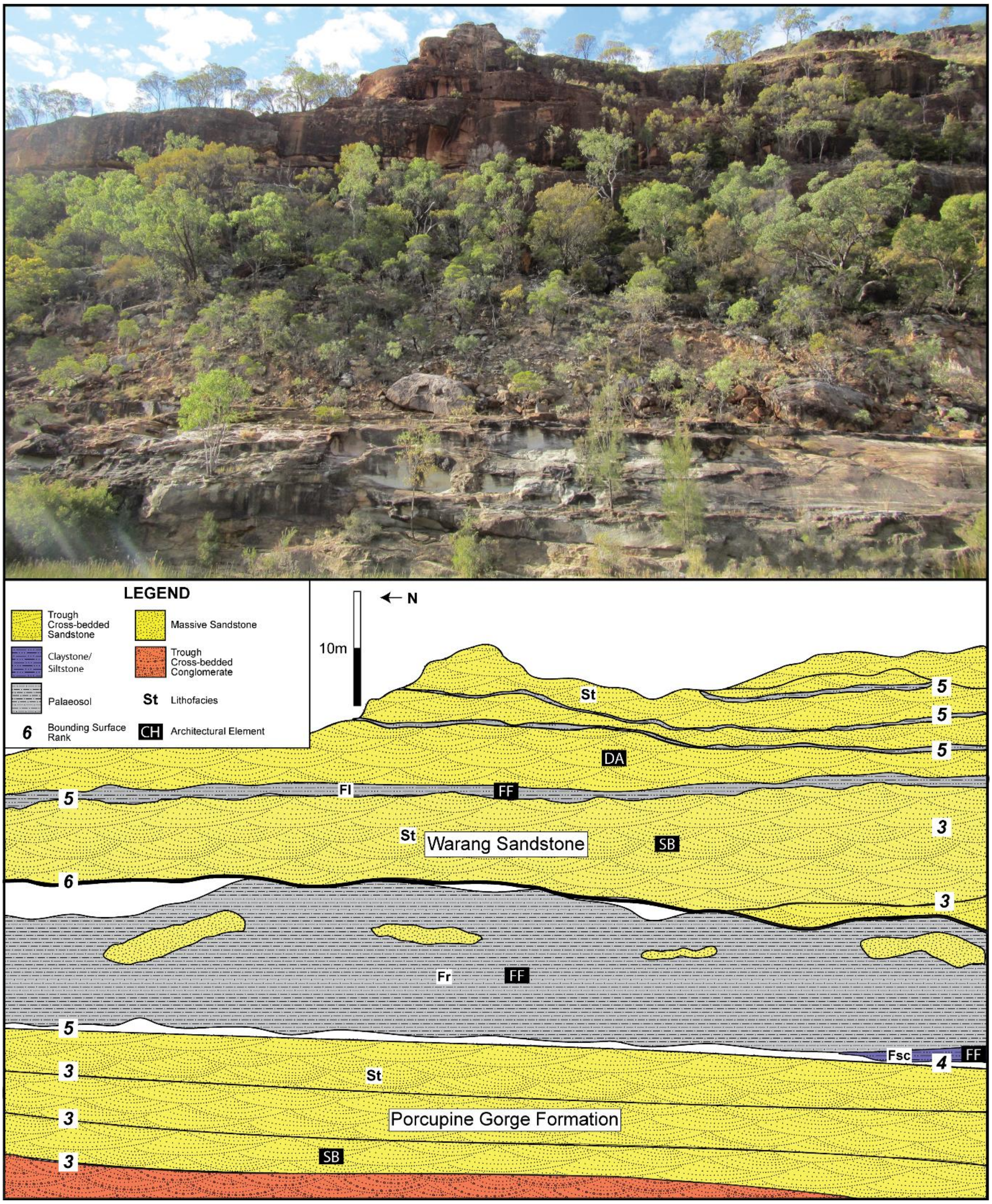

Figure 6 – Photomosaic of the Porcupine Gorge Formation and lower Warang Sandstone showing the distribution of lithofacies and architectural elements in the successions.

Interpretation

The Porcupine Gorge Formation is interpreted as a braided fluvial system. This fining upwards sequence most likely represents an autocyclic environmental shift from a high-energy scour and channel-fill deposit of the main river channel (GB and SB) towards deposition into either a localised backswamp (Fsc; FF), or proximally on the floodplain (Fl and Fr; FF).

The Gt and St deposits are indicative of transportation and deposition under a high-energy unidirectional flow regime (Anderton, 1985; Miall, 1992; Ekes, 1993; Scherer et al., 2015). The accumulation of these stacked sandstone bodies characterises the element SB which, when exposed in benches within the gorge, can be interpreted to represent mid-channel barforms oriented parallel to flow within a laterally extensive (>150 m) braidplain channel (CH) (Miall, 1977; Flores et al., 1984; Bordy et al., 2016). Multiple scour and 3rd order reactivation surfaces suggest repeated avulsion and migration of active channels, which is consistent with a high sediment load (e.g. Cant and Walker, 1978; Bristow, 1993; Miall, 2010). Amalgamation of the Gt and St co-sets is consistent with decreased accommodation space, which causes a lateral migration of the channel and reworking and destruction of the floodplain deposits (Wright and Marriott, 1993). The erosional basal surface and accumulation of granules and pebbles of quartz, with minor mud clasts, suggests recycling of the underlying Betts Creek beds. Low dispersion in palaeocurrent directions is consistent with a braided system. Based on the well-developed nature of the fining-upwards pattern, the Porcupine Gorge Formation is reasonably similar to the Donjek-type braided river (Miall, 1977).

The presence of conchostracans in the lower FF body indicates the occurrence of a small inland freshwater body such as a lake or pond (Tasch, 1969, Webb, 1979, Frank, 1988). Though there are known examples of conchostracans occurring in brackish deposits to marginal marine or marine settings (e.g. Kozur and Seidel, 1983; Kozur and Weems, 2010), the additional evidence of wood and plant material, and close association with fluvial braid bars, suggests a freshwater environment. In addition, the preservation of carbonaceous plant fragments suggests water-logged and anoxic conditions, likely in an abandoned channel or topographic low distal to the main channel (Davies-Vollum and Wing, 1998; Davies-Vollum and Kraus, 2001). The distal inference is supported by the limited occurrence of sandstone lenses (two; interpreted as major flooding events), and the evident maintenance of anoxic conditions for extended periods of time. This suggests a localised backswamp deposit on the floodplain.

Preservation of thin laminations, weak ripple stratification in the lithofacies Fl and Fr is characteristic of the element FF. Mottling of the claystone facies is indicative of the development of roots and, in combination with bioturbation in the form of vertical burrows (*Skolithos*) and weathering, likely caused the destruction of other sedimentary structures, leaving only very weak horizontal bedding. The presence of slickensides in the highly oxidised claystone suggests repeated shrinking and swelling due to frequent wetting and drying of the sediments (Retallack, 2001; Soares et al., 2020). These data suggest this interval was subjected to subaerial exposure with cyclic wet and dry periods, likely the result of seasonal flooding events, and the development of soil horizons. Palaeogeographical and palaeoclimatology data for eastern Australia suggests a warm temperate and humid climate during the Middle–Late Triassic (Grant-Mackie et al., 2000; McKellar, 2004; Turner et al., 2009), which is conducive to high rainfall events. This upper FF unit is, then, interpreted as a mature palaeosol horizon (Besly and Fielding, 1989; Kraus and Aslan, 1993; Soares et al., 2020). Infrequent but repeated sandy intervals suggest proximity to the main channel (Retallack, 2001; Bordy et al., 2016).

Warang Sandstone

Description

The Warang Sandstone has a dip of between 2–6° to the SSW in Porcupine Gorge, and is exposed for ~2.4 km along a NNE-SSW transect in Porcupine Gorge, and reaches a thickness of ~43 m. Due to the inaccessible vertical cliff faces of this unit, a split section was required to measure the entire thickness. The Warang Sandstone is white on fresh surfaces and red to orange on weathered surfaces. It is characterised by quartzose sandstone with a greasy kaolinitic texture that is moderately sorted and dominated by sub-angular to sub-rounded, medium- to coarse sand-sized grains. Outcrop exposures are mostly homogeneous, composed of alternating intervals of medium- to coarse-grained sandstones (SB) that are overlain by thin siltstones and claystones (FF), with a single pebble conglomerate unit near the top of the formation (GB) (Fig. 7). Three discrete SB elements dominate the formation that are ~12 m, ~15 m, and ~22 m thick, respectively, from bottom to top. Each SB body is tabular, primarily composed of lithofacies St with rare Sr or Sh towards the tops of individual sets, and traceable through the gorge for >2 km. Individual sets of cross-bedded sandstone (St) that make up the unit range between 0.1–3 m thick, with the average coset thickness ~0.5 m. Internal bounding surfaces are typically 3rd order. Granules and pebbles of quartz and rhyolite are common at the base of many sets, following the bedding plane.

Rare DA and CH elements are also present in the formation. The DA element predominantly consists of lithofacies Sp and typically bounded by 4th order surfaces, whereas the CH element contains lithofacies St and is bounded by 4th or 5th order surfaces (Fig. 8). These two architectural elements are not typically extensive, and usually only between 1 m and 3 m in thickness. CH elements are up to 10 m wide, whereas DA elements are up to 50 m wide. A single 1.5 m-thick GB element, composed of Gt, was identified at the top of the third SB sandstone unit and is separated by a 4th order surface (Fig. 7). This GB element is normally graded and characterised by pebble-sized quartz and rhyolite clasts.

Three tabular to sheet-like exposures of architectural element FF, consists of almost exclusively of lithofacies Fl with rare Fm and Fr, were recognised between each of the major

SB units in the formation. Internally, these elements are white to yellow, thinly laminated siltstones (<10 mm) and are stacked to a maximum thickness of 0.8–1.2 m. They extend laterally for between 50–150 m, and are traceable downstream for 100–500 m. Aside from the thin lamination and minor ripple cross-stratification, these deposits are featureless due to weathering, or are deeply oxidised to purple and red. The uppermost of these FF elements is 2 m thick and contains red-white mottling and root traces (Fm and Fr).

Palaeocurrents were measured in the middle and upper SB units. The middle unit measurements showed a flow dispersion between 171–204° and a vector mean of 180°. The upper unit measurements were slightly more varied, ranging between 166–235°, but most measurements were between 170–190°, with a vector mean of 188°.

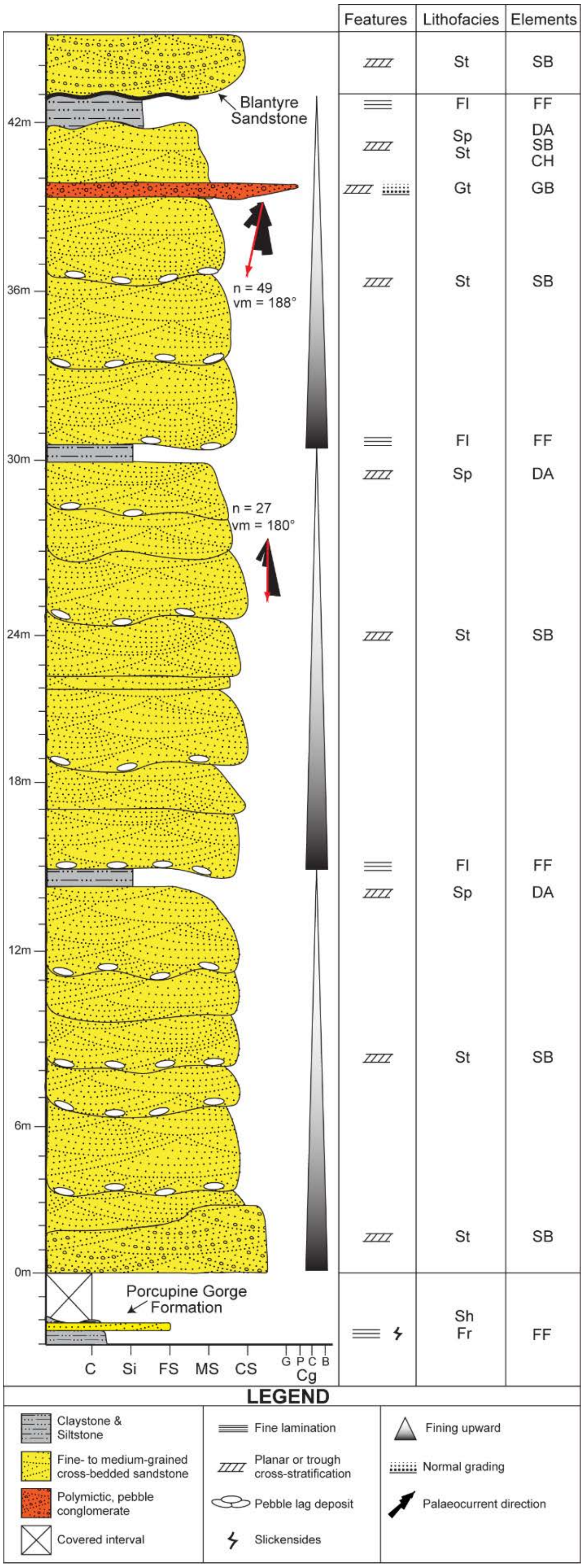

Figure 7 – Sedimentary lithofacies and architectural elements of the Warang Sandstone in composite section from Porcupine Gorge National Park, northern Queensland.

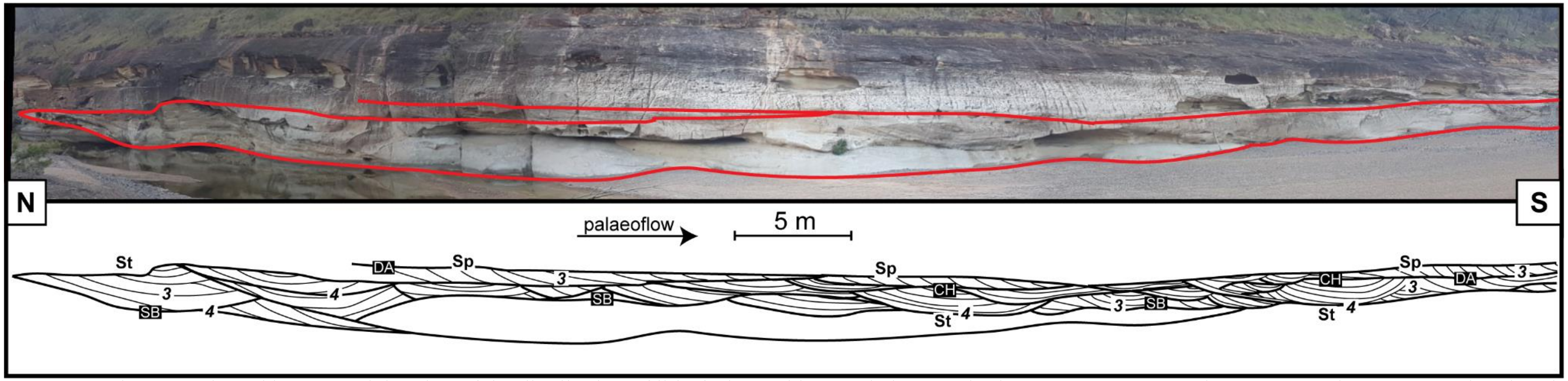

Figure 8 – Photomosaic and interpreted drawing of the distribution of lithofacies architectural elements in the upper Warang Sandstone, Porcupine Gorge National Park, northern Queensland. Numbers represent bounding surface hierarchy.

Interpretation

The Warang Sandstone is a sand-dominated braided fluvial system characterised by multistorey tabular sandbodies of the element SB, with less abundant tabular DA and lenticular CH, and a single tabular GB. The dominance of the SB bodies with abundant pebble lag deposits at the bases of cross-bed sets indicates continuous and significant scour and fill (3rd to 4th order), reworking in-channel barforms during avulsion and migration of the main channel (Miall, 1977; Flores et al., 1984; Bordy et al., 2016). Ripple surfaces (Sr) towards the tops of cosets suggests waning of flow velocity due to seasonality or as a result of sudden channel migration and abandonment (Leeder, 2011); however, given the temperate climate at this time (Grant-Mackie et al., 2000; McKellar, 2004) the latter is most likely. The presence of some horizontal sand beds (Sh), interbedded between some of the St or Sp beds is interpreted as upper plane bed deposits and suggest periodic change in flow regime from lower to upper, likely during peak flow. Cross-cutting CH elements (5th order surfaces) also suggest infrequent but sudden channel migration (e.g. Miall, 1977; Jones et al., 2001; Colombera et al., 2013; Flood and Hampson 2014). Downstream accretionary forms (DA) are also interpreted as mid-channel longitudinal barforms after Miall (1994) and Scherer et al. (2015), and feature the downstream accumulation of Sp cosets during normal flow. The thin, lenticular GB element is interpreted to represent bed-load transport during high-velocity flow, such as a flood event (Miall, 1985). These data, in addition to low dispersion measured in the palaeocurrents, suggests a low-sinuosity and low-accommodation fluvial system typical of a braided-style channel system, and most closely resembles a Donjek-type (Miall, 1977).

Thin, sheet-like floodplain deposits (FF) in the Warang Sandstone, represent sporadic flooding events with deposition proximal to the main channel due to suspension settle out as flow energy waned (Miall, 1977; Flores et al., 1984; Bordy et al., 2016). The thin nature of these bodies, together with erosional upper surfaces, is consistent with this interpretation.

Mottling in the upper parts of the FF elements is indicative of subaerial exposure of the channel belt after a thin veneer of clay and silt settled out. The mottling is suggestive of periodic pedogenesis (Mack et al., 1993; Retallack, 2001; Batezelli et al., 2019), which may reflect seasonality or even aridity in the basin during the Late Triassic.

The relatively high kaolinite content of these fluvial deposits gives the Warang Sandstone its characteristic white colour in outcrop in both Porcupine Gorge and White Mountains National Parks, for which the latter is named. The kaolinitic, or clay-rich, nature of the Warang Sandstone has also been recognised from the nearby core logs (Gray, 1977; Balfe, 1979), which may suggest that the formation was subaerially exposed and experienced significant weathering which broke down contained feldspars prior to burial by the overlying Blantyre Sandstone. The formation has also likely experienced significant weathering after incision of the Porcupine Creek (Coventry et al., 1985).

Lower Blantyre Sandstone

Description

The Blantyre Sandstone is the most continuously exposed unit in the gorge, extending for >7 km of the studied area, and reaching a maximum thickness of ~180 m. Five stratigraphic sections of the lower Blantyre Sandstone were measured along a 2.1 km NNE-SSW transect in the most accessible areas of the gorge (Figs 9 and 10) and a photomosaic was created by studying the exceptional cliff exposure of the Pyramid rock feature (Fig. 12). The Blantyre Sandstone dips variably between 2–6° to the SSW. Compared to the Porcupine Gorge Formation and Warang Sandstone, the lower Blantyre Sandstone is typically coarser-grained, with considerable amounts of conglomerate and gravelly sandstones.

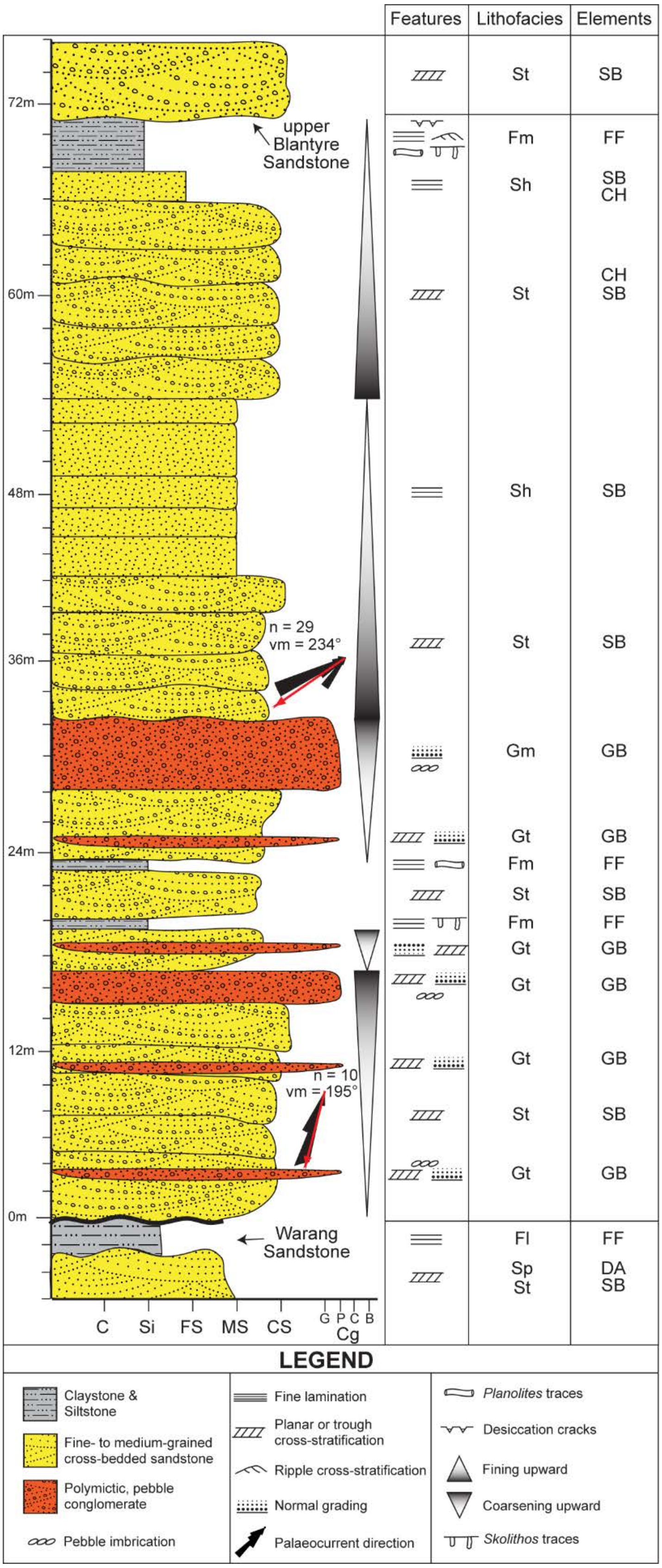

Figure 9 – Lithofacies and architectural elements of the lower Blantyre Sandstone.

The lower Blantyre Sandstone is composed of two distinct intervals. The lower interval is dominated by the architectural element SB, with locally common GB and FF elements (Fig. 11). The SB bodies are typically tabular and are dominated by the lithofacies St. These sandstone lithofacies are generally an oxidised yellow-brown and have a clayey feel. They are typically quartzose, ranging from sub-arkose to quartzarenite, locally micaceous, and are dominated by poorly-moderately sorted, angular to sub-rounded grains. In many of the measured sections of the lower Blantyre Sandstone, grain size generally coarsens upwards from dominantly medium-grained sandstone at the base to coarse-grained sandstones near the top. Despite generally coarsening upwards, there is a great deal of variability in grain size within each individual sandbody, which commonly display normal grading profiles. Each St set is up to 1.5 m thick with a lateral extent of ~150 m, and a downstream extent of at least 2 km. These sets are separated by 3rd or 4th order bounding surfaces. Sh sets are more common towards the top of this lower interval and tend to be finer-grained (medium sand) than the surrounding St sets (coarse sand), which are separated by 4th order surfaces. Palaeocurrents measured in these SB bodies range from 187–200° with a vector mean of 195°.

GB elements are tabular in geometry and consists of Gt lithofacies dominated by imbricated pebble- to cobble-sized, sub-rounded clasts of quartz, rhyolite, chert, recycled sandstone, weathered granite and intraformational mudstone in a coarse sand matrix. Individual GB units are between 1–4 m thick, externally bounded by 4th order surfaces, and internal 3rd order surfaces bound the Gt lithofacies. These beds are not laterally extensive, typically <50 m wide and extending downstream <100 m. Gt sets are normally graded with minor imbrication occurring in some of the beds. FF elements are thin (<1 m) and are composed of Fm with very rare Fl, in thin beds (<20 mm) with localised abundant vertical burrows (*Skolithos*) or horizontal burrows (*Planolites*) and desiccation cracks.

The upper interval is dominated by the elements CH, containing lithofacies St or Sh, and FF, containing the lithofacies Fl (Fig. 12). CH bodies are lenticular to irregular or tabular in shape, are between 2–8 m thick and extend laterally for at least 80 m – the horizontal extent of exposure on the Pyramid rock feature. The CH elements can be bounded by the FF elements or other CH elements at 5^{th} order surfaces. Fl lithofacies within the FF are predominantly weathered siltstones in massive or weakly laminated or ripple cross-stratified successions. A single example of the LA element, which is represented by low-angle inclined stratification of the lithofacies Sp and is 2 m thick and 6 m wide, bounds a CH element at a 5^{th} order surface. The Sp beds are oriented perpendicular to the measured flow of the remaining sandstone bodies. Palaeocurrents measured in the sandbodies of this upper interval ranged between 214–252° with a vector mean calculated at 234°.

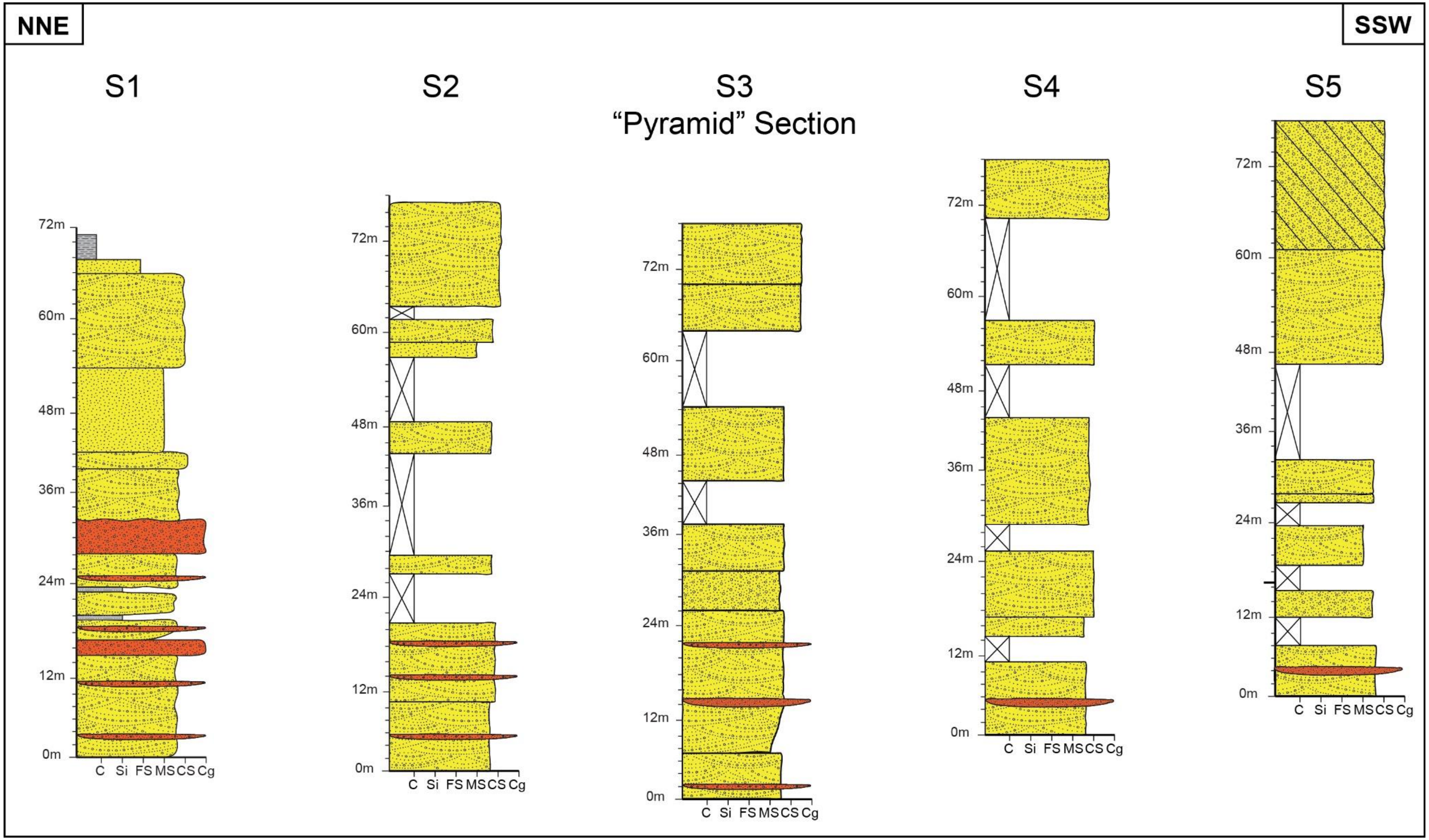

Figure 10 – Lithostratigraphic sections of the lower Blantyre Sandstone in Porcupine Gorge National Park, northern Queensland. Covered intervals (or very poor outcrop quality) in sections 2-5 are interpreted to represent the fine-grained architectural element FF.

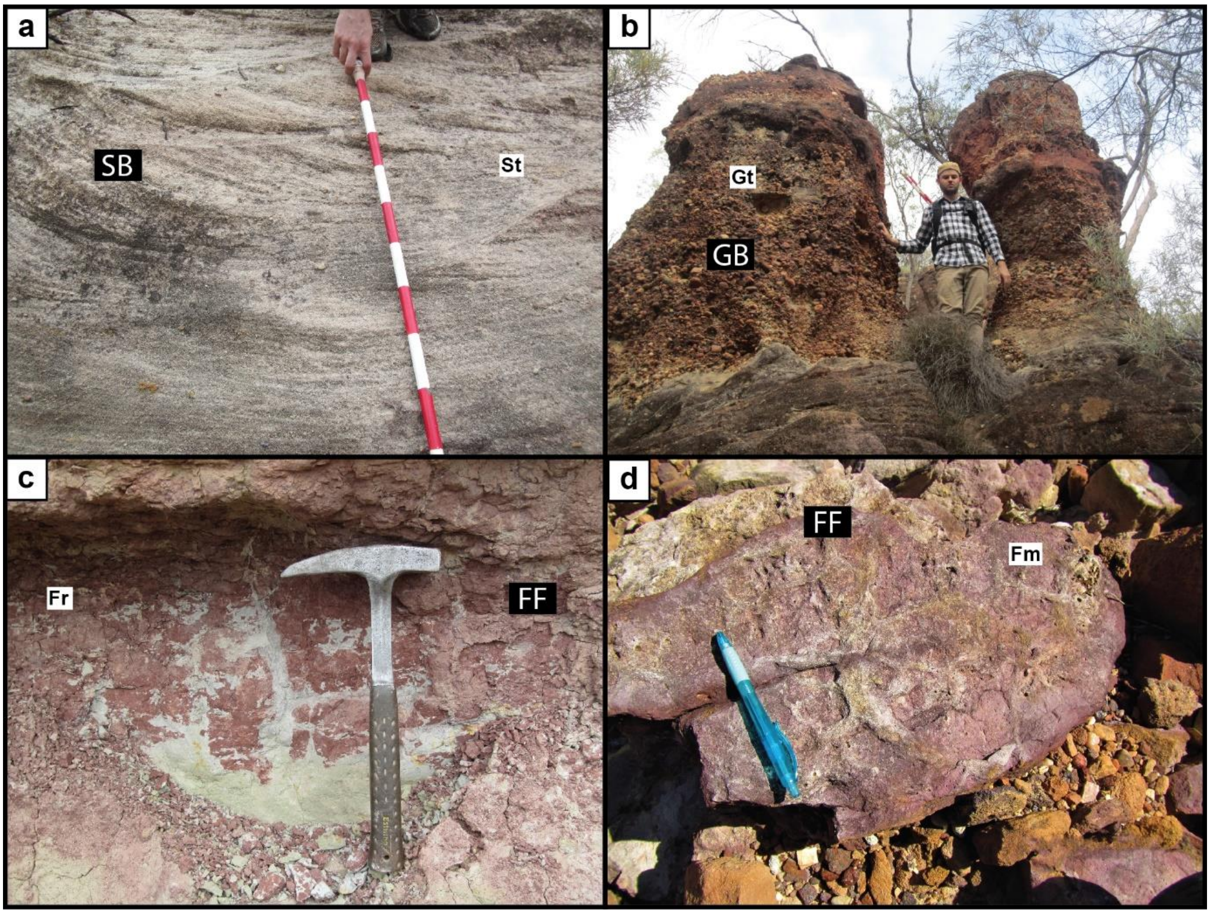

Figure 11 – Field photographs of the lower Blantyre Sandstone. (a) Amalgamated lithofacies St belonging to the architectural element SB. Jacob staff = 90 cm. (b) Thick Gt succession showing the element GB. Human scale = 1.8 m. (c) Rootlet traces in mottled claystone (Fr) of the element FF. Rock hammer = 32 cm long. (d) Horizontal burrows (*Planolites* and other indet. traces) in the lithofacies Fm, part of the element FF. Pencil scale = 15 cm.

Interpretation

The lower Blantyre Sandstone is interpreted as a braided fluvial system, similar to both the Porcupine Gorge Formation and Warang Sandstone. The lower, thick, tabular interval, which is primarily composed of the architectural elements SB and GB, with only very thin FF deposits, is indicative of high-energy transport and deposition, with the SB and GB units representing mid-channel bars (Miall, 1977; Flores et al., 1984; Bordy et al., 2016). Internal 3rd and 4th order bounding surfaces show frequent avulsion and migration of the active channel at scour and reactivation surfaces, consistent with high sediment load and low accommodation space in a braided fluvial setting (Cant and Walker, 1978, Bristow, 1993, Miall, 2010). The presence of Sh sets, interpreted here as upper plane bed deposits, indicates variable flow within the main channel that is likely caused by seasonality. The limited FF units are interpreted as overbank deposits (Miall, 1985; Colombera et al., 2013; Tucker et al., 2017). Palaeoflow shows low dispersion suggesting little sinuosity in the main channel belt, consistent with the braided interpretation. Despite an overall coarsening trend within the lower interval, the internal fining-upwards trends is suggestive of the Donjek-type braided deposit (Miall, 1977).

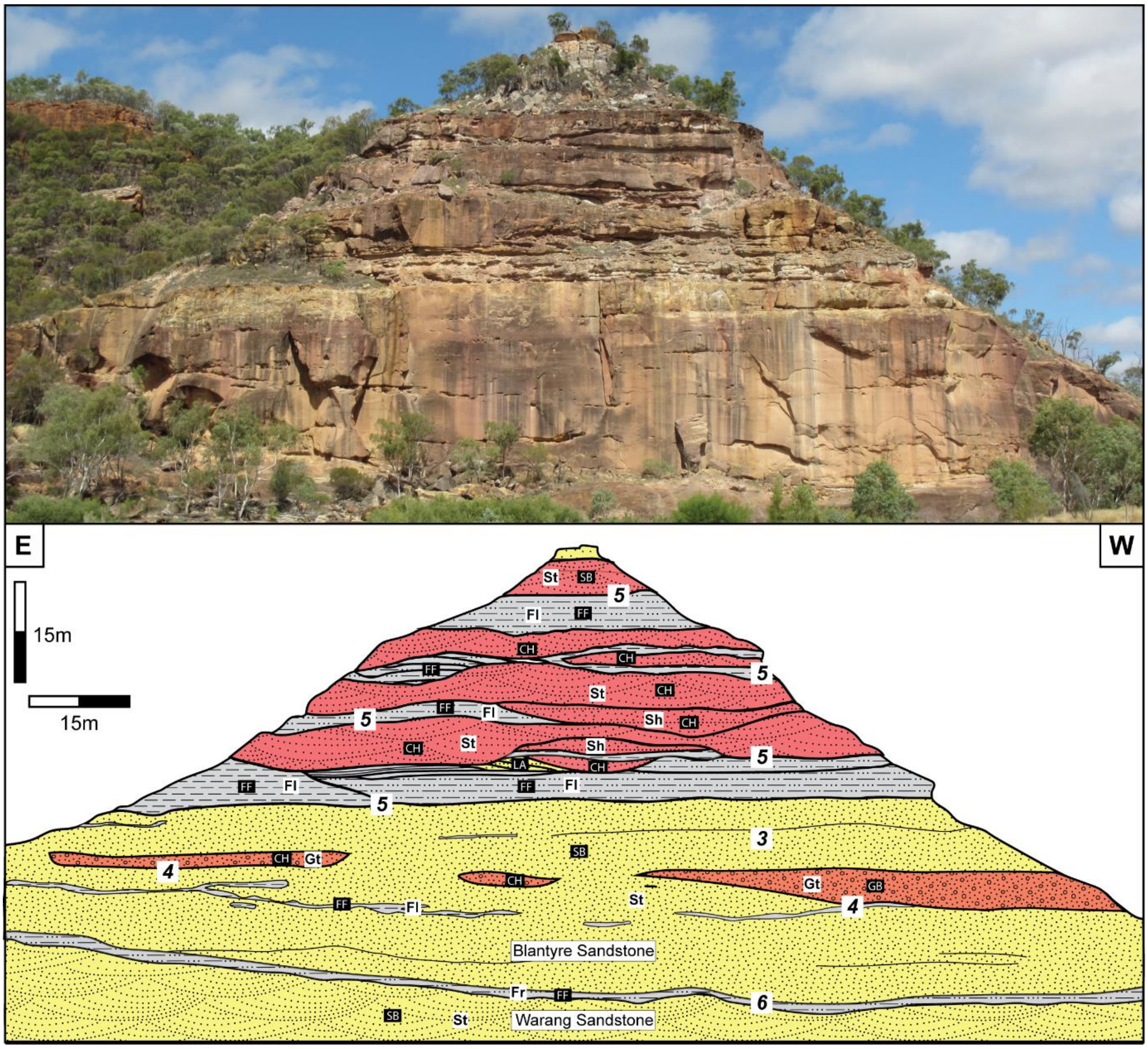

Figure 12 – Panel diagram of the Pyramid rock formation in Porcupine Gorge, including the uppermost Warang Sandstone and lower Blantyre Sandstone, showing the distribution of lithologies, facies associations and architectural elements. CH elements are red, SB elements are given in yellow, and FF elements in grey. S3 (Fig. 10) measures up left-hand side of the Pyramid.

The upper interval preserves a greater amount, and thicker units, of FF elements and associated lithofacies, typically well-developed with *Skolithos* and *Planolites* burrows and desiccation cracks (Fm, Fl). Channel forms (CH), both lenticular or irregularly shaped, are also much more distinct in this interval and are sometimes isolated, that is, completely bounded between FF units (Fig. 12). The sandy and gravelly deposits are still dominant, however, representing 55% to 70% of the interval. Preservation of these channel deposits, and a decreased sand/mud ratio, suggests an increased amount of accommodation space during deposition (Wright and Marriott, 1993; Hornung and Aigner, 1999; Huerta et al., 2011). Palaeocurrents from the second interval showed little sinuosity in the measured flow directions, suggesting that a meandering system is unlikely (Leeder, 2011). Further, the dominance of bed-load sediments (gravelly and sandy) over mixed-load sediments (fine-grained facies) and the sparseness of lateral accretion (LA) surfaces is consistent with a high-energy braided system (Miall, 1985; Colombera et al., 2013; Tucker et al., 2017).

Upper Blantyre Sandstone

Description

The upper Blantyre Sandstone (Fig. 13) is composed of four separate intervals, each composed of yellow to white, quartz-rich, clast-supported sandstone. The constituent sandstone is angular to sub-rounded and moderately to well-sorted. The basal 20.8 m interval is composed of the tabular architectural elements SB, with lithofacies St and Sr; and DA, containing the lithofacies Sp or St. These elements are separated by 4th order bounding surfaces and internally by 3rd order surfaces. Within the SB bodies, individual amalgamated St sets dip 10–15°, range from 0.1–1 m in thickness and commonly fine upwards and grade into Sr lithofacies at the tops of the sets. These sets extend laterally for >150 m and are traceable downstream for >200 m.

Granules of quartz or rare rhyolite can be seen on some of the bedding planes. Stacked Sp sets within DA bodies dip variably between 10–20°, with a thickness of 0.2–2 m and a lateral extent of >150 m and downstream extent of >200 m. Very thin (<0.2 m), laterally impersistent, sheet-like FF elements (Fm), separated by 4th order surfaces, with *Planolites* and *Skolithos* traces, are recognised in this interval, but are not extensive laterally or downstream (<100 m).

The second interval (28 m thick) consists of a series of three very weakly defined coarsening-upwards sequences, dominated by the tabular outcropping architectural elements SB and DA consisting mainly of St and Sp lithofacies, respectively, with minor GB elements, particularly lithofacies Gm and Gt. Sets of the lithofacies St and Sp are typically fine- to medium-grained, occurring in thin units up to 0.15 m thick. Two thin (~0.2 m thick) lenticular bodies of massive matrix-supported conglomerates (Gm), and one 2 m thick, trough cross-bedded conglomerate (Gt) cross-cut through these sandstones at 4th order bounding surfaces. These conglomerates are poorly to moderately sorted, with sub-rounded clasts up to 3 cm in diameter consisting of quartz with rare rhyolites and mud clasts within a coarse sandstone matrix. Palaeocurrents were measured in cross-beds on the top and bottom of this interval; the lower measurements range from 178–205°, with a vector mean of 189° calculated, and the upper measurements range between 85–140°, with an average of 124°.

The third interval (20 m thick) consists of two tabular SB elements, consisting of the lithofacies St, each being ~6 m thick and fining upwards from medium to fine sand, and coarse to medium sand, respectively. These units are separated from each other and the element above by 4th order bounding surfaces. The top of this interval consists of an ~8 m-thick channel scour and fill complex (CH), composed of alternating layers of massive and thinly laminated siltstone and sandstone (Fm and Fl). Horizontal burrows (*Planolites* and indet. traces), U-shaped burrows (*Arenicolites*) and almond-shaped traces (*Lockeia*) are abundant within the lowermost part of this siltstone interval and minor mottling was also observed. Palaeocurrents in this interval ranged from 196–250°, with a vector mean of 227°.

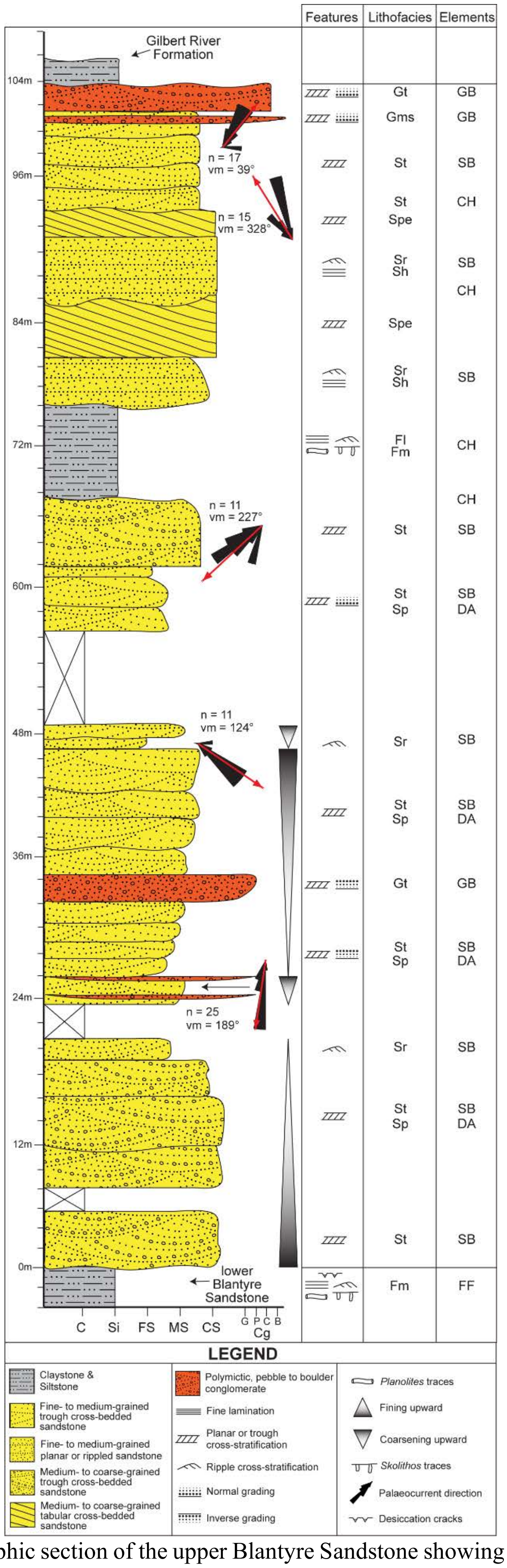

Figure 13 – Lithostratigraphic section of the upper Blantyre Sandstone showing the distribution of lithofacies and architectural elements in Porcupine Gorge National Park, northern Queensland.

The uppermost interval (28 m thick) consists of a series of alternating lenticular to irregular units of CH, dominated by the lithofacies Sh and Sr with minor St, and tabular sets of the lithofacies Spe, characterised by the high-angle tabular cross-bedded sandstone (Fig. 14). The Sh and St sets are typically medium- to coarse-grained and amalgamate into lenticular or irregular sandbodies between 0.3–5 m thick. These CH units are externally bounded by 4th to 5th order surfaces, and internally the Sh and Sr sets are separated by 2nd to 3rd order surfaces. The Spe sets are 0.5–8 m thick, but typically between 0.5–2 m thick, with individual beds either fining or coarsening upwards from medium to coarse sand, which is quartz arenitic, sub-rounded and very well-sorted. The angle of the cross-bed sets is between 27–32°, with the toes of each bed flattening out at the lower contact. Coarse- to granule-sized quartz grains have also been observed accumulating in toe deposits (grainfall). Each bed displays a pinstripe pattern with the colour alternating between white, orange, and yellow. The boundaries between the CH elements and the Spe facies are sharp, with the upper boundaries of the Spe sets often eroded into or cross-cut by the CH at 4th to 5th order surfaces (Fig. 3c, Fig 14c, d). Palaeocurrents were measured in two separate St intervals, with the lower interval ranging between 292–350°, average 328°; and the upper interval ranging between 016–090°, average of 039°.

The upper part of the uppermost interval consists of two tabular GB elements that cross-cut CH bodies, containing St lithofacies, at 4th order surfaces. The lower conglomerate (Gms; 0.3 m thick) is composed of sub-rounded to rounded pebble- (1 cm) to boulder- (26 cm) sized clasts in a massive coarse-grained, quartzose sandstone matrix. Conglomerate clasts are dominated by quartz and rhyolite, with less abundant chert, and rare intraformational mud clasts. The upper conglomerate (Gt) is composed of a single set, up to 2 m thick, with the clasts sub-angular to sub-rounded, well sorted, and dominated by quartz with rare rhyolite pebble-sized clasts (3 cm to 6 cm). It is separated from SB units by 4th order bounding surfaces.

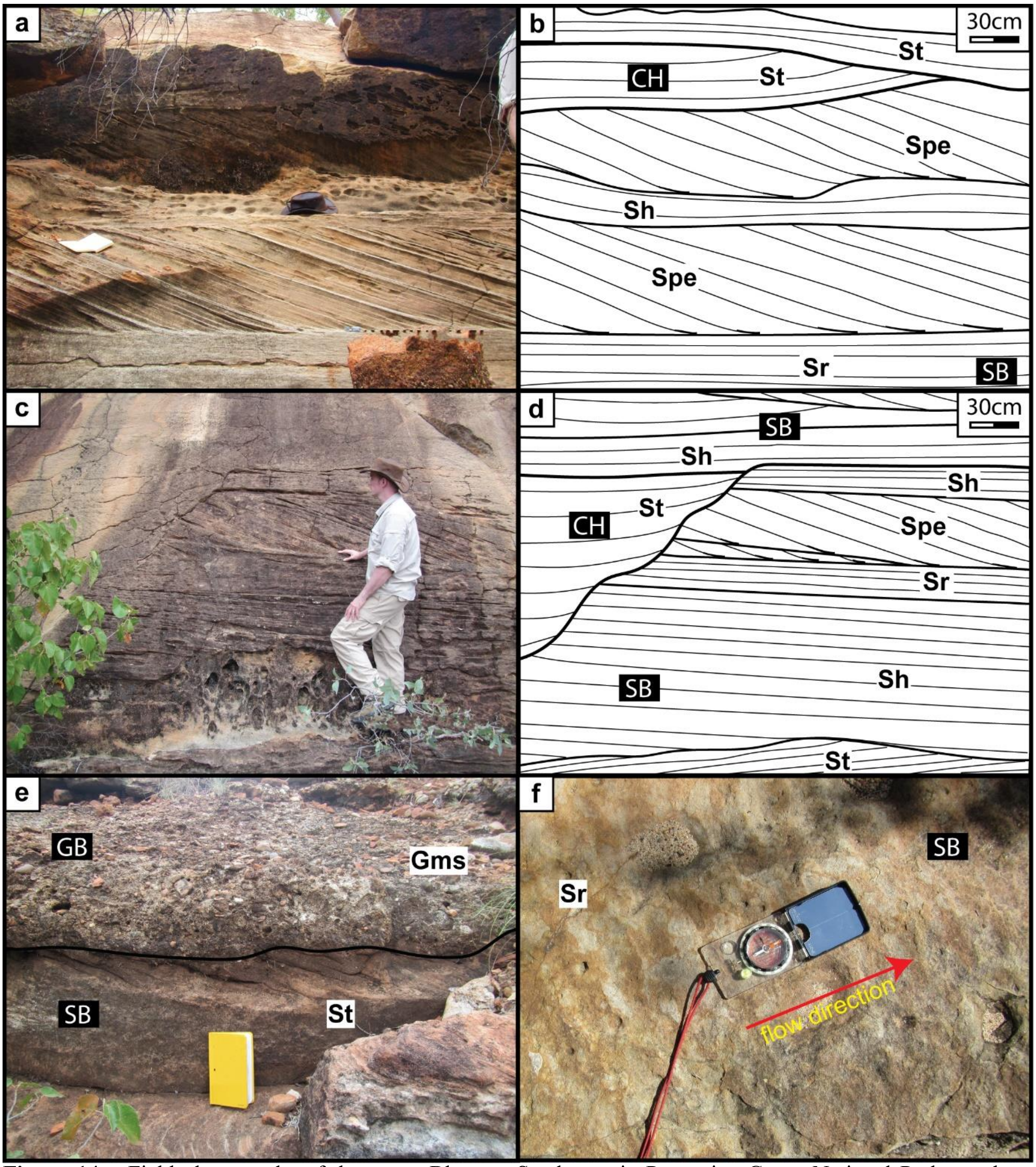

Figure 14 – Field photographs of the upper Blantyre Sandstone in Porcupine Gorge National Park, northern Queensland. (a) and (b), (c) and (d) Photographs and interpretations showing the strong cross-cutting relationship between the Spe lithofacies and the associated CH and SB elements. (e) The Gms lithofacies, representing a debris flow, and its relationship with the SB element. Book scale = 20 cm. (f) Top down view of unidirectional ripple cross-stratified beds, Sr, of the lower part of the upper Blantyre Sandstone, part of the element SB. Flow direction = 189°. Compass scale = 18 cm.

Interpretation

The upper Blantyre Sandstone is characterised by bed-load processes and sand-dominated lithofacies represented by the architectural elements SB and DA with some GB (Fig. 15). FF elements are poorly preserved within this succession. The abundance of SB elements with common granule or pebble lag surfaces is indicative of continuous scour and fill that rework mid-channel barforms (Miall, 1977; Flores et al., 1984; Bordy et al., 2016). DA elements, too, are interpreted as mid-channel bars preserved as Sp cosets accumulated during normal flow (Miall, 1994; Scherer et al., 2015; Ielpli et al., 2014).

The lowermost interval fines upwards from a coarse-grained St lithofacies into a fine- to medium-grained Sr lithofacies and likely represents a succession of mid-channel bar forms, with ripple cross-lamination preservation occurring due to periods of lower energy flow (Miall, 1977, 2010; Colombera and Mountney, 2019). These features may indicate seasonality or ephemerality in the stream. Fine-grained sandy facies and siltstones preserving *Planolites* and *Skolithos* traces are further evidence to suggest channel fill under lower-energy regimes, which is consistent with seasonality. The overall fining-upward pattern is similar to that of the Donjek-type braided river of Miall (1977).

The second interval, occurring as coarsening upwards-sequences and dominated by the same St and Sp lithofacies, with a much higher abundance of the Sp lithofacies representing the element DA which is formed by deposition of simple downstream dunes. These deposits, in addition to Gt lithofacies, are again representative of mid-channel bar-form deposits. The shift in palaeoflow from the base to the top of this interval, separated by a thick conglomerate unit, likely resulted from migration of the active stream across the braidplain by avulsion resulting from extreme flow conditions or differential topography on the floodplain. The increase in grain size suggests an increase in energy in the system, with the second interval better reflecting the Platte-type braided river of Miall (1977).

The third interval, with the two fining-upwards tabular sandstones (St) capped by a thick channelised fine-grained lithofacies succession (Fm and Fl; CH), is interpreted as a return to the Donjek-type braided river system. The presence of finer-grained lithofacies in a channel element suggests lower-energy deposition, and the *Planolites*, *Arenicolites*, and *Lockeia* traces further support this interpretation. Mottling of the sediments towards the upper surface of the channel fill suggests complete abandonment and migration of the active stream, allowing for pedogenesis to occur. The higher dispersion pattern of the palaeocurrents measured in this interval is further indicative of lower energy flow in the system; however, the coarse nature of the sediments in addition to the lack of floodplain deposits in the interval suggests a braided river setting more than a meandering setting.

The cross-cutting relationships observed in the fourth interval between the Spe sets and the CH element containing St, Sh, or Sr lithofacies indicates frequent avulsion and migration of the channels. These relatively thin Spe beds, interpreted as aeolian-derived sediments, occurring in stratigraphic continuity with fluvial lithofacies both above and below, is not immediately indicative of a semi-arid or arid depositional environment, which is consistent with the high palaeolatitudes of the study area in the Jurassic (~60°S; Veevers, 2006; Scotese, 2016). Instead, this complex cross-cutting relationship is interpreted to represent the remobilisation of fluvial braid-bar tops by aeolian processes, similar to those described in Simpson et al (2008). In their work, strong winds, such as coastal winds, during periods of low flow/discharge in the river within an arid to semi-arid climate were invoked to account for remobilisation. Despite no direct evidence for proximity to a marine environment in the upper Blantyre Sandstone (e.g. marine fossils or microfossils, deltaic or marine lithofacies), a growing body of evidence suggests that the Great Artesian Basin was twice infiltrated by the sea in the Jurassic, once in the Early Jurassic (Martin et al., 2018; Bianchi et al., 2018;

La Croix et al., 2019) and again in the Late Jurassic (Wainman and McCabe, 2019). Wainman and McCabe (2019) suggest a southward-transgressing seaway had already flooded the Hughenden area by the Late Jurassic, which would be consistent with the switch in palaeodrainage at the top of the formation from southwards towards the centre of the Eromanga Basin to northwards towards the transgressing sea. This suggests that a transition to marginal-marine and shallow-marine deposits would exist to the north and west, possible evidence of which is observed in the southern Carpentaria Basin (E. Foley, pers. comm.).

Alternatively, Trewin (1993) and Bongiolo and Scherer (2010) have shown that reworking of medium- to coarse-grained fluvial deposits into aeolian dunes can occur in an arid environment between seasonal fluvial discharge events without strong coastal winds. In Trewin's (1993) study area, however, such winds are said to produce low-angle dunes in thin deposits of less than 2 m, which is inconsistent with the steeper and thicker deposits (<8 m) observed in Porcupine Gorge. Whilst the high palaeolatitude of Australia during the Jurassic would suggest lower rainfall and higher seasonality and allow for desert environments to form, aeolian deposits are not found in any other Jurassic units in the GAB (e.g. Vine et al., 1964; Vine and Paine, 1974; Balfe, 1979; Wainman and McCabe, 2019).

A potential driver for sudden increased aridity and a shift towards a mixed fluvial-aeolian setting may be a rapid uplift of the eastern Australian margin, as outlined by Cheng et al. (2020), causing kilometre-scale relief to be formed. Such uplift events are known to cause a change in climate conditions, including increased aridity. An example of aridity caused by uplift is the Tibetan Plateau during the late Cainozoic (e.g. Yang et al., 2018); and the aridity here was subsequently increased due to the rain shadow effect of the Himalayas. However, whether this Jurassic uplift event in Australia had any impact on climate is not known.

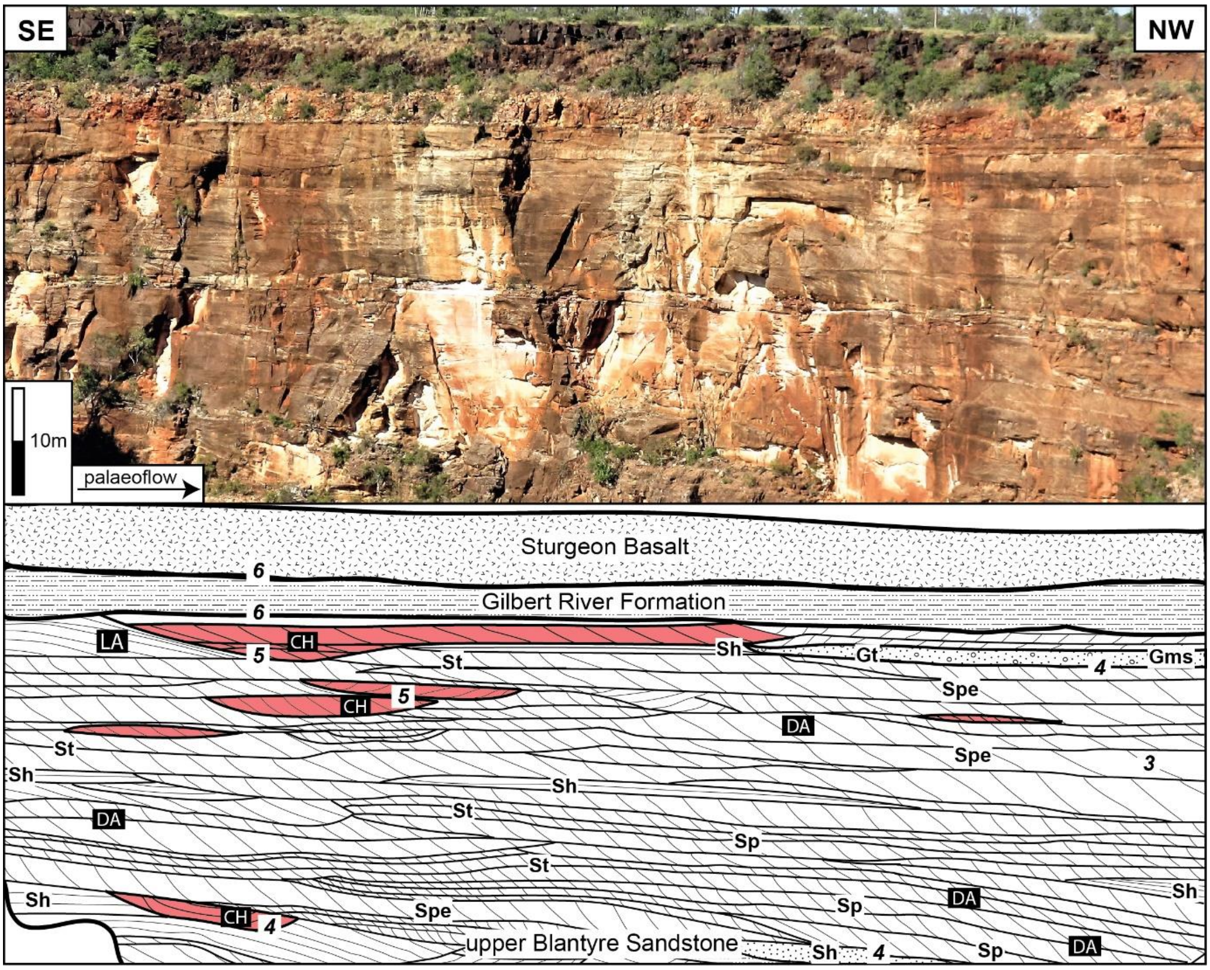

Figure 15 – Alluvial architecture and lithofacies distribution of the upper Blantyre Sandstone in Porcupine Gorge National Park, northern Queensland.

The uppermost part of the fourth interval is interpreted as a return to only fluvial deposition. An exception to this is a massive polymictic pebble to cobble conglomerate (Gms; Table 1). This conglomerate exhibits no internal structure, is poorly sorted, and contains a large range in clast size (2–20 cm) with a random orientation of the clasts. From this evidence it is consistent with a debris flow, likely from an alluvial fan (e.g. Miall, 1985, 1988; Blair and McPherson, 1999; Boggs Jr., 2014). The lithology of the pebbles is consistent with that of the conglomerates in most other formations in the succession, indicating the same probable source for each. The proximity of the study area to the basin margin, where highlands were developing, further supports the debris flow interpretation. However, the second and uppermost conglomerate (Gt) is was more likely associated with high-energy fluvial deposition, based on the presence of cross-bedding and clast imbrication. No palaeoflow orientation was determined due to the lack of 3D exposure of the conglomerate. Overall distribution of these FA within the upper unit suggests a braided fluvial system.

Discussion

Evolution of a Long-lived Fluvial System in Eastern Australia

Deposition in a continental setting during much of the Triassic and Jurassic is confirmed from the lithofacies and alluvial architecture of the Porcupine Gorge Formation, Warang Sandstone and Blantyre Sandstone, which is consistent with most previous interpretations (e.g. Vine et al., 1964; Vine and Paine, 1974; Gray, 1977; Balfe, 1979; Struckmeyer and Totterdell, 1990). Indeed, each of these formations is considered to have been deposited by bed-load-dominated, braided fluvial systems, draining internally from the margins of the intracratonic Galilee and Eromanga basins. There is limited evidence to suggest that the marine flooding experienced in other parts of the basin during this time had a significant influence on sedimentation. This implies that the generation of accommodation space in the Galilee and Eromanga basins was primarily tectonic in origin, and associated with subsidence by compression or extension associated with plate interactions along the eastern Australian margin (e.g. de Caritat and Braun, 1992; Waschbursch et al., 2009; Van Heeswijck, 2010). Most workers have suggested a dominantly compressional westward-verging subduction regime during most of this time (Veevers, 2006; Tucker et al., 2016; Hoy and Rosenbaum, 2017; Hoy et al., 2018), but clear evidence of arc magmatism versus rifting or back-arc extension is limited. Nonetheless, given the lack of significant variation in fluvial style in the Late Triassic and Middle Jurassic, there may have been general tectonic stability during this time. This is consistent with the hypothesis that the eastern margin was being peneplained at this time following the final compression event of the Hunter-Bowen Orogeny, which created kilometre-scale relief as it deformed the easternmost Tasmanides (Korsch et al., 2009; Cheng et al., 2020). Westward drainage during peneplanation may have provided the sediments necessary for the continuation of deposition into the Galilee Basin in the Late Triassic.

Regionally extensive and long-lived fluvial sedimentation in the Mesozoic in Porcupine Gorge began in the Late Triassic with deposition of the Porcupine Gorge Formation following a 20 Ma hiatus after formation of the latest Permian Betts Creek beds. A major unconformity, marked by an erosional surface and palaeosol development, separates these two units. The lowermost 9 m of the Porcupine Gorge Formation is composed of amalgamated to stacked sets of trough cross-bedded gravels and sandstones, separated by up to 4^{th} order bounding surfaces, and an apparent lack of floodplain deposits. Such a high sand to mud ratio, in combination with coarser grain size, is generally consistent with high-energy fluid flow in a low-accommodation setting. In a sequence stratigraphic framework, these deposits can be characterised as a lowstand depositional system, with sediments filling an incised valley (e.g. Wright and Marriott, 1993; Catuneau, 2006; Benvenuti and Del Conte, 2013; Sato and Chan, 2016). The preservation of mature soils (palaeosols) developing on the fluvial terraces is also suggested by these authors, which may be represented by the overlying 8.3 m-thick palaeosol. The low sinuosity of the palaeocurrents and proximity to the basin margin add support for the interpretation of a high-energy system, which allowed the rivers to move larger loads (e.g. Leeder, 2011).

This lowstand framework persisted as the Warang Sandstone, featuring several fining-upwards, amalgamated trough cross-bedded sandstones separated by thin laminated mudstones was deposited. In contrast to the Porcupine Gorge Formation, the bases of many troughs preserve pebble lag deposits, suggestive of a higher-energy system, and the numerous fining-upwards sequences show that it is more rhythmic in nature. The presence of CH forms cross-cutting at high angles to the average palaeoflow direction in the Warang Sandstone is a further indicator of high-energy fluid flow (e.g. Hjellbakk, 1997). The regional extensiveness of fluvial deposition of the Warang Sandstone on the margin of the Galilee Basin is extraordinary, with the deposits in Porcupine Gorge correlated with those of the White Mountains National Park, over 20 km away.

Detrital zircon geochronology and palynology from previous work (Chapter 2) suggests that a significant time gap exists between deposition of the Warang Sandstone and the lower Blantyre Sandstone (>50 Ma), and marks the inversion of the Galilee Basin and eventual subsidence of Eromanga Basin (e.g. Korsch et al., 2009; Van Heeswijck, 2010). The lower Blantyre Sandstone was also deposited in a low-accommodation braided river setting, with this depositional style reflected across most of the Great Artesian Basin where massive Jurassic fluvial sandsheets covered the Carpentaria Basin (e.g. Hampstead Sandstone or Garraway Sandstone), the Laura Basin (Dalrymple Sandstone), and the Surat and Eromanga basins (e.g. Hutton Sandstone) (Smart et al., 1971; Henry and Benade, 1982; Gray et al., 2002). The top of the lower Blantyre Sandstone, however, marks a change to an increased-accommodation setting. This is reflected in sandstone CH elements packaged within the FF successions (Fig. 12) and is the first and only example of such deposits in Porcupine Gorge. With the slight increase in accommodation, but still limited horizontal extent of these individual channels, a transgressive depositional system is considered a more likely interpretation of this interval (e.g. Wright and Marriott, 1993). This is also reflected in the palaeocurrents, with a slightly higher dispersion rate that is still within the range expected in a braided system, but also a more westerly flowing vector mean.

In the upper Blantyre Sandstone, a return to the lowstand depositional style is observed. However, the tabular cross-bedding and DA elements are more common than trough cross-bedding and SB elements, which suggests lower energy in the system and higher accommodation, with the sandstone accreting on the downstream surfaces of mid-channel bars and creating a stacked and tabular pattern (Cadle and Cairncross, 1993; Scherer et al., 2015; Bordy et al., 2016). This is in contrast to the higher-energy and lower accommodation systems where channel avulsion and migration are more common. The lowstand depositional style in the upper Blantyre Sandstone continues to the top of the formation, where reversal of the palaeoflow direction towards the north occurs, perhaps representing drainage into a transgressing seaway (Wainman et al., 2019) and also coincident with uplift on the eastern margin, which may have been a precursor to the current Great Dividing Range (Cheng et al., 2020).

Aquifer Characteristics of Mesozoic Sandbodies

Detailed qualitative outcrop analysis of the Porcupine Gorge Formation and the Warang and Blantyre sandstones reveals that these formations were deposited in bed-load-dominated braided river systems. Thick and laterally extensive sandbodies dominate each of the successive Mesozoic units, which are typically bounded by thin floodplain deposits, or high-order erosional bounding surfaces (4th or 5th). These vertically continuous and laterally extensive sandbodies provide excellent hydraulic conductivity which permits the groundwater to permeate throughout the basin, in contrast to mixed-load-dominated systems which provide much less transmissivity. The general paucity of laterally extensive fine-grained floodplain or other overbank depositional facies indicates a high degree of homogeneity within and between most formations. The dominance of these features, coupled with the preponderance of relatively high porosity in medium- to coarse-grained sandstone-dominated facies, suggests excellent hydraulic conductivity can be expected throughout this stratigraphic interval in this portion of the GAB.

The Porcupine Gorge Formation has not been previously identified as an aquifer, and so has not been targeted for porosity and permeability analyses. The analysis of its alluvial architecture and lithofacies conducted herein, however, has demonstrated the widespread occurrence of thick and laterally continuous sandbodies, which are bounded by floodplain deposits that confine the groundwater within the system, and which promote high hydraulic conductivity (Hornung and Aigner, 1999). The formation is also bounded by unconformities marked with mudstones on both the upper and lower surfaces, which would further contribute to the containment of the groundwater within the unit. The petrology of the sandstones of the Porcupine Gorge Formation revealed a significant clay percentage, likely kaolinite, that clogs the pores in the sandstone and reduces the overall hydraulic transmissivity of the unit. In comparison to the other Mesozoic formations in Porcupine Gorge, sandbodies in the Porcupine Gorge Formation are thinnest, and would not contain as much groundwater. Despite this, the formation has high lateral connectivity and homogeneity, and so is still considered likely to act as an aquifer or partial aquifer; however, analysis on the permeability and porosity needs to be completed to be certain.

The Warang Sandstone has been identified by Ransley et al. (2015) as a viable aquifer, and its supposed lithological correlative – the Clematis Group – has similarly been identified as an aquifer (Moya et al., 2014). Gray (1977) measured porosity and permeability in the Warang Sandstone in GSQ Hughenden 5 and 6 and found that porosity ranges from 19%–23% and permeability from 1–1704 md. Petrological observations here and by other authors (e.g. Vine et al., 1964; Vine and Paine, 1974; Gray, 1977) indicate that the formation contains a significant level of kaolinite clay, which clogs the pores and decreases the hydraulic transmissivity potential, and explains the relatively low permeability readings from core. However, these permeability readings are on average higher than floodplain readings (i.e. generally <10 md; Hornung and Aigner, 1999), which are characteristic of aquitards or aquicludes. The overall lateral and vertical continuity and homogeneity of the sandy facies in the Warang Sandstone is a good indicator for hydraulic transmissivity. These thick sandbodies are then bounded by the muddy facies, which stops the groundwater from leaving the system. From this, it is suggested that the Warang Sandstone is an aquifer.

The Blantyre Sandstone is correlated with the Hutton Sandstone (Vine et al., 1964; Balfe, 1979; Chapter 2), which is considered an important aquifer in the GAB (Moya et al., 2014; Ransley et al., 2015). In GSQ Hughenden 6, which is <1 km from Porcupine Gorge and closely mirrors the outcrop, the porosity measurements average 26%, and the permeability ranging from 609–9153 md (Gray, 1977), which far exceed respective values from the Warang Sandstone. The exact depths at which these measurements were taken were not given; however, due to its higher percentage of muddy facies, it is likely that many of the lower permeability values were collected from the lower Blantyre Sandstone with the larger percentage of fine-grained facies, whereas the higher permeability values were collected from the mud-poor upper Blantyre Sandstone. In Porcupine Gorge, the sandy facies distributions in the lower and upper Blantyre Sandstone units are consistent with high lateral and vertical connectivity. Fewer mudstone layers in the upper Blantyre Sandstone and increased homogeneity of the sandbodies suggests increased hydraulic connectivity potential, whereas the increased mud content – particularly in the higher-accommodation interval – would decrease the hydraulic connectivity in the lower Blantyre Sandstone. Overall, of the Mesozoic formations studied herein, the upper Blantyre Sandstone and its lithological correlatives have the greatest potential for groundwater to transfer across the GAB.

The above evidence shows that the exposure of highly permeable sandstones in Porcupine Gorge may be advantageous for its potential to be a groundwater recharge point for the correlative aquifer units in the GAB (Ransley et al., 2015). The stratigraphic dip of the Mesozoic succession in the Hughenden area is between 2–6° due to its proximity to the basin margin and Great Dividing Range, which would allow the groundwater to flow southwards towards the depocentres in the middle of the artesian system.

Conclusions

The north-eastern Galilee and Eromanga basins were the location of a laterally extensive and long-lived intracontinental fluvial system throughout the Triassic and Jurassic. This fluvial system was dominated by bed-load deposition under very low- to low-accommodation conditions and with limited floodplain preservation. The Porcupine Gorge Formation, Warang Sandstone and Blantyre Sandstone were found to have similar repetitive patterns of sandy lithofacies and architectural elements consistent with high-energy braided fluvial systems. In the upper Blantyre Sandstone, increased aridity facilitated the reworking of some of these fluvial braid bars into aeolian dunes. The overall domination of bed-load deposits suggests a proximal setting with the rivers draining from the basin margins into a depocentre located to the south of the study area. This style of deposition in intracratonic basins was advantageous for producing fluvial sandbodies with high sand to mud ratios that are laterally extensive and connected and characterise high-quality aquifers.

The lack of direct evidence for a marine incursion, or evidence for marginal-marine or paralic facies in the Jurassic is an important finding for the reconstruction of palaeoenvironments in the Eromanga Basin. This finding seemingly conflicts with a growing body of evidence that suggests the Great Artesian Basin experienced periodic transgressions, including flooding through the Carpentaria and Surat basins in the Middle to Late Jurassic. However, a palaeodrainage reversal in the upper Blantyre Sandstone may provide indirect evidence of an incursion.

Chapter 4:
Sedimentary provenance and palaeodrainage history of the north-eastern Galilee and Eromanga basins, Queensland

Abstract

The Phanerozoic tectono-sedimentary evolution of Eastern Australia is generally well understood, with considerable agreement on the plate dynamics and basin development during the Palaeozoic to early Mesozoic, and during the late Mesozoic to Cenozoic. However, basin development and plate tectonic patterns during the mid-Mesozoic, particularly for north-eastern Australia, remain enigmatic due to the scarcity of well-preserved magmatic rocks of this age along the continental margin. To decipher the tectonic framework and drivers of basin development during this time, sedimentary provenance analysis, involving palaeocurrent measurements, pebble counts, sandstone petrography, and U–Pb detrital zircon geochronology, was conducted on upper Palaeozoic to middle Mesozoic strata of the north-eastern Galilee and Eromanga basins. The results establish the presence of syn-depositional magmatism along the eastern margin of north-eastern Queensland during the Triassic and Jurassic; however, sandstone petrography and detrital zircon geochronology indicate that these were distal sources that account for only a small proportion of the total sediment input into the study region during this time. Sandstone petrography indicates that the Triassic to Middle Jurassic samples primarily plot in the sub-mature subarkose to sublitharenite petrofacies, with a subtle increase in compositional maturity in Upper Jurassic sandstones. The Triassic samples point towards a recycled orogen provenance whereas the Jurassic samples plot in the cratonic interior provenance field; hence most of the syn-depositional volcanic input into the basin during this time was likely through distal airfall ash deposits. However, it is possible that minor erosion of intrusive, arc-related rocks may have internittently entered the basin from the east. Palaeocurrent and detrital zircon provenance analysis demonstrates that fluvial drainage patterns during the late Permian to Middle Jurassic were dominated by south to south-west palaeoflow with sediment sourced from the Etheridge Province and the Kennedy Igneous

Association to the north. A significant Late Jurassic palaeocurrent reversal (flow to the north/north-east) is documented in the upper Blantyre Sandstone, which is interpreted to reflect an uplift event on the eastern Australian margin. This drainage reversal is confirmed by a change in the detrital zircon provenance evidenced by input of zircon populations eroded from the Anakie Province, located to the south-east of the study area. These populations are characterised by polyphase zircons that were likely recycled from the central Australian Musgrave Complex, the Ross-Delamerian Orogen, and Patterson-Petermann Orogen. As the basin filled, palaeoflow shifted to west-south-west in the Early Cretaceous, with the dominant detrital zircon population returning to Kennedy Igneous Association sources. Lower Cretaceous strata also yield significant syn-depositional detrital zircons, with a range of 135–120 Ma grains that are interpreted to be sourced from the Whitsunday Volcanic Province. This study not only demonstrates that sediments for the northern Galilee and Eromanga basins are primarily sourced from Palaeozoic terranes to the north-north-east, but also documents the presence of a continuum of Mesozoic magmatic zircons whose sources lie somewhere to the east of the present coastline of north-eastern Australia, which most likely entered the basin as airfall deposits.

Introduction

The early Cambrian to Late Triassic Tasman Orogenic Zone dominates the geology of eastern Australia (Glen, 2005, 2013; Rosenbaum, 2018). The sequence is composed of five subduction-related orogenic terranes – the Delamerian, Lachlan, Thomson, Mossman, and New England orogens (Glen, 2013) – which record and describe much of eastern Australia's tectonic evolution through the Phanerozoic. This long-lived, westward-driven subduction system also influenced the development of some of eastern Australia's most important sedimentary basin systems, including the Carboniferous to Triassic Galilee-Bowen-Cooper(±Sydney-Gunnedah) basin system, and the Jurassic to Cretaceous Eromanga-Carpentaria-Surat-Laura(±Clarence-Moreton basin) system, collectively referred to as the Great Artesian Basin (GAB). Deposition into the GAB ceased in the Late Cretaceous when the subduction zone retreated eastward, opening the Tasman Sea and removing pieces of continental crust that now make up the Lord Howe Rise, Solomon Islands, New Caledonia, and Zealandia (Crawford et al., 2003; Mortimer et al., 2008, 2015; Adams et al., 2009; Tapster et al., 2014). This retreat and associated back arc-rifting is thought to have resulted in isostatic rebound of the eastern margin of the continent, leading to formation of a continental divide (Great Dividing Range), and the final phase of basin fill within the GAB (Gurnis et al., 1998; Veevers, 2006; Müller et al., 2016).

Despite our knowledge of the evolution of the eastern Australian margin, Palaeozoic to Mesozoic sedimentary basin development remains comparatively poorly understood. The influence of the subduction margin on basin evolution in north-eastern Australia from the Late Triassic to Late Cretaceous, particularly the Jurassic, is poorly constrained. Attempts to resolve the tectono-sedimentary history of this region during this time have been made difficult by a paucity of preserved magmatic rocks of this age range along the eastern margin of the continent (Turner et al., 2009). In lieu of this, sedimentary provenance analysis of interior basins in

Eastern Australia have been shown to be a useful proxy to help address these questions (e.g. Bryan et al, 1997, 2000; Wainman et al., 2015, 2018b; Tucker et al., 2016).

In this study, we present results of a detailed sedimentary provenance analysis of Permian to Cretaceous strata from the north-eastern Galilee and Eromanga basins in northern Queensland. This multi-faceted investigation combines field methods such as palaeocurrent analysis and pebble counts with laboratory methods such as sandstone petrography and U–Pb detrital zircon geochronology to establish a palaeodrainage model for north-eastern Australia in the late Palaeozoic and Mesozoic. The data presented here, together with a number of other studies to the south (e.g. Wainman et al., 2015, 2018a, b) can then be used to test the influence of the eastern Australian subduction zone on Jurassic and Cretaceous basin development.

Geology and Stratigraphy

Galilee Basin

The Carboniferous to Triassic intracratonic Galilee Basin covers an area of 247,000 km^2 across central Queensland (Fig. 1). It is bounded to the east by the Devonian to Carboniferous Drummond Basin, to the north by the Etheridge and Croydon provinces of the North Australian Craton, and to the north-east by the Charters Towers and Greenvale provinces of the Thomson Orogen, and the Broken River Province of the Mossman Orogen. The Galilee Basin can be subdivided into three depocentres: the Lovelle Depression in the north-west, the Koburra Trough in the north-east, and the Powell Depression in the south. The Galilee Basin is coeval with the Bowen Basin to the east and the Cooper Basin to the south-west. Sedimentation was continuous across the Nebine Ridge between the Galilee and Bowen basins from the upper Permian (Vine et al., 1973; Fielding et al., 2000; Phillips et al., 2017a, b), but sediment transfer between the Galilee and Cooper basins was blocked by the Canaway Ridge (Hoffman, 1988).

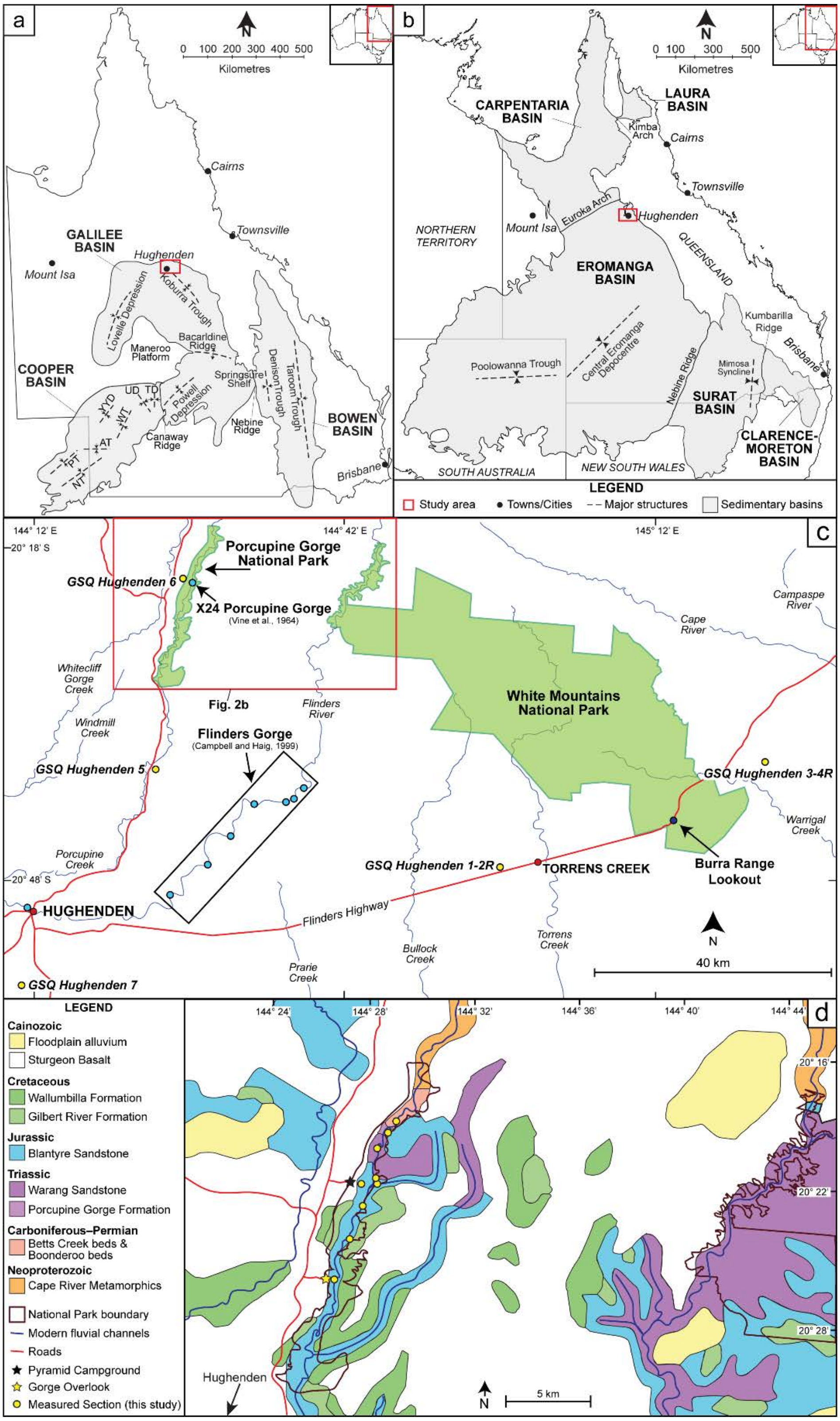

Figure 1 – (a) and (b) Basin extent and structural elements of the Galilee and Eromanga basins. (c) Map of the Upper Flinders River area showing the locations of Porcupine Gorge and White Mountains national parks as well as all of the GSQ Hughenden drill cores. (b) Local geology of the Porcupine Gorge National Park, north of Hughenden.

The formation of the Galilee Basin is much debated. Initial development has been attributed to either passive thermal subsidence (Van Heeswijck, 2010; 2018), foreland-style subsidence as a result of lithospheric flexure from the uplifting Anakie Province (de Caritat and Braun, 1992), or a response to the prolonged application of a dextral rotational force couple (Evans and Roberts, 1980). The stratigraphic continuity between the Galilee and Bowen basins from the upper Permian has led some authors to infer a shared tectonic history (e.g. de Caritat and Braun, 1992; Phillips et al., 2018b). This shared history is usually summarised in three events: early Permian extension, followed by passive thermal subsidence, and foreland-related subsidence in the late Permian to Triassic in the Bowen Basin while thermal subsidence continued in the Galilee Basin (Phillips et al., 2018b). This late Permian foreland subsidence is suggested to have created a single depositional system with the Galilee Basin developing as a platform basin proximal to the foreland-style Bowen Basin (de Caritat and Braun, 1992; Phillips et al., 2018b). A final compressive phase of the Hunter-Bowen Orogeny is widely interpreted to have inverted the Galilee Basin and ended deposition (e.g. Van Heeswijck, 2010, 2018).

Eromanga Basin

The Early Jurassic to Late Cretaceous intracratonic Eromanga Basin covers 1.2 million km^2 across much of Queensland and South Australia, and parts of the Northern Territory and New South Wales (Fig. 1). It overlies the Galilee and Cooper basins in Queensland and South Australia. The Eromanga Basin is bounded to the north-west by the Mount Isa Province and to the east by the Galilee Basin and New England Orogen. It contains two depocentres, including the Poolowanna Trough in the south-west, and the Central Eromanga Depocentre in the centre of the basin. Sedimentation was continuous across the Nebine Ridge between the south-eastern

Eromanga Basin and Surat Basin during the Early Jurassic to Early Cretaceous (Wake-Dyster et al., 1987). Sediment transfer between the Eromanga and Carpentaria basins across the Euroka Arch in the north was active only during the late Middle Jurassic (Smart and Senior, 1980), with rivers draining northward. The Ceduna Delta in the Great Australian Bight off the South Australian coast is interpreted to have become the ultimate depocentre for sediments from the Eromanga Basin during the Late Cretaceous from continental-scale basin drainage not unlike the Murray-Darling and Lake Eyre basins of today (MacDonald et al., 2013; Lloyd et al., 2016).

Table 1 – Lithostratigraphy of the north-eastern Galilee and Eromanga basins, including previous age data, lithology, depositional environments and correlations across basin boundaries. Each letter in parentheses corresponds to a different basin: (B) Bowen Basin, (G) Galilee Basin, (S) Surat Basin, (C) Carpentaria Basin, (E) Eromanga Basin. Key: U–Pb DZ = U–Pb detrital zircon geochronology; AFT = apatite fission-track dating. Compiled and modified from Vine et al. (1964), Gray (1977), Balfe (1979), Almond (1983), Gray et al. (2002), I'Anson et al. (2018).

Sedimentary Unit	Age	Stratigraphic Relationship to Underlying Unit	Lithology	Thickness (m)	Depositional Setting	Current Stratigraphic Correlations
Wallumbilla Formation	Barremian-Albian	Conformable	Marine siltstone, claystone, labile sandstone	6 – 156	Shallow marine	Wallumbilla Formation (E, S, C)
Gilbert River Formation	Aptian (U–Pb DZ)	Conformable	Medium- to coarse-grained sandstones, pebble conglomerates, minor siltstone	16 – 105	High-energy braided fluvial, mixed aeolian/braided fluvial	Cadna-owie Formation (E), Gilbert River Formation (E, C), Bungil Formation (S)
Hooray Sandstone	Barremian (U–Pb DZ)	Unconformable	Medium- to very coarse-grained sandstone, minor conglomerate, siltstone	18	High-energy braided fluvial, paludal	Gubberamunda Sandstone-Orallo Formation-Mooga Sandstone (S), Gilbert River Formation (E)
Injune Creek Group	Oxfordian-Tithonian (U–Pb DZ)	Unknown	Fine- to medium-grained sandstones, interbedded siltstones/sandstones, siltstone	33	Low-energy fluvial, lacustrine	Injune Creek Group (S), Ronlow beds, Blantyre Sandstone (in part) (E)
Blantyre Sandstone	Bajocian-Bathonian (palynology)	Unconformable	Medium- to very coarse-grained sandstone, pebble-cobble conglomerates, mudstones	76 – 184	High-energy braided fluvial	Upper Evergreen Formation-Hutton Sandstone-lower Injune Creek Group (E, S), Hampstead Sandstone (C)
Hutton Sandstone	Aalenian-Callovian (palynology; U–Pb geochronology)	Unconformable	Fine- to coarse-grained, quartzose sandstone, pebble conglomerates, minor mudstone	142	Fluvial, lacustrine (paludal)	Hutton Sandstone (S), Blantyre Sandstone (in part) (E)
Moolayember Formation	Anisian-Carnian (palynology; AFT)	Conformable	Fine- to medium-grained sandstone, claystone, siltstone, coal, minor limestone, conglomerate, tuff bands	150	Fluvial, lacustrine	Warang Sandstone (in part; G), Moolayember Formation (G, B)
Warang Sandstone	Upper Triassic (U–Pb DZ)	Unconformable	White, medium- to coarse-grained, kaolinitic sandstones, minor claystone	<340	High-energy braided fluvial	Upper Clematis Group, lower Moolayember Formation (G, B)
Porcupine Gorge Formation	Upper Triassic (U–Pb DZ)	Unconformable	Fine- to coarse-grained sandstone, pebble conglomerate, weathered interbedded mudstone/sandstone	18	High-energy braided fluvial, palaeosol	Glenidal Formation (Clematis Group) (B)
Betts Creek beds	upper Permian (U–Pb DZ; palynology)	Unconformable	Medium- to coarse-grained sandstone, pebble conglomerate, carbonaceous claystone/siltstone, coal	46 – 366	Alluvial/coastal-plain	Betts Creek Group, Bandanna Sandstone, Colinlea Sandstone (G)

Formation of the Eromanga Basin is similarly debated. The difficulty in determining the exact formation mechanism of the eastern Australian basins is exacerbated by uncertainty in the position of the eastern Australian plate margin during the Jurassic and Early Cretaceous. Often widely regarded as an intracratonic sag basin, the Eromanga Basin has also been interpreted to be a back-arc basin (Matthews et al., 2011), or a retro-arc foreland basin in an effort to account for accelerated subsidence curves (Gallagher, 1990; Tucker et al., 2016). This latter hypothesis would suggest placement of the subduction zone of the eastern margin proximal to the present-day coastline; however, no evidence for foreland tectonics has been observed eastward of the Eromanga Basin in the Surat or Clarence-Moreton basins, casting doubt on this interpretation. Other authors have instead interpreted that the margin's position was much further to the east and suggested that basin subsidence was a result of failed incipient rifting (e.g. Fielding, 1996; Yago and Fielding, 1996). Other mechanisms invoked to account for subsidence in the Eromanga Basin include thermal contraction of the lithosphere (Gallagher and Lambeck, 1989), deep crustal metamorphism (Middleton, 1980), and subduction-related dynamic platform tilting (Gallagher, 1990; de Caritat & Braun, 1992; Gallagher et al., 1994; Russell & Gurnis, 1994; Gurnis et al., 1998; Waschbursch et al., 2009). Individually, none of these models is able to fully explain the evolution of the Eromanga Basin, and so a complex combination of these models is considered more likely (Waschbursch et al., 2009).

Local Geology and Stratigraphy

A well-exposed transect through the Galilee and Eromanga basin successions is accessible on the north-eastern margin of these basins in the deeply incised Porcupine Gorge, ~65 km north of the town of Hughenden in North Queensland. The 25 km long and 100-150 m deep gorge reveals a ~350 m thick succession of southerly-dipping Permian to Cretaceous sedimentary strata (Fig. 1b; Fig. 2; Table 1) (Ch. 2; Ch. 3). The succession unconformably overlies

Precambrian basement rocks mapped as the Cape River Metamorphics, which are exposed in the northernmost reaches of the gorge. Miocene to Pleistocene basalt flows of the Sturgeon Sub-province cap the sedimentary sequence and are responsible for the formation of the steep-walled cliffs of the gorge. The Galilee and Eromanga basin deposits are also recorded in stratigraphic drill cores from the Geological Survey of Queensland (GSQ) in the Hughenden region in GSQ Hughenden 1-2R, 3-4R, 5, 6 and 7 (Fig. 1c).

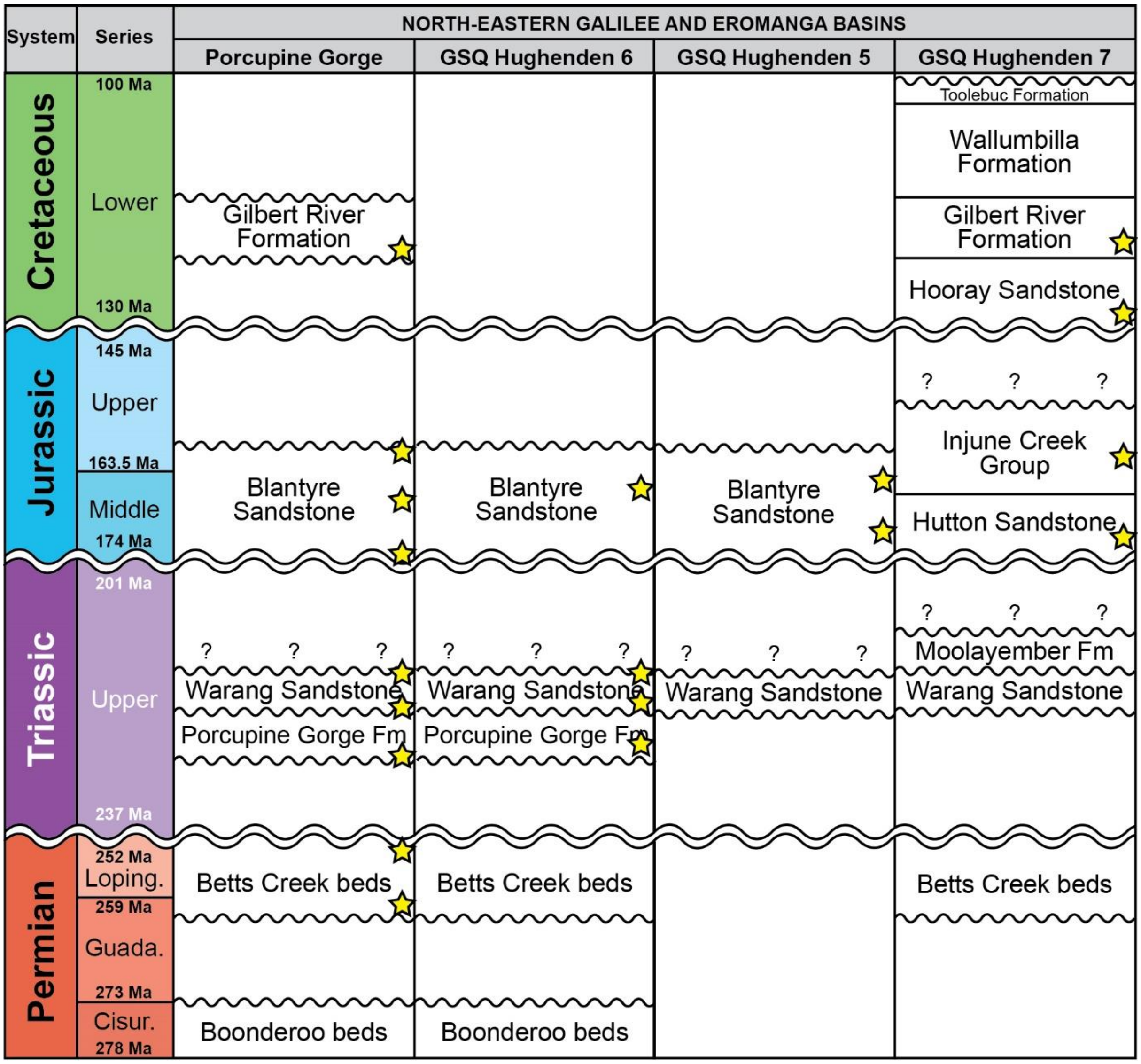

Figure 2 – Local stratigraphy of the Hughenden area compiled from Gray (1977), Balfe (1979) and Chapter 2. Yellow stars indicate where detrital zircon samples were collected.

Methods

Fieldwork

Detailed sedimentological and stratigraphic analysis was undertaken in Porcupine Gorge National Park between 2014 and 2017. Nine stratigraphic sections were measured (Appendix 4) where palaeocurrent measurements were collected and fluvial facies and architectural element analyses were undertaken to establish relationships between sedimentary petrology, alluvial architecture, and palaeo-dispersal directions. A total of 235 palaeocurrents were collected, including 12 from the Betts Creek beds, 29 from the Porcupine Gorge Formation, 76 from the Warang Sandstone, and 118 from the Blantyre Sandstone. Details of the fluvial facies and architecture exposed in cliff facies throughout the gorge are in Chapter 3.

Pebble Counts

Pebble counts were conducted on nine conglomerate intervals from three formations in Porcupine Gorge: two in the Betts Creek beds, four in the lower Blantyre Sandstone, and three in the upper Blantyre Sandstone (Appendix 5). No accessible conglomerates were encountered in either the Warang Sandstone or the Porcupine Gorge Formation in outcrop. The counts were achieved by placing a 50 cm x 50 cm grid over the conglomeratic interval and counting all clast types in each grid square to reduce bias.

Table 2 – Pebble count locations and total pebbles counted from the nine conglomerates in Porcupine Gorge. GPS coordinates given in WGS-84.

Formation	Coordinates	Total Pebbles Counted
Betts Creek beds	20° 19’ 45.89” S, 144° 28’ 7.70” E	64
	20° 19’ 45.25” S, 144° 28’ 6.87” E	159
Lower Blantyre Sandstone	20° 21’ 6.62” S, 144° 27’ 55.44” E	175
	20° 21’ 7.12” S, 144° 28’ 2.85” E	186
	20° 21’ 40.67” S, 144° 27’ 42.70” E	128
	20° 21’ 15.53” S, 144° 27’ 58.94” E	163
Upper Blantyre Sandstone	20° 24’ 31.38” S, 144° 26’ 12.22” E	384
	20° 24’ 31.31” S, 144° 26’ 12.31” E	137
	20° 24’ 4.94” S, 144° 26’ 23.82” E	315

Sandstone Petrography

Sampling

A total of 26 samples were collected from Porcupine Gorge and nearby cores, and standard thin sections were produced from these for sandstone petrography. Twenty-two samples were collected from Porcupine Gorge: two from the basal sandstone of the Porcupine Gorge Formation, three from the bottom and two from the top of the Warang Sandstone, and fifteen from different units in a section through the Blantyre Sandstone (Table 3). From core, a further four samples were collected (Table 3): two from the Blantyre Sandstone in GSQ Hughenden 5 at 104 m (H5B21) and 60 m depth (H5B21), one from the Porcupine Gorge Formation in GSQ Hughenden 6 at 200 m depth (H6B47), and one from the Hutton Sandstone in GSQ Hughenden 7 at 363 m depth (H7B107).

Analysis

Using a transmitted light-polarising microscope, the 26 thin sections were point counted using a modified Gazzi-Dickinson method to minimise compositional dependence on the grain size of each sample (Dickinson et al., 1983; Ingersoll et al., 1984). A total of 350 individual grains were counted in each thin section to ensure a valid statistical representation of their lithological composition. The total number of quartz (Q), feldspar (F), and lithic (L) grains were counted and plotted on QFL ternary diagrams to determine the sandstone classification after Folk (1974). These same samples were also plotted on QFL and QmFLt (monocrystalline quartz, feldspars, total lithics) ternary diagrams overlain with the tectonic field indicators from Dickinson et al. (1983) to establish possible provenance terranes. Textural and compositional maturity was determined for each sample based on the QFL proportions, and grain size, rounding, and sorting.

Table 3 – Outcrop detrital zircon and sandstone petrography samples from Porcupine Gorge and drill cores, and their associated coordinates, in stratigraphic order. Samples collected for thin section analysis are given in grey. GPS datum = WGS-84.

Sample Location	Sample	Formation	Age	Coordinates
Porcupine Gorge	Wall1	Gilbert River Formation	Early Cretaceous	20° 24' 31.33" S, 144° 26' 11.81" E
	GR1A	Blantyre Sandstone	Mid–Late Jurassic	20° 24' 31.33" S, 144° 26' 11.81" E
	GR1B			20° 24' 31.33" S, 144° 26' 11.81" E
	GRF-TS2			20° 24' 31.25" S, 144° 26' 13.6" E
	GRF-TS1			20° 24' 31.26" S, 144° 26' 13.87" E
	GRF01			20° 24' 31.36" S, 144° 26' 12.32" E
	BGR-TS1			20° 24' 14.29" S, 144° 26' 14.77" E
	BGR01			
	21/05/14-4			20° 20' 59.65" S, 144° 27' 47.88" E
	21/05/14-3			20° 20' 59.82" S, 144° 27' 48.01" E
	21/05/14-2			20° 21' 0.8" S, 144° 27' 48.34" E
	19/05/14-3			20° 20' 58.94" S, 144° 27' 45.89" E
	19/05/14-2			20° 20' 57.83" S, 144° 27' 47.77" E
	BSS-TS2			20° 21' 1.29" S, 144° 25' 50.81" E
	BSS-TS1			20° 21' 0.13" S, 144° 27' 49.63" E
	BSS-2004			20° 22' 28.19" S, 144° 27' 15.96" E
	B1A			20° 21' 15.01" S, 144° 27' 57.93" E
	B1B			20° 21' 15.01" S, 144° 27' 57.93" E
	B1C			20° 21' 15.01" S, 144° 27' 57.93" E
	BSSRhy			20° 22' 0.31" S, 144° 27' 32.41" E
	W1A	Warang Sandstone	Late Triassic	20° 21' 0.64" S, 144° 27' 57.85" E
	W1B			20° 21' 0.64" S, 144° 27' 57.85" E
	WSS-Top			20° 21' 5.16" S, 144° 27' 59.98" E
	WSS-0409			20° 20' 7.67" S, 144° 28' 8.84" E
	WSS-2908			20° 20' 7.26" S, 144° 28 '8.73" E
	WSS-2908			
	WSS-TS1			20° 20' 6.45" S, 144° 28' 8.63" E
	WSS-TS2			20° 21' 3.92" S, 144° 27' 57.56" E
	PGF01	Porcupine Gorge Formation		20° 20' 6.91" S, 144° 28' 8.48" E
	PGF-TS1			
	PGF-TS2			20° 20' 6.57" S, 144° 28' 8.18" E
	BCTuff01	Betts Creek beds	late Permian	20° 19' 58.22" S, 144° 28' 15.45" E
	BCB01			20° 19' 38.58" S, 144° 28' 4.53" E
GSQ Hughenden 5	H5B5	Blantyre Sandstone	Mid–Late Jurassic	20° 37' 60.00" S 144° 24' 0.00" E
	H5B7			
	H5B21			
	H5B21			
GSQ Hughenden 6	H6B8	Blantyre Sandstone		20° 20' 48.77" S 144° 27' 11.60" E
	H6B26	Warang Sandstone	Late Triassic	
	H6B38			
	H6B47	Porcupine Gorge Formation		
	H6B47			
GSQ Hughenden 7	H7B55	Gilbert River Formation	Early Cretaceous	20° 56' 60.00" S 144° 10' 60.00" E
	H7B59	Hooray Sandstone		
	H7B66	Injune Creek Group	Late Jurassic	
	H7B101	Hutton Sandstone	Mid Jurassic	
	H7B107			

U–Pb Detrital Zircon Geochronology

Nineteen detrital zircon samples were collected in the Hughenden region from outcrop and the three nearby stratigraphic cores. Sample locations are detailed in Tables 3. In Porcupine Gorge, two samples were collected from the Betts Creek beds, one from the Porcupine Gorge Formation, three from the Warang Sandstone, three from the Blantyre Sandstone and one from the Gilbert River Formation. Zircons from a rhyolite cobble out of a conglomerate unit in the lower Blantyre Sandstone (BSSRhy) in Porcupine Gorge were also dated using U–Pb zircon geochronology. In GSQ Hughenden 5, two samples of the Blantyre Sandstone were collected: H5B21 at 105 m and H5B5 at 60 m depth. In GSQ Hughenden 6, one sample was collected from the Porcupine Gorge Formation (H6B47; 199 m), two from the Warang Sandstone at 169 m (H6B38) and 120 m (H6B26), and one from the Blantyre Sandstone (H6B8; 53.5 m). In GSQ Hughenden 7, one sample was collected from each of the Hutton Sandstone (H7B101; 341 m), Injune Creek Group (H7B66; 230 m), Hooray Sandstone (H7B59; 198 m) and Gilbert River Formation (H7B55; 184 m). Mineral separation and analytical methods (including instrument set-up) for these samples are found in Chapter 2.

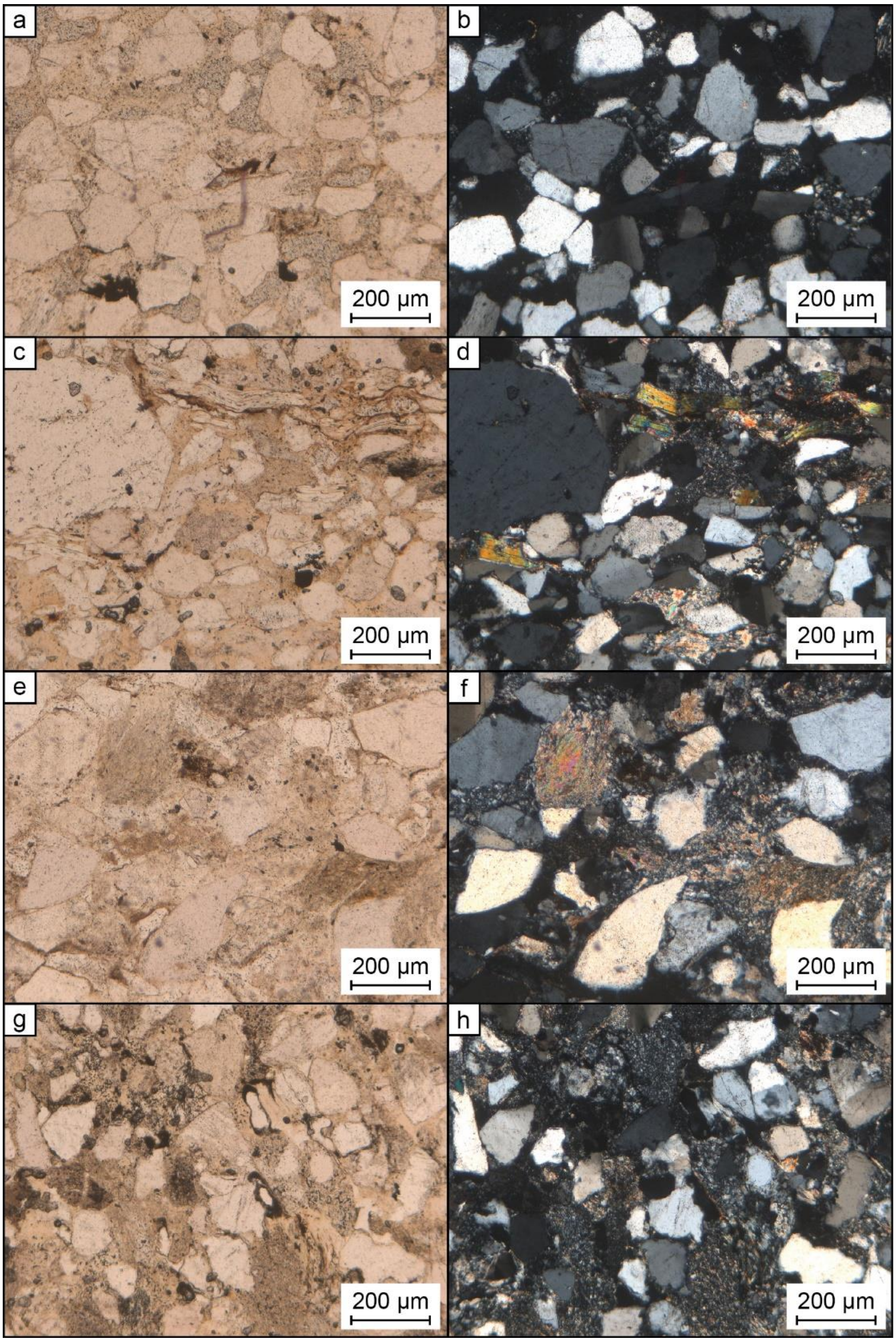

Figure 3 – Examples of the thin sections from the Triassic and Jurassic sandstones from the Hughenden area. (a) and (b), plane-polarised light (PPL) and cross-polarised light (XPL) images of the Upper Jurassic upper Blantyre Sandstone (GRF01; outcrop). (c) and (d), PPL and XPL of the Middle Jurassic Hutton Sandstone (H7B107; GSQ Hughenden 7). (e) and (f), PPL and XPL of the Upper Triassic Warang Sandstone (WSS-TS2; outcrop). (g) and (h), PPL and XPL of the Upper Triassic Porcupine Gorge Formation (PGF-TS2; outcrop).

Results

Palaeocurrent Analysis

Palaeocurrent measurements taken in Porcupine Gorge indicate a predominantly southerly flow direction (varying from south-east to south and south-west) from the upper Permian Betts Creek beds, Porcupine Gorge Formation, Warang Sandstone, and lower Blantyre Sandstone (Fig. 4; Appendix 6). Palaeocurrents were also measured by Allen and Fielding (2007a) from their study of the Betts Creek beds, where vector means of 142° in trough cross-beds of a conglomerate, and 198° and 188° from trough cross-beds in sandstone were calculated. In the upper Blantyre Sandstone palaeocurrent measurements become much more variable, shifting from south to south-east to south-west to north-west and finally to north-east (Fig. 4).

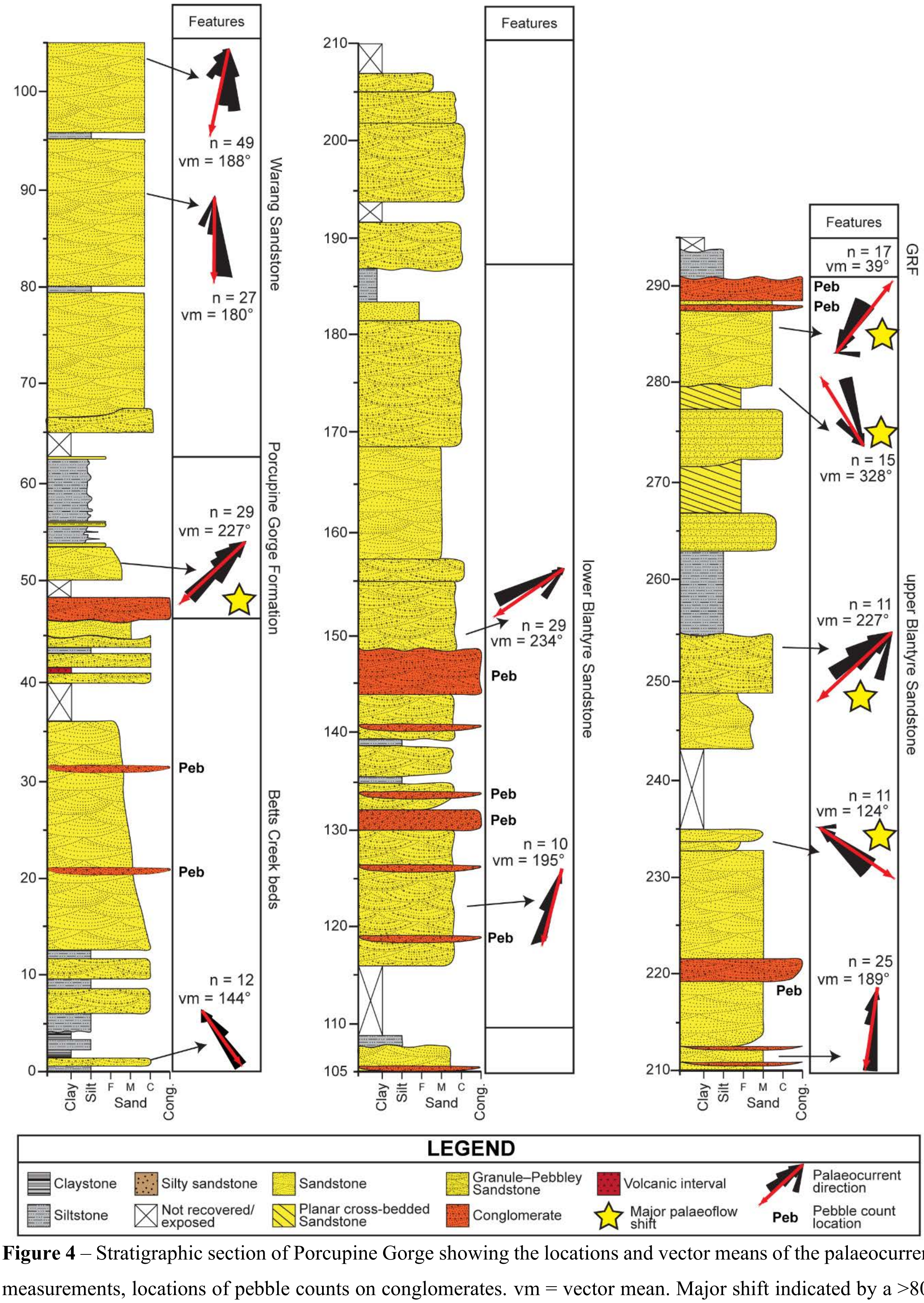

Figure 4 – Stratigraphic section of Porcupine Gorge showing the locations and vector means of the palaeocurrent measurements, locations of pebble counts on conglomerates. vm = vector mean. Major shift indicated by a >80° variation.

Pebble Counts

Conglomerates deposited in Porcupine Gorge include a diverse suite of clast types from nearby terranes (Table 4). Pebble counts in the Betts Creek beds are dominated by vein quartz and quartzite (50–86%) with subordinate recycled sandstone (8–16%), rhyolite (3–23%) and minor weathered granite, intraformational mudstone and chert (<5% each). The clasts in the lower Blantyre Sandstone are also dominated by vein quartz and quartzite (43–54%) with abundant rhyolite (34–38%), subordinate chert (6–11%), and minor intraformational mudstones (2–5%), recycled sandstone (2–3%) and weathered granite (1–2%). The upper Blantyre Sandstone is generally much more quartz rich, specifically vein quartz (54–96%), with varying abundance of rhyolite (1–44%) and rare chert and recycled sandstones (1% each).

Table 4 – Conglomerate clast types and possible source terranes from the Betts Creek beds and lower and upper Blantyre Sandstone in Porcupine Gorge.

Clast Type	Description	Likely Source Terranes
Vein quartz	White quartz	Carbo-Permian Kennedy Igneous Association
Metamorphic quartz/quartzite	White to grey quartzite	Precambrian Cape River Metamorphics (basement)
Rhyolite	Red or white, flow-banded or massive, commonly slightly weathered	Kennedy Igneous Association
Weathered granite	K-feldspar, quartz, and biotite-rich granite	Kennedy Igneous Association
Recycled sandstone	White to yellow, medium- to coarse-grained sandstone	Recycled Palaeozoic to Mesozoic basin rocks
Black chert	Opaque, massive, black chert	Volcanic origin – Kennedy Igneous Association
Intraformational mudstone	Grey to white mudstone	Recycled intraformational channel-bank mudstones – Palaeozoic to Mesozoic strata

Sandstone Petrography Results and Interpretation

Sandstone Classification

All 26 sandstone petrography samples from the Hughenden region are typically angular or sub-angular to sub-rounded and poorly to moderately sorted with grains ranging in size from fine sand to very coarse sand (texturally immature to mature; with maturity generally increasing up section). Quartz is the dominant mineral (81–97%) across all samples but is most abundant in the upper Blantyre Sandstone samples (Fig. 5). Feldspars are sparse (0.5–15%), occurring as equal parts K-feldspar and plagioclase crystals or dominated by K-feldspar (microcline). Lithic fragments are of rare to minor abundance (0–8%) in all samples and are mostly composed of sandstone or metasedimentary grains with a very rare lithic volcanic component (<0.1%) observed in only two samples (BSS-TS1 and H7B107). Muscovite and biotite micas are typically present as accessory minerals, becoming less abundant in the upper Blantyre Sandstone samples. The cement, where present, is dominated by chert, but quartz overgrowths and Fe-oxide are locally abundant in some samples (e.g. BSS-TS1 and B1A, respectively). Matrix is present at low abundances (<20%), but weathering of the feldspars has contributed to the formation of pseudomatrix in some samples.

The quartz fraction is dominated by monocrystalline (Qm) grains (50–75%), some of which display an undulose extinction, indicative of a metamorphic protolith. Polycrystalline quartz (Qp) is also strongly represented in total quartz (25–50%), which is consistent with a nearby metamorphic and/or plutonic source (e.g. basement terrane Cape River Metamorphics and the foliated granites of the Ravenswood and Lolworth batholiths).

In thin section, most feldspar grains are highly weathered and show significant alteration in the form of sericitisation or kaolinitisation which gives many of the rock units, particularly the Betts Creek beds and Warang Sandstone, a distinctive waxy feel in hand specimen. The kaolinitisation is not as apparent in core samples; however, there is no significant difference in the amount of weathering observed between thin sections from outcrop and core, indicating that weathering may also have taken place shortly after deposition and prior to, or during, burial.

The rare to minor abundance of metasedimentary lithic grains in thin section suggests a nearby metamorphic source, which is most likely the Cape River Metamorphics. Volcanic lithic grains, associated with the Kennedy Igneous Association to the east, are incorporated in many samples but in very low abundance (<0.1%). This assertion of rarity is contradicted by the high abundance of volcanic pebbles and cobbles within the conglomerates of the Betts Creek beds and Blantyre Sandstone, up to 44% in some samples, which suggests significant volcanic input into these units. This discrepancy may indicate high levels of chemical weathering or diagenesis has taken place and converted these volcanics to clay. These processes would then increase the ratio of pseudomatrix in the samples to be higher than currently measured.

Dickinson et al. (1983) and Weltje and von Eynatten (2004) highlighted some of the challenges of determining the correct sandstone classification and, therefore, the most accurate tectonic provenance fields of strongly quartzose samples, such as those presented herein. Most relevant to this study, however, are the local sedimentological factors, including climate (chemical weathering) and mechanical transport, that are known to modify sandstone modal compositions by preferentially weathering and removing feldspar and lithic grains prior to and even long after their deposition. Weathering of these grains seems to have taken place, in part during deposition. Given the humid, temperate climate that existed throughout the Middle Triassic–Early Jurassic (Grant-Mackie et al., 2000; McKellar, 2004; Turner et al., 2009). However following deposition, diagenesis is interpreted to have had a greater influence on the feldspar and volcanic lithic fractions. This is interpreted to have skewed the QFL results towards more quartzose compositions. The presence of distinctive domains of pseudomatrix and abundant chemical weathering of existing feldspar and lithic grains supports this assertion.

The QFL plots show a slightly higher proportion of lithics within the Porcupine Gorge Formation and Warang Sandstone, with these samples plotting on the boundary between the subarkose and sublitharenite fields of Folk (1974) (Fig. 5a). In the lower Blantyre Sandstone and Hutton Sandstone, the sections are less lithic-rich and more feldspathic, with most samples plotting in the subarkose field (Fig. 5d). The upper Blantyre Sandstone samples are the most quartzose, plotting on the boundary between subarkose and quartzarenite or within the quartzarenite field (Fig. 5d).

Tectonic Provenance

When the samples are plotted on QFL diagrams overlain by the tectonic fields of Dickinson et al. (1983) (Fig. 5b, e), five of the eight Porcupine Gorge Formation and Warang Sandstone samples plot within the recycled orogen field, with the remaining three approaching a craton interior signal. In contrast, the Blantyre and Hutton sandstones plot mostly within the craton interior field. The QmFLt diagrams show a different story (Fig. 5c, f), with all 26 samples now plotting within the recycled orogen fields of Dickinson et al. (1983), with no apparent correlation with age. Despite a strong metamorphic source indicated by the high percentage of Qp grains and the undulose extinction of the Qm grains, which is consistent with a recycled orogen or cratonic interior source, the intense weathering of the feldspars and lithics in these samples is likely masking much of the Kennedy Igneous Association signature observed in the pebble counts, and therefore the recycled magmatic arc provenance. Hence, making tectonic provenance interpretations based on these samples should be considered tenuous at best due to the effects of diagenesis documented in this study. However, the sandstone petrography still provides a reasonably clear picture of the provenance that suggests a primary metamorphic source in the North Australian Craton to the north of the study area (the Cape River Metamorphics), and secondary magmatic source from the Tasmanides to the east (the Kennedy Igneous Association). This is generally consistent with the palaeocurrent data, but detrital zircon geochronology is necessary to test and refine this interpretation.

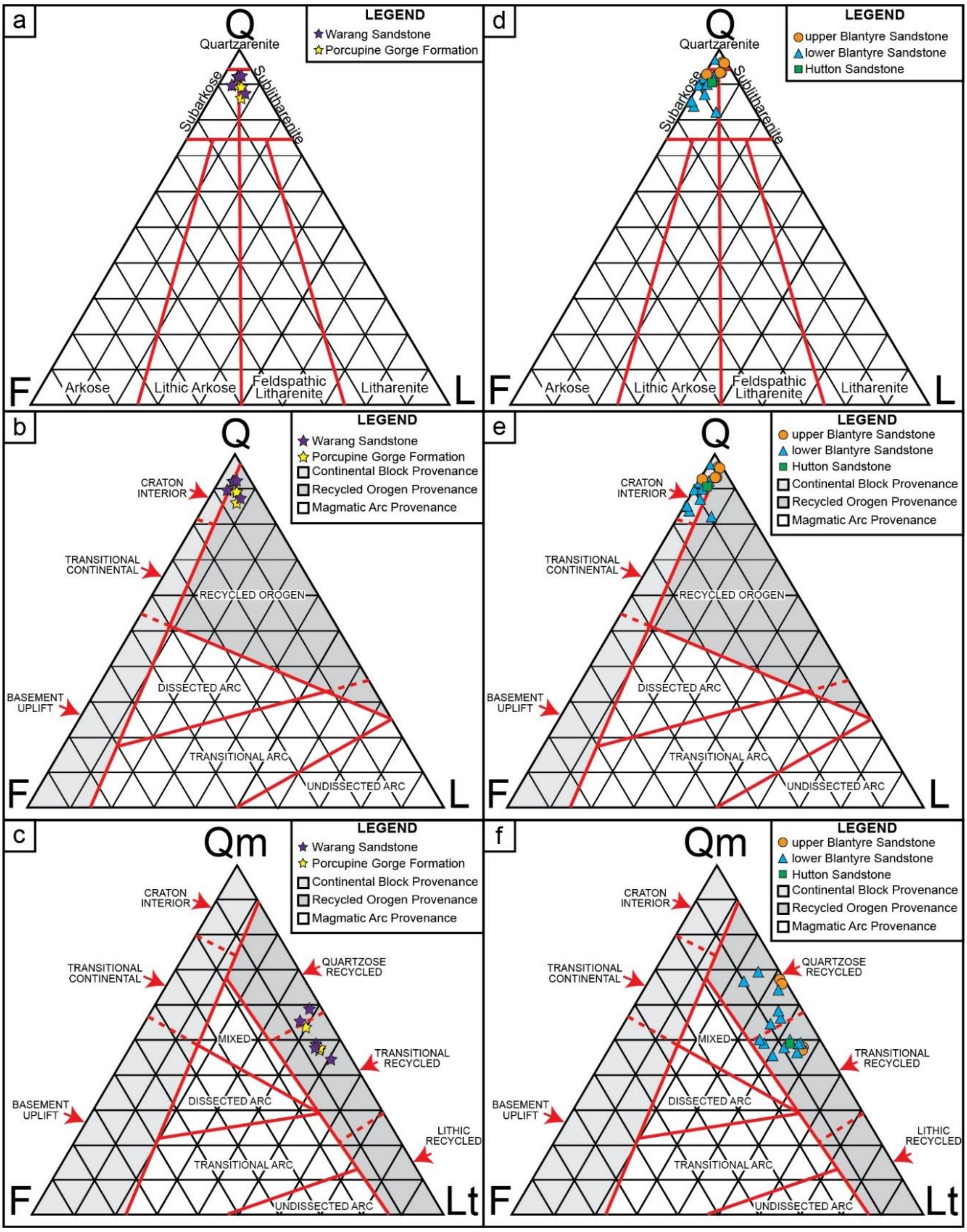

Figure 5 – (a) QFL sandstone classifications for the Porcupine Gorge Formation and the Warang Sandstone, (b) QFL diagram for the Porcupine Gorge Formation and Warang Sandstone with tectonic overlay, (c) QmFLt diagram for the Porcupine Gorge Formation and Warang Sandstone, (d) QFL sandstone classifications for the Hutton Sandstone and Blantyre Sandstone, (e) QFL diagram for the Hutton Sandstone and Blantyre Sandstone, (f) QmFLt diagram for the Hutton Sandstone and Blantyre Sandstone. Sandstone classifications are overlain with fields after Folk (1974); all QFL and QmFLt diagrams with overlain tectonic fields are after Dickinson et al. (1983).

U–Pb Detrital Zircon Geochronology

A total of 1682 concordant grains were analysed from the 19 detrital zircon samples collected from both core (n=10) and outcrop (n=9) in the Hughenden region. The spectra for each formation are in Fig. 6, separated by their study localities, and arranged into stratigraphic order. The samples are then clustered into their individual formations, which are further clustered into their corresponding time periods to establish provenance evolution in the region from the Permian to the Cretaceous. The relative probability plots for each individual period, as well as a composite spectrum, are shown in Fig. 7.

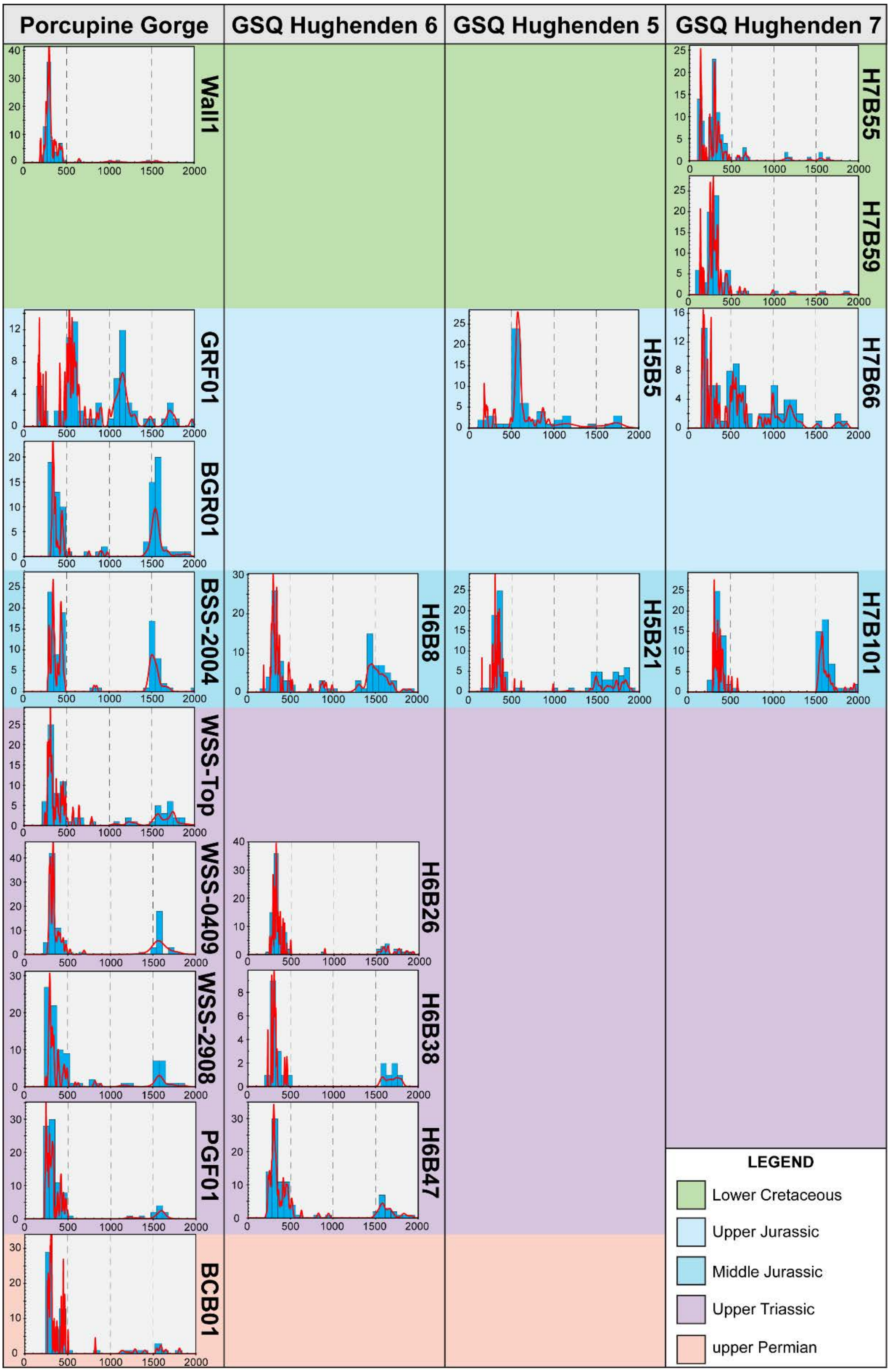

Figure 6 – Detrital zircon frequency distribution plots for all 19 samples from each of the separate locations in the Hughenden area (left to right represents N to S), arranged in stratigraphic order (youngest at the top, oldest at the bottom). Age on x-axis given in Ma, y-axis = frequency.

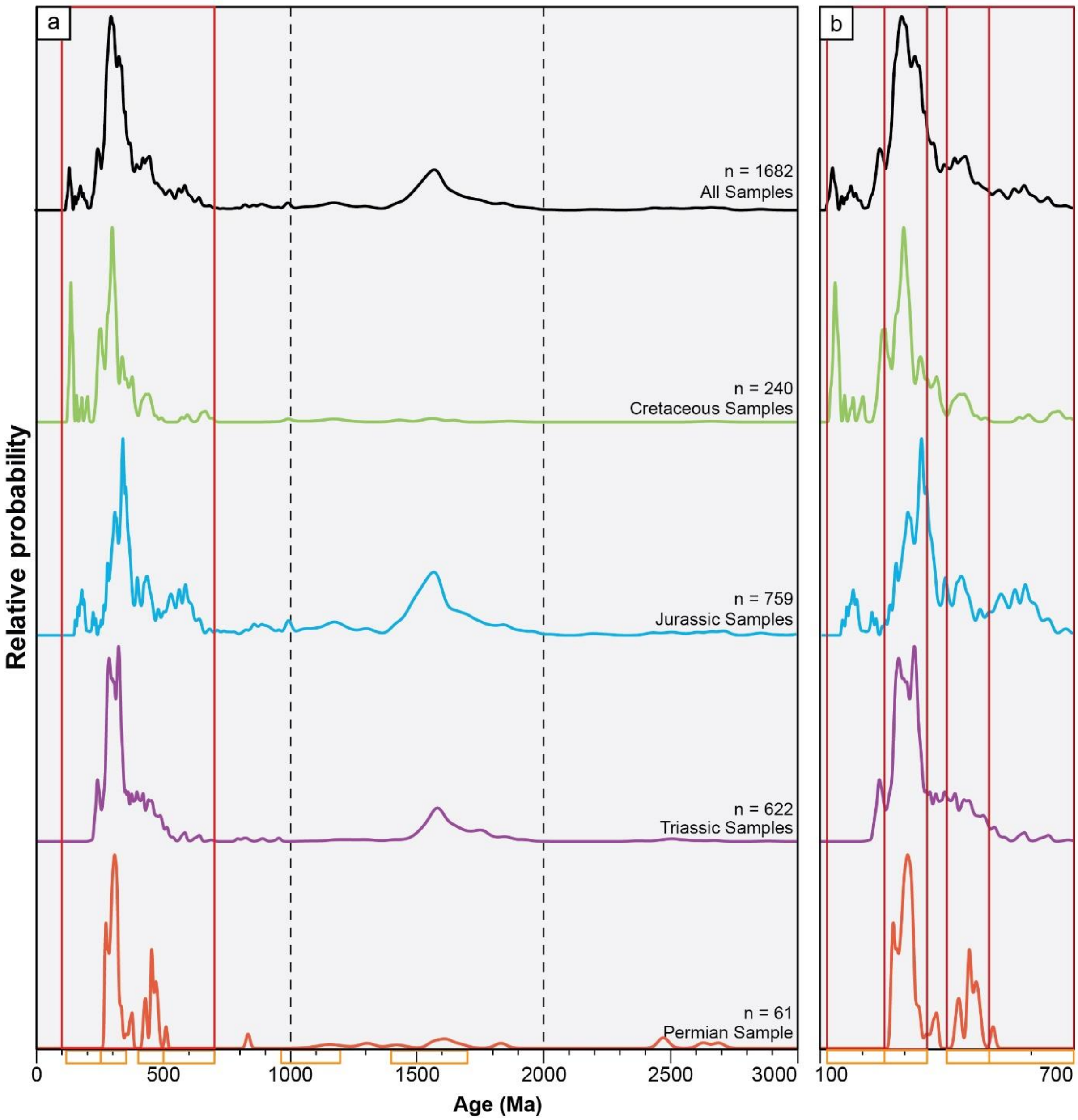

Figure 7 – Relative probability detrital zircon histograms combining all samples from each age group from the Hughenden area, to outline the evolution and change of detrital zircon populations from the Permian to the Cretaceous. (a) A composite relative probability plot for all samples in the Hughenden area illustrates the bimodal distribution in the detrital zircon spectrum. Orange boxes indicate main population ranges. (b) A close up of the 100-700 Ma spectra to compare populations across the different time periods.

The upper Permian Betts Creek beds sample (61 concordant grains) yielded a primary zircon population that clusters between 320–280 Ma, along with a minor age cluster between

450–400 Ma, and a small number of Proterozoic and Archean grains. A total of 181 concordant analyses were obtained from the Upper Triassic Porcupine Gorge Formation, along with an additional 441 concordant analyses on the Upper Triassic Warang Sandstone. In each sample primary zircon populations at 320–280 Ma and 1700–1400 Ma are present. A much smaller peak between 500–400 Ma is also evident in some of these samples. The Middle Jurassic Blantyre and Hutton sandstones (combined 543 concordant grains) showed the same two dominant peaks at 320–280 Ma and 1700–1400 Ma. However, in the Upper Jurassic Injune Creek Group and the upper Blantyre Sandstone samples (216 concordant grains combined), the 320–280 Ma and 1700–1400 Ma peaks are absent, and instead replaced by peaks at 1200–1000 Ma and 600–500 Ma. In one core sample from the upper Blantyre Sandstone (H5B5) the 1200–1000 Ma peak is much more subdued in comparison to the other two samples. A comparison of Middle and Upper Jurassic samples is shown in Figure 8. The Lower Cretaceous Hooray Sandstone and Gilbert River Formation samples yielded 240 concordant grains that are dominated by a primary peak clustered between 320–280 Ma, along with a second strong peak between 200–100 Ma. Syn-depositional Mesozoic populations were also recognised in Triassic to Cretaceous Hughenden samples PGF01, H7B66, H7B59, and H7B55. These populations are between 250–225 Ma, 180–160 Ma, 155–150 Ma, and 135–120 Ma (Fig. 6, 7b).

A Kolmogorov-Smirnov test (K-S test) was run (Table 5; Fig. 10) to compare the relative similarities across all samples. Samples are considered to be similar with a p-value of >0.05. Samples from the Betts Creek beds, Porcupine Gorge Formation, Warang Sandstone, Hutton Sandstone and lower Blantyre Sandstone (with two exceptions) generally show very strong correlations to each other. The upper Blantyre Sandstone and Injune Creek Group samples share few to no similarities with the other samples or to each other. The Hooray Sandstone and

Gilbert River Formation samples are all similar to each other, as well as similar to one of the Porcupine Gorge Formation samples (PGF01).

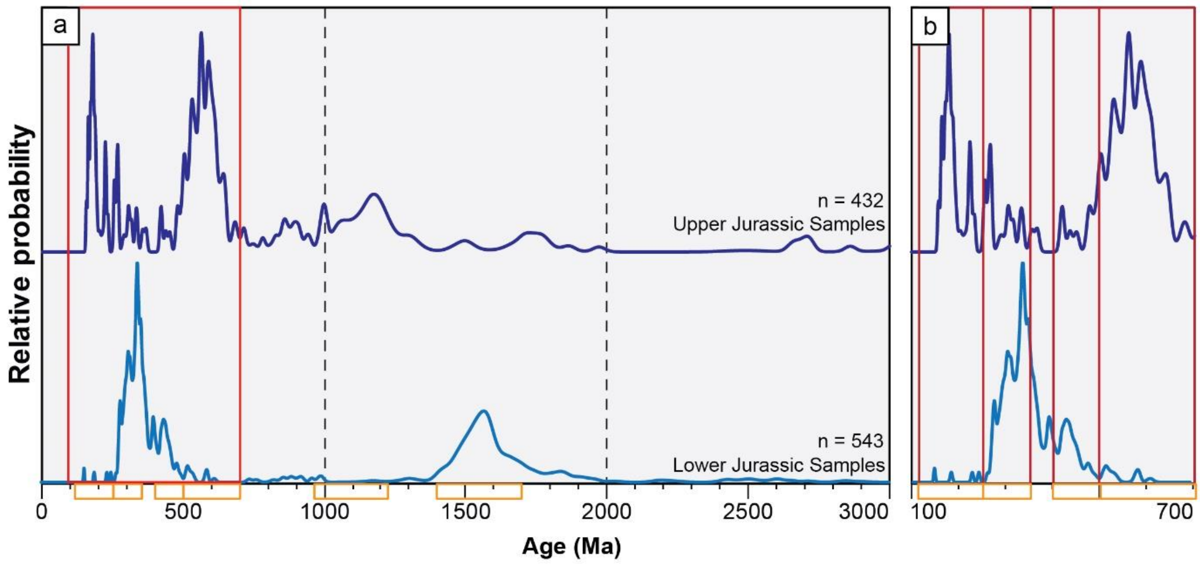

Figure 8 – Relative probability detrital zircon histograms of the Jurassic (Middle and Upper Jurassic) from the Hughenden region. Orange boxes indicate main population ranges. (a) Shows spectra from 0–3000 Ma. (b) Shows a close-up of the 100–700 Ma interval to compare populations.

Rhyolite Cobble Zircon Geochronology

Thirty zircon grains were analysed from a large rhyolitic cobble collected from a single conglomerate, approximately 8 m above the base of the lower part of the Blantyre Sandstone (118 m; Fig. 4). A single grain at 188.0 ± 6.3 Ma was excluded from further analysis as the age was considered too young, and likely a product of Pb-loss in the system. A cluster of three grains between 267–271 Ma was eliminated for the same reason. Six grains with dates between 459.9 ± 10.9 Ma and 2117.7 ± 42.3 Ma were excluded for being too old and a result of inheritance or recycling within the magma chamber. The remaining 20 grains ranged from 278–312 Ma, with a weighted mean calculated at 293.5 ± 4.2 Ma and the largest cluster of grains occurring between 285–300 Ma (Fig. 9).

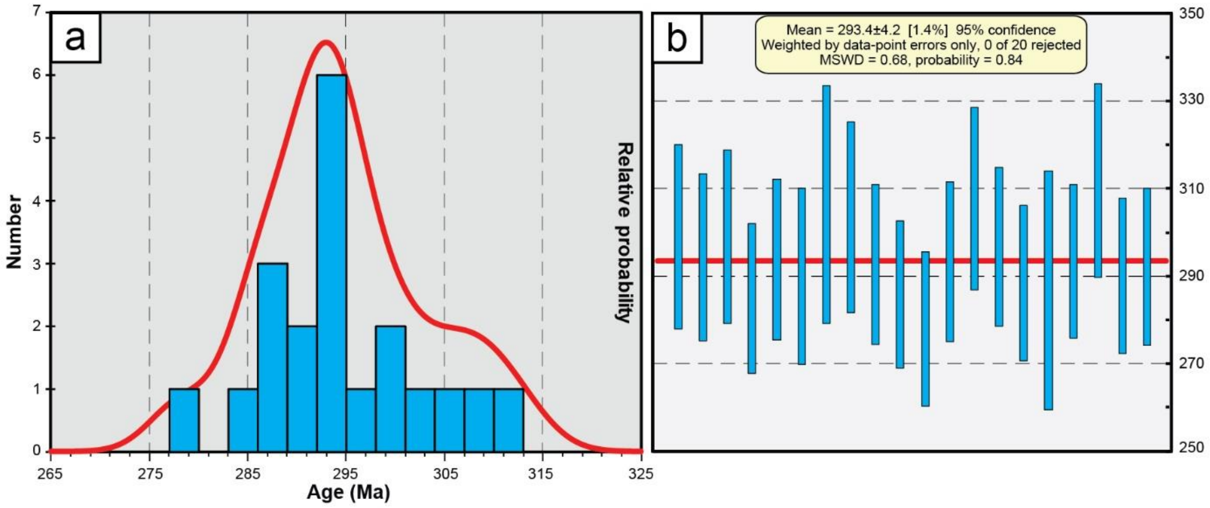

Figure 9 – (a) Probability density chart and (b) weighted average for the youngest grain population for the rhyolite cobbles found within the lower Blantyre Sandstone.

Table 5 – Kolmogorov-Smirnov Test results for all samples from the Hughenden region (core and outcrop). Results show that the upper Permian to Middle Jurassic samples generally share strong similarities with each other, the Upper Jurassic samples share few or no similarities with themselves or other samples, and the Lower Cretaceous samples are generally similar to one another. Cells highlighted indicate samples considered statistically significant (P>0.05).

K-S P-values using error in the CDF																			
	BCB01	PGF01	H6B47 (PGF)	WSS-2908	WSS-0409	H6B38 (WSS)	H6B26 (WSS)	WSS Top	BSS-2004	H6B8 (BSS)	H7B101 (Hutton)	H5B21 (BSS)	BGR01 (BSS)	H5B5 (BSS)	H7B66 (ICG)	GRF01 (BSS)	H7B59 (Hooray)	H7B55 (GRF)	Wall1 (GRF)
BCB01		0.030	0.975	0.993	0.481	0.010	0.177	0.373	0.000	0.001	0.000	0.022	0.000	0.000	0.000	0.000	0.002	0.000	0.005
PGF01	0.030		0.048	0.004	0.003	0.000	0.002	0.001	0.000	0.000	0.000	0.000	0.000	0.000	0.000	0.000	0.523	0.005	0.506
H6B47 (PGF)	0.975	0.048		0.820	0.723	0.011	0.147	0.451	0.001	0.000	0.000	0.047	0.000	0.000	0.000	0.000	0.000	0.002	0.001
WSS-2908	0.993	0.004	0.820		0.884	0.012	0.162	0.427	0.000	0.001	0.000	0.067	0.000	0.000	0.000	0.000	0.000	0.000	0.001
WSS-0409	0.481	0.003	0.723	0.884		0.036	0.307	0.310	0.001	0.004	0.001	0.106	0.000	0.000	0.000	0.000	0.000	0.000	0.000
H6B38 (WSS)	0.010	0.000	0.011	0.012	0.036		0.000	0.129	0.015	0.040	0.874	0.385	0.114	0.000	0.000	0.000	0.000	0.000	0.000
H6B26 (WSS)	0.177	0.002	0.147	0.162	0.307	0.000		0.002	0.000	0.000	0.000	0.011	0.000	0.000	0.000	0.000	0.000	0.000	0.000
WSS Top	0.373	0.001	0.451	0.427	0.310	0.129	0.002		0.033	0.032	0.005	0.475	0.001	0.000	0.014	0.000	0.000	0.000	0.000
BSS-2004	0.000	0.000	0.001	0.000	0.001	0.015	0.000	0.033		0.134	0.001	0.091	0.250	0.000	0.001	0.000	0.000	0.000	0.000
H6B8 (BSS)	0.001	0.000	0.000	0.001	0.004	0.040	0.000	0.032	0.134		0.001	0.210	0.016	0.001	0.000	0.000	0.000	0.000	0.000
H7B101 (Hutton)	0.000	0.000	0.000	0.000	0.001	0.874	0.000	0.005	0.001	0.001		0.039	0.081	0.000	0.000	0.000	0.000	0.000	0.000
H5B21 (BSS)	0.022	0.000	0.047	0.067	0.106	0.385	0.011	0.475	0.091	0.210	0.039		0.025	0.000	0.000	0.000	0.000	0.000	0.000
BGR01 (BSS)	0.000	0.000	0.000	0.000	0.000	0.114	0.000	0.001	0.250	0.016	0.081	0.025		0.000	0.000	0.000	0.000	0.000	0.000
H5B5 (BSS)	0.000	0.000	0.000	0.000	0.000	0.000	0.000	0.000	0.000	0.001	0.000	0.000	0.000		0.007	0.026	0.000	0.000	0.000
H7B66 (ICG)	0.000	0.000	0.000	0.000	0.000	0.000	0.000	0.014	0.001	0.000	0.000	0.000	0.000	0.007		0.024	0.000	0.000	0.000
GRF01 (BSS)	0.000	0.000	0.000	0.000	0.000	0.000	0.000	0.000	0.000	0.000	0.000	0.000	0.000	0.026	0.024		0.000	0.000	0.000
H7B59 (Hooray)	0.002	0.523	0.000	0.000	0.000	0.000	0.000	0.000	0.000	0.000	0.000	0.000	0.000	0.000	0.000	0.000		0.450	0.151
H7B55 (GRF)	0.000	0.005	0.002	0.000	0.000	0.000	0.000	0.000	0.000	0.000	0.000	0.000	0.000	0.000	0.000	0.000	0.450		0.014
Wall1 (GRF)	0.005	0.506	0.001	0.001	0.000	0.000	0.000	0.000	0.000	0.000	0.000	0.000	0.000	0.000	0.000	0.000	0.151	0.014	

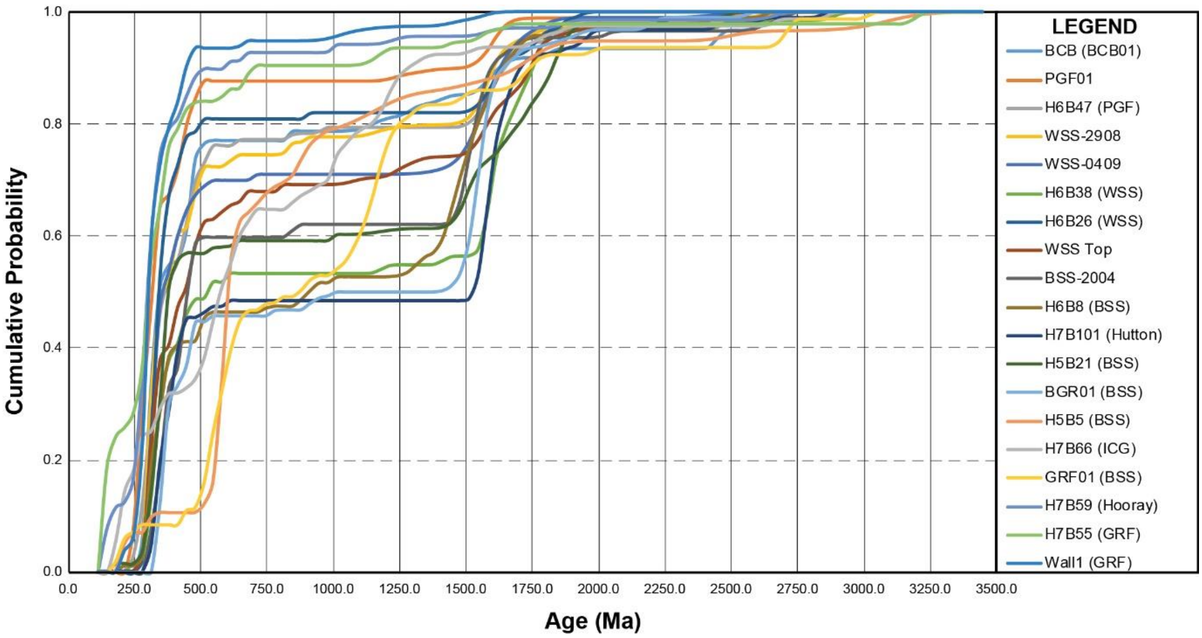

Figure 10 – Cumulative distribution frequency diagram of all detrital zircon samples from the Hughenden area.

Discussion

Sources of the detrital zircon populations

An inspection of the probability density plots of the 19 detrital zircon samples reveals a limited distribution of grain ages that occur predominantly between ~2000 Ma and ~120 Ma (Figs 6, 7, and 10). Within this range are nine important peaks, including five pre-Mesozoic population clusters at 1650–1500 Ma, 1200–1000 Ma, 700–500 Ma, 500–400 Ma, and 345–260 Ma, and four Mesozoic clusters at 250–225 Ma, 180–160 Ma, 155–150 Ma, and 135–120 Ma. Locations of possible source terranes are given in Figure 11.

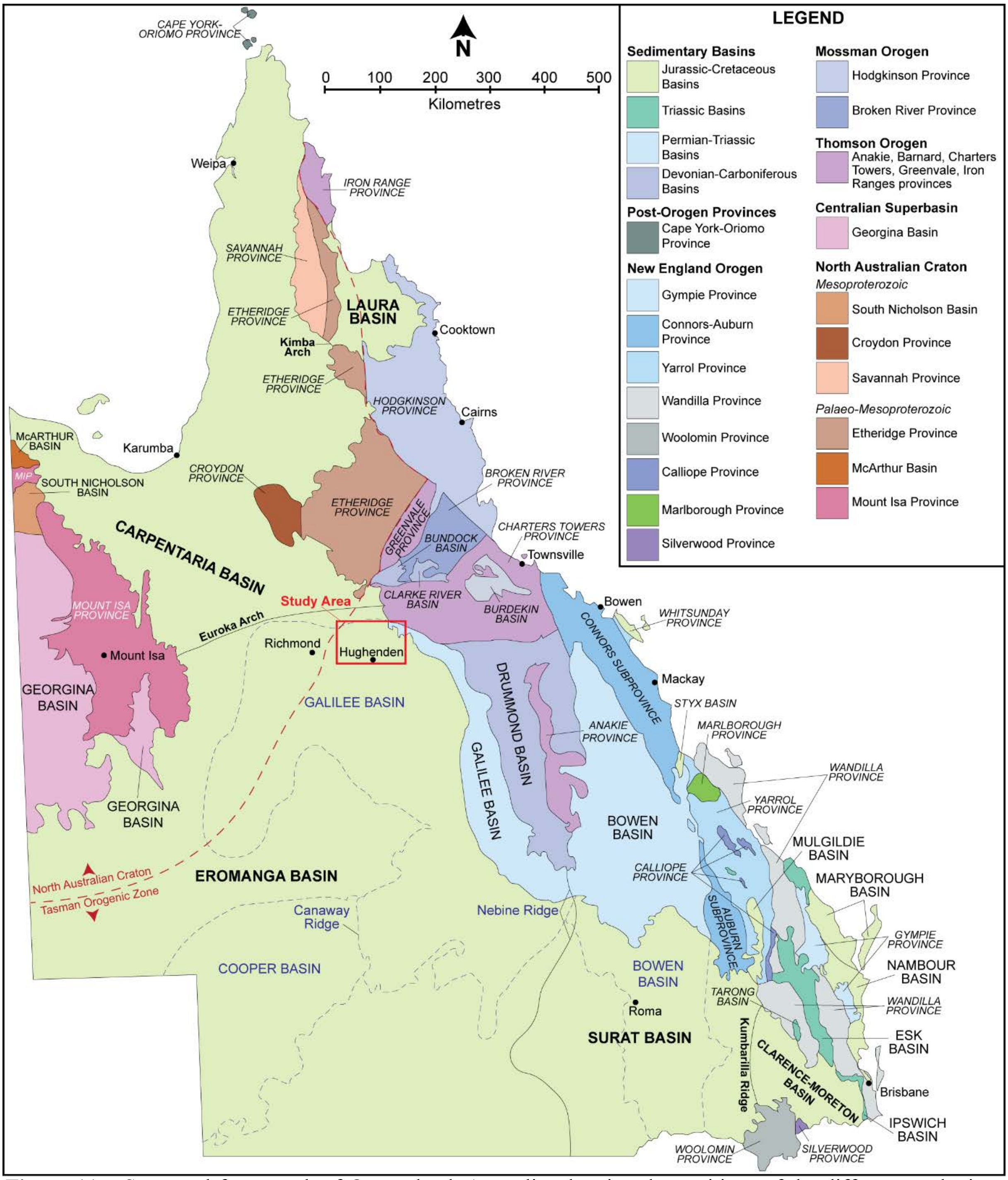

Figure 11 – Structural framework of Queensland, Australia, showing the positions of the different geologic – provinces that are possible source terranes for the important Palaeozoic to Mesozoic sedimentary basins. Modified from Withnall et al. (2013). Dotted lines indicate portions of Carboniferous to Triassic basins that are buried beneath the Jurassic to Cretaceous basins.

Late Palaeoproterozoic-early Mesoproterozoic (1700–1400 Ma) sources

The 1700–1400 Ma population is common to the Betts Creek beds, Porcupine Gorge Formation, Warang Sandstone and lower Blantyre Sandstone, with the relative frequency of this population increasing in the younger samples. It is absent from the upper Blantyre Sandstone, Hooray Sandstone and Gilbert River Formation. Overall, this cluster accounts for the second highest proportion of the detrital zircon analyses at 13.6%. Two potential sources within the North Australian Craton are now exposed that can account for this population: the Mount Isa Province, which is quite distal and to the west of the study area, and the much more proximal Etheridge Province to the north of the study area. The Etheridge Province is considered the provenance source for most of these grains because: 1) grain ages from individual provenance sources within the Etheridge Province (Nordsvan et al., 2018) are consistent with sub-peaks observed in this study; 2) the zircon grains in this population are euhedral to subhedral, which is consistent with a more proximal source area; 3) palaeocurrents from the Permian to Jurassic basin-fill strata indicate dominantly north to north-east sources (Fig. 4); 4) the Maneroo Platform (basement high) likely acted as a barrier to eastward sediment transfer from the Mt. Isa Province across the Lovelle Depression into the Koburra Trough.

In the Etheridge Province, granites of the Forsayth Supersuite provide excellent matches for the 1560–1550 Ma zircon populations documented in this study, and I-type and S-type granites within the Yambo Inlier are temporally comparable with the 1590–1560 Ma detrital zircon population (Withnall et al., 2013). At present, no clear magmatic rocks of the Etheridge Province are known to account for the 1550–1500 Ma and 1650–1590 Ma zircons in our study. However, detrital zircons collected from the Etheridge and Langlovale groups in the Georgetown area of Far North Queensland show ages within this 1650–1590 Ma period (Nordsvan et al., 2018). We interpret this older part of the population to be secondarily recycled from the Georgetown area of North Queensland.

Late Mesoproterozoic (Grenville: 1200–1000 Ma) sources

The 1200–1000 Ma population is found in an upper Blantyre Sandstone sample collected from Porcupine Gorge (GRF01) and the Injune Creek Group (H7B66) sample collected from the GSQ Hughenden 7 core, and appears as a minor peak in one other upper Blantyre Sandstone sample from GSQ Hughenden 5 (H5B5). It represents the smallest proportion of the total detrital zircon age spectrum at just 2.1%; however, it is the second largest population in each of these particular samples. This age range is broadly consistent with the North American Grenville orogenic age (Rino et al., 2008). Similar grain ages are present in different Proterozoic to Cambrian terranes across Australia, for example, the Halls Reward Metamorphics in North Queensland (Nishiya et al., 1999), the Bathampton Metamorphics from the Anakie Province in central Queensland (Fergusson et al., 2001), the Cape River and Argentine metamorphics of the Charters Towers Province in north Queensland (Fergusson et al., 2007a, b), and the Kanmantoo Group in South Australia (Ireland et al., 1998). Fergusson et al. (2007a, b) and Glen et al. (2017) inferred that the Mesoproterozoic central Australian Musgrave Complex previously extended to the eastern Australian margin, which would have permitted Musgrave-derived sediment to be transported into the Anakie Province and Charters Towers Province areas. Subsequent recycling of these terranes would provide the most direct source of these grains in northern Queensland. Northerly flowing palaeocurrents in the Upper Jurassic study units (Fig. 4) indicate that the Anakie Province is the more likely of these two sources for these samples.

Late Neoproterozoic-middle Cambrian (Pacific-Gondwanan: 700–500 Ma) sources

The 700-500 Ma age cluster, which is present in the upper Blantyre Sandstone and Injune Creek Group samples collected from the Hughenden area, accounts for 5.7% of the total zircon age spectrum. In Australia, this age range is commonly referred to as Pacific-Gondwanan and is roughly coincident with the Pan-African Orogeny (e.g. Rino et al., 2008). Detrital Pacific-Gondwanan zircon ages have been documented in the Cape River and Argentine metamorphics of the Charters Towers Province, and the Wynyard Metamorphics or Bathampton Metamorphics of the Anakie Province, but are typically less abundant than their Grenvillian counterparts (Fergusson et al., 2001, 2007a; Fergusson and Henderson, 2005; Shaanen et al., 2018). The 600–500 Ma component of the Pacific-Gondwanan signature is commonly attributed to the Ross-Delamerian orogenic belt that extends across the Antarctic and Australian continents, with the northernmost outcrops inferred in the Townsville area (Fergusson et al., 2007b). The older 700–600 Ma component of this signature has been attributed to granites of the western to central Australian Paterson-Petermann orogenies (Bagas, 2004; Martin et al., 2017). Palaeoflow in Upper Jurassic study units indicate that the most direct source of the Pacific-Gondwanan signature is from the Wynyard Metamorphics in the Anakie Province to the south-east of the study area.

Middle Cambrian-Lower Devonian (500–400 Ma) sources

The 500-400 Ma cluster is common to all 19 samples in the Hughenden area, accounting for 10.2% of the overall age distribution. This signal is most consistent with the granitoids of the Ravenswood, Lolworth and Reedy Springs batholiths, which belong to the magmatic arc-related Pama Igneous Association, and have intruded into the Charters Towers, Greenvale, and Etheridge provinces (Fergusson and Henderson, 2013). Palaeocurrent results are consistent with this interpretation (Fig. 4).

Early Carboniferous-late Permian (345–260 Ma) sources

The most significant and consistently represented zircon population in this study (except for the upper Blantyre Sandstone and Injune Creek Group samples) is the 345–260 Ma population, which accounts for 34.6% of the total zircon grains. Such a large peak that is near-ubiquitous indicates a source terrane that was consistently exposed at surface and was proximal to the study area. This age signature is consistent with the Kennedy Igneous Association. The peak ages at 320–280 Ma are roughly coincident with the Pennsylvanian-Sakmarian (~320–295 Ma) and Artinskian-Capitanian episodes (~290–260 Ma) in the province. These episodes resulted in widespread, predominantly felsic, arc-related magmatism across much of north-eastern Australia, from the southern Jardine Subprovince (Savannah and Iron Range provinces) in Cape York in the north to the Burdekin Falls Subprovince (Charters Towers and Thalanga provinces) in the south (Champion and Bultitude, 2013). We interpret the Kennnedy Igneous Association, particularly the more northerly Burdekin Falls Subprovince, to account for the dominance of these grain ages in all of the Hughenden samples.

The rhyolite boulder sample collected from the lower Blantyre Sandstone presents both ages (312 Ma–267 Ma) and lithology (felsic igneous) that matches the Kennedy Igneous Association. The abundance of rhyolite clasts in the conglomerates of the Porcupine Gorge succession is temporally and spatially consistent with a primary source area in the Kennedy Igneous Association.

Triassic (250–225 Ma) sources

The Triassic cluster is the dominant proportion of the Mesozoic spectra and accounts for 2.7% of the total age spectrum (Fig. 12). Palaeocurrents in the Porcupine Gorge Formation and Warang Sandstone in Porcupine Gorge demonstrate that south to south-south-westerly flowing stream transported sediment into the study area. Neither intrusive nor extrusive bodies are presently known to the north of the study area from where these grains are derived. To the south and south-east of the Hughenden area, however, Triassic granitoids of comparable age are exposed within the New England Orogen (e.g. Purdy, 2013, and references therein; Rosenbaum, 2018). Continuation of the New England Orogen beneath the Queensland Plateau has been inferred from isotopic studies (Mortimer et al., 2008; Shaanan et al., 2018), and it likely continued further to the north towards the Mossman Orogen off the present-day coastline. Following retreat of the eastern Australian margin in the Late Cretaceous, the New England Orogen was rifted away and buried as the Coral Sea opened. Continuation of this terrane into north-eastern Queensland would provide a potential source for the Triassic detrital zircon population encountered in the Hughenden area.

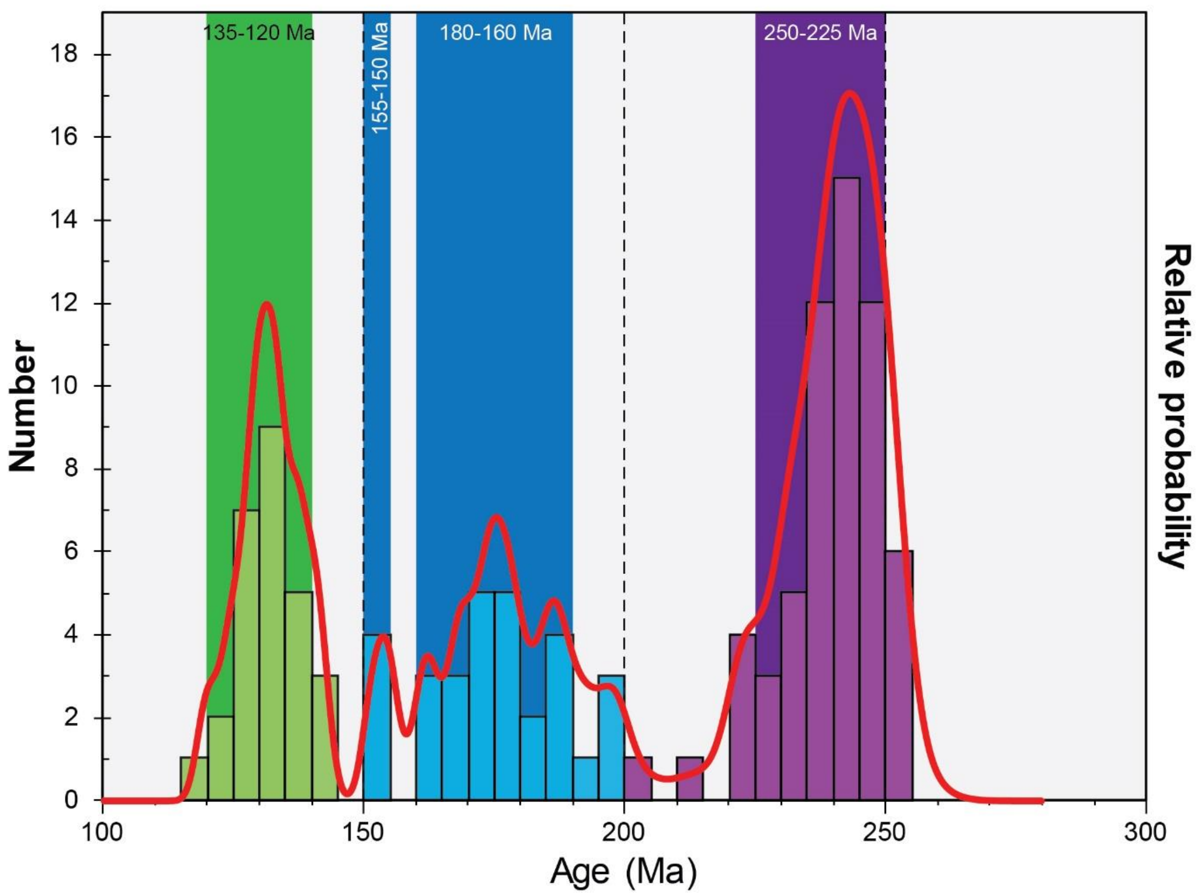

Figure 12 – U–Pb detrital zircon histogram and frequency distribution of the four dominant Mesozoic clusters from all samples.

Jurassic (180–160 Ma and 155–150 Ma) sources

Jurassic detrital zircon grains are the least common of the Mesozoic populations in the study area, only becoming apparent in the upper Blantyre Sandstone, Injune Creek Group, Hooray Sandstone and Gilbert River Formation. The source of these grains remains enigmatic given the questions regarding the presence or absence and location of a volcanic arc at this time, and the lack of preserved primary igneous bodies on the eastern Australian margin. Recently, however, several Middle to Late Jurassic tuffs were identified by Wainman et al. (2015, 2018a, b) in the southern Eromanga Basin, Surat Basin and Clarence-Moreton Basin. These tuffs have ages consistent with those of the detrital zircons recovered in the north-eastern Eromanga Basin samples, which indicates likely syn-depositional recycling of correlative airfall tuffs closer to the study area. These grain ages were interpreted by Wainman et al. (2015, 2019) to be consistent with derivation from a volcanic arc on the eastern margin. Given the sparsity of Jurassic grain ages in the Hughenden samples, however, it is likely the grains were transported great distances prior to deposition, suggesting the arc was located distal to the study area.

Early Cretaceous (135–120 Ma) sources

The Early Cretaceous grain ages account for 1.4% of the total age spectrum for the Hughenden samples, but are the second most dominant Mesozoic cluster. Although no palaeocurrents were measured in Cretaceous units in the Porcupine Gorge region, the 135–120 Ma detrital zircon cluster is interpreted to have been derived from sources to the east based on the dominance of Kennedy Igneous Association grains. The Whitsunday Volcanic Province (c. 135–95 Ma; Bryan et al., 2000, 2012), which is preserved on the present-day eastern Australian margin, represents the most likely option for the provenance of these Cretaceous grains

(Tucker et al., 2016). This area is somewhat to the south of the study area but would have likely extended further north prior to formation of the Coral Sea rift.

Permian–Cretaceous palaeodrainage evolution of north-eastern Australia

Despite palaeocurrents measured in the Betts Creek beds indicating a south-south-easterly flowing drainage pattern, the detrital zircon spectrum shows very little input from the Etheridge Province located directly to the north. Instead, the dominant two zircon populations seem to be derived from the Kennedy Igneous Assocaition and the Lolworth, Ravenswood and Reedy Springs batholiths (Pama Igneous Association) to the north-east (Fig. 13). We interpret this to reflect uplift of the nearby Kennedy Igneous Association, which would have effectively blocked transport of sediments into the basin from the Etheridge Province until the Late Triassic to Middle Jurassic, when input from the Etheridge Province increased. A continued increase in the abundance of sediment of this source in the younger formations likely resulted from slow exposure of this terrane through continued erosion of overlying units.

Provenance patterns determined for the Porcupine Gorge Formation, Warang Sandstone, and lower Blantyre Sandstone reveal strong similarities with each other. Palaeocurrents from each formation indicate south to south-westerly flow; and detrital zircon signatures indicate sources in the Etheridge and Charters Towers provinces, which is consistent with the craton interior and recycled orogen tectonic terranes indicated by the sandstone petrography, as well as sources from the Kennedy and Pama igneous associations (Fig. 13). This similarity is remarkable given the ~60 M.y age difference between these Triassic and Jurassic formations (~230–170 Ma). Indeed, the Hunter-Bowen Orogeny, which is known to have vertically deformed continental strata in the Bowen Basin and New England Orogen on a kilometre-scale and took place between the deposition of the Warang and Blantyre sandstones, appears to have had little to no effect on the provenance signatures in the study area. Instead, when sedimentation resumed after the hiatus between the Galilee and Eromanga basins, the same terranes began to be eroded and form the primary provenance source again. This is further evidenced in the detrital zircon record where the ages of the youngest grain populations increase in the younger stratigraphic units by the continuous removal of contemporaneous Mesozoic sources. Despite no direct deformation of the Galilee Basin strata by the Hunter-Bowen Orogeny, intense deformation further to the east may have resulted in the formation of a drainage barrier that has since been eroded away, blocking sediments that would otherwise be draining westward off the volcanic arc.

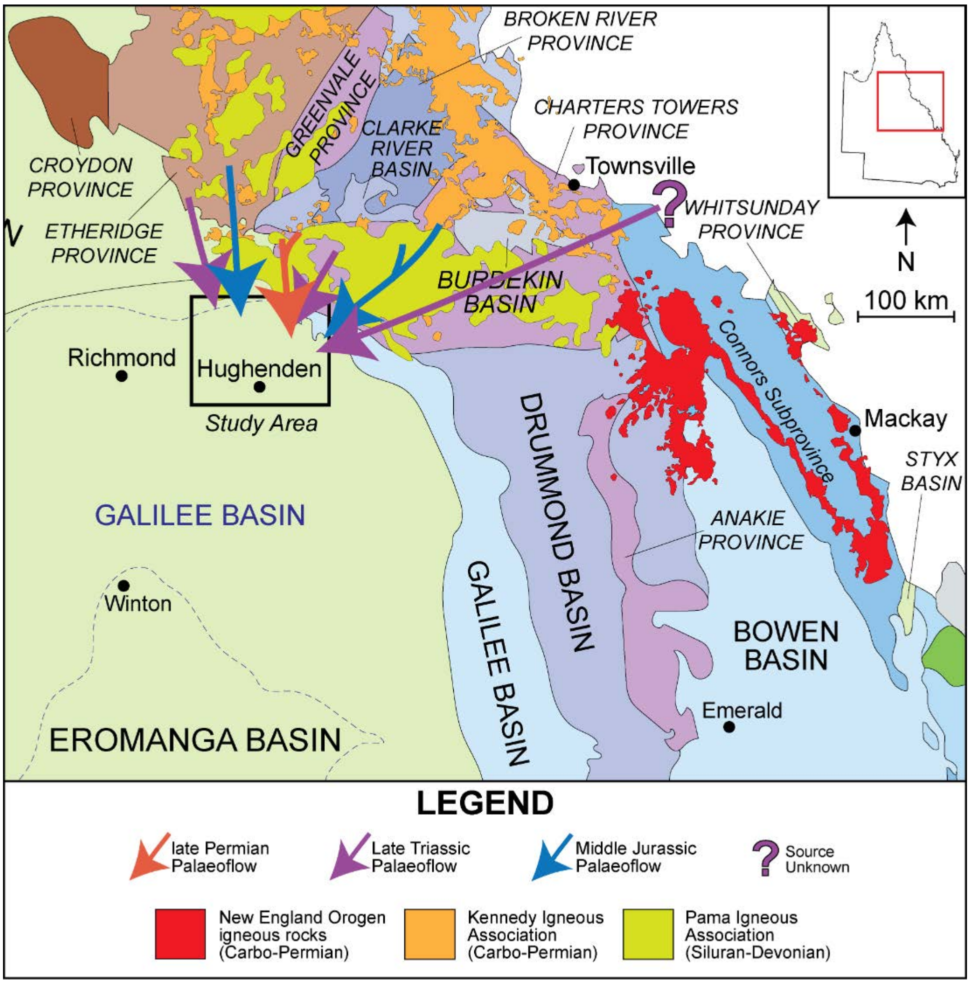

Figure 13 – Palaeodrainage model for the upper Permian to Middle Jurassic strata of the Hughenden area.

In the Upper Jurassic units in both Porcupine Gorge and the GSQ Hughenden 7 drill core a distinctive provenance change is observed for the first time. Palaeocurrents measured in the upper Blantyre Sandstone reveal a reversal from south-westerly to north-easterly, north-westerly, and easterly palaeoflow (Figs 4 and 14). A completely different detrital zircon signature is also recorded in samples H5B5, GRF01 and H7B66, with the 1700–1500 Ma and 320–280 Ma peaks replaced by 1200–1000 Ma and 700–500 Ma peaks. Contemporaneous Jurassic detrital zircon grains and Triassic grain ages are also present in these Upper Jurassic samples, a source that was entirely lacking from the Middle Jurassic samples. The thin sections for this same interval in the Hughenden region (H5B5, GR1, etc) also show a much higher quartz content, further confirming a provenance shift. This supports recent interpretations of Early-Middle Jurassic uplift of the north-eastern Australian continental margin based on (U-Th)/He zircon and apatite thermochronology data by Cheng et al. (2020; Appendix 1) from the Kennedy Igneous Association between the Whitsundays and Cairns regions. Cheng et al. (2020) also investigated detrital zircon samples collected in the north-eastern Eromanga Basin, and concluded that considerable denudation and uplift occurred to the east of the basin during this time.

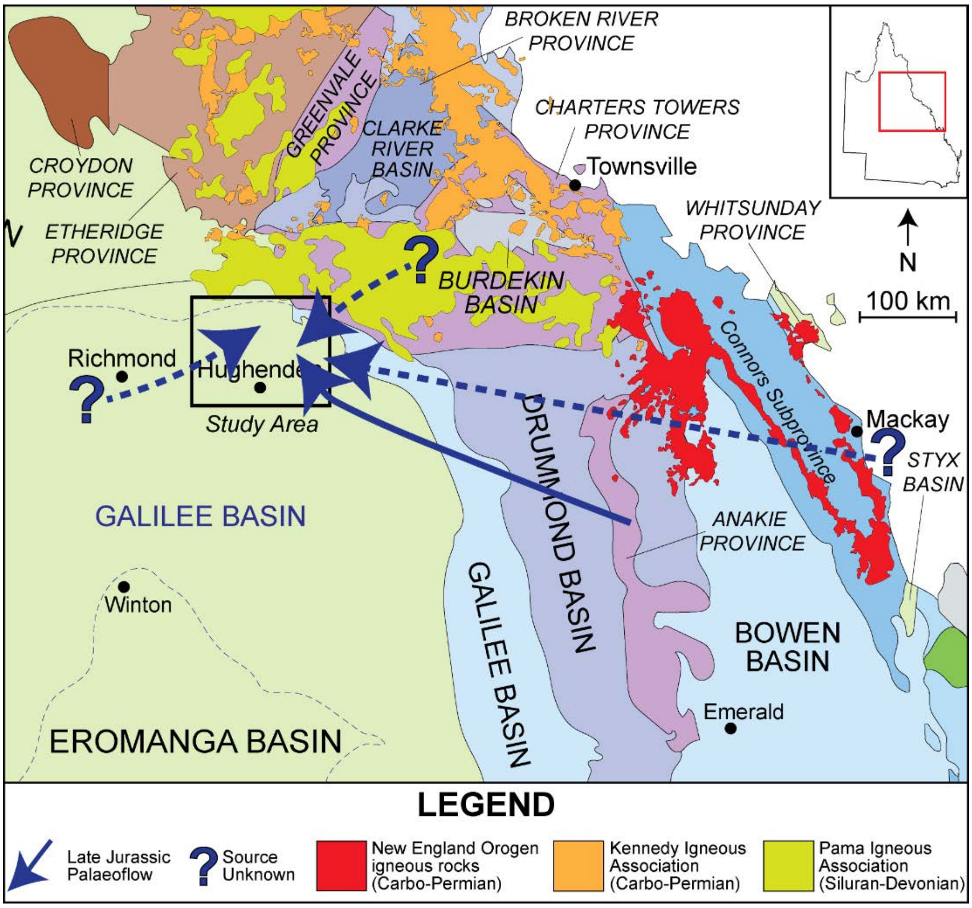

Figure 14 – Palaeodrainage model for the Upper Jurassic of the Hughenden area. Directions of the arrows shows the multiple source directions caused by sudden palaeocurrent reversals (from Fig. 4).

Cretaceous detrital zircons were identified only in drill core samples, so no palaeocurrents were measured. The provenance of these units is, however, different again from that of the underlying Upper Jurassic strata (Fig. 15). The 600–500 Ma and 1200–1000 Ma peaks are no longer present; however, the 320-280 Ma peak is again present and is the most prominent, similar to the Permian to Middle Jurassic samples. The only other significant zircon populations are those that have peaks in the Triassic, Jurassic, and Cretaceous. Drainage directly from the east or east-south-east would explain Kennedy Igneous Association source and the lack of 1700-1400 Ma grains, and would also account for the young Cretaceous grains.

The 135-120 Ma Cretaceous population was likely derived from the Whitsunday Volcanic Province, which is also located to the east of the study area (Fig. 15).

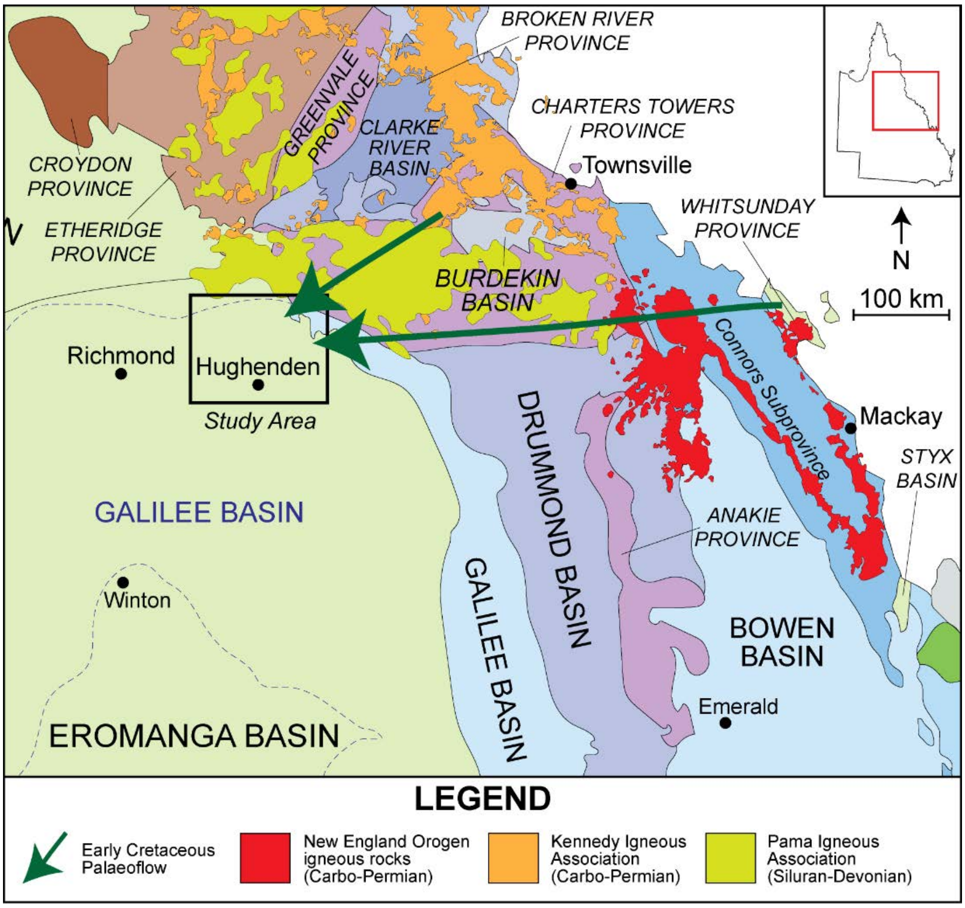

Figure 15 – Palaeodrainage model for the Lower Cretaceous of the Hughenden area.

The accumulation of Mesozoic grains within the Upper Jurassic and Lower Cretaceous samples in the study area (e.g. GRF01, H7B59, H7B55) suggests that magmatic activity was continuously depositing volcanogenic sediments onto eastern Australia. A lower overall abundance of these Mesozoic grains in comparison to those of the Kennedy Igneous Association or the Etheridge Province suggests they were likely sourced from more distal terranes and deposited as airfall tuffs or occasionally draining from proximal intrusive arc-related sources. This continuous volcanic activity is consistent with the growing body of evidence that suggests a volcanic arc was present on or near the eastern Australian margin throughout the Mesozoic (e.g. Veevers, 2006; Tucker et al., 2016; Wainman et al., 2015, 2019b).

Conclusions

This study provided a comprehensive sedimentary provenance investigation into upper Permian to Lower Cretaceous strata of the north-eastern Galilee and Eromanga basins in Queensland. In lieu of well-preserved Mesozoic magmatic rocks on the eastern margin, a model for the palaeodrainage evolution of northern Queensland was determined through a combination of palaeocurrent analysis, pebble counts, sandstone petrography, and U–Pb detrital zircon geochronology.

Fluvial palaeodrainage patterns in the late Permian to Middle Jurassic were dominated by southerly to south-westerly flow with the detrital zircon provenance suggesting the subarkosic to sublitharenitic sandstones were predominantly derived from the Etheridge Province and Kennedy Igneous Association. Sandstone petrography indicates a recycled orogenic terrane for the Triassic samples and a craton interior source for the Jurassic samples, which indicates that syn-depositional Triassic grains were likely deposited by distal airfall tuffs or by erosion of minor intrusive rocks in the east. Uplift of the eastern Australian margin in the Jurassic resulted in a reversal in palaeocurrents in the Late Jurassic upper Blantyre Sandstone (north or north-east), as well as the recording of different source terranes in the detrital zircon spectra. The erosion of the Anakie Province – the result of reworking of Central Australian orogenic terranes – replace the Etheridge Province and Kennedy Igneous Association. Jurassic zircons are also recorded for the first time in the study area. Early Cretaceous basin fill was again dominated by the Kennedy Igneous Association but, with a clear contemporaneous Whitsunday Volcanic

Province peak in place of the Etheridge Province, sources to the east-south-east are inferred despite the lack of palaeocurrent evidence.

The Mesozoic signals in the detrital zircon spectra suggest continuous magmatic input into eastern Australian basins but, given the low abundance relative to other sources, was likely derived from a volcanic arc located distally to the east.

Chapter 5:
Refined age and geological context of two of Australia's most important Jurassic vertebrate taxa (*Rhoetosaurus brownei* and *Siderops kehli*), Queensland

Abstract

Australia's Jurassic vertebrate fossil record remains extremely sparse with only two dinosaur taxa and two temnospondyl amphibians identified to date. Of these, the spectacular and extremely well-preserved giant amphibian, *Siderops kehli*, and the only known pre-Cretaceous sauropod in Australia, *Rhoetosaurus brownei*, are perhaps the most important. The age of both specimens, and the stratigraphic context of *Rhoetosaurus brownei*, are weakly constrained and imprecisely defined, limiting our understanding of their evolutionary relationships within a broader Gondwanan context. To clarify and contextualise the evolutionary relationships and ages of these two iconic Jurassic taxa, we used U–Pb detrital zircon geochronology to date the sandstone matrix from around the bones of the historic museum specimens. The robust maximum depositional age for *Siderops* was calculated at 176.6 Ma ± 2 Ma, indicating that it is no older than late Toarcian, which refines existing biostratigraphic estimates. The *Rhoetosaurus* maximum depositional age determined is 162.6 ± 1.1 Ma, no older than early Oxfordian, demonstrating that the fossils are younger than expected, and definitely recovered from the Walloon Coal Measures.

Graphical Abstract

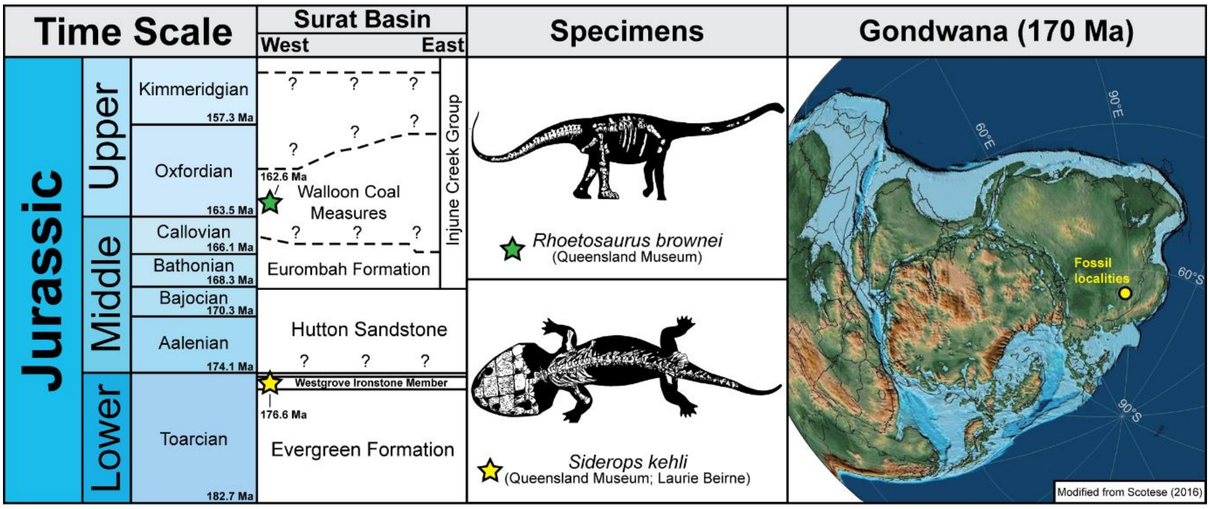

Introduction

The Australian Jurassic vertebrate fossil record is conspicuous for its extreme scarcity of tetrapod remains, with only two dinosaurs (*Rhoetosaurus brownei* and *Ozraptor subotaii* [Longman, 1926; Long and Molnar, 1998]), two temnospondyls (*Siderops kehli* and *Austropelor wadleyi* [Longman, 1941; Warren and Hutchinson, 1983]), and a handful of indeterminate plesiosaurs (Thulborn and Warren, 1980; Warren and Hutchinson, 1983; Kear, 2012) identified to date. Footprints from a variety of theropod and ornithopod dinosaurs in the Lower Jurassic of Queensland clearly demonstrate that the faunal record was more diverse than currently established (Thulborn, 1994; Cook et al., 2010, and references therein).

Of the known Jurassic tetrapods, perhaps the most important are *Siderops kehli*, an almost complete temnospondyl amphibian (Warren and Hutchinson, 1983), and *Rhoetosaurus brownei*, the only described pre-Cretaceous Australian sauropod (Longman, 1926; Nair and Salisbury, 2012). *Siderops*, along with two partially articulated freshwater plesiosaur specimens, were discovered on the Kolane cattle station in southeast Queensland (Fig. 1) in an oolitic ironstone (Westgrove Ironstone Member) of the Evergreen Formation (Warren and Hutchinson, 1983; Kear, 2012). The *Rhoetosaurus* specimen was collected from the banks of a gully feeding the Eurombah Creek on Taloona Station, in southeast Queensland (Fig. 1). Longman (1926) identified the horizon as a lower part of the Walloon Series, which is now called the Walloon Coal Measures. At the time, the Walloon was considered Lower Jurassic, but presently the age of the unit is considered Middle to Upper Jurassic (Callovian to Tithonian) based on extensive new high-precision ID-TIMS U–Pb geochronology of volcanic tuffs from throughout the succession (Wainman et al., 2018a, b).

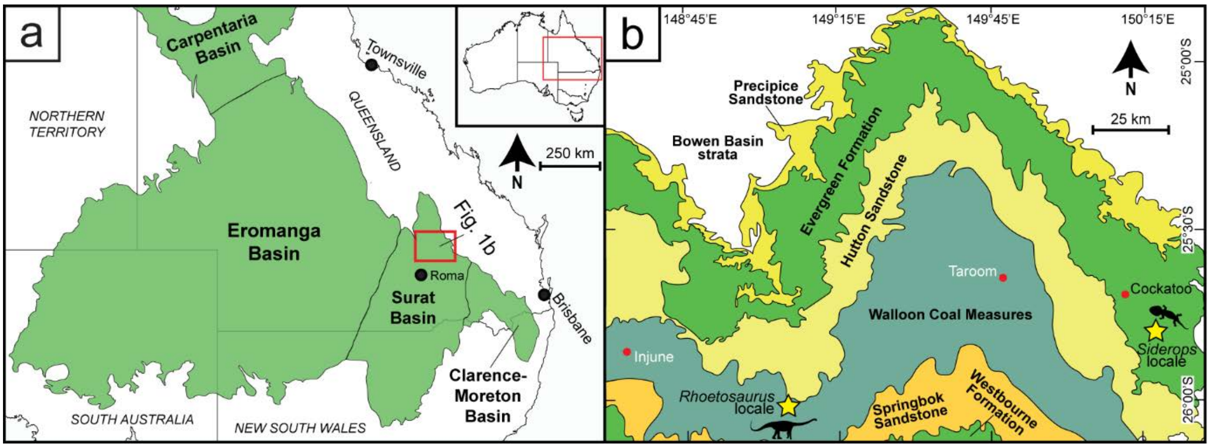

Figure 1 – (a) Map of the Great Artesian Basin in central eastern Australia highlighting the location of the study areas in the Surat Basin. (b) Geological map of the study area, the fossil locations are given by the yellow stars; modified from MinesOnlineMaps v2.5.

Subsequent review papers and references relating to the *Rhoetosaurus* have caused some confusion by relisting the specimen's stratigraphic horizon. Between 1966 and 1990, most authors listed the specimen as having been discovered in the Injune Creek Beds and being either Lower or Middle Jurassic in age (Hill et al., 1966; Molnar, 1980, 1982, 1984; McIntosh, 1990). The Injune Creek Beds were later was upgraded to the Injune Creek Group of which the Walloon Coal Measures is a part. In a later publication by Molnar (1991) the specimen was instead said to have been derived from the Hutton Sandstone. Though no explanation was provided, it is possible that this was done to retain the original Lower Jurassic interpretation by Longman (1926). Molnar's (1991) Hutton Sandstone reinterpretation was then used by most subsequent workers in their reviews of the specimen (Grant-Mackie et al., 2000; Upchurch et al., 2004; Turner et al., 2009; Kear and Hamilton-Bruce, 2011), except for Glut (1997) who retained the Injune Creek Beds and Middle Jurassic interpretations. Nair and Salisbury (2012) completed the most recent work on *Rhoetosaurus* in which they evaluated previously undescribed fossil materials and confirmed the original stratigraphic horizon as being the Walloon Coal Measures. However, they also noted that some authors had also applied the name

Eurombah Formation to outcrop nearby to this fossil-bearing horizon (Swarbrick et al., 1973). The Eurombah Formation is now considered to lie stratigraphically below the Walloon Coal Measures. On geological maps of the region produced by Forbes (1968) and Exon (1971), the Eurombah Formation is not included and outcrop exposures on the Eurombah Creek near the fossil locality are mapped as either Hutton Sandstone or Injune Creek Group. The possibility that the *Rhoetosaurus* site may fall within the Eurombah Formation must be weighed against the original lithological description of the sandstone matrix on the fossils given in Longman (1926) as being a highly calcareous. This is inconsistent with Swarbrick et al.'s (1973) definition of the Eurombah Formation as being non-calcareous. Indeed, these workers used this criterion to distinguish the Eurombah Formation from the calcareous sandstones of the Walloon Coal Measures. However, a lack of continuous exposure in the area, and a variable lithology of the sediment encasing the *Rhoetosaurus* specimen (S. Salisbury, pers. comm.), has meant that verifying which unit the locality is in is extremely difficult. This stratigraphic uncertainty hinders our understanding of how *Rhoetosaurus* fits in temporally with sauropod evolution in Gondwana and the rest of the world.

Volcaniclastic sedimentary deposits in the Winton Formation have shown their utility in providing maximum depositional ages for Cretaceous dinosaur taxa in Australia (Tucker et al., 2013). However, until now there has been no attempt to chronostratigraphically refine the age of any Jurassic tetrapod fauna in Queensland. This project aims to test if sediment matrix collected directly off the original fossils in museum collections can be dated via U–Pb detrital zircon geochronology using laser ablation-inductively coupled plasma-mass spectrometry (LA-ICP-MS) to constrain the maximum depositional ages of *Rhoetosaurus brownei* and *Siderops kehli,* and to provide clarity on the stratigraphy of their host sandstones. Better age constraints will have significant implications for our understanding of the Gondwanan, and perhaps global, evolutionary and palaeobiogeographic context of these taxa.

Geological Context

Both the *Siderops kehli* and *Rhoetosaurus brownei* localities are situated within the Surat Basin (Figs 1 and 2). The Jurassic to Cretaceous Surat Basin covers an area of 247 000 km^2 across southern Queensland and northern New South Wales, overlying the Permian to Triassic Bowen Basin (Green, 1997). Evidence for widespread Jurassic volcanism along the east coast of Australia remains tantalisingly sparse, with only a few known primary volcanic rocks of this age (Turner et al., 2009). U–Pb detrital zircon studies from Cretaceous deposits in the northern Eromanga Basin have revealed the presence of multiple discrete Jurassic zircon populations, suggesting that an extensive volcanic arc system was likely active throughout the Jurassic (Tucker et al., 2013, 2016). Wainman et al., (2015, 2018a, b) confirmed the presence of a series of primary volcanic ash beds throughout the Middle to Upper Jurassic succession in the Eromanga, Surat and Clarence-Moreton basins in a study of drill cores. Palynological work in the Walloon Coal Measures suggested a late Bathonian to middle Callovian age (~167-164 Ma) (Helby et al., 1987; McKellar, 1998); however, Wainman et al. (2015, 2018a, b) applied U–Pb chemical abrasion-isotope dilution-thermal ionisation mass spectrometry (CA-ID-TIMS) zircon geochronology to very precisely date the volcanic tuffs within the Walloon Coal Measures, which range between early Callovian and early Tithonian (~165-151 Ma).

Despite the presence of abundant volcanic detritus and primary volcanic ash beds in the Middle to Upper Jurassic basin strata of eastern Australia, very little is known about the chronostratigraphy of the Lower Jurassic succession in these interior basins, and whether explosive volcanism was also present during this time. The Westgrove Ironstone Member of the Evergreen Formation, which yielded *Siderops kehli* and the two partial, freshwater plesiosaur skeletons, is considered to be Lower Jurassic based on palynology (de Jersey and Paten, 1964; Reiser and Williams, 1969). Green et al. (1997) assigned the Westgrove Ironstone Member to the APJ32 palynozone, which corresponds to the upper Lower Jurassic of Price (1997). Later work confirmed this age, indicating these ironstone beds span the *Corollina torosa* to *Callialasporites turbatus* palynozones, which suggests a lower Toarcian age (Turner et al., 2009; Kear, 2012). Palynological investigations of the Hutton Sandstone in the Surat Basin suggest a slightly younger, late Toarcian to Callovian age assigned to the APJ33 and APJ41 zones (Price et al., 1985; Price, 1997; Gray et al., 2002). The upper limit of the Hutton Sandstone in the Surat Basin, more recently, has been refined to late Bajocian via high-precision U–Pb geochronology (Wainman et al., 2018a).

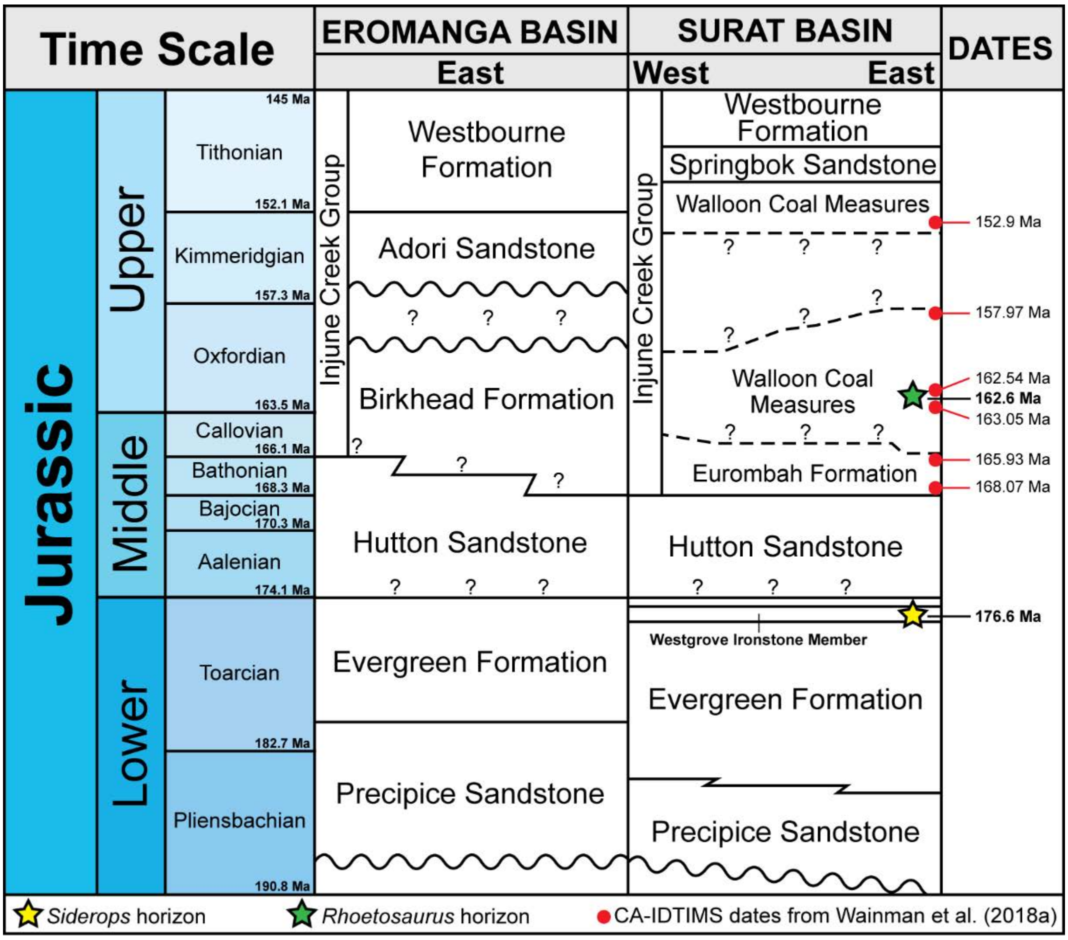

Figure 2 – Refined Jurassic stratigraphy of the eastern Eromanga Basin and the Surat Basin, the green and yellow stars indicate stratigraphic position of the fossil specimens. Modified from Cook et al. (2013), Hamilton et al. (2014) and Wainman et al. (2015, 2018a, b).

Materials and Methods

Detrital Zircon Geochronology

Sandstone matrix material was collected directly from the bones of the *Rhoetosaurus* (QM F1659) and *Siderops* (QM F7882) specimens, which are housed in the Queensland Museum collection in Brisbane, Australia. Each sample underwent heavy mineral separation at James Cook University, Townsville, Australia (JCU), involving crushing, milling, and magnetic and heavy liquid (LST) separations. Zircons were then hand-picked from the heavy concentrates under a binocular microscope, with special emphasis on picking the freshest, most acicular grains. The samples were mounted using epoxy resin, which was then polished to expose the zircons. These were then imaged using a scanning electron microscope with cathodoluminescence detector (SEM-CL) to identify the best grains and locations for analyses. U–Pb geochronology was performed using LA-ICP-MS (Teledyne Analyte G2 193 nm Excimer Laser with HeLex II Sample Cell and a Thermo iCAP-RQ ICP-MS) at the Advanced Analytical Centre at JCU. Instrumental tuning, dating methodology and analytical details are outlined in the supplementary materials. The analytical results were processed using Iolite (https://iolite-software.com/). The software was used for downhole fractionation calibration, instrumental drift correction and propagated error estimation. The method is similar to that described in Paton et al. (2010, 2011). Probability density plots and weighted mean ages were calculated using Isoplot (Ludwig, 2008). Maximum depositional ages were calculated by determining the weighted mean of the youngest cluster of concordant grains (where $n \geq 3$) with overlapping ages (within 1σ error) for each sample (see Dickinson and Gehrels, 2009).

Results

Zircon Morphology

Most of the detrital zircons imaged under cathodoluminescence show typical igneous growth zoning patterns (Fig. 4), consistent with a volcanic origin (Corfu et al., 2003). The mostly acicular and euhedral nature of the zircons is evidence for minimal transport from the source terrains. These zircon grains were likely reworked from the abundant tuffs in the local Jurassic Surat Basin sequence and redeposited into younger stratigraphy.

Rhoetosaurus sample (QM F1659)

A total of 118 zircons were analysed from the *Rhoetosaurus* sample (QM F1659), which produced 69 concordant ages. The youngest single grain age is 161.4 ± 1.7 Ma, whereas the youngest coherent zircon population (n = 7), including this youngest grain, yields a weighted mean age of 162.6 ± 1.1 Ma (MSWD = 0.53) (Fig. 3a, b; Fig. 4). This is a robust Oxfordian maximum depositional age that is consistent with recent high precision U–Pb CA-ID-TIMS zircon geochronology of intercalated volcanic tuffs from the Walloon Coal Measures reported by Wainman et al. (2018a, b).

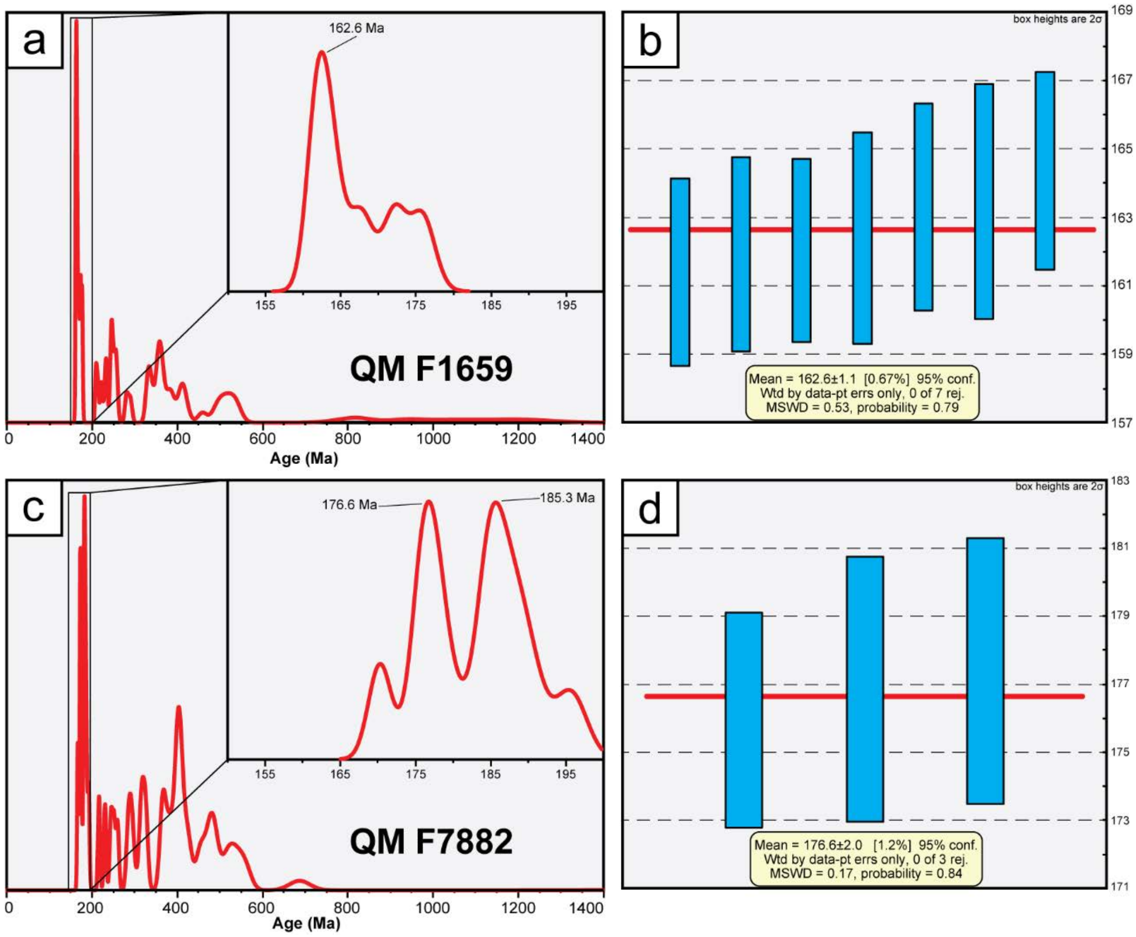

Figure 3 – (a) Relative probability plot of QM F1659 (*Rhoetosaurus*) also showing a dominant Jurassic peak (inset). (b) Weighted mean of the youngest seven grains from sample QM F1659. (c) Relative probability plot of QM F7882 (*Siderops*) showing the dominant Jurassic peaks (inset). (d) Weighted mean of the youngest population from sample QM F7882.

Siderops sample (QM F7882)

A total of 83 grains were analysed for the *Siderops* sample (QM F7882), resulting in 52 concordant ages. The youngest single grain age is calculated to 170.3 ± 1.8 Ma; however, the 1σ errors of this grain and the next youngest grain at 176.0 ± 1.8 do not overlap and, therefore, the youngest grain cannot reliably be considered part of the same cluster and is excluded (Dickinson and Gehrels, 2009). A coherent population of young grains (n = 3) was determined and yields a preferred and slightly more conservative maximum depositional age of 176.6 ± 2.0 Ma (MSWD = 0.17) (Fig. 3c, d; Fig. 4). This age constrains the maximum depositional age of *Siderops*, as well as the two partially articulated freshwater plesiosaur specimens from the Westgrove Ironstone Member of the Evergreen Formation (QM F10440 and QM F10441; Thulborn and Warren, 1980), to the upper Toarcian.

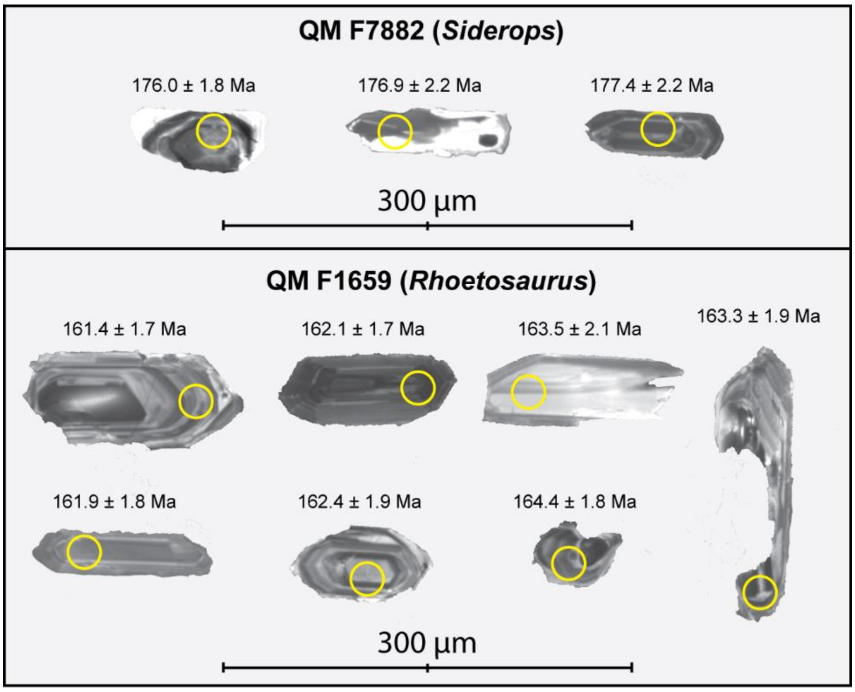

Figure 4 – Morphology and cathodoluminescence images of the detrital zircons that provided the youngest, maximum depositional ages for each sample. Yellow circle represents the 25 µm analysis spot used for by LA-ICP-MS.

Discussion

Age and Implications for *Rhoetosaurus brownei*

In this study, the Oxfordian (Upper Jurassic) maximum depositional age reported for *Rhoetosaurus brownei* not only refines the age of this taxon but also resolves the longstanding confusion over the true stratigraphic provenance of the fossil material. The results eliminate the possibility that the fossils were collected from the Hutton Sandstone (e.g. Molnar, 1991; Upchurch et al., 2004; Turner et al., 2009; Kear and Hamilton-Bruce, 2011) as the 162.6 Ma date is clearly inconsistent with the ~182-168 Ma age of the Hutton Sandstone, which is consistent with the Nair and Salisbury's (2012) documentation of the site. Rather, based on comparison with the high-precision chronostratigraphy for the Walloon Coal Measures by Wainman et al. (2015, 2018a, b) in the nearby Pleasant Hills 25 drill core, the weighted mean maximum depositional age of 162.6 ± 1.1 Ma correlates with the base of the Walloon Coal Measures, just above the Eurombah Formation, in the western Surat Basin. Hence, both the sedimentological evidence for the host sandstones being strongly calcareously cemented and the U–Pb zircon maximum depositional age presented here strongly support the interpretation that the site falls within the base of the Walloon Coal Measures, rather than the underlying Eurombah Formation or Hutton Sandstone. This fits very well with original site and lithological descriptions provided by Longman (1926). The youngest detrital zircon population identified in this study is interpreted to have been sourced from syn-depositional volcanic ash, and hence effectively records the true depositional age (see Fig. 10 of Wainman et al., 2018b). A discussion on the biostratigraphic implications of these ages are given in Wainman et al. (2015).

In the most recent study on *Rhoetosaurus*, Nair and Salisbury (2012) suggested a phylogenetic placement within Gravisauria but outside of Eusauropoda. Basal sauropods have been historically recognised as a common component of Early to Middle Jurassic faunas in western Pangea; however, in the early Late Jurassic, the record of non-neosauropodan sauropods begins to diminish and neosauropods become the more dominant component of dinosaurian faunas (Mannion et al., 2013, 2019; Rauhut et al., 2015; and references therein). The Oxfordian age of *Rhoetosaurus* implied by the detrital zircon age in this study shows that, in southeastern Gondwana, non-neosauropod sauropods likely existed beyond the early Late Jurassic. Sparse occurrences of Late Jurassic non-neosauropod sauropods have also recently been discovered in China and Europe (Mannion et al., 2019). The refined age for the *Rhoetosaurus* given here provides greater context to the hereto scant occurrences of dinosaurian faunas from the Jurassic fossil record of Australia, and provides a target for future palaeontological exploration.

Age and Implications for *Siderops kehli*

The upper Toarcian (upper Lower Jurassic) age presented in this study is entirely consistent with the original Westgrove Ironstone Member stratigraphic assignment of the specimen. It refines the previously assigned lower Toarcian age reported for the unit, and its associated fauna (Green et al., 1997; Turner et al., 2009; Kear, 2012), into the upper Toarcian. This suggests the need for recalibration of the APJ32 zone of Price (1997) from the lower Toarcian to upper Toarcian, and with it, the upper boundary of the *Araucariacites fissus* Association Zone. Further, the APJ33 zonation, including the lower *Camarozonosporites ramosus* Association Zone will also likely have to be recalibrated into the Aalenian (lower Middle Jurassic), which would also constrain the maximum age of the Hutton Sandstone to the Aalenian across the Surat and Eromanga basins.

Chigutisauridae, which *Siderops kehli* is phylogenetically nested within, is the longest surviving temnospondyl family, extending from the Early Triassic to Early Cretaceous in Gondwana (Dias-da-Silva et al., 2012). The two youngest chigutisaurids have been discovered in Australia, which are the Early Jurassic taxon *Siderops kehli* (Warren and Hutchinson, 1983; herein), and the Early Cretaceous taxon *Koolasuchus cleelandi* from Victoria, southern Australia (Warren et al., 1997). The refined age control presented in this study not only confirms the previous Early Jurassic age assignment of *Siderops*, but also illustrates the possibility for tighter age constraints for all chigutisaurids, many of which previously relied on biostratigraphic age controls, and may have implications for our understanding of their palaeobiogeographic and evolutionary history across Gondwana in the Mesozoic.

Implications for detrital zircon studies in Australia

This study, like a number of other recent similar studies, demonstrates the utility of detrital zircon geochronology for constraining the age of important continental vertebrate faunas in lieu of identifiable volcanic ash beds, and as a valuable supplement to refining biostratigraphy. Indeed, the application of detrital zircon geochronology to continental sedimentary successions, where biostratigraphy is typically imprecise, is proving to be a powerful tool for helping to refine the Jurassic-Early Cretaceous Spore-Pollen and Dinocyst zonation for Australia, as well as globally. Until very recently, the existence of widespread volcanic influence within Mesozoic basins of eastern Australia was mostly speculation (e.g., Bryan et al., 1997, 2012), with only a few known and even fewer dated volcanic ash beds from anywhere in the Jurassic-Cretaceous sedimentary succession of eastern Australia. However, work by Tucker et al. (2013, 2016, 2017), MacDonald et al., (2013), Lloyd et al., (2016; and references therein), Wainman et al. (2015, 2018a, b) and others now strongly supports the notion of long-lived volcanism along the east coast of the continent through much of the Mesozoic, demonstrating the potential for systematically developing a chronostratigraphy in parallel with refining the biozones across the Great Artesian Basin.

Supplementary Materials 1: LA-ICP-MS U–Pb Set-Up and Dating Method

Data acquisition was carried out at the Advanced Analytical Centre of James Cook University, using a Photon Machines Analyte.G2 193 nm ArF Excimer laser ablation system connected to a Thermo iCAP-RQ ICP-MS. The ablation cell was connected to the iCAP-RQ via Tygon tubing. Ablation was conducted in a HelEx II Active 2-Volume Cell using high-purity He as the carrier gas, which was subsequently mixed with argon and nitrogen gases prior to introduction into the ICP-MS.

The Thermo iCAP-RQ ICP-MS uses a unique 90° cylindrical ion lens known as the Right Angular Positive Ion Deflection ('RAPID') lens for optimum ion focusing and transmission. Completely off-axis design of the RAPID lens together with a new proprietary Qcell collision/reaction cell delivers a class leading background noise. The ICP-MS was regularly optimized using auto tune on a solution basis. It was tuned further for maximum sensitivity in laser ablation mode using glass NIST 610 under robust plasma conditions (U/Th = ~1) while maintaining oxide production rates (ThO/Th) to below 0.5%. All key tuning parameters are listed in Table 1. These conditions provide excellent analyte sensitivity with controlled ablation. Along with a small volume three-way mixing bulb the setup results in smooth time-integrated analytical signals. RSD of ^{238}U, ^{232}Th, and ^{206}Pb signals during line scan of NIST 610 is typically better than 2%. Detailed method is similar to that described in Spandler et al. (2016) and Tucker et al. (2013).

Conventional spot analyses were used for data acquisition of unknown samples. Laser fluence was set to ~3 J/cm^2 at the sample surface with a laser repetition rate and a beam diameter of 5 Hz and 30 µm, respectively. Each individual analysis contains 30 s background and 40 s sample integration. Analytes include ^{29}Si (10 ms), ^{49}Ti (20 ms), ^{91}Zr (10 ms), ^{200}Hg (10 ms), ^{204}(Pb + Hg) (10ms), ^{206}Pb (30 ms), ^{207}Pb (70 ms), ^{208}Pb (10 ms), ^{232}Th (10 ms), and ^{238}U (20 ms). Integration time of a single sweep is set to be ~0.2 s, so each sweep corresponds with a single laser shot in general. Each series of 10 zircon grains of unknown age were intercalated with two analyses of each standard (GJ1, Plesovice, and Temora 2). GJ1 was used for fractionation correction and instrumental drift calibration while Plesovice and Temora 2 were used for quality control. NIST 610 standards were analysed at the start and end of the run for calibration of Th and U concentrations.

Iolite v3.63 was used for data reduction using the U_Pb_Geochron4 data reduction scheme. Method is similar to that described in Paton et al. (2010). Principally, Iolite calculates raw U/Pb ratios after background subtraction. It then models the downhole fractionation based on the raw ratios and applies the fitted pattern to unknowns. Finally, it calibrates the instrumental drift according to the real time fluctuation of downhole fractionation corrected ratios of the primary standard. Isoplot 4.15 was used for Concordia and weighted mean average plots. Grains with discordance greater than 15% were omitted from interpretation.

Supplementary Table 1. Typical setup of the LA-ICP-MS at James Cook University.

Thermo iCAP-RQ	
Forward power	1450 W
Plasma gas	15 L/ min Argon
Auxiliary gas	0.8 L/min Argon
Make-up gas	0.5 L/min Argon
Shield torch	none
Sampling depth	5 mm
Photon Machines Analyte.G2 193 nm ArF Excimer laser	
Wavelength	193 nm
Pulse length	< 5 ns
Energy density	~3 J/cm^2
Carrier gas	0.8 (MFC1) +0.3 (MFC2) L/min Helium
Nitrogen	4 mL/min
Ablation style	Line scan
Scan speed	3 µm/s
Spot size	50 µm
Repetition rate	5 Hz

Supplementary Materials 2: U–Pb LA-ICP-MS Dating Tables

See thesis digital appendices.

Chapter 6:

Thesis Summary

Summary of Thesis Conclusions

This project recognised a significant gap in our knowledge of eastern Australian geology from the Middle Triassic–Early Cretaceous, despite these rocks containing some of the more important hydrocarbon and groundwater resources in the country, as well as globally unique Mesozoic fossil-bearing horizons. Our understanding of this period is greatly hindered by a lack of contemporaneous igneous bodies along eastern Australia in help interpret the tectonic setting during the mid-Mesozoic; however, this limitation can be partially addressed through investigation of coeval basin infill. The goal of this thesis was to provide lithostratigraphic, sedimentological, geochronological, and provenance context to understanding the tectonic, palaeogeographic and palaeoenvironmental framework of eastern Australia during this time. The Porcupine Gorge study area in northern Queensland presents an unmatched opportunity to investigate a long-lived Mesozoic depositional record from a single outcrop locality; which, when coupled with nearby stratigraphic drill cores, provides a useful record for addressing the main scientific questions proposed in this thesis.

Chapter 2 utilised a combination of lithostratigraphy, U–Pb zircon geochronology and palynology to identify two new sedimentary units within the Permian–Cretaceous stratigraphy in northern Queensland. The Galah Tuff Bed, dated at 251.5 ± 2.5 Ma, is a volcanic tuff horizon in the uppermost section of the Betts Creek beds. We suggest this is a correlative of the Yarrabee Tuff located in the Bowen Basin and provides strong evidence for extensive volcanism in the upper Permian throughout eastern Australia. The second newly defined unit in this study is the Upper Triassic Porcupine Gorge Formation, which records a previously unrecognised fluvial succession in the north-eastern Galilee Basin. In addition, marked changes in the thickness, age and sedimentology of the Jurassic and Cretaceous deposits in the gorge and regionally were identified, including refined maximum depositional age brackets (MDA) for the Injune Creek Group (MDA of 161.9 ± 3.1 Ma), Hooray Sandstone (MDA of 129.7 ± 2.3 Ma) and Gilbert River Formation (MDA of 122.5 ± 4 Ma). The discovery of Mesozoic detrital zircons from these units provides further support to the growing body of evidence that suggests interior basins were filled by a westward-draining volcanic arc off the eastern continental margin. The refined MDAs for many of these units are younger than the age ranges suggested by previously proposed palynozones, which indicates that Mesozoic palynozones for eastern Australia not well calibrated to the geological time scale. The work highlights the importance of future studies in these basins focused on using high-precision geochronological methods, such as chemical abrasion-isotope-dilution-thermal ionisation mass spectrometry (CA-ID-TIMS), to recalibrate Australian palynozones.

In Chapter 3, detailed sedimentological analysis of the Mesozoic stratigraphy in Porcupine Gorge (and nearby wells) revealed the presence of a long-lived fluvial system on the north-eastern margin of the Galilee and Eromanga basins. Twelve lithofacies and six architectural elements were identified within these sandy bed-load-dominated fluvial successions. The Porcupine Gorge Formation, Warang Sandstone, and upper Blantyre Sandstone record very similar sand- and gravel-dominated, low-sinuosity braided channel systems suggesting persistent low-accommodation depositional settings along the basin margin over most of the Mesozoic. However, during a brief interval in the Middle Jurassic, fluvial channels of the lower Blantyre Sandstone show a distinctive shift in morphology and style to higher-sinuosity channels with stable banks and lower sand to mud ratio. This 20 m-thick interval, which is interpreted to have occurred in a higher-accommodation setting, possibly in a transgressive systems tract, is potentially the result of a transgressing seaway in the Jurassic, as evidenced elsewhere in the Carpentaria and Surat basins. Aeolian deposition in the upper Blantyre Sandstone may point to increased aridity in the basin, which may have been driven by uplift of the eastern Australian margin in the Jurassic. The patterns of facies and alluvial architecture recognised in the Porcupine Gorge Formation, Warang Sandstone and Blantyre Sandstone – each representing a correlative unit from known aquifer-bearing units in the GAB – show significant lateral and vertical homogeneity within the sand bodies, which suggests the potential for excellent hydraulic connectivity. In addition, each of the formation boundaries, often represented by mudstones at unconformities, presents excellent confining units preventing loss of groundwater out of the system. From this, and despite the high clay content in some of these sand bodies, the Porcupine Gorge Formation, Warang Sandstone, and Blantyre Sandstone are all considered viable aquifers. The work done here shows the importance of utilising facies and alluvial architecture analysis to better characterise the fluvial aquifers within the GAB, which will lead to a better understanding of the ability of the system to recharge. This will be important going forward as climates shift and the population relying on groundwater in the GAB increases.

Chapter 4 reports on a sedimentary provenance investigation, utilising a combination of palaeocurrents, pebble counts, sandstone petrography, and U–Pb detrital zircon geochronology of the upper Permian to Lower Cretaceous strata of the north-eastern Galilee and Eromanga basins to reconstruct the palaeodrainage history during this time. Palaeocurrents in the upper Permian to Middle Jurassic were dominated by south to south-westerly flow, and sandstone petrography and detrital zircon results are consistent with this, suggesting northern and eastern sources in the Etheridge Province and the Kennedy Igneous Association.

A shift in palaeoflow to the north and north-east in the Late Jurassic is consistent with a change in detrital zircon populations that reflects a primary source in the Anakie Province to the south-east of the study area. This provenance shift is interpreted to be the result of an uplift of the eastern Australian margin (see co-authored paper in Appendix 1). Another provenance shift in the Early Cretaceous occurred, causing a switch back to bedrock sources in the Kennedy Igneous Association and new input of recycled volcanolithic sediment from the Whitsunday Volcanic Province to the east. In fact, numerous syn-depositional Mesozoic detrital zircon populations (mostly minor peaks) were documented in this study from multiple formations and are interpreted to be recycled from a distal volcanic arc-related sources on the eastern margin of the Australian continent.

Chapter 5 expands on the U–Pb detrital zircon studies utilised in Chapter 4 but focuses on applying these techniques to addressing long-standing questions about the age of several of Australia's most important Jurassic vertebrate fossil localities in eastern Australia. Specifically, this chapter investigates the potential to apply detrital zircon dating to sandstone matrix material still attached to fossilised bones from historic museum fossil collections. In collaboration with the Queensland Museum, matrix from the giant amphibian *Siderops kehli,* collected in the 1980s from the Evergreen Formation*,* was analysed, revealing a MDA for this taxon of 176.6 ± 2.0 Ma (upper Toarcian), which considerably refines the age of this taxon. Similarly, matrix from Queensland's only Jurassic dinosaur, *Rhoetosaurus brownei* (collected in 1926), was dated, revealing an MDA of 162.6 ± 1.1 Ma (lower Oxfordian). The refined age determination for this taxon is particularly significant, as it resolves an extended debate over its true stratigraphic provenance, and confirms an age consistent with the Walloon Coal Measures, as originally reported, but which contrasts with later interpretations that it may have come from the older Hutton Sandstone.

Future Work

This study was conducted as part of the larger Jurassic Arc Project. The results presented herein will be combined with a number of additional studies being conducted elsewhere in the Great

Artesian Basin to provide a holistic understanding of the tectonic framework of the eastern Australian margin during the Mesozoic. Future Lu-Hf geochemical analysis will be conducted on the Mesozoic grains from this study, along with other studies on coeval deposits in the Surat, Maryborough, Carpentaria, Laura, Papuan and other basins with the aim of building a large dataset of combined U–Pb and Lu-Hf data from detrital zircons and tuff zircons to better understand the tectono-magmatic provenance of these zircons, and to understand the source and nature of the volcanoes/plutons that produced these enigmatic grains that entered the basin during this time.

These results have also opened up new avenues to resolve outstanding correlation issues within the Triassic strata of the Galilee and Bowen basins. A comprehensive detrital zircon study on this succession, in addition to a detailed palynological investigation, could not only be used to better constrain the ages and correlations of these formations but could also better characterise the Triassic-Jurassic boundary and the effect of the Hunter-Bowen Orogeny on sedimentary deposition in the Triassic. This will also impact our understanding of the evolution of the Galilee and Bowen basins.

The successful application of detrital zircon dating of fossil matrix in Chapter 5 has also opened up new pathways to contextualise fossils in museum collections around the world where the local stratigraphy is unconstrained by primary igneous horizons such as tuff beds.

References

Adams, C.J., Cluzel, D., Griffin, W.L. 2009. Detrital-zircon ages and geochemistry of sedimentary rocks in basement terranes and their cover rocks in New Caledonia, and provenances at the Eastern Gondwanaland margin. *Australian Journal of Earth Sciences 56*, pp. 1023-1047.

Allen, J.R.L. 1983. Studies in fluviatile sedimentation: bars, bar-complexes and sandstone sheets (low-sinuosity braided streams) in the Brownstone (L. Devonian), Welsh Borders. *Sedimentary Geology 33*, pp. 237-293.

Allen, J.P. and Fielding, C.R. 2007a. Sedimentology and stratigraphic architecture of the Late Permian Betts Creek Beds, Queensland, Australia. *Sedimentary Geology 202*, pp. 5-34.

Allen, J.P. and Fielding, C.R. 2007b. Sequence architecture within a low-accommodation setting: an example from the Permian of the Galilee and Bowen basins, Queensland, Australia. *AAPG Bulletin 91*, pp. 1503-1539.

Almond, C.S. 1983. Stratigraphic drilling report – GSQ Eromanga 1. *Queensland Government Mining Journal 84*, pp. 358-368.

Anderson, M.P. 1989. Hydrogeological facies models to delineate large-scale spatial trends in glacial and glaciofluvial sediments. *Geological Society of America Bulletin 101*, pp. 501-511.

Anderson, M.P., Aiken, J.S., Webb, E.K., Mickelson, D.M. 1999. Sedimentology and hydrogeology of two braided stream deposits. *Sedimentary Geology 129*, pp. 187-199.

Ayaz, S.A., Martin, M., Esterle, J., Amelin, Y., Nicoll, R.S. 2016. Age of the Yarrabee and accessory tuffs: implications for the upper Permian sediment-accumulation rates across the Bowen Basin. *Australian Journal of Earth Sciences 63*, pp. 843-856.

Bagas, L. 2004. Proterozoic evolution and tectonic setting of the northwest Paterson Orogen, Western Australia. *Precambrian Research 128*, pp. 475-496.

Balfe, P.E. 1979. Stratigraphic drilling report – GSQ Hughenden 7. *Queensland Government Mining Journal 80*, pp. 282-293.

Batezelli, A., Ladeira, F.S.B., Do Nascimento, D.L., Da Silva, M.L. 2019. Facies and palaeosol analysis in a progradational distributive fluvial system from the Campanian–Maastrichtian Bauru Group, Brazil. *Sedimentology 66*, pp. 699-735

Bell, P.R., Fanti, F., Hart, L.J., Milan, L.A., Craven, S.J., Brougham, T., Smith, E. 2019. Revised geology, age, and vertebrate diversity of the dinosaur-bearing Griman Creek Formation (Cenomanian), Lightning Ridge, New South Wales, Australia. *Palaeogeography, Palaeoclimatology, Palaeoecology 514*, pp. 655-671.

Benvenuti, M. and Del Conte, S. 2013. Facies and sequence stratigraphic modelling of a Upper Pliocene–Lower Pleistocene fluvial succession (Valdelsa Basin, central Italy). *Sedimentary Geology 294*, pp. 303-314.

Besly, B.M. and Fielding, C.R. 1989. Palaeosols in Westphalian coal-bearing and red-bed sequences, Central and Northern England. *Palaeogeography, Palaeoclimatology, Palaeoecology 70*, pp. 303-330.

Bianchi, V., Zhou, F., Pistellato, D., Martin, M., Boccardo, S., Esterle, J. 2018. Mapping a coastal transition in braided systems: an example from the Precipice Sandstone, Surat Basin. *Australian Journal of Earth Sciences 65*, pp. 483-502.

Black, L.P., Kamo, S.L., Allen, C.M., Dais, D.W., Aleinikoff, J.N., Valley, J.W., Mundil, R., Campbell, I.H., Korsch, R.J., Williams, I.S. and Foudoulis, C. 2004. Improved $^{206}Pb/^{238}U$ microprobe geochronology by monitoring of a trace-element-related matrix effect;

SHRIMP, ID-TIMS, ELA-ICP-MS and oxygen isotope documentation for a series of zircon standards. *Chemical Geology 205*, pp. 115-140.

Blair, T.C. and McPherson, J.G. 1999. Grain-size and textural classification of coarse sedimentary particles. *Journal of Sedimentary Research 66*, pp. 6-19.

Boggs Jr., S. 2014. Transport and deposition of siliciclastic sediment. In: Boggs Jr., S. (Ed.), Principles of Sedimentology and Stratigraphy (5th Edition). Pearson Education Limited, Essex, UK.

Bongiolo, D.E., Scherer, C.M.S. Facies architecture and heterogeneity of the fluvial-aeolian reservoirs of the Sergi formation (Upper Jurassic), Reconcavo Basin, NE Brazil. *Marine and Petroleum Geology 27*, pp. 1885-1897.

Bordy, E.M., Head, H., Runds, M.J. 2016. Palaeoenvironment and provenance in the early Cape Basin of southwest Gondwana: sedimentology of the Lower Ordovician Piekenierskloof Formation, Cape Supergroup, South Africa. *South African Journal of Geology 119.2*, pp. 399-414.

Bristow, C.S. and Best, J.L. 1993. Braided rivers: perspectives and problems. In: Best, J.L. and Bristow, C.S. (Eds), Braided Rivers, Geological Society Special Publication No. 75, pp. 1-11.

Bryan, S.E., Constantine, A.E., Stephens, C.J., Ewart, A., Schon, R.W., Parianos, J. 1997. Early Cretaceous volcano-sedimentary successions along the eastern Australian continental margin: Implications for the break-up of eastern Gondwana. *Earth and Planetary Science Letters 153*, pp. 85-102.

Bryan, S.E., Ewart, A., Stephens, C.J., Parianos, J., Downes, P.J. 2000. The Whitsunday Volcanic Province, Central Queensland, Australia: lithological and stratigraphic investigations of a silicic-dominated large igneous province. *Journal of Volcanology and Geothermal Research 99*, pp. 55-78.

Bryan, S.E., Cook, A.G., Allen, C.M., Siegel, C., Purdy, D.J., Greentree, J.S., Uysal, I.T. 2012. Early-mid Cretaceous tectonic evolution of eastern Gondwana: From silicic LIP magmatism to continental rupture. *Episodes 35*, pp. 142-152.

Burger, D. 1973. Spore zonation and sedimentary history of the Neocomian, Great Artesian Basin, Queensland. Geological Society of Australia Special Publication 4, 87-118.

Burger, D. and Kemp, E.M. 1972. Notes on the Carboniferous to Cretaceous palynology of the Buchanan, Muttaburra, Tangorin and Hughenden 1:250,000 sheet areas, Queensland. *Bureau of Mineral Resources, Geology and Geophysics Record 1972/99*, 26 pp.

Burger, D. and Senior, B.R. 1979. A revision of the sedimentary and palynological history of northeastern Eromanga Basin, Queensland. *Australian Journal of Earth Sciences 26*, pp. 121-133.

Buys, J., Spandler, C., Holm, R.J., Richards, S.W. 2014. Remnants of ancient Australia in Vanuatu: implications for crustal evolution in island arcs and tectonic development of the southwest Pacific. *Geology 42*, pp. 939-942.

Cadle, A.B. and Cairncross, B. 1993. A sandy, bed-load dominated fluvial system deposited by lateral-accretion: Permian Karoo Sequence, South Africa. *Sedimentary Geology 85*, pp. 435-455.

Campbell, M., Rosenbaum, G., Shaanan, U., Fielding, C.R., Allen, C. 2015. The tectonic significance of lower Permian successions in the Texas Orocline (Eastern Australia). *Australian Journal of Earth Sciences 62*, pp. 789-806.

Campbell, R.J. and Haig, D.W. 1999. Bathymetric change during Early Cretaceous intracratonic marine transgression across the northeastern Eromanga Basin, Australia. *Cretaceous Research 20*, pp. 403-446.

Cant, D.J. and Walker, R.G. 1976. Development of a braided-fluvial facies model for the Devonian Battery Point Sandstone, Quebec. *Canadian Journal of Earth Sciences 13*, pp. 102-119.

Casey, D.J. 1970. Northern Eromanga Basin. Geological Survey of Queensland Record 1970/41.

Catuneau, O. 2006. *Principles of Sequence Stratigraphy*. Elsevier, Amsterdam, The Netherlands.

Champion, D.C. and Bultitude, R.J. 2013. Kennedy Igneous Association. In: Jell, P.A. (Ed.), Geology of Queensland, Geological Survey of Queensland, Brisbane, Queensland, pp. 473-514.

Cheng, Y., Todd, C.N., Henderson, R.A., Danisik, M., Sahlstrom, F., Chang, Z., Corral, I. 2019. Jurassic uplift and erosion of the northeast Queensland continental margin: evidence from (U-Th)/He thermochronology combined with U–Pb detrital zircon age spectra. *Australian Journal of Earth Sciences*, in review.

Collins, S. 2009. High stand or low stand: A geochemical and petrological insight into the cyclicity and depositional environment of the Wallabella Coal Member, Tinowon Formation, Bowen Basin. BSc Honors thesis, School of Earth Sciences, University of Queensland, Unpublished. St Lucia Qld.

Colombera, L. and Mountney, N.P. 2019. The lithofacies organization of fluvial channel deposits: a meta-analysis of modern rivers. *Sedimentary Geology 383*, pp. 16-40.

Colombera, L., Mountney, N.P., McCaffrey, W.D. 2013. A quantitative approach to fluvial facies models: methods and example results. *Sedimentology 60*, pp. 1526-1558.

Cook, A.G., Bryan, S.E., Draper, J.J. 2013. Post-orogenic Mesozoic basins and magmatism. In: Jell, P.A. (Ed.), Geology of Queensland 2013, Geological Survey of Queensland, Brisbane, Queensland, pp. 515-57

Cook, A.G., Saini, N., Hocknull, S.A. 2010. Dinosaur footprints from the lower Jurassic of Mount Morgan, Queensland. *Memoirs of the Queensland Museum 55*, pp. 135-146.

Corfu, F., Hanchar, J.M., Hoskin, P.W.O., Kinny, P. 2003. Atlas of zircon textures. In: Hanchar, J.M. and Hoskin, P.W.O. (Eds.), Zircon, Reviews in Mineralogy and Geochemistry 53, Mineralogical Society of America and the Geochemical Society, pp. 469-500.

Coutts, D.S., Matthews, W.A., Hubbard, S.M. 2019. Assessment of widely used methods to derive depositional ages from detrital zircon populations. *Geoscience Frontiers*, DOI: 10.1016/j.gsf.2018.11.002.

Coventry, R.J., Stephenson, P.J., Webb, A.W. 1985. Chronology of landscape evolution and soil development in the upper Flinders River area, Queensland, based on isotopic dating of Cainozoic basalts. *Australian Journal of Earth Sciences 32*, pp. 433-447.

Crawford, A.J., Meffre, S., Symonds, P.A. 2003. 120 to 0 Ma tectonic evolution of the southwest Pacific and analogous geological evolution of the 600 to 220 Ma Tasman Fold Belt System. *Geological Society of Australia Special Publication 22*, pp. 377-397.

Davies-Vollum, K.S. and Wing, S.L. 1998. Sedimentological, taphonomic, and climatic aspects of Eocene swamp deposits (Willwood Formation, Bighorn Basin, Wyoming). *Palaios 13*, pp. 28-40.

Davies-Vollum, K.S. and Kraus, M.J. 2001 A relationship between alluvial backswamps and avulsion cycles: an example from the Willwood Formation of the Bighorn Basin, Wyoming. *Sedimentary Geology 140*, pp. 235–249.

Day, M. and Kocurek, G. 2017. Aeolian dune interactions preserved in the ancient rock record. *Sedimentary Geology 358*, pp. 187-196.

de Caritat, P. and Braun, J. 1992. Cyclic development of sedimentary basins at convergent plate margins – 1. Structural and tectono-thermal evolution of some Gondwana basins of eastern Australia. *Journal of Geodynamics 16*, pp. 241-282.

de Jersey, N.J., & McKellar, J.L. 1980. Triassic palynology of the Warang Sandstone (Northern Galilee Basin) and its phytogeographic implications. In Cresswell, M. M., & Vella, P. (Eds.), *Proceedings of the Fifth International Gondwana Symposium* (pp. 31-35), Wellington, New Zealand.

de Jersey, N.J., Paten, R.J. 1964. Jurassic spores and pollen grains from the Surat Basin. *Geological Survey of Queensland Publication 322*, 18pp.

de Keyser, F., & Lucas, K.G. 1968. *Geology of the Hodgkinson and Laura Basins, North Queensland*. Canberra, ACT: Bureau of Mineral Resources, Geology and Geophysics, Bulletin, 84, 279 pp.

Dias-da-Silva, S., Sengupta, D.P., Cabreira, S.F., da Silva, L.R. 2012. The presence of *Compsocerops* (Brachyopoidea: Chigutisauridae) (Late Triassic) in southern Brazil with comments on chigutisaurd palaeobiogeography. *Palaeontology 55*, pp. 163-172.

Dickinson, W.R., Beard, L.S., Brackenridge, G.R., Erjavec, J.L., Ferguson, R.C., Inman, K.F., Knepp, R.A., Lindberg, F.A., Ryberg, P.L. 1983. Provenance of North American Phanerozoic sandstones in relation to tectonic setting. *Geological Society of America Bulletin 94*, pp. 222-235.

Dickinson, W.R., Gehrels, G.E. 2009. Use of U–Pb ages of detrital zircons to infer maximum depositional ages of strata: a test against a Colorado Plateau Mesozoic database. *Earth and Planetary Letters 288*, pp. 115-125.

Draper, J.J. (ed.) 2002. *Geology of the Cooper and Eromanga basins, Queensland*. Queensland Minerals and Energy Review Series, Queensland Department of Natural Resources and Mines, Brisbane, 92 pp.

Drochmann, T.K. (2015). *Sedimentology and provenance analysis of Jurassic and Early Cretaceous strata in the Carpentaria Basin*. Honours Thesis (unpub.), James Cook University, Townsville, Australia.

Ekes, C. 1993. Bedload-transported pedogenic mud aggregates in the Lower Old Red Sandstone in southwest Wales. *Journal of the Geological Society, London 150*, pp. 469-471.

Evans, P. R. (1964). *A correlation of some deep wells in the north-eastern Eromanga Basin, Central Queensland*. Canberra, ACT: Bureau of Mineral Resources, Geology and Geophysics, Record, 1964/197, 17 pp.

Evans, P.R. 1980. Geology of the Galilee Basin. In: Henderson, R.A. and Stephenson, P.J. (Eds.), The Geology and Geophysics of Northeastern Australia. Geological Society of Australia, Queensland Division, Brisbane, Queensland, Australia, pp. 299-305.

Evans, P.R. and Roberts, J. 1980. Evolution of central eastern Australia during the late Palaeozoic and early Mesozoic. *Australian Journal of Earth Sciences 26*, pp. 325-340.

Exon, N.F. 1971. Roma, Queensland 1:250 000 Geological Series. Explanatory Notes, Bureau of Mineral Resources, Geology and Geophysics, Canberra, Australian Capital Territory.

Exon, N.F., Senior, B.R, 1976. The Cretaceous of the Eromanga and Surat basins. Bureau of Mineral Resources Journal of Australian Geology and Geophysics Volume 1, Geoscience Australia, Canberra, pp. 33-50.

Exon, N.F., Quilty, P.G., Lafoy, Y., Crawford, A.J., Auzende, J-M. 2004. Miocene seamounts on northern Lord Howe Rise: lithology, age and origin. *Australian Journal of Earth Sciences 51*, pp. 291-300.

Fergusson, C.L., and Henderson, R.A. 2013. Thomson Orogen. In: Jell, P.A. (Ed.), Geology of Queensland, Geological Survey of Queensland, Brisbane, Queensland, pp. 136-145.

Fergusson, C.L., and Henderson, R.A. 2015. Early Palaeozoic continental growth in the Tasmanides of northeast Gondwana and its implications for Rodinia assembly and rifting. *Gondwana Research 28*, pp. 933-953.

Fergusson, C.L., Carr, P.F., Fanning, C.M., Green, T.J. 2001. Proterozoic-Cambrian detrital zircon and monazite ages from the Anakie Inlier, central Queensland: Grenville and Pacific-Gondwana signatures. *Australian Journal of Earth Sciences 48*, pp. 857-866.

Fergusson, C.L., Henderson, R.A., Lewthwaite, K.J., Philips, D., Withnall, I.W. 2005. Structure of the Early Palaeozoic Cape River Metamorphics, Tasmanides of north Queensland: evaluation of the roles of convergent and extensional tectonics. *Australian Journal of Earth Sciences 52*, pp. 261-277.

Fergusson, C.L., Henderson, R.A., Fanning, C.M., Withnall, I.W. 2007a. Detrital zircon ages in Neoproterozoic to Ordovician siliciclastic rocks, northeastern Australia: implications for the tectonic history of the East Gondwana continental margin. *Journal of the Geological Society, London 164*, pp. 215-225.

Fergusson, C.L., Henderson, R.A., Withnall, I.W., Fanning, C.M., Phillips, D., Lewthwaite, K.J. 2007b. Structural, metamorphic, and geochronological constraints on the alternating compression and extension in the Early Palaeozoic Gondwana Pacific margin, northeastern Australia. *Tectonics 26*, doi: 10.1029/2006TC001979

Fielding, C.R. 1996. Mesozoic sedimentary basins and resources in eastern Australia – a review of current understanding. *Geological Society of Australia, Abstracts 43*, pp. 180-185.

Fielding, C.R., Gray, A.R.G., Harris, G.I., Salomon, J.A. 1990. The Bowen Basin and overlying Surat Basin. In: Finlayson, D.M. (Ed.), The Eromanga-Brisbane Transect: a guide to basin development across Phanerozoic Australia in southern Queensland. Bureau of Mineral Resources, Geology and Geophysics, Canberra, pp. 105-116.

Fielding, C.R., Sliwa, R., Kassan, J. 2000. A new palaeogeographic synthesis of the Bowen central Queensland. In: Beeston, J.W. (Ed.), Proceedings of the Bowen Basin Symposium. Geological Society of Australia, Coal Geology Group and Bowen Basin Geologists Group, Rockhampton, pp. 287-302.

Flood, Y.S. and Hampson, G.J. 2014. Facies and architectural analysis to interpret avulsion style and variability: Upper Cretaceous Blackhawk Formation, Wasatch Plateau, Central Utah, USA. *Journal of Sedimentary Research 84*, pp. 743-762.

Flores, R.M., Blanchard, L.F., Sanchez, J.D., Walter, E., Muldoon, W.J. 1984. Paleogeographic controls of coal accumulation, Cretaceous Blackhawk Formation and Star Point Sandstone, Wasatch Plateau, Utah. *Geological Society of America Bulletin 95*, pp. 540-550.

Folk, R.L. (Ed.) 1974. Petrology of Sedimentary Rocks. Hemphill Publishing Company, Austin, Texas, USA.

Forbes, R.R. 1968. Taroom, Queensland 1:250 000 Geological Series. Explanatory Notes, Bureau of Mineral Resources, Geology and Geophysics, Canberra, Australian Capital Territory.

Frank, P.W. 1988. Conchostraca. *Palaeogeography, Palaeoclimatology, Palaeoecology 62*, pp. 399-403.

Fryberger, S. G. and Schenk, C. J. 1988. Pinstripe lamination: a distinctive feature of modern and ancient eolian sediments. *Sedimentary Geology 55*, pp. 1-15

Gallagher, K. 1990. Permian-Cretaceous subsidence history along the Eromanga-Brisbane geoscience transect. *Bulletin of the Bureau of Mineral Resources, Australia 232*, pp. 133-151.

Gallagher, K., Dumitru, T.A., Gleadow, A.J.W. 1994. Constraints on the vertical motion of eastern Australia during the Mesozoic. *Basin Research 6*, pp. 77-94.

Gallagher, K. and Lambeck, K. 1989. Subsidence, sedimentation and sea-level changes in the Eromanga Basin, Australia. *Basin Research 2*, pp. 115-131.

Gallagher, S.M., Wood, G.R., Lemon, N.L. 2008. Birkhead Formation chronostratigraphy on the Murteree Horst, South Australia: identifying and correlating reservoirs and seals. *PESA Eastern Australasian Basin Symposium III*, Sydney, 14-17 September, pp. 169-190.

Galloway, W.E. and Hobday, D.K. 1996. (Eds.) Terrigenous Clastic Depositional Systems Applications to Fossil Fuel and Groundwater Resources, 2nd Edition. Springer-Verlag, Berlin, Germany 489 pp.

Ghazi, S. and Mountney, N.P. 2009. Facies and architectural element analysis of a meandering fluvial succession: The Permian Warchha Sandstone, Salt Range, Pakistan. *Sedimentary Geology 221*, pp. 99-126.

Glen, R.A., 2005. The Tasmanides of eastern Australia. In: Vaughan, A.P.M., Leat, P.T., Pankhurst, R.J. (Eds.), Terrane Processes at the Margins of Gondwana. Geological Society, London, Special Publications 246, pp. 23-96.

Glen, R.A., 2013. Refining accretionary orogen models for the Tasmanides of eastern Australia. *Australian Journal of Earth Sciences 60*, pp. 315-370.

Glen, R.A., Fitzsimons, I.C.W., Griffin, W.L., Saeed, A. 2017. East Antarctic sources of extensive Lower-Middle Ordovician turbidites in the Lachlan Orogen, southern Tasmanides, eastern Australia. *Australian Journal of Earth Sciences 64*, pp. 142-224.

Glut, D.F. 1997. Dinosaurs the Encyclopedia. McFarland & Company, Inc., Publishers, Jefferson, North Carolina. 1075 pp.

Grant-Mackie, J.A., Aita, Y., Balme, B.E., Campbell, H.J., Challinor, A.B., MacFarlan, D.A.B., Molnar, R.E., Stevens, G.R., Thulborn, R.A. 2000. Jurassic palaeobiogeography of Australasia. In: Wright, A.J., Young, G.C., Talent, J.A., Laurie, J.R. (Eds.), Palaeobiogeography of Australasian faunas and floras. *Memoir of the Association of Australasian Palaeontologists 23*, Geological Society of Australia, pp. 311-353.

Gray, A.R.G. 1977. Stratigraphic drilling in the Hughenden 1:250 000 sheet area, 1974-75. *Queensland Government Mining Journal 78*, pp. 382-392.

Gray, A.R.G., McKillop., M., McKellar, J.L. 2002. Eromanga Basin Stratigraphy. In: Draper, J.J. (Ed.), Geology of the Cooper and Eromanga basins, Queensland. Queensland Government Department of Natural Resources and Mines, Brisbane, Queensland, pp. 30-59.

Green, P.M. 1997. Geological Setting. In: Green, P.M. (Ed.), The Surat and Bowen basins, South-East Queensland. Queensland Minerals and Energy Review Series, Queensland Department of Mines and Energy, Brisbane, Australia, pp. 4-6.

Green, P.M., Carmichael, D.C., Brain, T.J., Murray, C.G., McKellar, J.L., Beeston, J.W., Gray, A.R.G. 1997. Lithostratigraphic units in the Bowen and Surat basins, Queensland. In: Green, P.M. (Ed.), The Surat and Bowen basins, South-East Queensland. Queensland

Minerals and Energy Review Series, Queensland Department of Mines and Energy, Brisbane, Australia, pp. 41-108.

Gurnis, M., Muller, R.D., Moresi, L. 1998. Cretaceous vertical motion of Australia and the Australian-Antarctic Discordance. *Science 279*, pp. 1499-1503.

Habermehl, M.A. 1980. The Great Artesian Basin, Australia. *BMR Journal of Australian Geology and Geophysics 5*, pp. 9-38.

Habermehl, M.A. 1983. Hydrogeology and hydrochemistry of the Great Artesian Basin, Australia. In: Papers on the International Conference on Groundwater and Management, Sydney. Australian Water Resources Council Conference Service 8, pp. 83-98.

Habermehl, M.A. 2001. Wire-line logged waterbores in the Great Artesian Basin, Australia – Digital data of logs and waterbore data acquired by AGSO. Bureau of Rural Sciences Publication, Canberra, Australia.

Hamilton, S., Esterle, J., Sliwa, R. 2014. Stratigraphic and depositional framework of the Walloon Subgroup, eastern Surat Basin, Queensland. *Australian Journal of Earth Sciences 8*, pp. 1061-1080.

Hawkins, P.J. 1977. Galilee Basin – Prospect Review. Petroleum in Queensland: a stocktake for the future, Proceedings, Petroleum Exploration Society of Australia, Queensland Branch, Brisbane, Australia, 47 pp.

Hawkins, P.J. and Green, P.M. 1993. Exploration results, hydrocarbon potential and future strategies for the northern Galilee Basin. *APEA Journal 33*, pp. 280-296.

Hawkins, P. J., & Williams, L. J. 1990. *Review of the geology and economic potential of the Laura Basin*. Brisbane, QLD: Queensland Department of Resource Industries, Record, 1990/2, 41 pp.

Helby, R., Morgan, R. and Partridge, A.D. 1987. A palynological zonation of the Australian Mesozoic. In: Studies in Australian Mesozoic Palynology, edited by Jell, P.A., pp. 1-94, Association of Australasian Palaeontologists Memoir 4.

Henry, R.L. and Benade, D.R. 1982. Annual report of exploration activities in Authority to Prospect 226C, North Queensland. 1st January 1981 – 31st December 1981, report no. 363, Utah Development Company, Exploration Department, Brisbane, unpublished report held by the Geological Survey of Queensland as CR9813C.

Hill, D., Playford, G., Woods, J.T. 1966. Jurassic fossils of Queensland. Queensland Palaeontological Society, Brisbane, 32 pp.

Hjellbakk, A. 1997. Facies and fluvial architecture of a high-energy braided river: the Upper Proterozoic Seglodden member, Varanger Peninsula, northern Norway. *Sedimentary Geology 114*, pp. 131-161.

Hoffman, K.L. 1988. Revision of the limits of the Adavale Basin and Warrabin Trough, southwest Queensland. *Geological Survey of Queensland Record 1988/18*, 10 pp.

Holcombe, R.J. Stephens, C.J., Fielding, C.R., Gust, D.A., Little, T.A., Sliwa, R., Kassan, J., McPhie, K., Ewart, A. 1997. Tectonic evolution of the northern New England Fold Belt: the Permian-Triassic Hunter-Bowen event. *Geological Society of Australia, Special Publication 19*, pp. 52-65.

Hornung, J. and Aigner, T. 1999. Reservoir and aquifer characterization of fluvial architectural elements: Stubensandstein, Upper Triassic, southwest Germany. *Sedimentary Geology 129*, pp. 215-280.

Hoy, D. and Rosenbaum, G. 2017. Episodic behaviour of Gondwanide deromation in eastern Australia: insights from the Gympie Terrane. *Tectonics 36*, pp. 1497-1520.

Hoy, D., Rosenbaum, G., Mortimer, N., Shaanan, U. 2018. Hunter-Bowen deformation in South Percy Island, northeastern Australia. *Australian Journal of Earth Sciences 65*, pp. 175-190.

Huerta, P., Armenteros, I., Silva, P.G. 2011. Large-scale architecture in non-marine basins: the response to the interplay between accommodation space and sediment supply. *Sedimentology 58*, pp. 1716-1736.

Huggenberger, P., Aigner, T. 1999. Introduction to the special issue on aquifer-sedimentology: problems, perspectives and modern approaches. *Sedimentary Geology 129*, pp. 179-186.

Hunter, R.E. 1977. Basic types of stratification in small eolian dunes. Sedimentology 24, pp. 361-387.

Hunter, R.R. 1981. Stratification styles in eolian sandstones: some Pennsylvanian to Jurassic examples from the Western Interior, U.S.A. In: Ethridge, F.G. and Flores, R.M (Eds), Recent and Ancient Nonmarine Depositional Environments: Models for Exploration, Society for Sedimentary Geology Special Publication 31, pp. 315-329.

I'Anson, A., Deighton, I., Muller, R.D., Dutkiewicz, A., Heine, C. 2018. Burial and exhumation history of the Galilee Basin, Australia: Implications for unconventional hydrocarbon prospectivity. *AAPG Bulletin 102*, pp. 483-507.

Ielpi, A., Gibling, M.R., Bashforth, A.R., Lally, C., Rygel, M.C., Al-Silwadi, S. 2014. Role of vegetation in shaping Early Pennsylvanian braided rivers: architecture of the Boss Point Formation, Atlantic Canada. *Sedimentology 61*, pp. 1659-1700.

Ingersoll, R.V., Bullard, T.F., Ford, R.L., Grimm, J.P., Pickle, J.D., Sares, S.W. 1974. The effect of grain size on detrital modes: a test of the Gazzi-Dickinson point counting method. *Journal of Sedimentary Research 54*, pp. 103-116.

Ireland, T.R., Flottmann, T., Fanning, C.M., Gobson, G.M., Priess, W.V. 1998. Development of the early Paleozoic Pacific margin of Gondwana from detrital-zircon ages across the Delamerian orogen. *Geology 26*, pp. 243-246.

Jackson, S.E., Pearson, N.J., Griffin, W.L. and Belousova, E.A. 2004. The application of laser ablation-inductively coupled plasma-mass spectrometry to in situ U–Pb zircon geochronology. *Chemical Geology 211*, pp. 47-69.

Jinnah, Z.A. and Roberts, E.M. 2011. Facies associations, paleoenvironment, and base-level changes in the Upper Cretaceous Wahweap Formation, Utah, U.S.A. *Journal of Sedimentary Research 81*, pp. 266-283.

Jones, A. 2003. Sedimentological record of the late Palaeozoic Gondwanan glaciation in Queensland. PhD Thesis, Department of Earth Sciences, The University of Queensland, Brisbane, Australia.

Jones, A.T. and Fielding, C.R. 2004. Sedimentological record of the late Palaeozoic glaciation in Queensland, Australia. *Geology 32*, pp. 153-156.

Jones, J.G. and Veevers, J.J. 1983. Mesozoic origins and antecedents of Australia's Eastern Highlands. *Australian Journal of Earth Sciences 30*, pp. 305-322.

Jones, S.J., Frostick, L.E., Astin, T.R. 2001. Braided stream and flood plain architecture: the Rio Vero Formation, Spanish Pyrenees. *Sedimentary Geology 139*, pp. 229-260.

Kear, B.P. 2012. A revision of Australia's Jurassic plesiosaurs. Palaeontology 55, 1125-1138.

Kear, B. P., Hamilton-Bruce, R.J. 2011. Dinosaurs in Australia: Mesozoic Life from the Southern Continent. CSIRO Publishing, Collingwood, Victoria, Australia, 190 pp.

Klingbeil, R., Kleineidam, S., Asprion, U., Aigner, T., Teutsch, G. 1999. Relating lithofacies to hydrofacies: outcrop-based hydrogeological characterisation of Quaternary gravel deposits. *Sedimentary Geology 129*, pp. 299-310.

Kocurek, G. 1991. Interpretation of ancient eolian sand dunes. *Annual Review of Earth and Planetary Sciences 19*, pp. 43-75.

Korsch, R.J., Totterdell, J.M., Fomin. T., Nicoll, M.G. 2009. Contractional structures and deformational events in the Bowen, Gunnedah and Surat Basins, eastern Australia. *Australian Journal of Earth Sciences 56*, pp. 477-499.

Kozur, H.W. and Weems, R.E. 2010. The biostratigraphic importance of conchostracans in the continental Triassic of the northern hemisphere. In: Lucas, S.G. (Ed.), The Triassic Timescale, Geological Society, London, Special Publication 334, pp. 315-417.

Kraus, M.J. and Aslan, A. 1993. Eocene hydromorphic paleosols: significance for interpreting ancient floodplain processes. *Journal of Sedimentary Petrology 63*, pp. 453-463.

La Croix, A.D., Wang, J., He, J., Hannaford, C., Bianchi, V., Esterle, J., Undershultz, J.R. 2019. Widespread nearshore and shallow marine deposition within the Lower Jurassic Precipice Sandstone and Evergreen Formation in the Surat Basin, Australia. *Marine and Petroleum Geology 109*, pp. 760-790.

Laurie, J.R., Bodorkos, S., Nicoll, R.S., Crowley, J.L., Mantle, D.J., Mory, A.J., Wood, G.R., Backhouse, J., Holmes, E.K., Smith, T.E., Champion, D.C. 2016. Calibrating the middle and late Permian palynostratigraphy of Australia to the geologic time-scale via U–Pb zircon CA-IDTIMS dating. *Australian Journal of Earth Sciences 63*, pp. 701-730.

Leeder, M. 2011. Sedimentology and Sedimentary Basins: From Turbulence to Tectonics, 2nd Edition. Wiley-Blackwell, Oxford, United Kingdom, 1056 pp.

Li, P-F., Rosebnaum, G., Rubatto, D. 2012. Triassic asymmetric subduction rollback in the southern New England Orogen (eastern Australia): the end of the Hunter-Bowen Orogeny. *Australian Journal of Earth Sciences 59*, pp. 965-981.

Lloyd, J., Collins, A.S., Payne, J.L., Glorie, S., Holford, S., Reid, A.J. 2016. Tracking the Cretaceous transcontinental Ceduna River through Australia: the hafnium isotope record of detrital zircons from offshore southern Australia. *Geoscience Frontiers 7*, pp. 237-244.

Long, J.A., Molnar, R.E. 1998. A new Jurassic theropod dinosaur from Western Australia. *Records of the Western Australian Museum 19*, pp. 121-129.

Longman, H.A. 1926. A giant dinosaur from Durham Downs, Queensland. *Memoirs of the Queensland Museum 8*, pp. 183-194.

Longman, H.A. 1941. A Queensland fossil amphibian. *Memoirs of the Queensland Museum 12,* pp. 29-32.

Ludwig, J.R. 2008. User's Manual for Isoplot 3.70: A geochronological toolkit for Microsoft Excel. Berkeley Geochronology Center Special Publication No. 4, Berkeley, California.

MacDonald, J.D., Holford, S.P., Green, P.F., Duddy, A.R., King, R.C., Backe, G. 2013. Detrital zircon data reveal the origin of Australia's largest delta system. *Journal of the Geological Society, London, 170*, pp. 3-6.

Mack, G.H., James, W.C., Monger, H.C. 1993. Classification of paleosols. *Geological Society of America Bulletin 105*, pp. 129-136.

Mannion, P.D., Upchurch, P., Barnes, R.N., Mateus, O. 2013. Osteology of the Late Jurassic Portuguese sauropod dinosaur *Lusotitan ataliensis* (Macronaria) and the evolutionary history of basal titansauriforms. Zoolological Journal of the Linnean Society 168, 98-206.

Mannion, P.D., Upchurch, P., Schwarz, D., Wings, O. 2019. Taxonomic affinities of the putative titanosaurs from the Late Jurassic Tendaguru Formation of Tanzania: phylogenetic and biogeographic implications for eusauropod dinosaur evolution. Zoological Journal of the Linnean Society 185, 784-909.

Martin, E.L., Collins, W.J., Kirkland, C.L. 2017. An Australian source for Pacific-Gondwanan zircons: implications for the assembly of northeastern Gondwana. *Geology 45*, pp. 699-702.

Martin, M., Wakefield, M., Bianchi, V., Esterle, J., Zhou, F. Evidence for marine influence in the Lower Jurassic Precipice Sandstone, Surat Basin, eastern Australia. *Australian Journal of Earth Sciences 65*, pp. 75-91.

Marzolf, J. E. 1988. Controls on late Paleozoic and early Mesozoic eolian deposition of the western United States. *Sedimentary Geology 56*, pp. 167-191.

Matthews, K.J., Hale, A.J., Gurnis, M., Muller, R.D., DiCaprio, L. 2011. Dynamic subsidence of Eastern Australia during the Cretaceous. *Gondwana Research 19*, pp. 372-383.

McIntosh, J.S. 1990. Sauropoda. In: Weishampel, D.B. Dodson, P. and Osmolska, H. (Eds.), The Dinosauria, 1st edition. University of California Press, Berkeley, California, pp. 259-322.

McKellar, J.L. 1977. Palynostratigraphy of core samples from the Hughenden 1:250 000 Sheet area, northern Galilee and Eromanga basins. *Queensland Government Mining Journal 78*, pp. 393-399.

McKellar, J.L. 1979. Palynostratigraphy of core samples from GSQ Hughenden 7. *Queensland Government Mining Journal 80*, pp. 295-302.

Metcalfe, I., Crowley, J.L., Nicoll, R.S., Schmitz, M. 2015. High-precision U–Pb CA-TIMS calibration of middle Permian to Lower Triassic sequences, mass extinction and extreme climate-change in eastern Australian Gondwana. *Gondwana Research 28*, pp. 61-81.

Miall, A.D. 1977. A review of the braided-river depositional environment. *Earth Science Reviews 13*, 1-62.

Miall, A.D. 1985. Architectural-element analysis: a new method of facies analysis applied to fluvial deposits. *Earth-Science Reviews 22*, 261-308.

Miall, A.D. 1988. Architectural elements and bounding surfaces in fluvial deposits: anatomy of the Kayenta Formation (Lower Jurassic), southwest Colorado. *Sedimentary Geology 55*, pp. 233-262.

Miall, A.D. 1994. Reconstructing fluvial macroform architecture from two-dimensional outcrops: examples from the Castlegate Sandstone, Book Cliffs, Utah. *Journal of Sedimentary Research B64*, pp. 146-158.

Miall, A.D. 1996. The Geology of Fluvial Deposits: Sedimentary Facies, Basin Analysis, and Petroleum Geology. Springer-Verlag, Berlin, 582 pp.

Miall, A.D. 2006. The Geology of Fluvial Deposits: Sedimentary Facies, Basin Analysis, and Petroleum Geology, 4th corrected printing. Springer-Verlag, Berlin, 599 pp.

Miall, A.D. 2010. The Geology of Stratigraphic Sequences, Second Edition. Springer, Berlin Heidelberg, 532 pp.

Miall, A.D. and Jones, B.G. 2003. Fluvial architecture of the Hawkesbury Sandstone (Triassic), near Sydney, Australia. *Journal of Sedimentary Research 73*, pp. 531-545.

Michaelson, P., Henderson, R.A., Crosdale, P.J., Fanning, C.M. 2001. Age and significance of the Platypus Tuff Bed, a regional reference horizon in the upper Permian Moranbah Coal Measures, north Bowen Basin. *Australian Journal of Earth Sciences 48*, pp. 192-192.

Middleton, M.F. 1980. A model of intracratonic basin formation, entailing deep crustal metamorphism. *Geophysical Journal of the Royal Astronomical Society 62*, pp. 1-14.

Molnar, R.E. 1980. Australian late Mesozoic terrestrial tetrapods: some implications. Mémoires de la Société Géologique de France (Nouvelle Série) 139, pp. 131-143.

Molnar, R.E. 1982. A catalogue of fossil amphibians and reptiles in Queensland. *Memoirs of the Queensland Museum 20*, pp. 613-633.

Molnar, R.E. 1984. Ornithischian dinosaurs in Australia. In: Reif, W.E., Westphal, F. (Eds.), Third Symposium on Mesozoic Terrestrial Ecosystems, Short Papers. Attempto Verlag, Tubingen, pp. 151-156.

Molnar, R.E. 1991. Fossil reptiles in Australia. In: Vickers-Rich, P., Monaghan, J.M., Baird, R.F. and Rich, T.H. (Eds.), Vertebrate Palaeontology of Australasia. Pioneer Design Studio, Monash University Publications Committee, Melbourne, Australia, pp. 605-702.

Mortimer, N., Hauff, F., Calvert, A.T. 2008. Continuation of the New England Orogen, Australia, beneath the Queensland Plateau and Lord Howe Rise. *Australian Journal of Earth Sciences 55*, pp. 195-209.

Mortimer, N., Turnbull, R.E., Palin, J.M., Tulloch, A.J., Rollet, N., Hashimoto, T. 2015. Triassic-Jurassic granites on the Lord Howe Rise, northern Zealandia. *Australian Journal of Earth Sciences 62*, pp. 735-742.

Mortimer, N., Campbell, H.J., Tulloch, A.J., King, P.R., Stagpoole, V.M., Wood, R.A., Rattenbury, M.S., Sutherland, R., Adams, C.J., Collot, J., Seton, M. 2017. Zealandia: Earth's Hidden Continent. *GSA Today 27*, doi: 10.1130/GSATG321A.1.

Moya, C.E., Raiber, M., Cox, M.E. 2014. Three-dimensional geological modelling of the Galilee and central Eromanga basins, Australia: New insights into aquifer/aquitard geometry and potential influence of faults on inter-connectivity. *Journal of Hydrology: Regional Studies 2*, pp. 119-139.

Moya, C.E., Raiber, M., Taulis, M., Cox, M.E. 2015. Hydrochemical evolution and groundwater flow processes in the Galilee and Eromanga basins, Great Artesian Basin, Australia: A multivariate statistical approach. *Science of the Total Environment 508*, pp. 411-426.

Müller, R.D., Flament, N., Matthews, K.J., Williams, S.E., Gurnis, M. 2016. Formation of Australian continental margin highlands driven by plate-mantle interaction. *Earth and Planetary Science Letters 441*, pp. 60-70.

Nair, J.P., Salisbury, S.W. 2012. New anatomical information on *Rhoetosaurus brownei* Longman, 1926, a Gravisaurian sauropodomorph dinosaur from the Middle Jurassic of Queensland, Australia. *Journal of Vertebrate Paleontology 32*, pp. 369-394.

Nishiya, T., Watanabe, T., Yokoyama, K., Kuramoto, Y. 2003. New isotopic constraints on the age of the Halls Reward Metamorphics, North Queensland, Australia: Delamerian metamorphic ages and Grenville detrital zircons. *Gondwana Research 6*, pp. 241-249.

Nordsvan, A., Collins, W.J., Li, Z., Spencers, C.J., Pourteau, A., Withnall, I.W., Betts, P.G., Volante, S. 2018. Laurentian crust in northeast Australia: implications for the assembly of the supercontinent Nuna. *Geology*, doi: 10.1130/G39980.1

Norvick, M. 1974. Permian and late Carboniferous palynostratigraphy of the Galilee Basin, Queensland. *Bureau of Mineral Resources, Geology and Geophysics Report 219*, 174 pp.

Partridge, A.D. 2006. Jurassic-Early Cretaceous dinocysts zonations NWS Australia: 1st update of HMP 2004. In Monteil, R. (coord.), *Australian Mesozoic and Cenozoic Palynology Zonations – updated to the 2004 Geologic Time Scale* (8 pp). Canberra, ACT: Geoscience Australia, Record 2006-23.

Paton, C., Woodhead, J.D., Hellstrom, J.C., Hergt, J.M., Greig, A., Maas, R. 2010. Improved laser ablation U–Pb zircon geochronology through robust downhole fractionation correction. Geochemistry Geophysics Geosystems 11, doi: 10.1029/2009GC002618

Paton, C., Hellstrom, J., Paul, B., Woodhead, J., Hergt, J. 2011. Iolite: Freeware for the visualisation and processing of mass spectrometric data. *Journal of Analytical Atomic Spectrometry 26*, pp. 2508-2518.

Phillips, L.J., Esterle, J.S., Edwards, S.A. 2017a. Review of Lopingian (upper Permian) stratigraphy of the Galilee Basin, Queensland, Australia. *Australian Journal of Earth Sciences 64*, pp. 283-300.

Phillips, L.J., Edwards, S.A., Bianchi, V., Esterle, J.S. 2017b. Paleo-environmental reconstruction of Lopingian (upper Permian) sediments in the Galilee Basin, Queensland, Australia. *Australian Journal of Earth Sciences 65*, pp. 587-609.

Phillips, L.J., Crowley, J.L., Mantle, D.J., Esterle, J.S., Nicoll, R.S., McKellar, J.L., Wheeler, A. 2018a. U–Pb geochronology and palynology from Lopingian (upper Permian) coal measure strata of the Galilee Basin, Queensland, Australia. *Australian Journal of Earth Sciences 65*, pp. 153-173.

Phillips, L.J., Verdel, C., Allen, C.M., Esterle, J.S. 2018b. Detrital zircon U–Pb geochronology of Permian strata in the Galilee Basin, Queensland, Australia. *Australian Journal of Earth Sciences 65*, pp. 465-481.

Price, P.L., Filatoff, J., Williams, A.J., Pickering, S.A., Wood, G.R. 1985. Late Palaeozoic and Mesozoic palynostratigraphic units. CSR Oil and Gas Division Palynology Facility Report 274/225. Department of Resource Industries Open File report CR 14012, 20, (unpub.), Queensland Department of Employment, Economic Development and Innovation, Brisbane, Australia.

Price, P.L. 1997. Permian to Jurassic palynostratigraphic nomenclature of the Bowen and Surat basins. In: Green, P.M. (Ed.), The Surat and Bowen basins, South-East Queensland.

Queensland Minerals and Energy Review Series, Queensland Department of Mines and Energy, Brisbane, Australia, pp. 137-178.

Purdy, D.J. 2013. Granitoids of the northern New England Orogen. In: Jell, P.A. (Ed.), Geology of Queensland, Geological Survey of Queensland, Brisbane, Queensland, pp. 399-444.

Ransley, T.R., Radke, B.M., Feitz, A.J., Kellett, J.R., Owens, R., Bell, J., Stewart, G., Carey, H. 2015. Hydrogeological atlas of the Great Artesian Basin. Geoscience Australia, Australian Government, Canberra, Australian Capital Territory, 130 pp.

Rauhut, O.W.M., Carballido, J.L., Pol, D. 2015. A diplodocid sauropod dinosaur from the Late Jurassic Canadon Calcareo Formation of Chubut, Argentina. Journal of Vertebrate Paleontology 35, e982798, doi: 10.180/02724634.2015.982798

Raza, A., Hill, K. C., & Korsch, R. J. 2009. Mid-Cretaceous uplift and denudation of the Bowen and Surat basins, eastern Australia: relationship to Tasman Sea rifting from apatite fission-track and vitrinite-reflectance data. *Australian Journal of Earth Sciences, 56*, pp. 501-531.

Reiser, R.F., Williams, A.J. 1969. Palynology of the Lower Jurassic sediments of the northern Surat Basin, Queensland. Geological Survey of Queensland Publication 339, Palaeontological Paper 15, 24 pp.

Retallack, G.J. 2001. Cenozoic expansion of grasslands and climatic cooling. *The Journal of Geology 109*, pp. 407-426.

Rino, S., Kon, Y., Sato, W., Maruyama, S., Santosh, M., Zhao, D. 2008. The Grenvillian and Pan-African orogens: World's largest orogenies through geologic time, and their implications on the origin of superplume. *Gondwana Research 14*, pp. 51-72.

Roberts, E.M. 2007. Facies architecture and depositional environments of the Upper Cretaceous Kaiparowits Formation, southern Utah. *Sedimentary Geology 197*, 207-233.

Rosenbaum, G. 2018. The Tasmanides: Phanerozoic tectonic evolution of eastern Australia. *Annual Review of Earth and Planetary Sciences 46*, pp. 291-325.

Russell, M. and Gurnis, M. 1994. The planform of epeirogeny: vertical motions of Australia during the Cretaceous. *Basin Research 6*, pp. 63-76.

Sato, T. and Chan, M.A. 2015. Fluvial facies architecture and sequence stratigraphy of the Tertiary Duchesne River Formation, Uinta Basin, Utah, U.S.A. *Journal of Sedimentary Research 85*, 1428-1454.

Scherer, C.M.S., Goldberg, K., Bardola, T. 2015. Facies architecture and sequence stratigraphy of an early post-rift fluvial succession, Aptian Barbalha Formation, Araripe Basin, northeastern Brazil. *Sedimentary Geology 322*, pp. 43-62

Scotese, C.R. 2016. PALEOMAP PaleoAtlas for GPlates and the PaleoData Plotter Program, PALEOMAP Project, http://www.earthbyte.org/paleomap---paleoatlas---for---gplates/

Shaanan, U., Rosenbaum, G., Sihombing, F.M.H. 2018. Continuation of the Ross-Delamerian Orogen: insights from eastern Australian detrital-zircon data. *Australian Journal of Earth Sciences 65*, pp. 1123-1131.

Simpson, E.L., Hilbert-Wolf, H.L., Simpson, W.S., Tindall, S.E., Bernard, J.J., Jenesky, T.A., Wizevich, M.C. 2008. The interaction of aeolian and fluvial processes during deposition of the Upper Cretaceous capping sandstone member, Wahweap Formation, Kaiparowits Basin, Utah, U.S.A. *Paleogeography, Palaeoclimatology, Palaeoecology 270*, 19-28.

Smart, J. and Senior, B.R. 1980. Jurassic-Cretaceous basins of northeastern Australia. In: Henderson, R.A. and Stephenson, P.J. (Eds.), The Geology and Geophysics of Northeastern Australia. Geological Society of Australia, Queensland Division, Brisbane, Queensland, Australia, pp. 315-328.

Smart, J., Grimes, K.G., Doutch, H.F. 1971. New and revised stratigraphic names – Carpentaria Basin. *Queensland Government Mining Journal 73*, pp. 190-201.

Smith, T.E. and Mantle, D.J. 2013. *Late Permian palynozones and associated CA-IDTIMS dates tuffs from the Bowen Basin, Australia*. Record 2013-46, Canberra, ACT: Geoscience Australia.

Soares, M.V.T., Basilici, G., da Silva Marinho, T., Martinelli, A.G., Marconato, A., Mountnet, N.P., Colombera, L., Mesquita, A. F. Vasques, J.T., Abrante Junior, F.R., Ribeiro, L.C.B. 2019. Sedimentology of a distributive fluvial system: The Serra de Galga Formation, a new lithostratigraphic unit (Upper Cretaceous, Bauru Basin, Brazil). *Geological Journal*, doi:10.1002/gj.3987, 25 pp.

Spandler, C. Hammerli, J., Sha, P., Hilbert-Wolf, H., Hu, Y., Roberts, E., Schmitz, M. 2016. MKED1: A new titanite standard for in situ analysis of Sm-Nd isotopes and U–Pb geochronology. *Chemical Geology 425*, pp. 110-126.

Struckmeyer, H.I.M. and Totterdell, J.M. 1990. *Australia: Evolution of a Continent*, Australian Government Publishing Service, Canberra, Australia, 97 pp.

Swarbrick, C.F.J. 1975. Surat Basin. In: Knight, C.L., Traves, D.M., King, D. (Eds.), Economic Geology of Australia and Papua New Guinea – 2. Coal. The Australasian Institute of Mining and Metallurgy Monograph Series No. 6, Parkville, Victoria, Australia.

Swarbrick, C.F.J., Gray, A.R.G., Exon, N.F. 1973. Injune Creek Group – Amendments and an addition to stratigraphic nomenclature in the Surat Basin. *Queensland Government Mining Journal 74*, pp. 57-63.

Tapster, S., Roberts, N.M.W., Petterson, M.G., Saunders, A.D., Naden, J. 2014. From continent to intra-oceanic arc: Zircon xenocrysts record the crustal evolution of the Solomon island arc. *Geology 42*, pp. 1087-1090.

Tasch, P. 1969. Branchiopoda, order Conchostraca. In: Moore, R.C. (Ed). Treatise on invertebrate Paleontology. R, Arthropoda 4, pp. 141-163.

Thulborn, R.A. 1994. Ornithopod dinosaur tracks from the Lower Jurassic of Queensland. *Alcheringa 18*, pp. 247-258.

Thulborn, R.A., Warren, A.A. 1980. Early Jurassic plesiosaurs from Australia. *Nature 285*, pp. 224-225.

Todd, C.N., Roberts, E.M., Knutsen, E.M., Rozefelds, A.C., Huang, H-Q., Spandler, C. 2019. Refined age and geological context of two of Australia's most important Jurassic vertebrate taxa (*Rhoetosaurus brownei* and *Siderops kehli*), Queensland. *Gondwana Research 76*, pp. 19-26.

Tucker, R.T., Roberts, E.M., Hu, Y., Kemp, A.I.S., Salisbury, S.W. 2013. Detrital zircon age constraints for the Winton Formation, Queensland: Contextualizing Australia's Late Cretaceous dinosaur faunas. *Gondwana Research 24*, pp. 767-779.

Tucker, R.T., Roberts, E.M., Henderson, R.A., Kemp, A.I.S. 2016. Large igneous province of long-lived magmatic arc along the eastern margin of Australia during the Cretaceous? Insights from the sedimentary record. *Geological Society of America Bulletin*, doi: 10.1130/B31337.1

Tucker, R.T., Roberts, E.M., Darlington, V., Salisbury, S.W. 2017. Investigating the stratigraphy and palaeoenvironments for a suite of newly discovered mid-Cretaceous vertebrate fossil-localities in the Winton Formation, Queensland, Australia. *Sedimentary Geology 358*, pp. 210-229.

Turner, S., Bean, L.B., Dettman, M., McKellar, J.L., McLoughlin, S., Thulborn, R.A. 2009. Australian Jurassic sedimentary and fossil successions: current work and future prospects for marine and non-marine correlation. *GFF 131*, pp. 49-70.

Upchurch, P., Barrett, P.M., Dodson, P. 2004. Sauropoda. In: Weishampel, D.B. Dodson, P. and Osmolska, H. (Eds.), The Dinosauria, 2nd edition. University of California Press, Berkeley, California, pp. 259-322.

Van Heeswijck, A. 2004. The structure and hydrocarbon potential of the northern Drummond Basin and northeastern Galilee Basin, central Queensland, Australia. In: Boult, P.J., Johns, D.R. and Lang, S.C. (Eds.), Eastern Australasian Basin Symposium II, Petroleum Exploration Society of Australia Special Publication, pp. 319-330.

Van Heeswijck, A. 2006. The structure, sedimentology, sequence stratigraphy and tectonics of the northern Drummond and Galilee basins, Central Queensland, Australia. PhD Thesis, James Cook University, Townsville, Australia.

Van Heeswijck, A., 2010. Late Paleozoic to early Mesozoic deformation in the northeastern Galilee Basin, Australia. *Australian Journal of Earth Sciences 57*, pp. 431-451.

Van Heeswijck, A. 2018. Fluvial sequences and basin development in the northern Galilee Basin. *Australian Journal of Earth Sciences 65*, pp. 367-389.

Veevers, J.J. 2006. Updated Gondwana (Permian-Cretaceous) earth history of Australia. *Gondwana Research 9*, pp. 231-260.

Vine, R.R. 1973. The Galilee Basin. *Bureau of Mineral Resources, Geology and Geophysics Record 1973/53*, 26 pp.

Vine, R.R. and Paine, A.G.L. 1974. Explanatory notes on the Hughenden 1:250 000 geological sheet. *Bureau of Mineral Resources, Geology and Geophysics*, Australian Government Publishing.

Vine, R.R., Casey, D.J., Johnson, N.E.A. 1964. Progress report, 1963, on the geology of part of the north-eastern Eromanga Basin, Queensland. *Bureau of Mineral Resources, Geology and Geophysics Record 1964/39*, 394pp.

Wainman, C.C. and McCabe, P.J. 2019. Evolution of the depositional environments of the Jurassic Walloon Coal Measures, Surat Basin, Queensland, Australia. *Sedimentology 66*, pp. 1673-1699.

Wainman, C.C., McCabe, P.J., Crowley, J.L., Nicoll, R.S. 2015. U–Pb zircon age of the Walloon Coal Measures in the Surat Basin, southeast Queensland: implications for the paleogeography and basin subsidence. *Australian Journal of Earth Sciences 62*, 807-816.

Wainman, C.C., Hannaford, C., Mantle, D., McCabe, P.J. 2018a. Utilizing U–Pb CA-TIMS dating to calibrate the Middle to Late Jurassic spore-pollen zonation of the Surat Basin, Australia to the geological time-scale. *Alcheringa 42*, pp. 402-414.

Wainman, C.C., McCabe, P.J., Crowley, J.L. 2018b. Solving a tuff problem: Defining a chronostratigraphic framework for Middle to Upper Jurassic nonmarine strata in eastern Australia using uranium-lead chemical abrasion-thermal ionization mass spectrometry zircon dates. *AAPG Bulletin 102*, pp. 1141-1168.

Wainman, C.C., Reynolds, P., Hall, T., McCabe, P.J., Holford, S.P. 2019. Nature and origin of tuff beds in Jurassic strata of the Surat Basin, Australia: Implications on the evolution of the eastern margin of Gondwana during the Mesozoic. *Journal of Volcanology and Geothermal Research 377*, pp. 103-116.

Wang, J., La Croix, A.D., Gonzalez, S., He, J., Undershultz, J. 2019. Sequence stratigraphic analysis of the Lower Jurassic Precipice Sandstone and Evergreen Formation in the Surat Basin, Australia: Implications for the architecture of reservoirs and seals for CO_2 storage. *Marine and Petroleum Geology 102*, pp. 829-843.

Wake-Dyster, K.D., Sexton, M.J., Johnstone, D.W., Wright, C., Finlayson, D.M. 1987. Deep seismic profiling across the Nebine Ridge, Surat Basin, Kumbarilla Ridge and Clarence Moreton Basin in southern Queensland. *Exploration Geophysics 16*, pp. 218-222.

Warren, A.A., Hutchinson, M.N. 1983. The last Labyrinthodont? A new Brachyopoid (Amphibia, Temnospondyli) from the Early Jurassic Evergreen Formation of Queensland, Australia. *Philosophical Transactions of the Royal Society of London 303*, pp. 1-62.

Warren, A.A., Rich, P.V., Rich, T.H. 1997. The last, last labyrinthodonts? *Palaeontologica A 247*, pp. 1-24.

Waschbursch, P., Korsch, R.J., Beaumont, C. 2009. Geodynamic modelling of aspects of the Bowen, Gunnedah, Surat and Eromanga Basins from the perspective of convergent margin processes. *Australian Journal of Earth Sciences 56*, pp. 309-334.

Webb, J.A. 1979. A reappraisal of the palaeoecology of Conchostracans (Crustacea: Branchiopoda). *Neues Jahrbuch für Geologie und Paläontologie, Abhandlungen 158*, pp. 259-275.

Weltje, G.J. and von Eynatten, H. 2004. Quantitative provenance analysis of sediments: review and outlook. *Sedimentary Geology 171*, pp. 1-11.

Willcox, J.B., Sayers, J., Stagg, H.M.J., van de Beuque, S. 2001. Geological framework of the Lord Howe Rise and adjacent ocean basins. In: Hill, K.C. and Bernecker, T. (Eds.), Eastern Australasian Basins Symposium, a refocused energy perspective for the future. Petroleum Exploration Society of Australia Special Publication, pp. 211-225.

Withnall, I.W., Henderson, R.A., Champion, D.C., Jell, P.A. 2013. Introduction. In: Jell, P.A. (Ed.), Geology of Queensland, Geological Survey of Queensland, Brisbane, Queensland, pp. 1-22.

Withnall, I.W., Draper, J.J., Mackenzie, D.E., Knutson, J., Blewett, R.S., Hutton. L.J., Bultitude, R.J., Wellman, P., McConachie, B.A., Bain, J.H.C., Donchak, P.J.T., Land, S.C., Domagala, J., Symonds, P.A., Rienks, I.P. 1997. Review of Geological Provinces and Basins of North Queensland. In: North Queensland Geology, Bain, J.H.C., and Draper, J.J. (eds.). Australian Geological Survey Organisation Bulletin/Queensland Department of Mine and Energy, Queensland, pp. 449-528.

Wood, G.D., Gabriel, A.M. and Lawson, J.C. 1996. Palynological techniques – processing and microscopy. In: Palynology: Principles and applications, American Association of Stratigraphic Palynologists Foundation 3, Jansonius, J., and McGregor D.C. (eds.), pp. 29-50, Publishers Press, Salt Lake City, Utah.

Wray, R.A.L. 2009. Phreatic drainage conduits within quartz sandstone: Evidence from the Jurassic Precipice Sandstone, Carnarvon Range, Queensland, Australia. *Geomorphology 110*, pp. 203-211.

Wright, V.P. and Marriott, S.B. 1993. The sequence stratigraphy of fluvial depositional systems: the role of floodplain sediment storage. *Sedimentary Geology 86*, pp. 203-210.

Yago, J.V.R. and Fielding, C.R. 1996. Sedimentology of the Middle Jurassic Walloon Coal Measures in the Great Artesian Basin, eastern Australia. *Geological Society of Australia, Abstracts 43*, pp. 574-575.

Yang, R., Yang, Y., Fang, X., Ruan, X., Galy, A., Ye, C., Meng, Q., Han, W. Late Miocene intensified tectonic uplift and climatic aridification on the northeastern Tibetan Plateau: evidence from clay mineralogical and geochemical records in the Xining Basin. *Geochemistry, Geophysics, Geosystems 20*, pp. 829-851.

Zappa, G., Bersezio, R., Felletti, F., Giudici, M. 2006. Modeling heterogeneity of gravel-sand, braided stream, alluvial aquifers at the facies scale. *Journal of Hydrology 325*, pp. 135-153.

Appendix 1

Cheng, Y., **Todd, C.N.**, Henderson, R.A., Danisik, M., Sahlstrom, F., Chang, Z., Corral, I., 2020. Jurassic uplift and erosion of the northeast Queensland continental margin: evidence from (U-Th)/He thermochronology combined with U–Pb detrital zircon age spectra. *Australian Journal of Earth Sciences*, https://doi.org/10.1080/08120099.2020.1714730.

This image has been removed
due to copyright restrictions

Appendix 2

Roberts, E.M., **Todd, C.N.**, Aanen, D.K., Nobre, T., Hilbert-Wolf, H.L., O'Connor, P.M., Tapanila, L., Mtelela, C., Stevens, N.J., 2016. Oligocene termite nests with *in situ* fungus gardens from the Rukwa Rift Basin, Tanzania, support a Paleogene African origin for insect agriculture. *Plos One*, 11, doi: 10.1371/journal.pone.0156847

PLOS | ONE

RESEARCH ARTICLE

Oligocene Termite Nests with *In Situ* Fungus Gardens from the Rukwa Rift Basin, Tanzania, Support a Paleogene African Origin for Insect Agriculture

Eric M. Roberts[1]*, Christopher N. Todd[1], Duur K. Aanen[2], Tânia Nobre[3], Hannah L. Hilbert-Wolf[1], Patrick M. O'Connor[4,5], Leif Tapanila[6], Cassy Mtelela[1,7], Nancy J. Stevens[4,5]

1 Department of Earth and Oceans, James Cook University, Townsville, Queensland, 4811 Australia, 2 Laboratory of Genetics, Wageningen University, Droevendaalsesteeg 1, Radix West, Building 107, 6708 PB, Wageningen, The Netherlands, 3 Institute of Mediterranean Agricultural and Environmental Sciences (ICAAM), Universidade de Évora, Núcleo da Mitra, Ap. 94, 7002–554, Évora, Portugal, 4 Department of Biomedical Sciences, Heritage College of Osteopathic Medicine, Ohio University, Athens, Ohio, 45701, United States of America, 5 Center for Ecology and Evolutionary Studies, Ohio University, Athens, Ohio, 45701, United States of America, 6 Department of Geosciences and Idaho Museum of Natural History, Idaho State University, Pocatello, Idaho, 83209, United States of America, 7 Department of Geology, University of Dar es Salaam, P.O. Box 35052, Dar es Salaam, Tanzania

* eric.roberts@jcu.edu.au

Citation: Roberts EM, Todd CN, Aanen DK, Nobre T, Hilbert-Wolf HL, O'Connor PM, et al. (2016) Oligocene Termite Nests with *In Situ* Fungus Gardens from the Rukwa Rift Basin, Tanzania, Support a Paleogene African Origin for Insect Agriculture. PLoS ONE 11(6): e0156847. doi:10.1371/journal.pone.0156847

Editor: Faysal Bibi, Museum für Naturkunde, GERMANY

Received: December 10, 2015

Accepted: May 20, 2016

Published: June 22, 2016

Data Availability Statement: All relevant data are within the paper and its Supporting Information files.

Funding: This research was supported by the US National Science Foundation (NSF EAR_0617561, EAR_0854218, EAR 0933619), National Geographic Society (CRE), and funding from Ohio University and James Cook University. TN was supported by a Marie Curie fellowship (FP7-PEOPLE-2012-CIG Project Reference 321725) and by the Portuguese Foundation for Science and Technology (SFRH/BCC/52187/2013).

Abstract

Based on molecular dating, the origin of insect agriculture is hypothesized to have taken place independently in three clades of fungus-farming insects: the termites, ants or ambrosia beetles during the Paleogene (66–24 Ma). Yet, definitive fossil evidence of fungus-growing behavior has been elusive, with no unequivocal records prior to the late Miocene (7–10 Ma). Here we report fossil evidence of insect agriculture in the form of fossil fungus gardens, preserved within 25 Ma termite nests from southwestern Tanzania. Using these well-dated fossil fungus gardens, we have recalibrated molecular divergence estimates for the origins of termite agriculture to around 31 Ma, lending support to hypotheses suggesting an African Paleogene origin for termite-fungus symbiosis; perhaps coinciding with rift initiation and changes in the African landscape.

Introduction

Termites are among the most diverse and ecologically important groups of insects in modern ecosystems, playing a critical role as natural decomposers of plant tissues. Termites typically rely on gut symbionts to decompose organic matter. However, members of the subfamily Macrotermitinae have turned to agriculture by developing a highly specialized, symbiotic relationship with fungi of the genus *Termitomyces* (Basidiomycotina). The fungus-growing termites cultivate fungi in gardens/chambers inside the colony and then exploit the ability of the fungi to convert recalcitrant, nitrogen-poor, plant material into a more easily digestible,

Appendix 3

Roberts, E.M., **Todd, C.N.**, Were termites the world's first farmers?

Australasian Science, March/April 2017

This image has been removed due to copyright restrictions

Appendix 4

Stratigraphic Section Locations

Formation(s)	Coordinates	Notes
Betts Creek beds	20° 20’ 9.46” S, 144° 28’ 5.38” E	
Porcupine Gorge Formation	20° 20’ 6.57” S, 144° 28’ 8.18” E	
Warang Sandstone	20° 20’ 12.63” S, 144° 28’ 1.98” E	Part 1
	20° 20’ 16.57” S, 144° 27’ 58.3” E	Part 2
Lower Blantyre Sandstone	20° 21’ 6.4” S, 144° 27’ 57.83” E	S1
	20° 21’ 7.09” S, 144° 28’ 0.78” E	S2
	20° 21’ 40.6” S, 144° 27’ 42.59” E	S3
	20° 21’ 15.1” S, 144° 27’ 59.76” E	S4
	20° 22’ 24.73” S, 144° 27’ 19.7” E	S5
Upper Blantyre Sandstone	20° 24’ 30.77” S, 144° 26’ 15.91” E	

Appendix 5

Pebble Count Data

Betts Creek beds

Vein Qtz	Meta Qtz	Rhy	Granite	Sandstone	IF Mud	Chert	Plag	Total
21	11	15	3	10	4	-	-	64
137		4	2	13	-	3	-	159

Lower Blantyre Sandstone

Vein Qtz	Meta Qtz	Red Rhy	Flow Rhy	Granite (weathered)	Sandstone	Chert	IF Mud	Total
34	42	50	15	4	5	20	5	175
42	47	38	32	0	6	12	9	186
27	42	36	7	2	3	8	3	128
37	46	42	16	2	3	11	6	163

Upper Blantyre Sandstone

Alluvial Fan						
Qtz-Qtzite	**Rhy**	**Granite**	**Sst**	**Chert**	**Mica**	**Total**
210	170	0	0	4	0	384
Upper Conglomerate						
125	10	0	1	1	0	137
Basal Fluvial Conglomerate						
305	3	0	0	3	4	315

Appendix 6

Palaeocurrent Data

Formation	Coordinates	Measurements
Betts Creek beds	20° 19’ 38.02” S, 144° 28’ 4.52” E to 20° 19’ 42.20” S, 144° 28’ 5.21” E	138, 148, 147, 146, 172, 144, 136, 138, 142, 127, 151, 142
Porcupine Gorge Formation	20° 20’ 1.15” S, 144° 28’ 12.93” E to 20° 20’ 6.16” S, 144° 28’ 6.26” E	240, 242, 244, 244, 236, 232, 224, 225, 228, 222, 238, 212, 210, 217, 230, 228, 212, 208, 220, 208, 212, 223, 222, 225, 211, 223, 233, 255, 250
Warang Sandstone	20° 20’ 35.66” S, 144° 27’ 54.39” E to 20° 20’ 42.01” S, 144° 27’ 55.30” E	172, 185, 180, 172, 172, 174, 175, 176, 183, 172, 171, 172, 178, 170, 172, 180, 178, 171, 183, 200, 200, 204, 202, 201, 185
	20° 20’ 50.89” S, 144° 27’ 56.93 E to 20° 21’ 12.17” S, 144° 27’ 58.77” E	170, 173, 168, 167, 178, 172, 173, 173, 176, 183, 177, 176, 176, 166, 170, 168, 182, 181, 182, 182, 235, 210, 210, 210, 252, 224, 224, 188, 190, 194, 210, 190, 190, 190, 185, 220, 200, 209, 204, 185, 180, 160, 188, 230, 235, 210, 215, 200, 208
Lower Blantyre Sandstone	20° 21’ 6.43” S, 144° 27’ 55.25” E to 20° 21’ 5.71” S, 144° 27’ 55.30” E	190, 192, 200, 187, 194, 198, 200, 195, 200, 190
	20° 21’ 5.18” S, 144° 27’ 44.94” E to 20° 21’ 6.14” S, 144° 27’ 44.65” E	218, 220, 216, 215, 245, 252, 245, 240, 242, 245, 242, 238, 346, 247, 250, 238, 242, 246, 240, 242, 242, 230, 232, 231, 214, 214, 217, 242, 208
Upper Blantyre Sandstone	20° 24’ 3.09” S, 144° 26’ 23.25 E to 20° 24’ 4.94” S, 144° 26’ 23.82” E	183, 188, 189, 182, 192, 188, 180, 200, 194, 186, 200, 195, 186, 205, 180, 190, 178, 179, 180, 185, 185, 200, 185, 190, 195
	20° 24’ 9.16” S, 144° 26’ 23.20” E	85, 112, 130, 130, 122, 126, 127, 125, 140, 135, 133, 130
	20° 24’ 31.60” S, 144° 26’ 14.95” E to 20° 24’ 30.96” S, 144° 26’ 14.70 E	212, 196, 198, 225, 228, 238, 240, 245, 250, 250, 232, 233
	20° 24’ 31.36” S, 144° 26’ 11.52” E to 20° 24’’ 31.75” S, 144° 26’ 12.65” E	325, 330, 310, 310, 320, 292, 305, 310, 340, 340, 345, 344, 350, 349, 349
		16, 45, 90, 97, 20, 13, 29, 38, 50, 27, 29, 35, 40, 33, 28, 38, 37